The University Of Sheffield.

The Role of Cancer Associated Fibroblasts in Bone Invasive Oral Squamous Cell Carcinoma

By:

Areeg Elmusrati

A thesis submitted in partial fulfilment of the requirements for the degree of Doctor of Philosophy

The University of Sheffield
Faculty of Medicine, Dentistry and Health
Department of Oral & Maxillofacial Pathology
School of Clinical Dentistry

February 2020

Acknowledgments

First of all, I would like to express my sincere and grateful appreciation to my supervisors, Professor Daniel W Lambert and Dr Syed Ali Khurram for their constant support, motivation, and guidance throughout my PhD. Your optimism and endless encouragement are highly appreciated.

I would like to thank the Libyan Consulate and Ministry of Scientific Research and Higher Education, Libya, for the financial assistance, and granting me the opportunity to excel academically.

I would also like to express my gratitude to my friends and colleagues at the School of Clinical Dentistry, for making the department an amazing place to work.

A special thanks to Brenka McCabe, Jason Heath, and Kirsty Franklin for the technical support, and for always being there to cheer me up when things don't go as planned.

Thank you to my loving parents and siblings for the encouragement and uplifting support throughout my education to whom I owe this all.

Publications

Elmusrati, A.A., Pilborough, A.E., Khurram, S.A. and Lambert, D.W., 2017. Cancer-associated fibroblasts promote bone invasion in oral squamous cell carcinoma. *British Journal of Cancer*, *117*(6), p.867.

Pink, R.C., Elmusrati, A.A., Lambert, D. and Carter, D.R.F., 2017. Royal Society Scientific Meeting: Extracellular vesicles in the tumour microenvironment. *Philosophical Transactions of the Royal Society B: Biological Sciences*, *373*(1737), p.20170066.

Prizes

Senior Colgate Prize, British Society of Oral and Dental Research (BSODR) 2019.

Third year oral presentation, School of Clinical Dentistry, Postgraduate Research Day 2019.

Second year poster presentation, School of Clinical Dentistry, Postgraduate Research Day 2018.

First year oral presentation, School of Clinical Dentistry, Postgraduate Research Day 2017.

Abstract

Bone invasion is a common feature of oral squamous cell carcinoma (OSCC) and is associated with poor prognosis. In this study, we report a novel role for cancer associated fibroblasts (CAF) in OSCC bone invasion, and provide additional evidence that two subsets of CAF, myofibroblastic and senescent fibroblasts, can both promote bone destruction via a mechanism involving receptor activator of nuclear factor kappa-B ligand (RANKL) and extracellular vesicles (EV).

Our results show two populations of CAF, alpha smooth muscle actin (αSMA) myofibroblastic, and αSMA and p16INK4a positive senescent, are present and show increased expression of RANKL in *ex vivo* OSCC bone resections. To examine the mechanism underlying this observation, senescence was experimentally induced in normal oral fibroblasts (NOF) by culturing to replicative mitotic exhaustion (S-NOF^{Rep}), or exposure of proliferating cells to hydrogen peroxide (S-NOF^{H2O2}) or cisplatin (S-NOF^{Cis}). Elevated expression of the molecular markers of senescence, p16INK4a and interleukin-6 (IL6), were seen; the latter is also a key component of the senescence-associated secretory phenotype (SASP) and mediator of bone absorption. Increased expression and secretion of RANKL was also detected in these cell cultures.

Osteoclastogenesis and pit formation on a synthetic bone substrate were significantly increased in response to primary CAF, myofibroblastic and senescent fibroblast-derived conditioned media. This mechanism was significantly attenuated by the senolytic drugs Alvespimycin (17-DMAG) and Navitoclax (ABT263). Moreover, to understand the mechanism by which OSCC and surrounding CAF communicate in the tumour microenvironment, EV were isolated from H357 oral cancer cell line, primary CAF from fresh OSCC tissue and experimentally induced senescent fibroblasts (S-NOF). EV from all cells contained RANKL, and significantly promoted osteoclastogenesis. Osteoprotegrin (OPG), a RANKL decoy receptor, antagonist and bone resorption regulator reduced osteoclastogenesis, providing further evidence of a role of RANKL in CAF-mediated bone destruction.

In conclusion, this work provides novel evidence that CAF play a functional role in bone invasion. The ability of senolytic drugs to reduce senescent CAF burden and inhibit osteoclastogenesis holds promise as a novel therapeutic approach in bone invasive OSCC.

Table of Contents

Acknowledgments i

Publications ii

Prizes ii

Abstract iii

List of Figures x

List of Tables xiv

Abbreviations xv

Chapter 1 *1*

Introduction and Literature Review *1*

1.1 Introduction 2

1.2 Bone physiology 6

1.2.1 Bone tissue 6

1.2.2 The dynamic mechanism of bone remodelling 7

1.3 Cellular and molecular mechanisms in bone invasion by tumours 10

1.4 Role of tumour microenvironment in cancer 12

1.4.1 Components of tumour microenvironment 13

1.4.2 Fibroblasts 17

1.4.3 Myofibroblasts 18

1.4.4 Myofibroblasts in oral cancer 19

1.4.5 Origin of cancer associated fibroblasts 21

1.4.6 Significance of CAF in tumour microenvironment 21

1.4.7 Senescence in fibroblasts 22

1.5 Extracellular vesicles: cellular messengers in tumour microenvironment 24

1.5.1 Classification biogenesis, and contents of EV 25

1.5.2 Extracellular vesicles in bone 28

1.5.3 Roles of extracellular vesicles in cancer and microenvironment 29

1.5.4 EV and cancer biomarkers and potential therapeutics 31

1.6 Bone Invasion in OSCC 32

1.6.1 Cytokines 32

1.6.2 Role of TGFβ dependent pathways in cancer progression 33

1.6.3 RANK, RANK ligand and OPG mechanisms. 36
1.6.4 “Vicious cycle” a cascade regulating bone integrity 39

1.7 Adjuvant therapeutic implications in cancer 40
1.7.1 Senotherapeutics 40

1.8 Summary 44

1.9 Project hypothesis, aims and objectives 45
1.9.1 Hypothesis 45
1.9.2 Aims 45
1.9.3 Objectives 45

Chapter 2 46

Materials and Methods 46

2.1 Clinicopathological analysis of OSCC bone resections 47

2.2 Immunohistochemical (IHC) analysis of OSCC incisional biopsies away from bone 47
2.2.1 IHC procedure 48
2.2.2 IHC evaluation 52
2.2.3 Double IHC analysis of senescence in myofibroblasts 53

2.3 Cell culture and propagation 55
2.3.1 Cell lines and culture conditions 55
2.3.2 Cell subculture and propagation 57
2.3.3 Collection of conditioned media from cultured cells 57
2.3.4 Indirect co-culture of human primary osteoblasts with H357 or CAF. 57
2.3.5 Treatment of fibroblasts with TGFβ1 60
2.3.6 Induction of senescence in NOF 61

2.4 Assessment of senescence 62
2.4.1 Senescence-associated β-galactosidase assay 62
2.4.2 Evaluation of accumulating lipofuscin in senescence, using Sudan B Black staining 63

2.5 mRNA expression analysis from cultured cells 64
2.5.1 Total RNA extraction and purification 64
2.5.2 Quantification of RNA concentration and purity 64
2.5.3 Reverse Transcription (RT) of RNA to complementary DNA (cDNA) 65

2.6 Quantitative Real-Time Polymerase Chain Reaction (qPCR) 66

2.6.1 qPCR protocol 66

2.7 Immunofluorescence (IF) 68

2.8 Enzyme-linked immunosorbent assay (ELISA) 69

2.8.1 ELISA detection of soluble RANK ligand 70

2.8.2 ELISA quantification 71

2.9 Osteoclastogenesis assay 71

2.9.1 TRAP staining 73

2.9.2 Pit formation 74

2.9.3 Nucleation staining for osteoclast verification 74

2.10 Evaluation of senotherapeutics 75

2.10.1 Optimisation of senolytic drugs 75

2.10.2 Evaluation of senotherapeutic toxicity on NOF viability 76

2.11 Extracellular vesicle (EV) isolation and analysis 77

2.11.1 Graded concentration centrifugation for EV isolation from conditioned media in culture 77

2.11.2 Size exclusion chromatography (SEC) for EV separation 79

2.11.3 Quantification of protein content in EV fractions to determine highest EV content 80

2.11.4 EV quantification by nano particle tracking 80

2.11.5 EV characterisation 81

2.11.6 Investigation of RANKL expression in EV 81

2.11.7 Osteoclastogenesis assay to examine EV functionality 81

2.12 Osteoprotegerin, a RANKL antagonist and regulator of osteoclast differentiation and activation 82

2.12.1 Optimisation of OPG 82

2.12.2 Investigating the role of OPG in antagonising RANKL expression 83

2.13 Statistical analyses 85

Chapter 3 86

The role of myofibroblastic CAF in the tumour microenvironment of bone invasive OSCC 86

3.1 Introduction 87

3.1.1 Aim 88

3.1.2 Experimental approach 88

3.2 Clinicopathological data **89**
3.2.1 Gender and Site 89
3.2.2 OSCC histological grade 91
3.2.3 Bone involvement 91
3.2.4 Metastasis 93
3.3 Evaluation of stromal marker αSMA and bone turnover markers RANKL and OPG expression in OSCC tissue away from bone **94**
3.3.1 Expression of αSMA in tumour microenvironment away from bone 95
3.3.2 RANKL and OPG expression 97
3.4 Double αSMA and RANKL expression in OSCC microenvironment **102**
3.5 Experimentally induced CAF and primary CAF isolated from OSCC express stromal marker αSMA **104**
3.6 OSCC derived CAF express soluble RANKL protein **107**
3.7 Expression of RANKL and OPG mRNA in primary human osteoblasts **108**
3.7.1 CAF increase RANKL and reduce OPG expression in human primary osteoblasts on a transcript level 108
3.8 OSCC cells, experimentally induced CAF, and CAF isolated from human OSCC tissue induce osteoclastogenesis **110**
3.9 Discussion **115**
Chapter 4 ***119***
Exploring the role of fibroblast senescence in bone invasion in OSCC ***119***
4.1 Introduction **120**
4.1.1 Aims 122
4.1.2 Experimental approach 122
4.2 Evaluation of senescence marker p16INK4a and DPP4 expression in *ex vivo* OSCC bone resections at tumour bone interface **123**
4.2.1 Expression of tumour suppressor gene p16INK4a in tumour microenvironment proximal to bone 123
4.2.2 Expression of senescence marker DPP4 (CD26) in tumour microenvironment proximal to bone 125
4.3 Senescent fibroblasts exhibit contractility features through the expression of αSMA in tumour microenvironment proximal to bone **127**

4.4 Characterisation of induction of senescence *in vitro* 129

4.5 Primary oral fibroblasts express Sudan B Black *in vitro* after experimental senescence induction 131

4.6 mRNA expression of p16INK4a and SASP factor IL6 is significantly higher in senescent fibroblasts 134

4.7 Experimentally induced senescent fibroblasts express stromal marker αSMA 136

4.8 Senescent oral fibroblasts express RANKL a transcript and protein 138

4.9 Senescent oral fibroblasts induce osteoclastogenesis 141

4.10 Senolytic drugs impede tumour progression and bone invasion, giving promising therapeutic benefits 146

4.10.1 The effect of senolytics Alvespimycin (17-DMAG) and Navitoclax (ABT263) on NOF viability 146

4.10.2 Senotherapeutics Alvespimycin (17-DMAG) and Navitoclax (ABT263) target senescence. 148

4.10.3 Senolytic drugs limit bone invasion by reducing osteoclast generation 152

4.11 Discussion 159

Chapter 5* *162

Extracellular vesicles: communicators in the OSCC microenvironment* *162

5.1 Introduction 163

5.1.1 Aims 164

5.1.2 Experimental approach 164

5.2 EV isolation from OSCC, NOF, CAF, myofibroblasts and senescent oral fibroblasts 165

5.2.1 Collection of EV from oral cancer and stromal cells 165

5.2.2 Quantification and size distribution of EV 165

5.3 Characterisation of EV expressed by oral cancer cells and NOF 168

5.4 EV isolated from OSCC, CAF and senescent fibroblasts express bone resorption marker RANKL 172

5.5 EV isolated from OSCC, CAF and senescent fibroblasts EV are instrumental in promoting bone invasion in OSCC 174

5.6 OPG antagonises RANKL production by EV isolated from OSCC, CAF and senescent fibroblasts and impedes bone invasion in OSCC **179**
5.6.1 Optimisation of RANKL antagonist OPG 179
5.6.2 OPG significantly reduces osteoclast generation 181
5.7 Discussion. **189**
Chapter 6 ***192***
Discussion ***192***
6.1 Introduction **193**
6.2 Myofibroblastic stroma in OSCC **195**
6.3 Senescence promotes OSCC bone invasion **200**
6.4 Senolytics, a promising therapeutic application in limiting bone invasion in OSCC **205**
6.5 Cell to cell communications in the tumour microenvironment are mediated by secreted EV **207**
6.6 Prospective implications in improvement of cancer therapies **210**
6.7 Conclusions **212**
6.8 Future work **213**
References ***214***

List of Figures

Chapter 1

Figure 1.1: Bone remodelling 8

Figure 1.2: Tumour microenvironment 13

Figure 1.3: Biogenesis of extracellular vesicles 26

Figure 1.4: Epithelial-mesenchymal transdifferentiation 35

Figure 1.5: Vicious cycle of bone invasion 39

Chapter 2

Figure 2.1: Indirect co-culture of human primary osteoblasts. 59

Figure 2.2: NOF treatment with TGFβ1. 61

Figure 2.3: Osteoclastogenesis assay. 72

Figure 2.4: Osteoclastogenesis assay protocol. 73

Figure 2.5: NOF viability test. 76

Figure 2.6: EV isolation by size exclusion chromatography. 79

Figure 2.7: The effect of OPG on osteoclastogenesis. 84

Chapter 3

Figure 3.1: Gender distribution in 407 bone invasive OSCC cases, 90

Figure 3.2: Site distribution of 407 bone invasive OSCC cases. 90

Figure 3.3: Grade of primary OSCC tumour. 91

Figure 3.4: Representative photomicrograph showing bone involvement distribution in OSCC cases with bone resection. 92

Figure 3.5: Bone involvement distribution in 407 OSCC cases with bone resection. 93

Figure 3.6: Distribution of metastasis in 407 OSCC samples with bone resection. 94

Figure 3.7: Representative photomicrographs showing IHC localisation of αSMA in incisional biopsies away from bone. 96

Figure 3.8: Quantification of αSMA expression in OSCC biopsy sections away from bone interface in selected cohort. 97

Figure 3.9: Representative photomicrographs showing IHC localisation of RANKL in incisional biopsies away from bone. 98

Figure 3.10: Representative photomicrographs showing IHC localisation of OPG in incisional biopsies away from bone. 99

Figure 3.11: Expression of RANKL and OPG in biopsies of tumour (away from bone interface) with superficial cortical bone resorption. 100

Figure 3.12: Expression of RANKL and OPG in tumour biopsies (away from bone interface) with confirmed cancellous bone involvement. 100

Figure 3.13: Expression of RANKL and OPG in stroma of OSCC (biopsies-away from bone interface) with only superficial cortical bone resorption. 101

Figure 3.14: Expression of RANKL and OPG in stroma of OSCC biopsies (away from bone interface) with definite cancellous bone invasion. 101

Figure 3.15: Representative photomicrographs showing IHC co-localisation of αSMA and RANKL. 103

Figure 3.16: Representative photomicrographs showing cytoplasmic αSMA. 105

Figure 3.17: Relative expression of αSMA mRNA in normal oral fibroblasts following TGFβ1 treatment and CAF isolated from OSCC 106

Figure 3.18: Soluble RANKL protein expression in CAF and NOF. 107

Figure 3.19: Relative expression of RANKL and OPG mRNA in HOB 109

Figure 3.20: Osteoclastogenesis assay. 113

Figure 3.21: Osteoclast and pit formation quantification. 114

Chapter 4

Figure 4.1: Representative photomicrographs showing IHC localisation of p16INK4a. 124

Figure 4.2: Quantification of p16INK4a expression in stromal cells of OSCC bone resections. 125

Figure 4.3: Representative photomicrographs showing IHC localisation of DPP4. 126

Figure 4.4: Quantification of DPP4 expression in stromal cells of OSCC bone resections. 127

Figure 4.5: Representative photomicrographs showing IHC co-localisation of αSMA and p16INK4a. 128

Figure 4.6: Representative photomicrographs of SA-β-Gal detection in NOF following exposure to different senescent inducers. 130

Figure 4.7: Quantification of SA-β-Gal positive cells. 131

Figure 4.8: Representative photomicrographs showing Sudan B Black histochemical staining in response to different senescence inducers. 132

Figure 4.9: Quantification of SBB positive cells. 133

Figure 4.10: Relative expression of p16INK4a and IL6 mRNA in senescent oral fibroblasts. 135

Figure 4.11: Representative photomicrographs showing immunofluorescence detection of αSMA. 137

Figure 4.12: Expression of mRNA RANKL and OPG in senescent oral fibroblasts. 139

Figure 4.13: Expression of soluble RANKL protein in senescent oral fibroblasts. 140

Figure 4.14: Osteoclastogenesis assay. 144

Figure 4.15: Senescent oral fibroblasts induce osteoclastogenesis. 145

Figure 4.16: Effect of senolytics on NOF viability. 147

Figure 4.17: Representative photomicrographs showing the effect of senolytics on S-NOF^{H2O2}. 149

Figure 4.18: Representative photomicrographs showing the effect of senolytics on S-NOF^{Cis}. 150

Figure 4.19: Evaluation of senescence following exposure to senolytics. 151

Figure 4.20: Osteoclastogenesis assay, the effect of senolytics on osteoclast generation. 156

Figure 4.21: Senolytics reduce osteoclast generation. 158

Chapter 5

Figure 5.1: EV size distribution analysis by nanoparticle tracking using ZetaView instrument. 167

Figure 5.2: Average number of EV produced by different cell types. 168

Figure 5.3. Characterisation of EV derived from primary NOF. 170

Figure 5.4. Characterisation of EV derived from OSCC cell line H357. 171

Figure 5.5: Soluble RANKL protein expression in EV isolated from OSCC, CAF, myofibroblasts and senescent oral fibroblast. 173

Figure 5.6: Osteoclastogenesis assay with EV isolated from conditioned media. 177

Figure 5.7: EV produced by OSCC, CAF, and senescent oral fibroblasts induce osteoclastogenesis. 178

Figure 5.8: Optimisation of RANKL antagonist recombinant human OPG. 180

Figure 5.9: Osteoclastogenesis assay with OPG treatment. 186

Figure 5.10: OPG significantly reduced osteoclast generation caused by H357, CAF, and senescent oral fibroblasts and derived EV. 188

List of Tables

Chapter 1

Table 1.1: Senolytic drugs and SCAP. 42

Chapter 2

Table 2.1: Details of primary antibodies used for IHC. 48

Table 2.2: IHC solutions and reagents. 50

Table 2.3: Details of secondary antibodies used for IHC. 51

Table 2.4: HistoQuest settings for haematoxylin measurement. 52

Table 2.5: HistoQuest settings for DAB and NovaRed measurement. 53

Table 2.6: Media used to propagate the specific cell strains. 56

Table 2.7: RT master mix components. 65

Table 2.8: TaqMan primers. 66

Table 2.9: Real time qPCR TaqMan master mix components. 66

Table 2.10: SYBR green primers. 67

Table 2.11: Real time qPCR SYBR green master mix components. 67

Table 2.12: ELISA reagents preparations. 70

Chapter 3

Table 3.1: Osteoclastogenesis assay: quantification of TRAP positive cells and pits formed. 111

Chapter 4

Table 4.1: Abbreviations used for different senescence induction methods 129

Table 4.2: Quantification of TRAP positive cells and pits formed. 142

Table 4.3: Quantification of TRAP positive cells and pits formed following senolytic drug exposure 153

Chapter 5

Table 5.1: Number of TRAP positive cells and pits formed following EV exposure 175

Table 5.2: Number of TRAP positive cells and pits formed following OPG exposure 182

Abbreviations

AJCC	American Joint Committee on Cancer Classification
Atp6v0d2	ATPase
Bcl-XL	B-cell lymphoma-extra large
Bim	Bcl-2 pro apoptotic protein
BMC	Bone marrow mice cells
BMP	Bone morphogenic proteins
BSA	Bovine serum albumin
CAF	Cancer associated fibroblasts
cDNA	Complementary DNA
COX	Cyclooxygenase
CSF	Colony-stimulating factor
CT	Cycle threshold
CTGF	Connective tissue growth factor
DC-STAMP	Dendritic cell-specific transmembrane protein
DPP4	Dipeptidyl peptidase 4
ECM	Extracellular matrix
EGF	Epidermal growth factor
EGFR	Epidermal growth factor receptor
EIF2	Eukaryotic initiation factor 2
ELISA	Enzyme-linked immunosorbent assay
EMT	Epithelial-mesenchymal transition
ESCRT	Endosomal sorting complex required for transport
EV	Extracellular vesicles
FAP	Fibroblast activation protein

FcRy	Fc receptor-related protein Y
FFPE	Formalin fixed paraffin embedded
FGF	Fibroblast growth factor
FITC	Flourescent isothiocynate
FSP	Fibroblast specific protein 1
GDF	Growth differentiation factor
HB-EGF	Heparin binding epidermal growth factor
H&E	Haematoxylin and Eosin
HGF	Hepatocyte growth factor
HIER	Heat induced epitope retrieval
HIF	Hypoxia inducible family
H_2O_2	Hydrogen peroxide
HPV	Human papilloma virus
HSP	Heat shock protein
HOB	Human osteoblasts
IDA	Absolute alcohol
IGF	Insulin-like growth factor
IHC	Immunohistochemistry
IFN-y	Interferon gamma
IF	Immunofluorescence
IL	Interleukin
LOX	Lysyl oxidase
LPS	Lipopolysaccharide
MCSF	Macrophage colony stimulating factor
MCP	Monocyte chemotactic protein
MHCII	Major histocompatibility class II
MMP	Matrix metalloproteinases
mRNA	Messenger RNA

NF-kB	Nuclear factor kappa B
OCIF	Osteoclast inhibitory factor
OPG	Osteoprotegrin
OSCC	Oral squamous cell carcinoma
PBS	Phosphate buffered saline
PDGF	Platelet derived growth factor
PG	Prostaglandin
PTH	Parathyroid hormone
PTH1R	Parathyroid hormone receptor
PTHrP	Parathyroid hormone related protein
qPCR	Quantitative polymerase chain reaction
RANK	Receptor activated nuclear factor kappa β
RANKL	Receptor activated nuclear factor kappa β ligand
ROI	Regions of interest
ROS	Reactive oxygen species
RT	Room temperature
SA-β-Gal	Senescence associated β galatosidase
SASP	Senescence associated secretory phenotype
SBB	Sudan b black
SCAP	Senescent cell anti apoptotic pathway
SEC	Size exclusion chromatography
SMA	Smooth muscle actin
S-NOF	Senescent oral fibroblasts
$S\text{-}NOF^{H2O2}$	Senescent oral fibroblasts induced by H_2O_2
$S\text{-}NOF^{Cis}$	Senescent oral fibroblasts induced by cisplatin
$S\text{-}NOF^{Rep}$	Senescent oral fibroblasts induced by replication
TAM	Tumour associated macrophages
TGF	Transforming growth factor

Th1	T-helper cells
TNF	Tumour necrosis factor related proteins
TRAP	Tartrate resistant acid phosphatase
VEGF	Vascular endothelial growth factor

Chapter 1

Introduction and Literature Review

1.1 Introduction

Cancer is a term used to describe uncontrolled proliferation of anaplastic cells, with invasion of proximal tissue and metastasis to regional sites and distant organs. Cancer is one of the leading causes of mortality worldwide, with an estimate of 8.2 million deaths recorded in 2012 (Cancer Research, UK, 2017).

Head and neck cancers are predominantly of epithelial origin. Oral squamous cell carcinoma (OSCC), comprises 95% of all neoplasia of the oral cavity, and approximately 30% of head and neck malignancies involving pharynx, nasal cavity, paranasal sinuses, oral cavity, and lips (Haddad and Shin, 2008). In reference to the State of Mouth Cancer UK Report 2018/2019, more than 8,300 people are diagnosed with oral cancer each year. It is the fourteenth most common cancer, in which over 78% are over the age of 55 (dentalhealth.org, 2019). Unfortunately, oral cancer has been on a rise to up to 33% in the last decade (Cancer Research UK, 2019).

OSCC has diverse risk factors, such as excessive alcohol consumption, tobacco, diet and genetics either affecting independently or synergistically. Over the past two decades, OSCC incidence has been increasing in young patients and in developed countries particularly. This escalation has been partly attributed to tonsillar and oropharyngeal cancers related to human papillomavirus (HPV), but the particular causes and mechanism of this rapid increase remain rather speculative (Warnakulasuriya, 2010; Cleary et. al, 2016; Office of National Statistics, 2017).

Oral cancer remains difficult to treat and one main reason is the lack of specific biomarkers and late detection of these lesions at an advanced stage. OSCC can

arise from histologically normal epithelium but usually develops within an existing potentially malignant lesion clinically presenting as erythroplakia or leukoplakia i.e. red or white lesions respectively (Colella et. al, 2008). Lesions can originate anywhere in the oral mucosa, but the gingiva, floor of mouth and tongue are considered the most frequent sites (Jimi et al., 2011).

Advanced OSCC is very aggressive, with a three-year survival rate of 40% often due to regional metastasis (National Cancer Intelligence Network (NCIN), 2013). As tumour cells proliferate and invade the connective tissue, the lesion expands in size and may lead to involvement of locoregional structures including the mandible, maxilla or facial bones. In fact, bone invasion is a hallmark of OSCC, upgrading the tumour stage and is seen in 12% to 56% of OSCCs (Chen et al., 2011). Maxillofacial bones (particularly maxilla and mandible) are closely associated with complex anatomical structures such as sinuses, nose, eyes, cranial nerves, and brain; therefore, OSCC infiltration can cause critical functional complications. Such cancers are difficult to treat and eradicate surgically due to the complex maxillofacial anatomy, difficult surgical access and attempt at preservation of functionality. The primary treatment modality for OSCC is surgery with adjuvant radio or chemotherapy. However, surgery can have associated morbidity with aesthetic and psychosocial impact on patients. Bone involvement is usually related to a poor prognosis, significantly deteriorating the patient's quality of life and postoperative outcome. Therapy and rehabilitation could be challenging, as principal functions such as speech, mastication, and swallowing can be adversely influenced. Despite these significant issues related to bone invasion in OSCC, its precise mechanism remains under-investigated and poorly understood (Quan et al., 2012).

Surgical radical resection with a healthy margin is the treatment of choice for OSCC patients presenting with bone involvement (Shah and Gil, 2009). The American Joint Committee on Cancer Classification (AJCC), recommends upgrading OSCC with bone invasion to a clinical (and pathological) primary tumour stage T4 (irrespective of any other parameters) with an overall stage (IV); the latter associated with a poor prognosis (Frederick et al., 2002). Shah and Lydiatt (1999) recorded the 5-year survival rate of patients with stage IV OSCC as 39%, compared to 53, 68 and 70% for stages III, II and I respectively, indicating its significance as a clinical issue. A retrospective study reviewing cases with histopathologically confirmed bone invasion reported that cancellous bone invasion (rather than superficial cortical bone resorption) is the prime factor that has a prognostic implication on survival. (Ebrahimi et al., 2011).

It has recently become increasingly evident that the stroma surrounding tumour (predominantly fibroblasts, inflammatory cells, and endothelial cells) plays a critical role in tumour advancement (De Wever et al., 2008). Marsh et al. (2011), amongst others, highlighted the importance of the tumour microenvironment in OSCC progression, showing that stromal features such as the presence of myofibroblast-like cells are more sensitive predictors of OSCC aggression, than other tumour features or TNM staging. Alpha smooth muscle actin (αSMA) expressing stromal myofibroblasts (cancer associated fibroblasts, peri-tumour fibroblasts or cancer activated fibroblasts) are apparent in numerous solid tumour microenvironments (Radisky et al., 2007). Xu et al. (2009) observed the transdifferentiation of myofibroblasts through TGFβ and postulated that cancer associated fibroblasts (CAF) could differentiate from epithelial cancer cells through epithelial mesenchymal transition (EMT). However, Marsh et al.

(2011) suggested that myofibroblasts are likely to originate from local mesenchymal cells and promote tumour progression by creating a microenvironment encouraging cancer growth and spread.

Nonetheless, the role of OSCC stroma in bone invasion remains largely unexplored. Ishikuro et al. (2008) reported the presence of intervening fibrous stroma at the OSCC and bone interface evident in mandibular bone invasion, in addition to expression of RANKL in cells surrounding osteoclasts in OSCC bone sections. Moreover, they co-cultured human OSCC cell lines with murine osteoblasts, reporting an amplification of RANKL and RANK mRNA expression. However, the outcome from this study is inconclusive to some extent, as stromal activation markers were not examined, nor did they study the effect of human osteoblasts co-cultured with CAF.

Bone invasion in oral cancer may be associated with an elevation in both osteoblastic and osteoclastic activity. Totsuka et al. (1991) reported two patterns of bone invasion in OSCC. In the expansile pattern, the tumour invades with a broad pushing invasive front, surrounded by fibrous stromal tissue. Alternatively, the infiltrative pattern of bone invasion is recognised as strands and nests of extensive discohesive infiltrating tumour cells (Müller and Slootweg, 1990). Cases with intermixed patterns are referred to as showing a mixed pattern of infiltration (Jimi et al., 2013).

1.2 Bone physiology

1.2.1 Bone tissue

Osseous (bone) tissue is a rigid but dynamic structure. It has both organic and inorganic constituents. In order to maintain tissue integrity, homeostasis must be achieved; hence conserving cellular equilibrium and bone structure. Numerous cell types regulate bone deposition, resorption, and architectural integrity. The basic unit modulating this mechanism are osteoclasts, which actively resorb osseous tissue, while osteogenic or osteoblast lineage cells (bone lining cells, pre-osteoblasts, osteoblasts, and osteocytes) are responsible for structural preservation (Kular et. al, 2012; Nanci, 2017).

Osteoblasts are derived from mesenchymal stem cells and are the sole cells accountable for bone matrix deposition. Upon stimulation, osteoblasts have the ability to differentiate through four different stages, starting as preosteoblasts and gradually maturing from osteoblast finally presenting as bone lining cells. Mature osteoblasts are mononuclear cuboidal cells that mainly secrete type 1 collagen, osteocalcin, and alkaline phosphatase, jointly responsible for bone foundation. On maturation, osteoblasts become surrounded by their secreted matrix or osteoid, and are referred to as osteocytes (Clarke, 2008).

Osteocytes are terminally differentiated bone cells embedded within mineralised bone. These cells are connected to other cells in bone matrix and surface and form signalling networks through their processes (Prideaux et al., 2016). Osteocytes predominantly function as mechanical receptors, resulting in initiation of bone remodelling by modulating osteoblasts and osteoclasts, however when generating osteoclasts in culture, the presence of these cells are not necessary (Marino et al., 2014).

Osteoclasts are large multinucleated tartrate resistant acid phosphatase (TRAP) staining cells, derived from fusion of haematopoietic monocytes, in a process termed osteoclastogenesis. Several factors are required to regulate osteoclastogenesis. Macrophage colony-stimulating factor (M-CSF), receptor for activation of nuclear factor kappa B (NF-κB) ligand (RANKL) expressed both by osteoblasts and stromal cells, and its receptor RANK present on osteoclast cell membranes, are necessary to promote osteoclast formation (Kular et al., 2012). Binding of RANK ligand to its receptor activates a signalling cascade resulting in osteoclastic differentiation of progenitor bone cells. However, RANKL can actively be antagonised in the presence of osteoprotegerin (OPG), which acts as a decoy receptor competing with RANKL binding to RANK, consequently inhibiting osteoclastogenesis (Jimi et al., 2013; Nanci, 2017).

1.2.2 The dynamic mechanism of bone remodelling

Remodelling is a complex synchronised process involving the coordinated functioning of two main cell types; the osteoblast, responsible for bone matrix synthesis as well as remineralisation; and osteoclasts, the principal cells in bone mass regulation and resorption.

The remodelling cycle initially commences with osteoclast recruitment to the bone surface, allowing activation and conservation of demineralisation, and resorption of bone matrix through secretion of enzymes, acid phosphatase and cathepsin B (Nanci, 2017). Osteoclast stimulation is activated by RANKL binding to its designated receptor in the presence of parathyroid hormone related protein (PTHrP), interleukin-11 (IL11), sclerostin, and prostaglandin (PG2) (Theill et al., 2002; Boyle et al., 2003; Wada et al., 2006). Following RANK attachment to its ligand, osteoclasts further release fusion proteins Atp6v0d2 (an ATPase) (Lee et

al., 2006), FcRy (Fc receptor-related protein Y), and DC-STAMP (dendritic cell-specific transmembrane protein) (Kukita et al., 2004). Moreover, osteoclast proliferation is escalated by osteoblast secretion of M-CSF, further triggering RANK activity.

Following attachment of osteoclasts to the bone surface, lysosomes are released to the binding sites, actively disintegrating bone matrix (Sims and Gooi, 2008). Throughout bone demineralisation and resorption, osteoclasts may disseminate bone forming proteins and growth factors TGFβ (Centrella et al., 1991), BMP (Harris et al., 1994), and IGF (Schmid et al., 1992), which upon activation stimulates osteoblast recruitment; facilitating bone formation (Mohan and Baylink, 1991) (Figure 1.1).

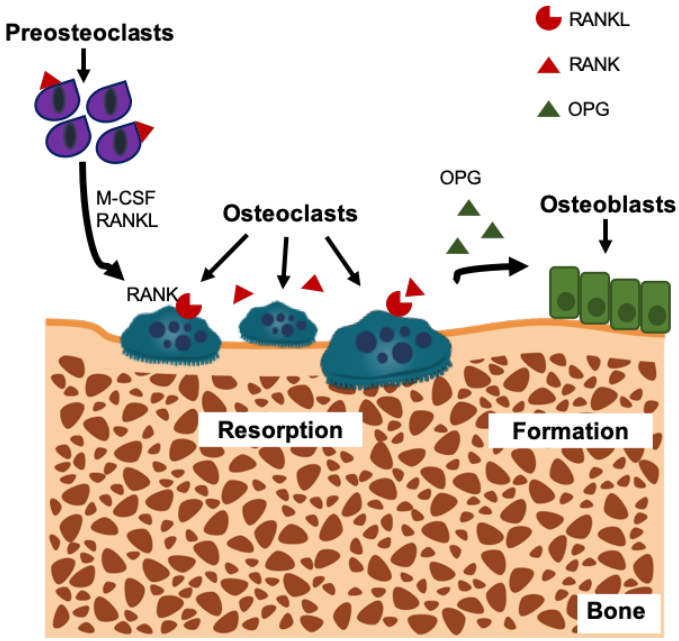

Figure 1.1: Bone remodelling. Bone remodelling is a continuous process that maintains the tissue integrity. In this mechanism, bone is resorbed by osteoclasts differentiated from haematopoietic cells in the presence of M-CSF and RANKL (preosteoclasts). OPG/OCIF released by osteoblasts blocks osteoclast generation and bone resorption, allowing osteoblasts to deposit new bone in resorptive areas.

A reverse interval of resorption follows, as the active osteoclastic bone degradation is halted, and osteoclasts undergo apoptosis, while osteoblast lineage cells proliferate and undergo differentiation. This stage is considered a transition from predominant osteoclast to osteoblast influence (Kular et al., 2012). Bone deposition proceeds primarily through osteoclast-osteoblast communication through ephrinB2 and its corresponding receptor EphB4 on osteoblasts, thus promoting osteoblast maturation (Zhao et al., 2006). However, this interaction could be impeded in the presence of PTH, hence depleting bone mineralisation due to an increase in unbound ephrinB2 (Allan et al., 2008). An equivalent pathway has been described which blocks both osteoblast and osteoclast differentiation in the presence of osteoclast inhibitory factor (OCIF) (Zhou et al., 2001).

In the termination stage, remodelling is halted as osteoblasts reverse differentiate into bone lining cells, and either remain on the bone surface or become entrapped in mineralised bone matrix as osteocytes. Sutherland et al. (2006), noted that osteocyte expression of sclerostin acts as a negative regulator of bone formation by diminishing osteoblast proliferation, decreasing matrix mineralisation, and promoting osteoblast apoptosis. It has recently been shown that neutralisation of sclerostin with a specific antibody elevates bone mass (McClung et al., 2014; Recker et al., 2015). Finally, following bone deposition fulfilment, osteoblasts migrate back to the bone surface, and matrix mineralisation progresses until a sufficient level is attained.

1.3 Cellular and molecular mechanisms in bone invasion by tumours

Previous literature has demonstrated the critical role osteoclasts play in bone invasion; however, the process by which neoplastic tumour cells and corresponding myofibroblastic stromal tissue destroys and penetrates osseous tissue still remains obscure. Quan et al. (2012) described three integrated stages in OSCC bone invasion.

Initially, tumour cells secrete proteolytic enzymes, proteases, disintegrating the extracellular matrix (ECM), and facilitating tumour cell infiltration. In addition, these enzymes trigger the differentiation of progenitor bone cells - osteoclast recruitment - further amplifying bone destruction. Collagen, elastin, and proteoglycans act as physical barriers in bone matrix. To enhance tumour migration and progression, tumour cell expression of zinc metalloenzymes, matrix metalloproteinases (MMP) has been shown to disrupt these barriers (Krane and Inada, 2008; Kessenbrock et al., 2010). A previous study co-cultured OSCC cells with osteoblasts and noticed amplification in MMP-2 expression by tumour cells, and increased MMP-9 expression in osteoblasts (Quan et. al, 2012). These findings are in agreement with similar research conducted earlier identifying the role of these proteolytic enzymes in OSCC invasion and distant metastasis (Krane and Inada, 2008).

Sinevici and O'Sullivan (2016) recently reviewed various oral cancer biomarkers and reported that the increase in MMP expression correlates with tumour behaviour and prognosis. Collagenase (MMP-1 and MMP-13), stromelysin (MMP-3, MMP-10, and MMP-11), and gelatinase (MMP-2 and MMP-9) have been shown to contribute to bone invasion. Primarily, gelatinase secretion disrupts

epithelial stability by triggering the destruction of the basement membrane and activation of growth factors TGF-β1, initiating EMT through SNAIL-regulated pathways. During EMT, keratinocytes exhibit morphological changes, and a loss in extra- and intracellular adhesions, featuring an increase in N-cadherin and a decline in E-cadherin adhesion molecules. *Ex vivo* expression of stromelysin (MMP-3) was detected in tumour boundaries of OSCC biopsies, further linking this biomarker to tumour progression, whereas MMP-10 and MMP-11 were associated with OSCC differentiation and direct invasion.

In the resorptive stage, bone deposition and destruction are regulated by tumour necrosis factor (TNF) related proteins, triad nuclear factor kappa B (NK-kB) activator receptor RANK binding to its ligand RANKL triggering osteoclastogenesis, or its decoy OPG promoting bone preservation. Preliminary studies have claimed to examine the role of stroma in bone invasive OSCC. In a previous study, RANKL positive fibroblasts were noticed surrounding tumour body in close proximity to bone, in addition to mRNA expression of RANKL in co-cultures of murine osteoblasts with a human OSCC cell line (Ishikuro et al., 2008). Unfortunately, this research did not investigate the role of human CAF in bone invasive OSCC.

Several cytokines have been noted to mediate bone destruction, of these interleukin-1β (IL1β) (Dewhirst et al., 1985; Cheng et al., 2014), IL6, IL11, and IL15 (Walsh et al., 2006; Brailo et al., 2012) being the most prevalent. Glenn (2004) noted that neoplastic lesions have the ability to react to growth stimulating cytokines, hindering tumour cell apoptosis and promoting invasion and metastasis. Another group reported IL6 and IL11 amplification in bone invasive OSCC as opposed to non-invasive OSCC (Shibahara et al., 2005). Furthermore,

significant amplification of IL6 on a protein and mRNA transcript level in human OSCC cell lines was reported to play a role in osteoclast generation (Tang et al., 2008; Hwang et al., 2012).

Bone is a rich reservoir of growth factors and upon OSCC induced destruction releases epidermal growth factor (EGF), connective tissue growth factor (CTGF) or transforming growth factor (TGF). These growth factors regulate osteoblasts and osteoclast recruitment in tumour progression and bone destruction (Matsuo and Irie, 2008; Quan et al., 2012). Huang et al. (2002) reported a decline in OSCC proliferation and invasion due to the obstruction of anti-EGF receptor (EGFR). The role of CTGF in neoplastic keratinocytes and osteoclasts of bone invasive OSCC was verified by the genesis of TRAP staining cells stimulated by recombinant (rh) CTGF *in vitro* (Shimo et al., 2008), further clarifying their previously published work (Shimo et al., 2004) on CTGF as a diagnostic biomarker in osteolytic conditions. However, more research is necessary to establish the significance of these growth factors in bone invasive OSCC.

1.4 Role of tumour microenvironment in cancer

Rudolph Virchow (1863) first suggested the importance of microenvironment in cancer progression. The study identified leukocytes surrounding solid tumour mass, and further hypothesised that cancer originated from chronic inflammation. However, this study focused on inflammation and didn't examine other components of the tumour microenvironment. Although when Paget (1889) suggested the 'seed and soil' phenomenon years later all the components were considered. Moreover, in 1982, Bissell et al. reported that tumour microenvironment (TME) was as crucial as genetic predisposition in the

development and progression of cancers. Understanding the TME is essential in establishing modern prognostic markers, and new generation therapeutics.

1.4.1 Components of tumour microenvironment

The TME in OSCC comprises diverse non-malignant cells integrated in a complex extracellular matrix (ECM). Collectively, these cells embedded in a matrix comprise the tumour stroma. The cross talk between neoplastic cells and surrounding stroma is constantly maintained, enabling tumour cell stimulation of the microenvironment, which as a result actively transmits paracrine signals increasing tumour cell proliferation and invasion (Figure 1.2).

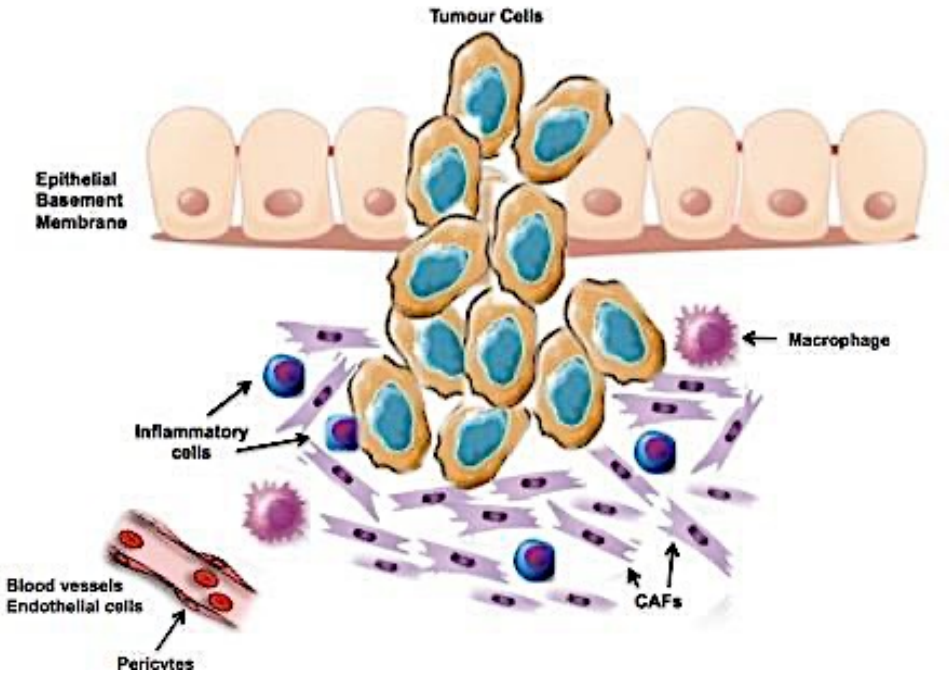

Figure 1.2: Tumour microenvironment. Tumorigenesis involves the co-existence of neoplastic cells, immune, stromal and endothelial cells embedded in an extracellular matrix. The tumour niche is a dynamic structure with access to various growth factors, and vascular supply. (Illustration generated using Photoshop software).

The main cellular components of the TME are fibroblasts, inflammatory cells, mesenchymal stem cells, pericytes, bone marrow derived cells, hematopoietic

and vascular endothelial cells, nerves and lipocytes (Joyce and Pollard, 2009). Weinberg (2013) estimated that these non-neoplastic cells could make up 90% of the tumour mass. Although these cells usually have a protective role in confining tumour progression, there is increasing evidence that the cells of the TME play an active role in tumour dissemination. Allen and Jones (2011) in a recent review, highlighted that tumour cells can initiate stromal activation through the expression of cytokines (growth factors and chemokines) and extracellular proteases, enhancing angiogenesis, and increasing malignancy progression.

1.4.1.1 Extracellular matrix

The cells of the TME are embedded in a complex mesh of proteins termed the extracellular matrix. The ECM is a network of proteoglycans, elastin, collagen, laminin and fibronectin that provide support for cells to adhere to (Boy, 2002). Stromal fibroblasts mainly synthesise and regulate this matrix. The ECM is a regulator of cellular morphology, by altering cell cytoskeleton, function and signalling (Kim et al., 2011). In addition, the mechanical properties of ECM have an impact on modulating tumour cell growth, differentiation and migration. A decline in ECM tensile strength has been reported to suppress malignant behaviour in breast cancer (Pazek et al., 2005). Lysyl oxidase (LOX), an enzyme secreted particularly by fibroblasts, has been shown to modulate tensile strength of the ECM by facilitating collagen and elastin cross-linkage, and elevating rigidity (Kagan and Li, 2003). This alters tumour behaviour, promoting invasiveness (Levental et al., 2009), and giving rise to the hypothesis and subsequent evidence that an increase in breast tissue densities, detected by mammography, is related to a higher risk of breast cancer (Martin and Boyd, 2008).

Significant modulation and remodelling of the ECM occur during tumour advancement, which can be regulated by different growth factors, such as PDGF, EGF, and TGFβ1 (Matrisian and Hogan, 1990), but is principally regulated by stromal fibroblast expression of proteases, particularly MMP (Kessenbrock et al., 2010). MMP degrade the ECM, contributing to tumourigenesis and metastasis through several pathways. Initially, MMP and other proteases trigger ECM degradation, facilitating a pathway for cellular dissemination and mobility, by releasing growth factors, PDGF, HB-EGF, and TGFβ1 (Joyce and Pollard, 2009). Moreover, proteases trigger proteolytic cleavage of dormant growth factors and MMP allowing their activation (Kessenbrock et al., 2010). Latent TGFβ1 is reportedly activated by MMP expression by stromal fibroblasts, stimulating EMT and tumour progression (Biere and Moses, 2006). However, MMP have also been reported to act as tumour obstructers rather than promoters (Gutierrez-Fernandez et al., 2008). By regulating angiogenesis, protease cleavage of plasminogen is reported to generate angiostatin, inhibiting angiogenesis, and suppressing tumour development (Houghton et al., 2006).

1.4.1.2 Angiogenesis and hypoxia

Angiogenesis is an essential factor for tumour genesis and survival (Carmeliet and Jain, 2000). Tumour and surrounding microenvironment express endothelial growth factors, mainly vascular endothelial growth factor (VEGF), which regulates neoangiogenesis (Carmeliet et al., 1996; Fukumura et al., 2001; Lin et at., 2017). Similarly, neoplastic tissue requires nutrient supply and waste removal more so than normal tissue (Papetti and Herman, 2002; Lin et at., 2017). During tumour development, due to the increase in proliferation of malignant cells, areas of hypoxia develop because of insufficient vascular supply. Although hypoxia is

sometimes considered a restraining factor for tumour development, several studies have shown otherwise (Zhu et al., 2017). Hypoxia-inducible family (HIF) proteins, expression in hypoxic tumour regions, have been noted to modulate cellular metabolism (Chen et al., 2010), proliferation, apoptosis (Carmeliet et al., 1998) and remodelling (Canning et al., 2001). In addition, Esteban et al. (2006), reported an up regulation of EMT, following a decline in epithelial E-cadherin expression.

1.4.1.3 Inflammation in tumour microenvironment

A state of inflammation increases the risk of malignancy. Colotta et al. (2009) reported that inflammation associated with cancers influenced genetic instability in cancer cells. The inflammatory milieu is composed of numerous immune cells, which secrete growth factors, cytokines, and proteolytic enzymes (TNF-alpha, TGFB, VEGF, Interleukins, MMP, cyclooxygenase 2 (COX-2), and CXC motif ligand 8 (CXCL8), further recruiting inflammatory cells, and altering the stromal phenotype (Murdoch et al., 2008). In particular, bone derived macrophages assemble in the TME through chemotactic signalling of VEGF, macrophage colony stimulating factor-1 (MCSF-1), and monocyte chemotactic protein-1 (MCP-1) (Bingle et al., 2002). This leads to an increased number of tumour-associated macrophages (TAM) (Hsu et al., 2010 and Ojalvo et al., 2010), which correlates with an unfavourable prognosis in a range of malignancies (Mantovani et al., 2017; Tan et al., 2016; Joyce and Pollard, 2009; Bingle et al., 2002).

TAM exhibit a characteristic phenotype and have been shown to express tumour-promoting factors VEGF (O'Sullivan et al., 1993), and EGF (Lewis et al., 2000), induce neoangiogenesis, while subsequently stimulating invasion and metastasis (Lewis and Pollard, 2006; Mantovani et al., 2006).

Briefly, macrophages can be classified according to their activity, as classically (M1) or alternatively activated (M2) (Kaneda et al., 2004). In conventional immunological reactions, M1 macrophages are recruited through T-helper cells (Th1), and cytokine, interferon gamma (IFN-γ) and lipopolysaccharide (LPS) in response to the presence of pathogens. M1 macrophages are characterised by highly expression of IL12, major histocompatibility class II (MHCII) and TNF-α. Contrastingly, during tissue wound occurrence, humoral, or in a pro-tumourigenic response, M2 differentiation is induced through Th2 cytokines IL4 and IL13, promoting angiogenesis by expressing amplified levels of IL10, and distinctive low levels of MHCII and IL12 (Mantovani et al., 2004; Mosser and Edwards, 2008; Joyce and Pollard, 2009; Laoui et al., 2011).

1.4.2 Fibroblasts

Decades ago, Tarin and Croft (1969), first reported fibroblasts as abundant cells located in mesenchymal connective tissue embedded in an extracellular matrix comprising fibronectin, and collagen type I. Fibroblasts, the predominant cells in the TME in most malignancies, contribute to tumour cell proliferation and spread, and are associated with ECM desmoplastic attachment, resulting in an increase in tensile strength or “stiffening” of the tissue (Cardone et al., 1997).

Several markers have been utilised to identify fibroblasts including vimentin, alpha smooth muscle actin (αSMA), fibroblast specific protein 1 (FSP1) and fibroblast activation protein (FAP). Unfortunately, due to the vast genetic diversity of fibroblasts, these markers are not considered as strong indicators, since no specific marker is exclusive for all fibroblast derivatives or subtypes (Kalluri and Zeisberg, 2006). However, αSMA is reliable and most commonly used (Shiga et al., 2015).

In addition, fibroblasts regulate matrix deposition, remodelling and progression, through expression of heterogeneous proteins, primarily collagen type I, III, IV and V (Hinz et al., 2007), fibronectin-1, and MMP (Kalluri and Zeisberg, 2006; Dewever er al., 2008; Kessenbrock et al., 2010).

1.4.3 Myofibroblasts

Cancer associated fibroblasts (CAF) share similar phenotypic characteristics to myofibroblasts found in granulation tissue during fibrosis, and wound contraction during healing (Gabbiani et al., 1994; Kalluri and Zeisberg, 2006; Hinz et al., 2007). Myofibroblasts are histologically defined as elongated spindled cells with elevated expression of alpha smooth muscle actin (αSMA) (Desmouliere et al., 2004; Hinz et al., 2007) and show increased secretion of MMP2, MMP3 and MMP9, enhanced proliferation (Rodemann and Muller, 1991), and amplification in cytokine and growth factor production (Bhowmick et al., 2004). However, it is important to note that pericytes, endothelial cells, myoepithelium, smooth muscle cells and myofibroblasts are also αSMA positive (Gabbiani et al., 1994; Desmouliere et al., 2004). Regardless, myofibroblasts are still referred to as αSMA positive cells, without conducting further characterisation assays based on location and morphology. Additionally, myofibroblasts comprise contractile microfilaments, which allow these cells to adhere to each other and the surrounding ECM (Hinz et al., 2007).

Myofibroblasts have been reported to differentiate from fibrocytes, pericytes, smooth muscle cells, mesenchymal cells and epithelial cells through EMT (Hinz et al., 2007; McAnulty et al., 2007; Mueller et al., 2007). Myofibroblastic differentiation can be triggered as a result of inflammation or neoplasia (Werner and Grose, 2003).

It has previously been shown that squamous carcinomas may directly enhance the myofibroblastic phenotype, through the expression of TGFβ (Lewis et al., 2004; Rønnov-Jessen and Bissell, 2009). In OSCC, myofibroblastic differentiation of normal oral fibroblasts (NOF) is induced through TGFβ dependent pathways, which has been shown to be amplified in the presence of IL1β (Lygoe et al., 2007; Anderberg and Pietras, 2009). Furthermore, carcinomas secrete chemotactic factors; platelet-derived growth factor A (PDGF-A), and fibroblast activation factor that are suggested to contribute to the accumulation of CAF in stroma (Tejada et al., 2006; Xouri and Christian, 2010). The close proximity and spatial arrangement of myofibroblasts in neovascularised areas, and tumour invasive fronts, implies the role of these fibroblasts in tumour invasion (Thode et al., 2011).

Santos et al. (2009), claimed that CAF may be a promising target in treating cancer due to their genetic stability, and phenotypic similarities of stromal fibroblasts across various cancers. Therefore, targeting stromal fibroblasts may hinder the progression of cancerous cells.

1.4.4 Myofibroblasts in oral cancer

Several previous studies on oral mucosa have reported that essential factors released by both keratinocytes and fibroblasts are paramount in epithelial differentiation and morphogenesis (Hill et al., 1984; Mackenzie and Dabelsteen, 1987). Costea et al. (2006) isolated premalignant human oral keratinocytes from dysplastic oral lesions and reported that *in vitro* invasion was only seen in the presence of fibroblasts. Their findings also showed that conditioned media from co-cultured fibroblasts and potentially malignant keratinocytes can yield this effect as spent media from mono-cultured fibroblasts was unable to produce this

outcome indicating a paracrine interrelation between tumour cells and associated fibroblasts. Interestingly, Gaggioli et al. (2007), reported a mechanical role of tumour associated fibroblasts in invasion. Co-cultures of squamous cell carcinoma keratinocytes and fibroblasts grown on collagen matrix showed fibroblast-led invasion, followed by tumour cells advancing in the ECM paths initially generated from cultured fibroblasts.

Two definite patterns of myofibroblasts associated with tumour stroma have been identified in published literature i.e. the 'spindle' and 'network' pattern. The former is characterised by spindle shaped morphology surrounding the tumour mass, to a maximum of three layers, while the latter is abundant throughout the whole depth of stroma (Kellermann et al., 2007; Vered et al., 2009).

Several recent studies have reported the correlation between αSMA positive myofibroblasts and cancer progression and invasion in TME (Rodrigues et al., 2015; Elmusrati et al., 2017; Smitha et al., 2019). Abundance of myofibroblasts have been associated with OSCC prognosis in various semi-quantitative histological studies (Kellermann et al., 2007; Vered et al., 2010). Kellermann et al., (2007) noted the correlation of αSMA positive myofibroblasts with tumour invasive front. Furthermore, Vered et al. (2010) reported that weak or negative αSMA expression in myofibroblasts was related with a significantly better disease free 5-year survival as opposed to OSCC patients with strong αSMA staining. The invasive front of OSCC, indicated by the band of tissue located between cancerous growth and normal tissue has been suggested to reflect tumour aggressiveness (Bryne et al. 1989; Bryne et al. 1991). This has led to the hypothesis of tumour-associated myofibroblasts being generated from neoplastic keratinocytes through EMT, following numerous studies involving

immunohistochemical analysis of antigen surface markers (Kellermann et al., 2007; Turley et al., 2008; Vered et al., 2010).

1.4.5 Origin of cancer associated fibroblasts

CAF configuration derives from heterogeneous aberrations presumably due to their diverse origin, but the process by which CAF arise still remain obscure (Kalluri and Zeisberg, 2006; Augsten 2014). Whilst the main source of CAF is commonly thought to be the activation of regional stromal fibroblasts (Kalluri and Zeisberg, 2006), alternative experimental models have demonstrated the lineage of CAF from genetically marked bone marrow originated cells (Direkze et al, 2006). Radisky and Radisky (2007), also suggested that normal or malignant epithelial cells undergoing EMT may be a source of myofibroblasts. However, it is still argued that CAF originate from transdifferentiation of fibrocytes, pericytes, smooth muscle, and mesenchymal stem cells.

1.4.6 Significance of CAF in tumour microenvironment

Barth et al. (2004), were amongst the first to report the presence of CAF in OSCC stroma, and later studies have further emphasised their significance. The presence of CAF in OSCC appears to be strongly correlated with tumour progression, invasion, recurrence, and poor patient outcome (Kawashiri et al., 2009; Vered et al., 2010). It has also been shown that activated fibroblasts are more sensitive and accurate predictors of OSCC recurrence and patient mortality compared to conventional parameters such as TNM staging (Marsh et al., 2011).

Most recently, Cirillo et al. (2016) conducted *in vitro* studies on OSCC by using CAF derived from genetically unstable OSCC cells (GU-OSCC), and genetically stable OSCC (GS-OSCC). The former was characterised by an abundant loss of heterozygosity, p16INK4a and TP53 genes, while the latter expressed wild type

p16INK4a and TP53 with minimum loss of heterozygosity. Their findings showed a correlation between increased expression of TGFβ1 & TGFβ2 in CAF from GU-OSCC, but not in CAF from GS-OSCC or normal fibroblasts suggesting that the sequential EMT and reduction in expression of cell adhesion molecules E-cadherin and vimentin results in epithelial dis-cohesion and invasion regulated through a TGFβ dependent signalling. Bhowmick et al. (2004) showed that mouse models with inactive TGFβ RII receptor inhibit tumour and surrounding stroma proliferation *in vivo*.

1.4.7 Senescence in fibroblasts

Hayflick (1965) reported that human extracted fibroblasts, despite being vital and metabolically functional, do not have the ability to proliferate indefinitely, and fail to propagate following considerable cell splitting. The irreversible state of growth arrest (at G1 phase) is termed senescence, unlike quiescence, which is characterised by amplification in p16INK4a (Prime et al., 2016). Senescent fibroblasts are also distinctive to myofibroblasts, as they express up-regulated levels of p16INK4a and p21.

Senescent CAF have been identified in tumour microenvironment (Hassona et al., 2013; Kabir et al., 2016), and premalignant lesions (Costea et al., 2013; Procopio et al., 2015). Several factors are responsible for fibroblasts undergoing senescence including exhaustive mitotic activity, permanent DNA damage induced as a result of oxidative stress from mitochondrial malfunction and uncontrolled cell division due to amplification of oncogene expression promoting genome replication (Di Micco et al., 2006), in addition to chemo and radiotherapy. Senescence can be induced *in vitro* by exposure to radiation, damaging DNA or

through treatment with hydrogen peroxide or anticancer therapeutic drugs such as cisplatin (Rodier and Campisi, 2011; Kabir et al., 2016).

In carcinomas, irreversible damage in cell recovery, or over exhausted DNA, results in senescence, which acts as an effective tumour suppressor. However, in contrast, senescence occurring in tumour-associated fibroblasts is a considered a key tumour promoter (Parkinson, 2010). Senescent fibroblasts express a vast range of pro-tumourigenic secretory proteins, which are jointly termed senescence associated secretory phenotype (SASP) (Kuilman and Peeper, 2009; Laberge et al., 2015). The SASP collectively comprises chemokines, inflammatory factors, osteopontin, growth factors (VEGF), proteases (MMP), extracellular proteins (collagen, laminin and fibronectin), reactive oxygen species (ROS), and interleukins (IL6 and IL8) (Coppe et al., 2008; Pazolli et al., 2009). Senescent cells promote tumours through enhancement of neoplastic proliferation, invasion, metastasis and therapeutic resistance (Prime et al., 2016; Kabir et al., 2016). During cancer therapy, cisplatin promotes apoptosis or induces senescence to suppress tumour growth (te Poele et al., 2002; Banito and Lowe, 2013).

Kabir et al. (2016) investigated the mechanism underlying SASP development in OSCC and reported that microRNA (miR-335) amplified in primary human CAF and experimentally induced senescent oral fibroblasts were able to regulate SASP expression and further promote OSCC cell migration following co-culture experiments. Moreover, on blocking miR-335 with celecoxib (an inhibitor of cyclo-oxygenase inhibitor 2, COX-2) the secretion of SASP factors decreased, reducing pro tumorigenic effects (Kabir et al., 2016).

Interestingly, several recent studies have shown the role of TGFβ as a regulator in tumour-senescence fibroblast crosstalk (Hassona et al., 2013; Hassona et al., 2014; Calon et al., 2014). In conjunction with reactive oxygen species (ROS), TGFβ induces fibroblast senescence and activation. Fibroblasts associated with genetically unstable OSCC (GU-OSSC) were noted to be senescent, due to the detection of amplified levels of ROS, TGFβ1, and TGFβ2, resulting in oxidative DNA damage (Hassona et al., 2013). Following senescence, CAF secrete increased levels of TGFβ and MMP2, which initiates EMT of neoplastic keratinocytes, leading to loss of cellular adhesion and promoting invasion (Prime et al., 2016).

The mechanisms of fibroblast activation and senescence have been suggested to be closely related. Hassona et al. (2013) claimed that these may be different phases of indistinguishable pathways. This was further verified as fibroblast senescence was demonstrated following TGFβ fibroblastic activation. Furthermore, both fibroblast phenotypes are SMA positive, and their tumour-promoting capabilities are mediated through similar pathways (Demehri et al., 2009; Alspach et al., 2014; Procopio et al., 2015).

1.5 Extracellular vesicles: cellular messengers in tumour microenvironment

Extracellular vesicles (EV) are microscopic plasma membrane-derived structures, made up of a lipid bilayer membrane and released extracellularly by a vast number of cells (Théry et al., 2002; Raposo and Stoorvogel, 2013; Andaloussi et al., 2013). Recently, EV have been gaining interest as a novel mode of cellular communication in biomedical research. EV are capable of

shuttling bioactive particles comprising nucleic acid as microRNA, mRNA, DNA, and proteins or lipids from one cell to another, leading to an interchange of genetic material and reprogramming of target cells. There is increasing evidence that EV expression is amplified in tumorigenesis, which has an impact on tumour progression, metastasis and chemotherapeutic drug resistance (Kahlert and Kalluri, 2013; Vader et al., 2014; Minciacchi et al., 2015; Becker et al., 2016). In addition, EV transfer their cargo from tumour cells to surrounding tumour microenvironment, disseminating growth factors and other mediators to altering extracellular milieu contributing to a more aggressive tumour pattern (Webber et al., 2010; Kahert and Kalluri, 2013; Becker et al., 2016).

1.5.1 Classification biogenesis, and contents of EV

Extracellular vesicle nomenclature has been conflicting and inconsistent over the past years. Based on their origin or biological role, the terms cardiosome (Waldenström et al., 2012), ectosome (Stein and Luzio, 1991), oncosome (Morello et al., 2013), argosome (Greco et al., 2001), and deteriosome (Yao et al., 1993) have been used. Currently, EV are widely classified in accordance to their mechanism of biogenesis to apoptotic bodies (1-5 μm) released by cells undergoing apoptosis, microvesicles/microparticles (100-1000 nm) formed by outward budding of the plasma membrane, and exosomes (30-100 nm) produced when multivesicular bodies fuse with the plasma membrane, releasing the intraluminal vesicles they carry out of the cell (Figure 1.3). However, these dimensions overlap making the separation of distinct subgroups challenging.

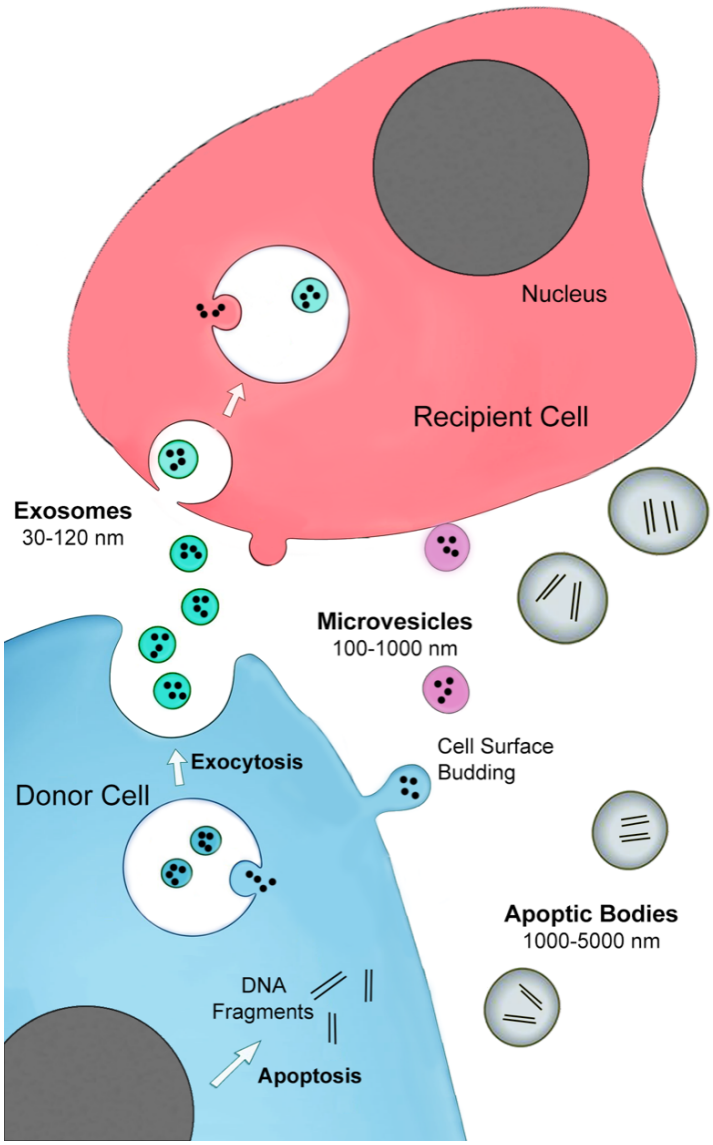

Figure 1.3: Biogenesis of extracellular vesicles. EV are widely classified in accordance to their mechanism of biogenesis to apoptotic bodies (1000-5000 nm) released by cells undergoing apoptosis, microvesicles (100-1000 nm) formed by outward budding of the plasma membrane, and exosomes (30-120 nm) produced when multivesicular bodies fuse with the plasma membrane, releasing the intraluminal vesicles they carry out of the cell. (Illustration generated using Photoshop software).

The exact mechanism behind the programmed sorting of cargo is still unclear. The endosomal sorting complex required for transport (ESCRT)-dependent and ESCRT independent messages have been proposed to control the sorting of EV

components (Trajkovic et al., 2008; Colombo et al., 2013). In addition, syndecan heparan sulfate proteoglycans has been reported to regulate EV biogenesis (Baietti et al., 2012; Kowal et al., 2014). EV secretion on the other hand, has been described to be regulated by Rab guanosine triphosphates (GTPases) (Hsu et al., 2010; Kowal et al., 2014), and by accumulation of calcium ions (Savina et al., 2003; Emmanouilidou et al., 2010). In cancer, the pH of the TME has been described to inversely modulate EV expression; at a low pH EV secretion from donor cell and uptake by recipient cell is amplified (Parolini et al., 2009). Furthermore, tumour suppressors and oncogenes have been reported to regulate EV secretion, influencing tumorigenesis and progression of cancer (Yu et al., 2005).

EV act as envelopes that shelter their cargo (RNA, DNA, proteins and lipids) from degradation in the ECM (Lässer et al., 2011). They interact with target cells via surface receptors, directly merge to cell membrane or are ingested by endocytosis, proceeding to the relocation of their contents to the recipient cell (Mulcahy et al., 2014). Various techniques for EV isolation have been described. Most commonly, ultracentrifugation solely or combined with size exclusion chromatography (SEC), and magnetic sorting or immune bead isolation have been used. Characterisation of the protein composition of tumour cell-derived EV has also been well defined using various proteomic methods. ExoCarta (www.exocarta.org) is a well-recognised tool, which identifies the most common miRNA, mRNA, and proteins found in EV.

1.5.2 Extracellular vesicles in bone

Bone is in continual dynamic equilibrium of resorption and deposition harmonised by a mineral metabolic process. Bone homeostasis involves several cell types comprising osteocytes, osteoblasts, osteoclasts and their precursors. Intercellular communication between these cells is mandatory to carry information from one cell to another, further regulating this process.

Primarily, bone forming cells or osteoblast derived EV play essential roles in intercellular communication in bone. Deng et al. (2015), reported that osteoblast EV expressed RANKL, and can promote RANK-RANKL interaction, initiating osteoclastogenesis. In addition, targeting osteoblast derived microvesicles can diminish bone loss (Deng et al., 2017). These results suggest that osteoblasts can initiate and activate osteoclast generation through secretion of EV without immediate cell to cell contact. Furthermore, Ge et al. (2015), revealed the proteomic analysis of osteoblast derived EV isolated from mouse MC3T3 osteoblasts, and reported the expression of an abundant amount of osteogenesis-related localised proteins, including eukaryotic initiation factor 2 (EIF2) signalling, which takes part in BMP induced osteoblast differentiation.

Secondarily, preosteoclasts and osteoclast derived EV play a key role in mineralisation metabolism in bone. Recently, Huynh et al. (2016) described that osteoclast EV express surface RANK, targeting osteoblasts through RANKL/RANK interaction, consequentially leading to RANKL expressing osteoblast EV promoting osteoclast generation in return. In addition, osteoclast EV expressing RANK, may impede osteoclastogenesis by binding to RANKL expressing osteoblast EV. Interestingly, Huynh et al. (2016) reported RANK in osteoclast derived EV but not in preosteoclasts. Preosteoclast EV can promote

osteoclast formation, and osteoclasts EV can block osteoclast generation, suggesting that preosteoclasts are functionally different and can be responsible for stabilisation of bone mineralisation.

Sato et al. (2017) found that osteocyte derived EV may transfer miRNA to the target cell via blood circulation, suggesting how osteocytes might be regulated regionally and systemically. Most recently, Qin et al. (2017) showed that osteocyte EV contained miRNA-218 inhibited sclerostin and promoted the differentiation of osteoblasts. Sclerostin and RANKL are the main molecules expressed by osteocytes, but unfortunately there is no evidence that they are found in osteocyte derived EV.

1.5.3 Roles of extracellular vesicles in cancer and microenvironment

Increasing evidence shows that EV play important roles in cancer. EV transport oncogenic nucleic acids and proteins to recipient cells, playing vital roles in tumour growth, progression, metastasis and therapeutic resistance. EV derived from malignant cells are capable of inducing dysplastic transformation in normal cells. Abd Elmageed et al. (2014), found that adipose-derived stem cells had a potential oncogenic transformation when exposed to EV isolated from prostate cancer. Similar results have also been reported in breast cancer, where miRNA containing EV silenced mRNA in non-neoplastic cells, resulting in transcriptome reprogramming and malignant transformation (Melo et al., 2014).

Tumours are composed of a heterogeneous population of neoplastic and non-neoplastic cells such as mesenchymal, immune cells and acellular ECM. Recently, tumour complexity has been further highlighted by the emergence of EV in tumour microenvironment. Cancer cell EV have the potential to

communicate with the surrounding host stroma, stimulating or restricting tumour progression.

Cancer derived EV have a significant impact on the tumour microenvironment by encouraging tumour angiogenesis, immune cell infiltration, and activation of resting fibroblasts to CAF, advancing tumour progression. Webber et al. (2010), reported that prostate cancer EV expressed TGFβ, and actively triggered myofibroblastic differentiation of normal fibroblast in tumour microenvironment, which promoted tumour growth. These results are in further agreement with Gu et al. (2012), where gastric cancer EV stimulated the differentiation of mesenchymal cells to CAF. Moreover, these findings were also observed in breast cancer (Cho et al., 2012). Interestingly, CAF communication with cancer cells favours tumour progression, affecting radiation and chemotherapy resistance. Boelens et al. (2014) demonstrated that EV expressed by CAF communicated with breast neoplastic cells initiating the NOTCH3 pathway to increase therapy resistance. Stromal derived EV have also been suggested to promote invasion and metastasis in breast cancer through Wnt-planar cell polarity signalling (Luga et al., 2012). Hence, EV communication between cancer and surrounding stromal fibroblasts adds another dimension to the complexity of TME, and synergistically mediates tumour growth and progression.

1.5.4 EV and cancer biomarkers and potential therapeutics

EV have been isolated from numerous biological fluids, including saliva, blood, tears, bile, urine, cerebrospinal fluid and breast milk. (Lässer et al., 2011; Raposo and Stoorvogel, 2013; De Toro et al., 2015). Cancer derived EV have been reported to be systemically elevated in circulation and may serve as a potential liquid biopsy for diagnostic and prognostic indicators in various malignancies (Nilsson et al., 2009; Corcoran et al., 2011; Melo et al., 2015). Therefore, it is conceivable that EV transmission in malignancy could be a potential target to enhance and monitor therapy response. Pitt et al. (2014) established immunotherapeutic anticancer agents using dendritic cell EV (dexosomes), which have gone through clinical trials for melanoma, lung and colorectal malignancy (Tan et al., 2010).

A novel strategy for treatment of advanced malignancies, is by the depletion of EV (Marleau et al., 2012). Amiloride, a drug used to treat hypertension, has been reported to halt EV biogenesis and limit colorectal cancer progression (Chalmin et al., 2010). However, advanced investigations are needed to assess the clinical safety of EV elimination.

Due to their various genomic contents along with their extensive distribution and biocompatibility, the utilisation of EV as diagnostic biomarkers and therapeutics delivering anticancer drugs has been gaining attention (Van den Boorn et al., 2010; Hu et al., 2012; Pascucci et al., 2014). Improving the current strategies to isolate a substantial amount of EV from donor cells, introduction of nanotechnologies to pack EV with targeted therapies, will enable the use of EV as natural cargo for anti-cancer drugs.

1.6 Bone Invasion in OSCC

Oral cancer involving the lateral tongue, alveolar ridge and floor of mouth, due to its anatomical proximity, frequently invades the maxilla or mandible, significantly worsening patient outcomes. A few studies have demonstrated the function of osteoclasts in bone invasive OSCC but it still remains speculative whether this is an osteoclastic or tumour/associated microenvironment driven mechanism.

1.6.1 Cytokines

OSCC secrete cytokines that have been reported to contribute to the process of osteoclastogenesis. Bone tissue is considered a reservoir for numerous cytokines and growth factors. This allows cell proliferation by maintaining malignant cellular division, inhibition of apoptosis, leading to progression of tumour growth and invasion of adjacent osseous tissue. Earlier research has claimed that osteoclast led bone destruction is the main element in tumour progression, invasion and metastasis.

Many factors are involved in tumourigenesis and progression. Interleukin-6 (IL6) has been shown to significantly intensify ECM degradation by prompting MMP expression stimulating bone resorption by enhancing ostoclastogenesis and hindering osteocyte and osteoblastic activation (Li et al., 2010). O'Brien et al. (1999) demonstrated how osteoblasts expressing RANKL can induce osteoclastic bone resorption via IL6. In addition, it has been suggested that osteoclasts and not tumour cells predominate in the process of bone invasion in mandibular resections of OSCC patients (Shibahara et al., 2005). The findings from this study revealed IL6, PTHrP and TNF-α expression in osteoclasts as well as tumour keratinocytes and associated tumour fibrous stroma in both bone

invasive and non-invasive groups. This study concluded that osteoclasts play an important role in OSCC bone invasion.

Furthermore, Kayamori et al. (2010), validated the expression of PTHrP and IL6 by conducting immunohistochemistry (IHC) on OSCC patient tissue samples. They noticed expression of PTHrP in neoplastic cells in comparison to IL6. However, similar IL6 expression was noted in both cancer and stromal cells. They further examined RANKL relevance by treating fibroblastic stromal cell lines with conditioned media collected from cultured OSCC cells and showed a relation between RANKL dependent osteoclast led bone destruction, and up regulation of IL6 and PTHrP. Recently, another study group showed both *in vitro* and *in situ*, that IL6 expression is more pronounced in stromal CAF than in tumour cells (Nagasaki et al., 2013). This evidence further validates the significant role of CAF, in addition to cancer cells, in bone invasive OSCC.

1.6.2 Role of TGFβ dependent pathways in cancer progression

Osseous tissue, precisely the bone matrix, is a reservoir of TGFβ. Pfeilschifter and Mundy (1987) showed presence of TGFβ in bone microenvironment, following osteoclast mediated bone destruction. In tumourigenesis and progression, TGFβ has a fundamental role in modulating cancer cell proliferation, differentiation and metastasis (Pickup et al., 2013). Throughout the preliminary course of tumour development, TGFβ exhibits tumour suppressive activity through growth inhibition, activation of cellular apoptosis (Massagué et al., 2000; Siegel and Massagué, 2003), and proteases inhibition (Ito et al., 2004). However, during advanced stages, this anti-tumourigenic effect subsides, and is replaced by a more aggressive EMT cancer progressive phase, through the stimulation of TGFβ expression, ligand activation for tumour growth promotion and pro-

oncogenic functionality including neoangiogenesis and invasion (Pickup et al., 2013).

The recognised TGFβ signalling pathway is involved in a broad superfamily, comprising bone morphogenic proteins (BMP), activins, and growth and differentiation factors (GDF) which are principal elements in differentiation, development, and cellular and humoral homeostasis (Weiss and Attisano, 2013). TGFβ1, β2, and β3 are the three main TGFβ ligands, which are encoded by distinct genes, but are activated through similar receptor signalling pathways (Massagué, 1998). Amongst these, TGFβ1 has been the focus in most tumourigenesis studies.

The release of TGFβ as a latent protein necessitates the presence of regulatory activation mechanisms, including metalloprotease cleavage by MMP9 and MMP2 (Yu and Stamenkovic, 2000), ECM protein thrombospodin (Schultz-Cherry and Murphy-Ullrich, 1993; Crawford et al., 1998), αvβ6 surface integrin (Munger et al., 1999), or by myofibroblastic contraction (Wipff et al., 2007). In carcinogenesis, TGFβ signalling process is mediated through two types of heteromeric cell surface transmembrane serine-threonine kinase receptors TGFβ receptor type I (TGFβ RI), and receptor type II (TGFβ RII). Following TGFβ1 ligand binding to the receptor II complex, TGFβ RII initiates and mediates phosphorylation of TGFβ RI, which sequentially phosphorylates Smad2 and Smad3 and co-joins Smad4, facilitating nuclear translocation and transcription regulation (Derynck and Feng, 1997; Piek et al., 1999; Itoh et al., 2000; Massagué et al., 2000; Derynck et al., 2001)

During the process of EMT, cell surface adhesion molecule transition occurs; this phenomenon is widely known as “cadherin switching”. In this transition epithelial surface antigen E-cadherin expression is replaced with N-cadherin, a mesenchymal marker, followed by an acquired tumour cellular expression of αSMA and vimentin cytoskeletal proteins (Wan et al., 2013) (Figure 1.4).

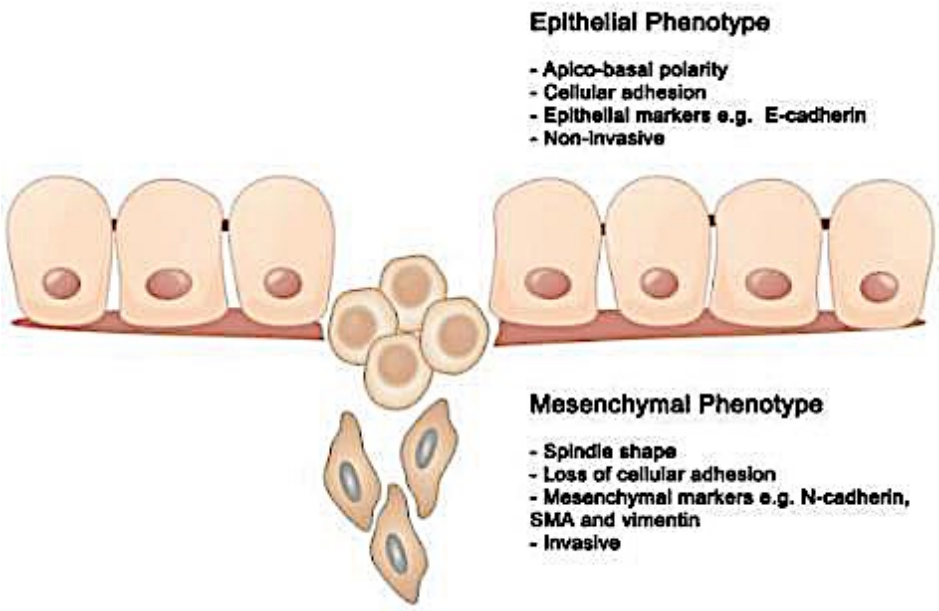

Figure 1.4: Epithelial-mesenchymal transdifferentiation. On cancer progression, several cytokines, and growth factors stimulate keratinocytes to differentiate to a mesenchymal phenotype. Promoting loss of cell adhesion, alteration in morphology and invasion. (Illustration generated using Photoshop software).

A considerable number of studies have shown the key role of TGFβ in modulating EMT, and consequential OSCC bone involvement (Quan et al., 2012; Quan et al., 2013; Hwang et al., 2014). A previous study reported morphological changes of neoplastic keratinocytes on transfection of V69 (a murine OSCC cell line) with TGFβ. This transformation was noted as changing from angular to an extended

spindle shape. *In vivo* transplantation of these cells into the floor of the mouth of murine models resulted in highly aggressive tumours (Davies et al., 2000). An *in vitro* study involved transfection of three alternative human head and neck cancer cell lines (SCC25, HN5 and TCA8113) with TGFβ1. In contrast to Davis et al. (2000), following the predetermined time span of three days, the TGFβ dependent amplification of MMP2 and MMP9 was noted to promote bone invasion through EMT initiation and sustaining osteoclast activity. Despite these findings, no morphological changes were detected in these studies (Qiao et al., 2010; Quan et al., 2013).

These opposing findings raise the possibility that morphological transformation may not be a prerequisite to obtain EMT features. The precise role of TGFβ on osteoclast activity and regulation, therefore, remains to be determined.

TGFβ has been reported to play a pro-tumourigenic role by inducing transdifferentiation of stromal fibroblasts to more stimulated/aggressive αSMA expressing myofibroblasts (Pickup et al., 2013). Treatment of normal human gingival fibroblasts (NOF) with TGFβ (0.5 to 10ng/ml) leads to αSMA surface antigen expression evident through immunofluorescence (Lewis et al., 2004). Moreover, when OSCC cell lines CA1, VB6 and 5PT were co-cultured with these fibroblasts, a significant up regulation in TGFβ protein expression was detected through an ELISA. This data demonstrates the important interaction between CAF and TGFβ in cancer progression.

1.6.3 RANK, RANK ligand and OPG mechanisms.

As mentioned earlier, the vital factors accountable for bone sustainability and structure are RANK, RANKL and its antagonist OPG. Alterations in functional equilibrium of these cytokines will either result in osteogenesis (higher OPG

expression) or osteolysis (higher RANKL levels). RANK/RANKL signalling cascade facilitates differentiation of bone lining cells, osteocytes and osteoblasts to osteoclasts, along with macrophage colony-stimulating factor (M-CSF) while OPG suppresses these signals.

OPG acts as a signal for osseous tissue deposition and preservation, alongside its bone resorption obstruction functionality (Simonet et al., 1997). OPG belongs to the TNK receptor family; it is an actively secreted protein, due to absence of a transmembrane element. Experimental studies conducted on murine specimens *in vivo* have shown that OPG administration can arrest tumour growth; prevent bone invasion and distant spread of prostate cancer (Armstrong et al., 2008). These findings reinforce the role of RANK/RANKL in promoting OSCC bone involvement. OSCC cells are known to secrete RANKL. Chuang et al. (2009) claimed that there was no significant difference in RANKL expression between bone invasive and non-bone invasive OSCC suggesting that oral cancer cells may have the capacity to stimulate osteoclastogenesis when in proximity to adjacent bone. However, on reviewing this study, noticeable limitations are noted as in some of the images the IHC staining does not appear to be specific. OPG expression was reported as absent in bone invasive lesions, however this expression was also negative in osteoblasts on bone surface, further making the data somewhat questionable. In addition, the tumour-bone proximity of the tested cohort was not acknowledged.

It is still uncertain whether all OSCC cells express RANKL or can induce osteoclastogenesis on their own. Tada et al. (2005) co-cultured aggressive human OSCC (BHY) cell lines derived from the lower alveolus with murine bone marrow cells (BMC). *In vitro* osteoclastic differentiation was weak, although

RANKL surface antigen was detected in BHY cells following flow cytometry. Following co-culture of BHY cancer cells with primary bone cells and BMC, significant numbers of osteoclasts were generated (TRAP stained and counted under light microscope). On administration of OPG, this process was significantly, but not absolutely inhibited. Inconsistent findings were reported for head and neck squamous cell carcinoma HSC-2 cell line. Osteoclastogenesis was profound when co-cultured with BMC murine marrow cells, however, these cells lacked RANKL expression. This highlights the importance of phenotypic characterisation in cancers and the diverse mechanisms involved in the complex milieu of OSCC bone invasion. In the former study, the expression of RANKL and failure of osteoclastogenesis suggested that the TME ceased to induce RANKL activation, while in the second study RANKL expression was suggested to be non-essential for bone resorption to occur. Furthermore, IHC analysis of bone invasive OSCC revealed lower OPG expression in fibrous stromal cells compared to normal mucosa. This raises the possibility that a decline in OSCC OPG expression in the presence of osteoblasts, rather than an amplified RANKL expression, may be more important in induction of osteoclastogenesis.

OSCC regulation of osteoclastic differentiation has also been investigated. Osteoclasts have relatively brief life spans and are subjected to prompt cellular apoptotic death in the absence of RANKL, IL6 and M-CSF. Prolonged osteoclast survival has been shown to be related to suppression of Bcl-2 pro apoptotic protein (Bim) in BHY cancer cells. These OSCC cells have also been demonstrated to induce osteoclastic pit-formation (Tada et al., 2009). Another research group injected human OSCC cells (B88) into nude mice and following tumour formation OPG treatment was administered. Obvious reductions in

tumour growth and osteoclast count were noticed, in addition to increased OSCC cell apoptosis. However, the *in vitro* approach showed no change in proliferation, suggesting that tumour and bone microenvironment plays an important role in OPG functionality (Shin et al., 2011).

1.6.4 "Vicious cycle" a cascade regulating bone integrity

The cascade involved in OSCC bone invasion, is considered a "vicious cycle" (Figure 1.5).

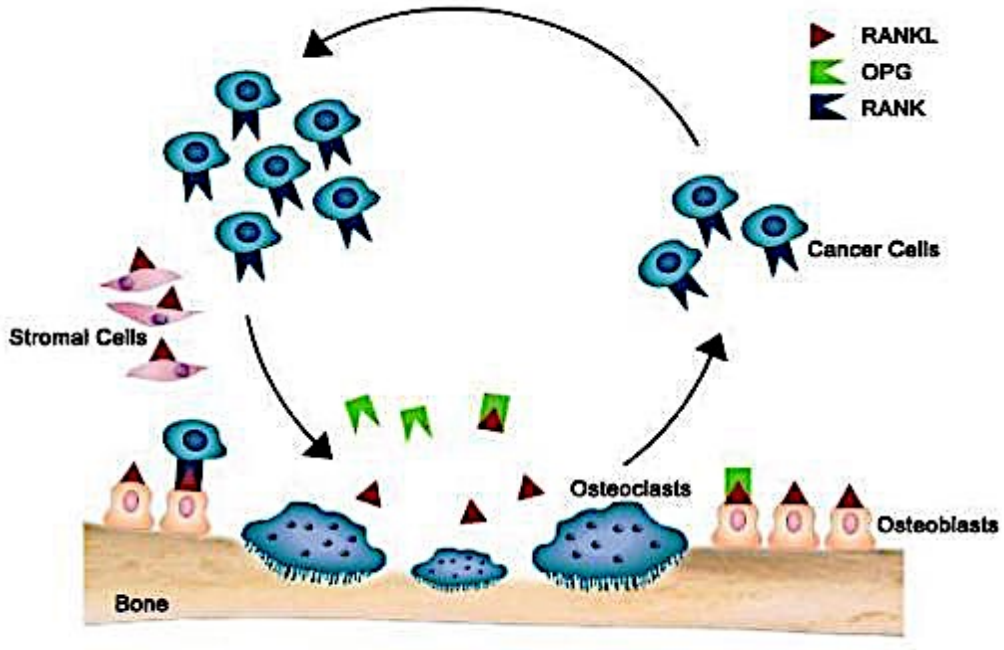

Figure 1.5: Vicious cycle of bone invasion. Bone integrity is maintained through TNF triad proteins. On binding of RANKL to its receptor RANK, osteoclastogenesis is initiated. However, if RANKL binds to its antagonist and decoy receptor OPG osteoclast generation is reduced, decreasing bone destruction. (Illustration generated using Photoshop software).

The cross talk between tumour and bone through intervening fibrous stroma or by direct contact regulates the dynamic advancement of bone destruction. Neoplastic keratinocytes secrete humoral factors. Amongst these growth factors, cytokines and hormones as PTHrP, which promotes osteoclast differentiation

through assembly of RANKL expressed osteoblasts and fibrous stromal cells (Chikatsu et al., 2000).

Both CAF and cancerous tumour cells have been shown to express RANKL (Mao et al., 2013) through the joining of the ligand to its receptor RANK located on progenitor bone cells, leading to induction of osteoclastogenesis. Consequently, the generated osteoclasts resorb osseous tissue. During this process growth factors IGF, TGFβ, and BMP are disseminated into the microenvironment, promoting further progression of cancer growth. This “vicious cycle” facilitates tumour cell proliferation promoting advanced bone invasion.

1.7 Adjuvant therapeutic implications in cancer

Cancer associated fibroblasts have been suggested to be good therapeutic targets due to their genetic stability and non-proliferative characteristics (Johansson et al., 2012; Kinugasa et al., 2014). In reference to OSCC, multiple studies support the evidence that CAF secreted hepatocyte growth factor (HGF) disrupts EGF expression (Wang et al., 2009; Yamada et al., 2010) conferring resistance to an antagonistic EGFR antibody; cetuximab, via CAF induced MMP (Johansson et al., 2012). However, normal resting oral fibroblasts were not included in this study which would have been useful for comparison with CAF.

1.7.1 Senotherapeutics

Senescent cells accumulate with ageing, as well as in pathologies of chronic disease. *In vitro* studies on these ageing cells have shown to impede or prevent age related diseases including osteoporosis, pulmonary fibrosis, cardiovascular disease, diabetes, and cancer (Zhu et al., 2014; Roos et al., 2016). Zhu et al. (2015) first identified senotherapeutics through the contradicting fact that senescent cells despite expressing SASP factors that should trigger cell death,

are resistant to apoptosis. In addition, proapoptotic pathways are amplified in senescence, yet these cells withstand apoptosis (Wang et al., 1995). Therefore, senescent cells depend on their pro-survival mechanisms to protect themselves from the pro-apoptotic SASP expression. Following this hypothesis, and thorough RNA bioinformatics evaluation, senescent cell anti apoptotic pathways (SCAP) were proposed (Table 1.1). Through this approach the survival proteins were described and targeting of these proteins led to selective apoptosis of senescent cells while sparing proliferative non senescent cells.

Table 1.1: Senolytic drugs and SCAP (Adapted from James et al., 2017)

SCAP	Senolytic agent	Effective In vivo
BCL-2, BCL-X_L family	Navitoclax (ABT263) Fisetin A1331852 A1155463	Yes
P13Kδ, AKT, ROS-protective	Quercetin Fisetin Piperlongumine	Yes
MDM2, P53, P21, Serpine (PAI-1&2)	Quercetin Fisetin FOX04-related peptide Dastinib (FOXO-p53 interaction)	Yes Yes
Ephrins	Dastinib (ephirin receptors) Piperlongumine	Yes
HIF-1α	Quercetin Fisetin	Yes
HSP-90	17-AAG (tanespimycin) Geldanamycin 17-DMAG (alvespimycin)	 Yes

The first senolytic drug adapted using this hypothesis were quercetin and dasatinib (Zhu et al., 2015), followed by a B-cell lymphoma 2 (BCL-2) family inhibitor navitoclax (Chang et al., 2016; Zhu et al., 2016). More recently the use of heat shock protein (HSP-90) has also been reported (Fuhrmann-Stroissnigg et al., 2017).

Targeting a single pro-apoptotic pathway cannot eliminate senescence in all cell types. However, combination of different senotherapeutics can have synergistic properties, increasing the range of senescent cells that can be eliminated (Zhu et al., 2015).

In age related bone loss, Farr et al. (2017) recently eliminated senescent cells in bone by stimulating apoptosis through targeted activation of caspase (INK-ATTC transgene), and administration of pharmacological senotherapeutic agents in mouse models. They further reported that on exposure to senescent cell conditioned media, osteoclast survival was significantly enhanced. Collectively, this data can be further used to understand the role of senescence in cancer related bone invasion, with potential therapeutic application to limit tumour spread and recurrence in bone following radio and chemotherapy.

1.8 Summary

The majority of head and neck cancers are diagnosed as OSCC. Although it is not one of the most common cancers, in the United Kingdom, more than 11,900 new cases of head and neck cancers were reported in 2016, with an increase in incidence of over 33% for new patients diagnosed with oral cancer in the last decade, and over 4000 oral cancer-related deaths reported annually (Cancer Research UK, 2019).

Bone invasion is a common feature of OSCC and is associated with a poor prognosis. A number of previous studies have attempted to explore the mechanism of OSCC associated bone invasion, however, the exact molecular mechanism in which OSCC invades bone still remains unclear. There is increasing evidence that the tumour microenvironment, predominantly composed of CAF, play a key role in tumour progression, but the role of CAF in bone invasion remains to be elucidated.

1.9 Project hypothesis, aims and objectives

1.9.1 Hypothesis

Cancer associated fibroblasts (CAF) play a functional role in OSCC bone invasion through a RANKL dependent pathway.

1.9.2 Aims

The aim of this study is to investigate whether CAF play a role in bone invasion and to identify underlying mechanisms of interactions between CAF and bone cells.

1. Investigate the role of fibroblasts in bone remodelling.
2. Examine the contribution to different subsets of CAF.
3. Understand the mechanism by which different subsets of CAF influence bone invasion in OSCC.
4. Assess the possibility of targeting CAF pharmacologically as an intervention for bone invasive OSCC.

1.9.3 Objectives

1. To investigate the abundance and role of myofibroblastic CAF in bone invasion and remodelling in OSCC.
2. To examine the different subsets of CAF, in particular those with a senescent phenotype, in the tumour microenvironment of bone invasive OSCC.
3. To examine whether EV influence bone invasion in oral cancer.

Data from this project will present novel information concerning the role of CAF tumour microenvironment in bone invasive OSCC.

Chapter 2

Materials and Methods

2.1 Clinicopathological analysis of OSCC bone resections

The local pathology database was used to identify OSCC cases with bone removal. OSCC bone resections diagnosed from 1994 to 2017 (407 cases) were identified from the Unit of Oral and Maxillofacial Pathology, School of Clinical Dentistry, University of Sheffield archive and the following information retrieved from pathology reports:

- Site (maxilla or mandible)
- Age
- Gender
- Grade of tumour differentiation (well, moderate, and poor)
- Bone invasion (Superficial cortical resorption or deep cancellous invasion)
- Regional metastasis

2.2 Immunohistochemical (IHC) analysis of OSCC incisional biopsies away from bone

10 OSCC cases that had undergone initial diagnostic incisional biopsies (1996 to 2016) were selected from the archive detailed in section 2.1.

Immunohistochemical staining was performed on 4 μm tissue sections to study *ex vivo* expression of a marker of myofibroblastic differentiation (αSMA), bone turnover markers (OPG and RANKL), and senescence markers dipeptidyl

peptidase-4 (DPP4/CD26) and p16INK4a (ethical approval ref.# 07/H1309/150).

Numerous pilot assays were carried out to optimise primary antibody dilutions to detect specific expression and reduce non-specific background staining, including determining the optimal antibody concentration, incubation time, blocking method and antigen retrieval technique (Table 2.1).

Table 2.1: Details of primary antibodies used for IHC.

Primary antibody	Dilution	Description	Details
αSMA	1:100	Mouse anti-human monoclonal antibody	Catalogue number A5228, Sigma Aldrich
RANKL	1:50	Rabbit anti-human polyclonal antibody	Catalogue number ab9957, Abcam
OPG	1:100	Rabbit anti-human polyclonal antibody	Catalogue number ab73400, Abcam
DPP4 (CD26)	1:100	Rabbit anti-human monoclonal antibody	Catalogue number 40134, Cell Signalling
p16INK4a	1:100	Rabbit anti-human monoclonal antibody	Catalogue number ab108349, Abcam

2.2.1 IHC procedure

OSCC formalin fixed paraffin embedded (FFPE) tissue sections were submerged in 100% xylene for 10 min at room temperature (RT) to deparaffinise the tissue samples. Sections were dehydrated by immersion in absolute alcohol for a further 10 min. Incubation in 3% (v/v) hydrogen peroxide in methanol (100%) for 20 min was used to block endogenous peroxidase at RT, followed by a wash in PBS,

ready for antigen retrieval (Table 2.2). Heat-induced epitope retrieval (HIER) was performed by microwaving sections in 0.01 M tri-sodium citrate buffer (pH 6) for 8 min on high power (Table 2.2). Slides were briefly allowed to cool, prior to blocking in serum corresponding to the species in which the primary antibodies were raised (100% horse serum for mouse (αSMA) antibody, and goat serum for rabbit (RANKL, OPG, DPP4/CD26 & p16INK4a antibody), at RT. After 30 min, the blocking serum was removed and 200 µl of primary antibody diluted in appropriate 100% serum was applied in a humidified chamber overnight at 4°C (Table 2.1). Exclusion of primary antibody served as a negative control.

On the subsequent day, sections were washed twice in PBS for 5 min at RT to remove unbound antibody. VECTASTAIN ELITE ABC Kits (Vector Laboratories) were utilised in accordance with the manufacturer's specifications (Table 2.3).

Table 2.2: IHC solutions and reagents.

Chemical reagents	Formulation
3% (v/v) Hydrogen Peroxide	70 ml Hydrogen Peroxide (H_2O_2) 230 ml Absolute Methanol
0.01 M Sodium Citrate Buffer	11.8 g/ml Sodium Citrate Tribasic
Phosphate Buffer Saline (PBS)	425 g/ml Sodium Chloride 58 g/ml Sodium Phosphate Dibasic 12.5 g/ml Potassium Phosphate 5 L Distilled Water
Secondary Biotinylated Antibody	Biotinylated Antibody Stock (1 drop) Blocking Serum (3 drops) 10 mL PBS
VECTASTAIN ELITE ABC	Reagent A (2 drops) Reagent B (2 drops) 5 ml PBS
Vector Nova Red Peroxidase	Reagent 1 (1 drop) Reagent 2 and 3 (2drops) H_2O_2 (2 drops) 5 ml distilled water
DAB Substrate Kit	Buffer stock solution (2 drops) DAB stock solution (4 drops) Hydrogen peroxide solution (2 drops) 5 ml distilled water

Table 2.3: Details of secondary antibodies used for IHC.

Secondary antibody	VECTASTAIN ELITE ABC Kit
Anti-human αSMA monoclonal antibody	Horse anti-Mouse IgG Catalogue number PK-6102
Anti-human RANKL polyclonal antibody	Goat anti-Rabbit IgG Catalogue number PK-6101
Anti-human OPG polyclonal antibody	Goat anti-Rabbit IgG Catalogue number PK-6101
Anti-human DPP4 polyclonal antibody	Goat anti-Rabbit IgG Catalogue number PK-6101
Anti-human p16INK4a polyclonal antibody	Goat anti-Rabbit IgG Catalogue number PK-6101

The secondary biotinylated antibody was applied to all sections, 1 drop diluted in 10 ml PBS, and incubated for 30 min at RT. The ABC solution was prepared at the same time and left to stand for 30 min prior to application (Table 2.2). After 30 min, the slides were washed in PBS and ABC solution was applied for a further 30 min, followed by two more washes in PBS.

Colour development was performed using the Nova RedTM Peroxidase Substrate Kit (Vector Laboratories) for the antibodies detecting αSMA, RANKL, and OPG and the reaction was stopped after 5 min by immersing slides in distilled water (Table 2.2). DAB Substrate Kit (Vector Laboratories), a chromogenic substrate that oxidises in the presence of peroxidase resulting in a brown colour, was used for DPP4 and p16INK4a. Slides were incubated with DAB for 6 min, then washed in distilled water for 5 min to stop the colour development. Finally, the sections were counterstained using haematoxylin (Thermo Electron, UK),

dehydrated in increasing concentrations of alcohol (90% then 100% respectively), and immersed in xylene (100%) using a Shandon linear staining appliance. Glass coverslips were used to seal the sections using a distyrene plasticizer xylene (DPX) mountant.

2.2.2 IHC evaluation

The stained slides were scanned using a high definition scanner TissueFAXS Slide Loader 120 Histo (Wien, Austria), and HistoQuest analysis software (Tissue Gnostics Imaging Solution, Austria) was utilised for IHC quantification. Three random regions of interest (ROI) per slide were selected covering an area of 0.5 mm^2 in tumour and stroma at the tumour invasive front and bone interface. The percentage positivity and staining intensity were measured and calculated by the software based on the recommended settings (Table 2.4 and 2.5).

Table 2.4: HistoQuest settings for haematoxylin measurement.

Nuclei size	**15**
Remove weakly stained objects	1
Remove small sized objects	1
Threshold	13

Table 2.5: HistoQuest settings for DAB and NovaRed measurement.

Ring mask	Yes
Use nuclei mask	No
Use identification cell mask	Outside
Internal radius	-0.28 μM
External radius	+0.28 μM
Maximum growing steps	2.2 μM

2.2.3 Double IHC analysis of senescence in myofibroblasts

Matched cases of OSCC bone resections were examined, using double IHC, for expression of αSMA (monoclonal anti-actin, α-smooth muscle antibody A5228; Sigma-Aldrich, Poole, UK, 1:100) and p16INK4a (monoclonal anti-p16INK4a antibody ab108349; Abcam, Cambridge) or RANKL (polyclonal anti-RANKL antibody ab9957; Abcam, Cambridge, UK; 1:50) (Table 2.1). Staining was conducted using the DoubleStain IHC Kit: mouse and rabbit on human tissue (Abcam ab210061, Cambridge, UK). Two distinct antigens expressed in human tissue were evaluated using HRP-Polymer anti-mouse IgG (Emerald green chromogen), and AP-Polymer anti-rabbit IgG (Permanent red chromogen), which also gives the benefit of co-localisation.

OSCC bone resections were deparaffinized as previously described in section (2.2.2). Sections were blocked in peroxidase blocking buffer (3% H_2O_2) for 10 min, then rinsed twice in distilled water. Antigen retrieval was conducted by HIER in citrate buffer (0.01 M sodium citrate buffer) for 8 min in a microwave at high power, and allowed to cool in the hot buffer for another 5 min before washing in

TBS-T wash buffer (50 mM Tris, 150 mM NaCl, 0.05% Tween 20, pH 7.6).

Slides were incubated in 300 µl of diluted mouse and rabbit primary antibodies (anti-αSMA, 1:100, anti-RANKL, 1:50 or anti-p16INK4a, 1:100) in TBS-T. Following a 60 min incubation, sections were washed in TBS-T wash buffer (3 times, 2 min per wash). A fresh mixture of rabbit AP polymer and mouse HRP polymer was prepared at a ratio of 1:1 and used promptly. 100 µl of the mixture was carefully added to the slides, to cover the sections, and incubated for 30 min in a humidifier. Slides were washed in TBS-T (3 times, 2 min per wash). Permanent Red staining was performed in accordance to manufacturer's instructions (10 µl Permanent Red Chromogen, 200 µl Permanent Red Activator, in 1 ml Permanent Red Substrate). Permanent red staining solution (100 µl) was applied to each slide. After 10 min, the sections were immersed in distilled water to stop the reaction.

Sections were counterstained by briefly dipping slides in haematoxylin for 30 sec, rinsed in water (1 min), dipped in PBS (10 sec) for colour development, and rinsed in TBS-T before proceeding to the anti-mouse Ig detection using Emerald green staining. 100 µl of Emerald chromogen was applied, and sections incubated in a humidifier (5 min). Following this, slides were rinsed with distilled water, dehydrated in graded ethanol (85%, 95%, 100% absolute ethanol), and xylene (20 sec). Sections were mounted using 50 µl limonene mounting medium (catalogue ab104141, abcam) supplied and covered with a glass coverslip. (catalogue ab104141, abcam) supplied and covered with a glass coverslip.

2.3 Cell culture and propagation

2.3.1 Cell lines and culture conditions

2.3.1.1 HOB

Human primary osteoblasts, a gift from Dr Keyvan Moharamzadeh, were isolated from bone chips collected following dental implant surgery (Sheffield Research Ethics Committee (15/LO/0116, STH Research Department: STH18551), and used at passage 2.

2.3.1.2 NOF

Primary normal oral fibroblasts were isolated from human gingival tissue, as previously described (Hearnden et al., 2009) (Sheffield Research Ethics Committee reference number 13/NS/0120, STH17021). NOF 803, 804 and 822 (from three different donors) were used at passage 3-7 to exclude the possibility of senescence (based on previous data obtained in the laboratory).

2.3.1.3 DENF 316

Primary normal oral fibroblasts were retrieved from the department archive bio-repository. These human fibroblasts were isolated from healthy gingival tissue, which was collected during molar tooth extraction at Charles Clifford Dental Hospital, University of Sheffield (Sheffield Research Ethics Committee reference number 04/Q2305/78). Fibroblasts were used between passages 5-7.

2.3.1.4 CAF

Primary human cancer associated fibroblasts (CAF 002, 003 and 004- from three different donors) were isolated from OSCC resection specimens (Elmusrati et al., 2017) from Sheffield Teaching Hospitals NHS Foundation Trust (Sheffield Research Ethics Committee reference number 13/NS/0120, STH17021) and used between passage 3-7.

2.3.1.5 H357

The human OSCC-derived cell line H357 was retrieved from the department bio-repository. The H357 cell line was originally established from a well-differentiated OSCC of the tongue excised from a 74-year-old Caucasian male patient (Prime et al., 1990). The primary tumour dimension was 20 mm in diameter with no regional lymph node spread or distant metastases.

2.3.1.6 RAW 264.7

The murine monocyte cell line RAW 264.6 was acquired from ATCC (ATCC, TIB-71) and used below passage 5.

The cells were cultured and propagated in Table 2.6.

Table 2.6: Media used to propagate the specific cell strains.

Cell lines	Nutrient Media
HOB **H357** **RAW 264.7**	Dulbecco's Modified Eagle's Medium (DMEM) 10% (v/v) Foetal Bovine Serum (FBS) 1% (v/v) Penicillin/ Streptomycin 1% (v/v) Amphotericin B (250 µg/ml) 1% (v/v) L-Glutamine
DENF 316 **NOF 803, 804 and 822** **CAF 002, 003 and 004**	DMEM 10% (v/v) FBS 1% (v/v) L-Glutamine

Cells were grown in 12 ml of their corresponding culture media in T75 cm^2 tissue culture treated surface flasks (Greiner Bio-one, Germany). Cells were incubated in 99% humidity, 5% carbon dioxide (CO_2), at 37°C until confluent and ready for use.

2.3.2 Cell subculture and propagation

After reaching near confluence (70-80%), all cells were trypsinised, reseeded, and allowed to further propagate. To achieve this, spent media was discarded, and attached cells were irrigated twice in 5 ml of sterile modified Dulbecco's PBS, without calcium or magnesium chloride (catalogue number D8537, Sigma-Aldrich). Following rinsing (2 x), PBS was removed from the culture flask, 3 ml of trypsin (catalogue number T3924, Sigma-Aldrich) was applied, and the cells allowed to detach in the incubator at 37°C for 5 min. Following trypsin neutralisation with 3 ml 10% FBS DMEM nutrient media, cells were re-suspended and centrifuged at 1000 xg for 5 min to obtain a cell pellet. The supernatant was discarded carefully to avoid dislodgment of pellet. Cells were re-suspended by adding 3 ml of nutrient media, gently agitated by pipetting up and down to disperse cells throughout fresh media, and 1 ml was added to new T75 cm^2 flasks containing 11 ml of the respective media. Cells were allowed to grow in humidified incubators as mentioned previously.

2.3.3 Collection of conditioned media from cultured cells

Cells were grown to 70-80% confluence, rinsed twice in PBS and incubated in 2.5 ml serum free media (1% L-glutamine in low-medium glucose DMEM) in T75 flask for 24 h. Collected media was centrifuged at 1000 xg for 5 min, filter sterilized, and stored at -80°C ready for use in functional assays.

2.3.4 Indirect co-culture of human primary osteoblasts with H357 or CAF.

HOB were cultured to 70-80% confluence in T75 flasks. Spent media was discarded, and 3 ml of trypsin was added, following a double rinse with PBS.

Flasks were returned to a humidified incubator (3-5 min), until cells could be dislodged from the attached surface by gentle agitation. Following neutralization (3 ml media) and centrifugation, a haemocytometer was used for cell counting, and the cell pellet was resuspended at the required density. HOB (300,000-500,000 cells) were seeded into 6-well plates (catalogue number 657/60, Greiner bio one), making sure the final volume was kept consistent (2 ml/well). Plates were left in humidified incubator overnight to allow cellular attachment.

On the next day, nutrient media was dispensed, osteoblasts were irrigated with PBS, and serum free media (2 ml/well) was added for 24 h. Allowing cells to culture in serum free media brings all cells into an arrest phase (G0 cell cycle) for consistency. Simultaneously, confluent OSCC cells (H357) or CAF (002, 003, 004) were rinsed in PBS and further serum starved in 5 ml media for 24 h. Serum free media (5 ml) in a T75 flask, served as a negative control.

The following day, serum free media from osteoblasts grown in 6 well plates was removed and replaced by 1 ml of conditioned filtered serum free media collected from OSCC cells and CAF in the bottom wells. In the upper wells, 1 ml/ well serum free media was added; these wells acted as negative controls (Figure 2.1). All plates (n=3) were incubated in 99% humidity, 5% CO_2 incubator at 37°C for 24 h.

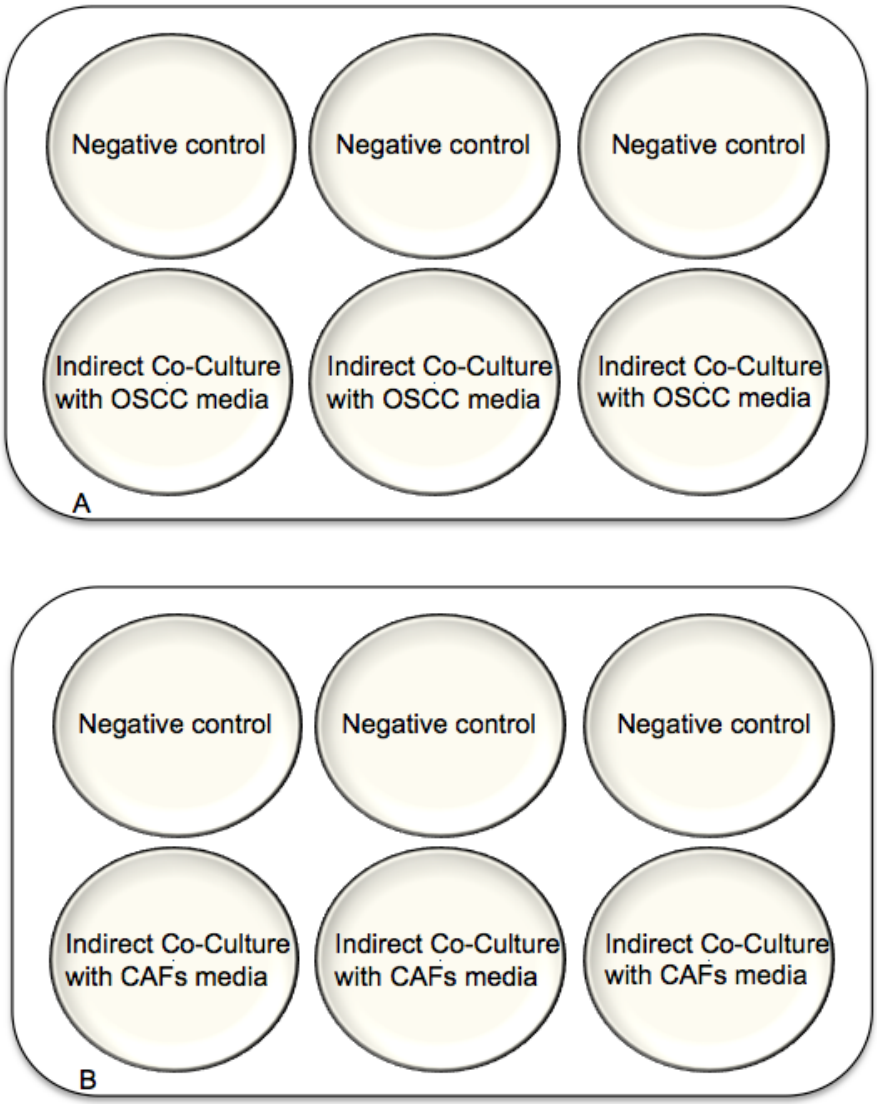

Figure 2.1: Indirect co-culture of human primary osteoblasts (300,000-500,000 HOB cells) treated with serum free conditioned media collected from **(A)** OSCC cells (H357) and **(B)** CAF (002, 003 and 004). Osteoblasts (HOB) treated in serum free media served as the negative control.

Finally, conditioned media was discarded, lysis buffer (350 µl, containing 1% β-mercaptoethanol) (RNeasy Mini Kit, Qiagen, UK) applied directly to wells and cells scraped (30 s) with small scrapers (Fisher Scientific, catalogue number 08-100-241). Following lysis, osteoblasts were collected in 1.5 ml eppendorf tubes, and RNA extraction was commenced promptly for optimal RNA yield.

2.3.5 Treatment of fibroblasts with TGFβ1

Normal oral fibroblasts were cultured in T75 flasks to 70-80% confluence. Media was discarded, and cells harvested by adding 3 ml of trypsin for 3 min (flasks were returned to humidified incubators to facilitate cell dislodgement). Following trypsin inactivation with DMEM nutrient media (3 ml), and centrifugation (1000 xg for 5 min), cells were quantified using a haemocytometer, and 250,000 cells seeded on sterile coverslips (VWR) (2 ml / well) in a 6 well plate for subsequent determination of αSMA expression and localisation using immunofluorescence (section 2.7).

For αSMA mRNA expression evaluation (section 2.5.1), DENF 316 and NOF (803, 804) were seeded at the 250,000 cells/well in 6 well plates. The cells were allowed to adhere to the 6 well plates for 24 h. On the following day, spent media was aspirated, fibroblasts were washed in PBS, and serum starved in serum free media (2 ml/ well) for 24 h. The next day, serum free media was aspirated, and three wells of fibroblasts were treated with 5 ng/ml (Bhowmick et al., 2004) recombinant human TGFβ1 (Catalogue number 240B, R&D Systems, UK) diluted in fresh serum free media (1 ml/ well). Fibroblasts in serum free media served as a negative control (Figure 2.2).

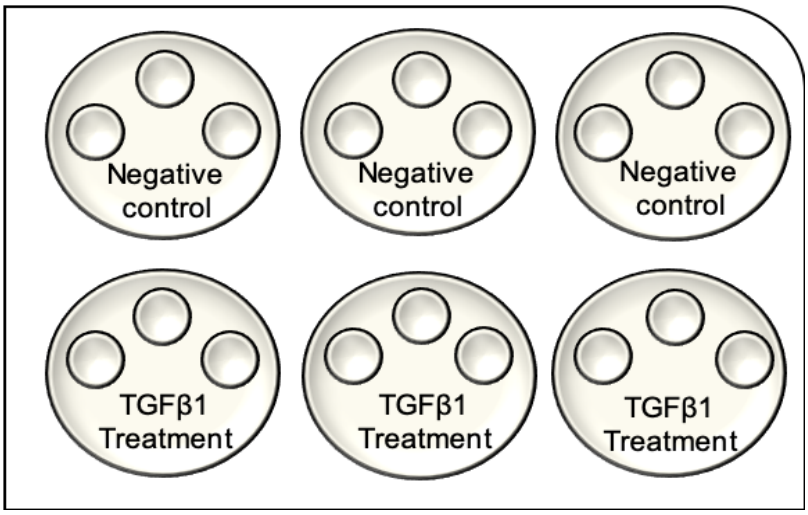

Figure 2.2: NOF treatment with TGFβ1. NOF 803, 804 and DENF 316 (250,000 cells / well) fibroblasts were seeded on coverslips in 6-well cell culture plates and treated with recombinant human TGFβ1 (5ng/ml). Fibroblast in serum-free media served as the negative control.

2.3.6 Induction of senescence in NOF

Hydrogen peroxide (H_2O_2), cisplatin, DNA damaging reagents, and replicative exhaustion techniques were selected to trigger senescence in fibroblast cell cultures (Kabir et al., 2016). Initially, primary human oral fibroblasts (NOF 803, 804, 822 & DENF 316) were seeded into T75 flasks with a cellular density of 500,000 cells/flask, when fibroblasts reached 70% to 80% confluence. Cells were next exposed to 500 μM H_2O_2 (catalogue number H/1750/15, Fisher Scientific) for 2 h, or 10 μM cisplatin (catalogue number BP809, Sigma Aldrich) for 24 h and allowed to incubate in a 99% humidified incubator in 5% CO_2 at 37°C. Following treatment, fibroblasts were rinsed twice with sterile PBS, 10 ml of fresh growth media was added, and the cells were allowed to grow in an incubator for 5 days. Senescence induction by replicative exhaustion was conducted by allowing primary oral fibroblasts to grow and propagate until passage 25, where cell count doubling time decelerated, and the number of cells of the former passage (passage 24, 3.5 million cells/flask) was similar to the latter (passage 25, 3.52

million cells/flask) after 10 days in culture . NOF cultured in growth media and not exposed to H_2O_2 served as the negative control.

2.4 Assessment of senescence

2.4.1 Senescence-associated β-galactosidase assay

It has been reported that senescent cells exhibit an accumulation and overexpression of endogenous lysosomal β-galactosidase, referred to a senescence-associated β-galactosidase (SA-β-gal), and regarded as a biomarker of cellular senescence. At pH 6, β galactosidase cleaves lysosomal X-Gal, which precipitates as a blue chromogen in senescent fibroblasts (Dimri et al., 1995).

To determine the extent of fibroblast senescence after H_2O_2, cisplatin treatment, and replicative exhaustion, senescence associated β galactosidase (catalogue number ab65351, Abcam) activity analysis was performed on low passage normal oral fibroblasts (Kabir et al., 2016).

Following senescence induction, fibroblasts were seeded (10,000 cells/well) into 12 well plates. NOF (10,000 cells/well) at a low passage (passage 4 or 5) seeded in a 12 well plate were also investigated for senescence, and served as a negative control. Fibroblasts were left overnight in a humidified incubator for cell attachment. On the next day, fibroblasts were rinsed with PBS, and 500 µl of fixative was applied for 15 min.

X-gal staining solution was prepared to a concentration of 20 mg/ml, and a mixture of 25 µl X-gal and 5µl 100X staining supplement was added to 470 µl of 1X staining reagent. Plates were placed in a dark hood, and 500 µl of the mixture

was added to each well. Plates were wrapped with aluminium foil and kept in a humidified incubator overnight.

Accumulation of β galactosidase in fibroblasts was analysed, and fibroblasts exposed to oxidative, genotoxic and replicative mitotic stress and NOF were evaluated at x20 magnification using Olympus CKX41 inverted microscope.

2.4.2 Evaluation of accumulating lipofuscin in senescence, using Sudan B Black staining

Sudan B Black (SBB) histochemical staining was conducted to examine lipofuscin accumulation, a recently described biomarker for cellular senescence (Georgakopoulou et al., 2013). SBB staining solution was prepared by dissolving 0.7 g Sudan B Black (Catalogue number 190160250, Arcos Organics) in 70% ethanol, covered with parafilm and thoroughly stirred overnight at RT. On the next day, the staining solution was filtered three times using filter paper (Catalogue number FB59031, Fisherbrand). Primary oral fibroblasts left untreated or exposed to H_2O_2, cisplatin, or replicative exhaustion were seeded onto 12 mm sterile glass coverslips (10,000 cells) and allowed to adhere overnight in a humidified incubator at 37°C and 20% O_2 saturation. On the following day, fibroblasts were rinsed twice in PBS followed by fixation in 3.7% formaldehyde for 5 min, washed in PBS and stained with SBB for 2 h. After incubation, coverslips were rinsed briefly with two changes of 70 % ethanol and washed with distilled water. Staining was visualised using a light microscope (Nikon Eclipse TS-100, Kingston-upon-Thames).

2.5 mRNA expression analysis from cultured cells

2.5.1 Total RNA extraction and purification

The cells were collected by adding 350 µl lysis buffer (RLY) to 3.5 µl beta-mercaptoethanol to cell pellet. Cell lysate was then promptly loaded into the provided ISOLATE II Filter (ISOLATE II RNA Mini Kit, BIOLINE, UK) placed into 2 ml collection tubes, and centrifuged for 1 min at 11,000 x g. Following filtration of lysate, 350 µl of 70% (v/v) ethanol was applied to the homogenized lysate and pipetted up and down (5-6 times). The lysate was then loaded into ISOLATE II RNA Mini Column, fitted into a 2 ml collection tube, and centrifuged for 30 s at 11,000 x g. After centrifugation, the flow-through was disposed, the column was fitted into a new 2 ml collection tube, and membrane-desalting buffer (350 µl) was applied to each sample column. Following centrifugation (11,000 x g for 1 min), the flow through was disposed of and the samples were subjected to three washes, 200 µl RW1 wash buffer (centrifuge 30 s at 11,000 x g), and 600 µl RW2 wash buffer (centrifuge 30 s at 11,00 x g). Finally, the samples were washed in 250 µl RW2 wash buffer (centrifuged 2 min at 11,000 x g), flow through was discarded, and ISOLATE II RNA Mini column was fitted into a 1.5 ml nuclease free collection tube ready for RNA elution. To obtain optimal RNA yield, 60 µl of nuclease free water was added to each column, and centrifuged 11,000 x g for 1 min. The eluted RNA was immediately placed on ice, ready for RNA quantification.

2.5.2 Quantification of RNA concentration and purity

The extracted RNA was measured using a Nanodrop (ND-1000) spectrophotometer (Thermo Scientific, VWR International; Illinois), and the concentration and purity of samples were observed at wavelength 260nm/280nm, with an optimal ratio of 2.0.

2.5.3 Reverse Transcription (RT) of RNA to complementary DNA (cDNA)

RNA (100µg) was reverse transcribed using High Capacity cDNA Reverse Transcription Kit (Applied Biosystems, USA), according to the manufacturer's instructions.

Reverse transcription master mix reaction (total volume 20 µl) was prepared (Table 2.7).

Table 2.7: RT master mix components.

Master mix reagents	Volume (total volume 5.8 µl)
Random primers	2 µl
Reverse transcriptase buffer	2 µl
Reverse transcriptase Multiscribe	1 µl
Deoxynucleotides (dNTPs)	0.8 µl

A total volume of 14.2 µl diluted mRNA was pipetted into each PCR tube (VWR International, USA), and 5.8 µl of the prepared master mix added to each sample respectively. To ensure all samples collected at the base of the tubes, samples were centrifuged for 15 s at 10,000 xg. Following this, the samples were placed in a DNA Engine DYAD (Bio-Rad Laboratories, USA) thermo-cycler, programmed at a selected setting of 25°C for 10 min, followed by an increase in temperature to 37°C for 2 h, and for 85°C for 5 min, prior to the samples being held at 4°C, ready for use or stored at -80°C for cDNA preservation.

2.6 Quantitative Real-Time Polymerase Chain Reaction (qPCR)

2.6.1 qPCR protocol

Following reverse transcription to cDNA, all samples were exposed to real time qPCR evaluation using Rotor-Gene Q PCR system (Qiagen, Germany). TaqMan primers (Life Technologies, Thermo Fisher Scientific, USA) or primers for SYBR quantification (Sigma) were utilized for DNA amplification (Table 2.8 and 2.10).

Table 2.8: TaqMan primers.

TaqMan primer	Details
RANKL	Reference code TNFSF11, Catalogue number PHP0034
OPG	Reference code TNFRSF1, Catalogue number PHC1684
IL6	part no. Hs00985639_ml

Table 2.9: Real time qPCR TaqMan master mix components.

Real time qPCR master mix	Volume (total volume 9.5 µl)
Primer/probe	0.5 µl
B2M reference gene	0.5 µl
Nuclease free water	3.5 µl
TaqMan Gene Expression Master Mix (Applied Biosystems, Catalogue number 4369016, Thermo Fisher Scientific)	5 µl

Table 2.10: SYBR green primers.

SYBR primer	Details
p16INK4a Forward	5' AATAACCTTCGGCTGACTGGCTG 3', Sigma-Aldrich
p16INK4a Reverse	5' TTATTCGCCTCCAGCAGCGCCCG 3', Sigma-Aldrich
αSMA Forward	5' GAAGAAGAGGACAGCACTG 3', Sigma-Aldrich
αSMA Reverse	5' TCCCATTCCCACCATCAC 3', Sigma-Aldrich
U6 Forward	5' CTCGCTTCGGCAGCACA 3', Sigma-Aldrich
U6 Reverse	5' AACGTTCACGAATTTGCGT 3', Sigma-Aldrich

Table 2.11: Real time qPCR SYBR green master mix components.

Real time qPCR master mix	Volume (total volume 9.5 µl)
Forward primer	0.5 µl
Reverse primer	0.5 µl
Nuclease free water	3.5 µl
qPCRBIO SyGreen Mix (Catalogue number PB20.1501, PCRBIOSYSTEMS)	5 µl

Human beta-2 microglobulin B2M (Catalogue number Hs00187842_m1, Life Technologies, Thermo Fisher Scientific, USA) was chosen as a reference gene for TaqMan primers (Kabir et al., 2016), while SYBR green amplifications were normalised using the U6 gene due to their low variation across samples, in accordance to Livak method (Livak and Schmittgen, 2001). A volume of 0.5 µl of cDNA was added to the qPCR master mix (9.5 µl) (Table 2.9 and Table 2.11). To exclude the possibility that signals were obtained from amplification of contaminating genomic DNA, 0.5 µl RNA (instead of DNA) was used as a negative control for all samples.

Samples were loaded into 0.2 ml PCR tubes (catalogue number 14230225, Fisherbrand) in triplicates, centrifuged briefly, to ensure collection of samples at

bottom of tube. A two-step setting was used for TaqMan primers, where the thermal profile commenced with a denaturation stage at 95°C for 10 s, followed by a decrease in temperature to 60°C for 45 s annealing and extension stage, this was repeated for 40 cycles. Gene expression of each sample was normalized to the corresponding endogenous gene B2M or U6 to obtain ΔCt. For SYBR green primer, three steps with melt setting, to generate a melt-curve, was used, where the thermal profile commenced with a denaturation stage at 95°C for 10 s, then a decrease in temperature to 60°C for 15 s, followed by 72°C for 20 s annealing stage, this was repeated for 40 cycles.

Finally, 2-ΔΔCt method was used to measure fold-change of gene of interest to relevant untreated samples (Livak, 2001).

2.7 Immunofluorescence (IF)

Following a 24 h stimulation of fibroblasts with TGFβ1, conditioned media was discarded, and 1 ml methanol used to wash the coverslips. Methanol was aspirated and 1 ml of fresh absolute methanol was added for cellular fixation for 15 min. The fixed fibroblasts were permeabilised in 1 ml 4 mM sodium deoxycholate (catalogue number 89905, ThermoFisher) for 15 min. Blocking buffer (2.5% bovine serum albumin (BSA) in PBS) (catalogue number A4503, Sigma-Aldrich) was prepared and applied at RT on a shaker to allow equal distribution of blocking solution for 15 min. The blocking reagent was discarded and monoclonal alpha smooth muscle actin FITC murine antibody (catalogue number A2547, Clone 1A4, Sigma-Aldrich), dissolved in 1:100 v/v in blocking buffer was applied for 1 h at 37°C.

Following antibody incubation, samples were washed in PBS (three times). Coverslips were carefully removed from wells, and mounted on glass slides (catalogue number 631-0108, VWR International) using a drop of Prolong gold DAPI containing mountant (catalogue number P36931, Thermo Fisher Scientific). Coverslips were placed in a slide box and allowed to attach to slides at 4°C for 24 h to ensure uniform staining of DAPI.

Images were taken at x40 magnification using an Axioplan 2 fluorescent microscope.

2.8 Enzyme-linked immunosorbent assay (ELISA)

NOF (803, 804, 822) and DENF 316 normal oral fibroblasts, NOF (803, 804, 822) exposed to senescence induction (at passage 25 or 5, 10 and 15 days after H_2O_2 or cisplatin exposure) and CAF 002, 003 and 004 were cultured in T75 flasks to 70-80% confluence and seeded in 6 well plates as previously mentioned. The plates were incubated for 24 h, to allow cell attachment.

On the following day, spent media was aspirated, fibroblasts were irrigated in PBS, and serum starved in serum free media (2 ml/ well) for 24 h. The next day, serum free media was aspirated and stored at -80°C in preparation for an enzyme linked immunosorbent assay (ELISA).

A sandwich duoSet ELISA kit (catalogue number DY626, R&D Systems) was conducted to demonstrate and evaluate soluble RANKL expression from CAF in comparison to NOF secretion *in vitro*. Required reagents were composed in accordance to manufacturer's instructions (Table 2.11).

Table 2.12: ELISA reagents preparations.

Reagents	Composition
PBS	1.5 mM KH_2PO_4 8.1 mM Na_2HPO_4 137 mM KCL
Wash Buffer	0.05% (v/v) Tween 20 in PBS
Reagent Diluent	1% (v/v) BSA in PBS
Substrate Solution	1:1 mixture of colour reagent A (H_2O_2) and colour reagent B (Tetramethylbenzidine)
Stop Solution	2 N H_2SO_4

2.8.1 ELISA detection of soluble RANK ligand

The capture antibody (murine anti-human RANK ligand) was diluted in PBS (180 µg/ml of antibody reconstituted in 1 ml PBS), and 100 µl of the working concentration was applied to the 96-well microplate (Greiner bio-one), to coat the bottom of each well. The plate was sealed (catalogue number 676001, Greiner bio-one) to prevent evaporation of diluent, and allowed to incubate overnight at RT.

On the next day, capture antibody was discarded, and each well was washed using 400 µl wash buffer (Table 2.12) twice. Extra care was taken following washing, and remnant wash buffer was removed by repetitive blotting of microplate on clean paper towels. Plates were blocked using 300 µl / well reagent diluent and left to stand for 1h at RT. Blocking reagent was aspirated, and the wells were washed as previously described.

Collected conditioned media from samples was diluted in Reagent Diluent and added to each well. Plates were sealed and allowed to stand for 2 h at RT. Sample supernatant was aspirated, and the wells were washed using the

washing buffer and blotted dry. Biotinylated Goat Anti-Human RANKL Detection antibody (9 µg/ml of antibody reconstituted in 1 ml in Reagent Diluent), and 100 µl per well was added, and incubated for 2 h at RT. Following aspiration, irrigation, and blotting, 100 µl streptavidin-HRP was applied to each well for 20 min, washed and blotted dry followed by addition of substrate solution (100 µl per well) for another 20 min at RT. Colour development was terminated by adding 100 µl of stop solution. Absorbance was instantly measured using TECAN (Magellan V7.2 software, Infinite M200) plate reader set at 450 nm with a correction wavelength of 570 nm.

2.8.2 ELISA quantification

Quantification was carried out using a standard curve in which the optical densities of the standards were plotted against standards' concentration. Subtraction of average standard (zero) from the average triplicate readings for each standard and sample was performed, and the equation (standard curve and the R2 values) was used to quantify RANKL (pg/ml) expression for all samples. The experiment was performed in triplicate.

2.9 Osteoclastogenesis assay

Murine monocyte/macrophage cells (RAW 264.7) were seeded in a 24 well Osteo Assay Surface plate (Catalogue number 3987, Corning, USA) (for osteoclastogenesis and pit forming assay), and on coverslips in 24 well plates (400 µl, approximately 20,000 cells/well). The cells were placed in a humidified incubator for 24 h, to allow cell attachment. On the following day, normal oral fibroblasts cultured in T75 flasks to 60-80% confluence, were treated with TGFβ1 (5 ng/ml). NOF, CAF, S-NOF, and H357 were rinsed twice with sterile PBS, and serum starved in 3 ml alpha MEM media (1% Pen/Strep. And 1% anti-fungal,

Amphotericin) for 24 h.

On day three, conditioned media was collected from serum-starved cells, and TGFβ1 treated oral fibroblasts, filtered, centrifuged (1000 xg for 5 min), and 400 µl per well added to RAW 264.7 cells (Figure 2.3). RAW 264.7 treated with recombinant RANKL (50 ng/ml) in serum free alpha MEM media served as a positive control, and RAW 264.7 in serum free alpha MEM media served as a negative control.

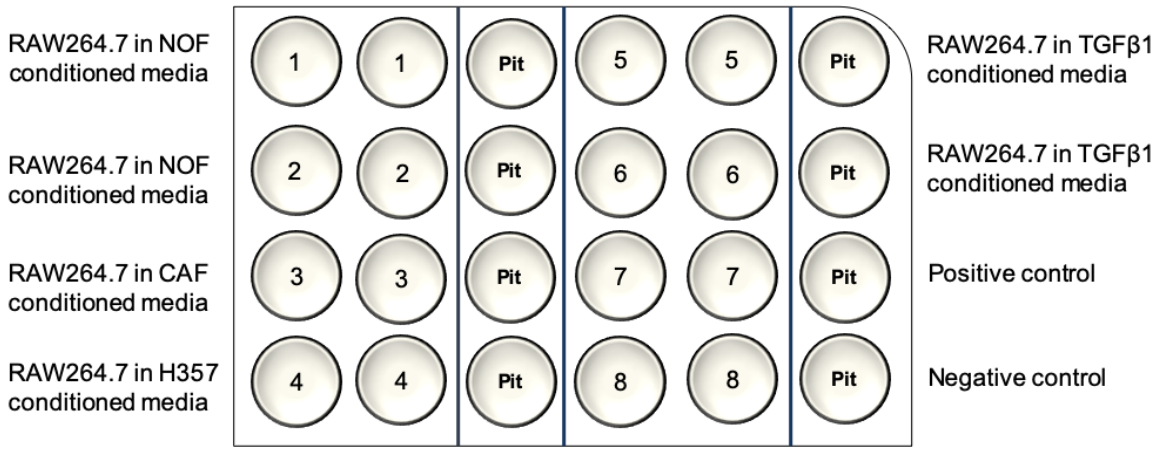

Figure 2.3: Osteoclastogenesis assay. Corning osteo surface 24 well plate seeded with 20,000 RAW 264.7 monocyte/macrophage cells (passage 5). Cells were subjected to a daily alpha MEM conditioned media change for 7 days. Samples included 1. Conditioned media from serum starved NOF. 2. Conditioned media from serum starved NOF. 3. Conditioned media from serum starved CAF. 4. Conditioned media from serum starved OSCC (H357). 5. Conditioned media from serum starved NOF treated with TGFβ1. 6. Conditioned media from serum starved NOF treated with TGFβ1. 7. Positive control, RAW 264.7 treated with 50 ng/ml recombinant RANKL. 8. Negative control, monocytes in serum free alpha MEM media. Two wells were designated for TRAP staining, and the third well was left to dry after day 7 to observe pit formation. The experiment was performed in triplicate.

Treatment of monocytes was continued for 7 days, with a daily change of conditioned media (collected from NOF, CAF and cancer cell lines). After 7 days, TRAP staining (2.9.1), pit forming (2.9.2), and nucleation staining (2.9.3) was performed to assess osteoclastogenesis (Figure 2.4).

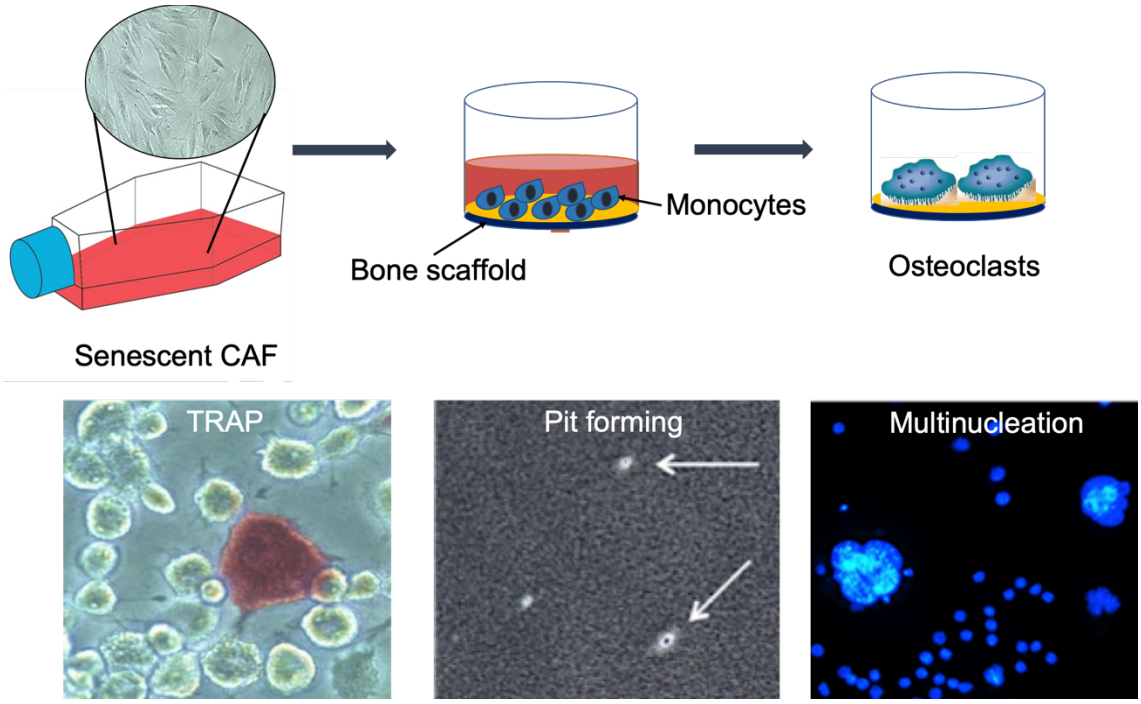

Figure 2.4: Osteoclastogenesis assay protocol. Conditioned media was collected for serum starved cells, and monocytes (20,000 per well) were seeded on a Corning osteo surface 24 well plate. Following seven days of daily media change, osteoclast generation was evaluated by TRAP staining, and for further verification, the ability to resorb bone and multinucleation was assessed.

2.9.1 TRAP staining

Tartrate-resistant acid phosphatase (TRAP) activity was assessed using the B-Bridge International (USA) assay kit (catalogue number AK04). Culture media was aspirated, and wells were irrigated with 400 µl of PBS. Following the wash, cells were fixed in 200 µl per well of Reagent 1, after 5 min, all wells were washed

with 1000 µl of distilled water, this was repeated three times. One vial of Chromogenic Substrate (Reagent 3) was diluted in 5 mL of Reagent 2 (Tartrate-containing Buffer). Following a brief vortex, to ensure all substrate has dissolved in buffer, 200 µl of Chromogenic Substrate was added to each well and incubated 37°C for 1 h (excess incubation was avoided to prevent precipitation of chromogenic substrate). When optimal staining was evident, wells were washed with distilled water to stop the reaction. Cells were evaluated and positive staining quantified under a light microscope (Nikon Eclipse TS-100), in three randomly selected high-power fields (magnification x 40).

2.9.2 Pit formation

Different wells of the 24 Osteo Surface plate were observed for active osteoclast resorptive pit formation assay (Figure 2.3). Initially, culture media was removed from wells, and 400µl of 10% (v/v) bleach (hypochloric acid) solution was added to each well. Plates were incubated at RT for 5min. Following incubation, wells were washed twice with distilled water, and allowed to dry in RT for 3-5 h. Single pits or pit clusters were analysed under a light microscope (Nikon Eclipse TS-100) in three randomly selected high-power fields (magnification x 40).

2.9.3 Nucleation staining for osteoclast verification

RAW 264.7 cells were seeded on coverslips in 24 well plates, at an approximate density of 20,000 cells/well, and allowed to propagate as described above (section 2.8). Medium was removed and the plates were washed with PBS followed by fixation in 3.7% formaldehyde for 5 min. Cells were dehydrated in acetone (5 min), and permeabilised with 0.1% TRITON X-100 in PBS. After thorough washing, coverslips were mounted on glass slides using SlowFade® Diamond Antifade Mountant with DAPI (catalogue number S36968,

ThermoFisher) for nuclear staining. Images were obtained using a fluorescent microscope.

2.10 Evaluation of senotherapeutics

2.10.1 Optimisation of senolytic drugs

Heat shock protein 90 (HSP90) inhibitor Alvespimycin (17-DMAG) (Catalogue number HY-12024, MedChem Express, USA), and B-cell lymphoma -2 (BCL-2) inhibitor Navitoclax (ABT263) (Catalogue number A3007, APExBIO Technology, USA) were used to target senescence. These drugs were selected due to their reported ability to promote apoptosis of senescent cells (Fuhrmann-Stroissnigg et al., 2017; Zhu et al., 2017). The drugs were reconstituted in DMSO (5 mM, and 10 mM respectively), then diluted in DMEM culture media to obtain a range of working solutions with graded concentrations. The concentrations 50 nM, 250 nM, 500 nM, and 750 nM were prepared for Alvespimycin (Fuhrmann-Stroissnigg et al., 2017), and 1μM, 2 μM, 3 μM, 4 μM, 5 μM, and 10 μM for Navitoclax (Zhu et al., 2016), aliquoted and stored at -20℃. Functional assessment of senotherapeutics was optimized by exposing both proliferating and senescent fibroblasts to a range of concentrations for 24 h.

Senescent oral fibroblasts, and proliferating NOF (passage 6) were seeded (5,000 cells/well) into 24 well plates and left overnight in a humidified incubator to allow cell adherence. On the next day, senescent fibroblasts as well as the low passage primary NOF were exposed to different concentrations of Alvespimycin and Navitoclax, and then incubated for 24 h at 37°C, in 99% humidity and 5% CO_2. Senescent fibroblasts and NOF not exposed to the senolytic drugs served as a negative control. Following treatment, the cells were rinsed in PBS and fixed in 3.7% formaldehyde for 5 min, and a Sa-β-Gal assay was performed to examine

the senescent burden in the cell population. This data was then compared to senescent cells not treated with the senolytics. In addition, a PrestoBlue cell viability test was conducted on both senescent and NOF exposed to the senotherapeutic, and the concentration of the optimized drugs that specifically initiated apoptosis in senescent fibroblasts and had no significant effect of NOF was used.

2.10.2 Evaluation of senotherapeutic toxicity on NOF viability

To investigate the effect of Alvespimycin and Navitoclax on cell survival and apoptosis on proliferating non-senescent fibroblasts. an experiment was set up similar to the one previously described in the senolytics optimizing assay (section 2.10). NOF were seeded (10,000 cells/ well) in a 12 well plate. NOF were treated with Alvespimycin or Navitoclax diluted in serum free DMEM media at graded concentrations (50 nM, 250 nM, 500 nM, and 750 nM and 1μM, 2 μM, 3 μM, 4 μM, 5 μM, and 10 μM respectively) (Figure 2.5) for 24 h.

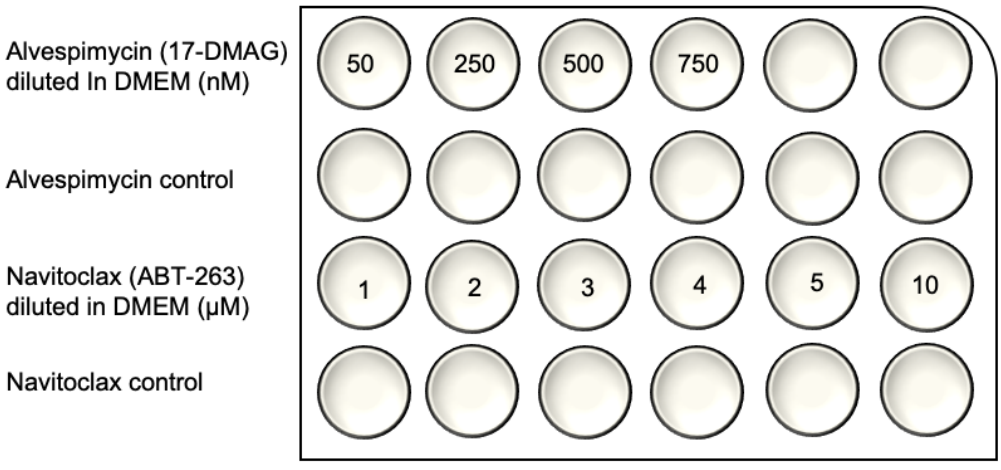

Figure 2.5: NOF viability test. 24 well plate seeded with 5,000 NOF cells (passage 5. Cells were subjected to treatment with senolytics Alvespimycin or Navitoclax and incubated for 24 h. Samples included NOF treated with Alvespimycin (50 nM, 250 nM, 500 nM, and 750 nM). NOF treated with Navitoclax (1μM, 2 μM, 3 μM, 4 μM, 5 μM, and 10 μM), negative control, NOF in DMEM media.

Following 24 h, a resazurin-based PrestoBlue cell viability reagent (catalogue number A13261, Life Technologies) was used at a dilution of 1:10 to assess NOF viability after senolytic treatment. PrestoBlue was applied to each well (40 µl PrestoBlue in 360 µl conditioned media / well). The 24 well plate was covered in aluminum foil and allowed to incubate in a humidified incubator for 1 h. Cell media was then collected and transferred to a 96 well plate (each sample was pipetted in duplicate). To correct background fluorescence control wells of media with no cells was added.

Fluorescence was measured using TECAN (Magellan V7.2 software, Infinite M200) plate reader set at an excitation wavelength of 560 nm with an emission wavelength of 590 nm. The mean of the fluorescent readings of the no cell controls was deducted from the values of each sample well. Relative fluorescence was plotted against time interval for the different senolytic drug concentrations and negative control.

2.11 Extracellular vesicle (EV) isolation and analysis

2.11.1 Graded concentration centrifugation for EV isolation from conditioned media in culture

To enhance the purity of the EV samples and reduce any contaminants, conditioned media collected from serum starved cells were exposed to graded concentration centrifugations and size exclusion chromatography (SEC) (Théry et al., 2018; Peacock et al., 2018) was conducted to isolate EV from cancer cells (H357), NOF (803, 804, 822), myofibroblasts (NOF treated with TGFB), CAF (002, 003, 004), and senescent fibroblasts (NOF exposed to H_2O_2 or cisplatin). Cells

were grown in three T175 flasks to confluence, rinsed twice in PBS and serum starved for 72 h in 20 ml serum free DMEM media supplemented with L-glutamine. A total volume of 60 ml of conditioned media was collected from serum starved cells was used for isolation of EV.

After 3 days, the conditioned media was collected into 50 ml centrifuge tubes and centrifuged at 300 xg for 10 min (J-26XP Beckman Coulter high speed centrifuge) to pellet cells and exclude large cellular debris. After the first spin, conditioned media was aspirated into a new 50 ml centrifuge tube, centrifuged at 2000 xg for 15 min, to pellet apoptotic bodies. After centrifugation the conditioned media was transferred to a new 50 ml tube, balanced and spun at 1000 x g for 45 min, to pellet large EV. Following the third centrifuge cycle, the conditioned media was filtered through a 0.22 μm filter,15 ml of the filtered media was transferred into Vivaspin protein concentrator spin columns (Catalogue number 28932363, GE Healthcare Life Sciences), balanced and centrifuged at 6000 xg for 20 min at 15˚C. After 20 min the media in the lower compartment of the concentrated centrifuge tubes were discarded and 15 ml of the filtered media was added to the top compartment of the centrifuge, and centrifuged at the same speed of 6000 xg, however the time was increased by 5 min. This procedure was repeated until all the filtered media was passed through concentration tubes and centrifuged at 6000 x g, while adding 5 min to each cycle.

SEC column preparation was performed by adding 14 ml sepharose suspended in ethanol (Catalogue number 17101404, GE Health Sciences) to each 10 ml flow column (Catalogue number 7321010, Bio-Rad) and allowed to settle for 2 h. A polystyrene fret was inserted and placed into the columns at a level 2 mm above

the top of the sepharose layer. The columns were then rinsed twice with 10 ml 0.03% Tween 20 in PBS to remove ethanol.

2.11.2 Size exclusion chromatography (SEC) for EV separation

Following the centrifugation, the concentrated sample of EV (0.5 ml – 1 ml) was transferred to the SEC columns. Immediately after the concentrated EV was allowed to flow through the fret filter, 10 ml of 0.03% Tween 20 in PBS was added to the columns. Fractions of EV (0.5 ml) were collected drop wise in 2 ml labelled eppendorf tubes (fractions 1-11) and stored at -20˚C (Figure 2.6).

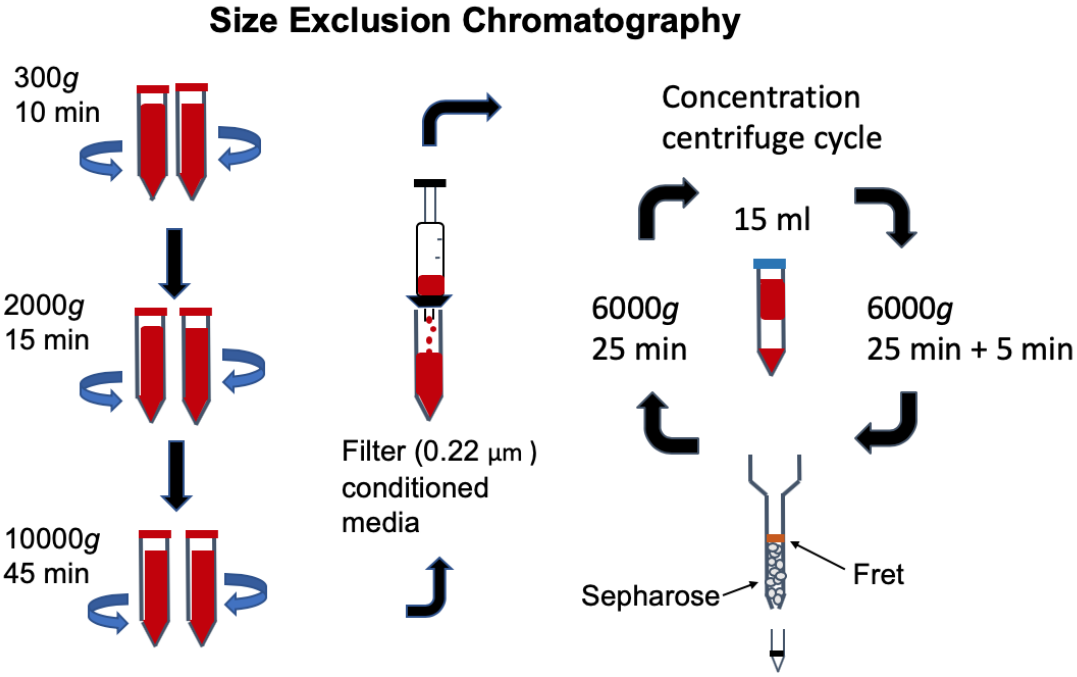

Figure 2.6: EV isolation by size exclusion chromatography. Conditioned media was collected centrifuged at graded speeds (300 xg, 2000 xg, and 10000 xg respectively). Following centrifugation, media was filtered, transferred to Vivaspin protein concentrator spin columns and centrifuged at 6000 xg for 25 min, adding 5 min to each spin until all the sample has been processed. Concentrated media was collected from the top chamber of the concentrator spin columns and loaded on to flow columns filled with sepharose beads. EV were collected in 2 ml eppendorf tubes (0.5 ml) in fractions (1-11).

2.11.3 Quantification of protein content in EV fractions to determine highest EV content

To identify the fraction of isolated EV with highest EV count, a BCA assay was carried out using the Pierce BCA Protein Assay Kit (catalogue number 23225, Thermo Fisher Scientific, UK). In accordance with the manufacturers' instructions, 10 µl of each fraction of EV for each sample or the diluted albumin standard (BSA) supplied (0, 0.0025, 0.25, 0.5, 0.75, 1, 1.5, 2 mg/ml of BSA) were pipetted into a 96 well plate, and 200 µl of the BCA working solution (reagent B to reagent A 1:50) was added to each well. All standards and samples were run in triplicate. The plate was covered and incubated for 30 min at 37℃. Following incubation, the plate was cooled to RT, and the optical density of the standards and samples were evaluated at 562 nm using a spectrophotometer plate reader TECAN (Magellan V7.2 software, Infinite M200). Quantification of protein concentration was carried out using a standard curve in which the optical densities of the standards were plotted against standards' concentration.

2.11.4 EV quantification by nano particle tracking

ZetaView (ZetaView® BASIC NTA – Nanoparticle Tracking Video Microscope PMX-120, Particle Matrix) was used to analyse the size and concentration of EV sub-populations. The ZetaView detects particles via light scattering and uses Brownian motion to quantify the size of the EV sample. The microscope was calibrated using a bead dilution in Milli-Q water (1:250,000). Video was acquired with a sensitivity of 85% and shutter value of 70 sec. Sample (1 ml diluted EV in PBS) was scanned at 11 positions (in triplicate), and particles were tracked using Brownian motion to obtain a mean value. Concentration as a mean percentage of the population was further calculated.

2.11.5 EV characterisation

Following quantification, an Exoview R100 (Nanoview Biosciences) – which uses antibody affinity-based technology for EV characterisation was used. EV markers CD9, CD63, and CD81 were selected, and antibodies against the specific tetraspanin antigen were labelled with fluorophores to detect the presence of EV. Samples were diluted in ExoView Incubation Solution (EV-TC-INC). 35 ul of sample was incubated on ExoView Tetraspanin Chips (EV-TETRA-C) placed in a 24 well plate for 16h at room temperature. Chips were washed three times in 1 ml of Incubation Solution for 3 mins on an orbital shaker. After washing chips were incubated with ExoView Tetraspanin Labelling Abs (EV-TC-AB-01) consisting of anti-CD81 Alexa-555, anti-CD63 Alexa-647 and anti-CD9 Alexa-488. All antibodies were diluted 1:600 in ExoView Blocking Solution (EV-TC-BSA-01). Chips were incubated in 250 ul of the antibody solution and 250 ul of Incubation Solution for 1 h at room temperature. All chips were then washed as before, once in Incubation Solution, three times in ExoView Wash Solution (EV-TC-WSH) and once in ExoView Rinse Solution (EV-TC-RNS) prior to drying. Samples were imaged on the ExoView R100 using the nScan 2.7 acquisition software. Data was analysed using ExoViewer 2.6.9 with the sizing thresholds set at 50 nm and 200 nm. Mouse IgG served as the negative control.

2.11.6 Investigation of RANKL expression in EV

Following EV isolation, quantification and characterisation, an ELISA was carried out as previously mentioned (section 2.8) to determine bone resorptive protein RANKL expression in EV.

2.11.7 Osteoclastogenesis assay to examine EV functionality

Functionality of EV was examined by carrying out an osteoclastogenesis assay. This assay was conducted as previously described (section 2.9). However,

instead of exposing monocytes to conditioned media collected from serum starved cells, these cells were exposed to EV isolated from the conditioned media resuspended in serum free alpha MEM media. Pit forming and nucleation assays were also performed to further verify osteoclast generation.

2.12 Osteoprotegerin, a RANKL antagonist and regulator of osteoclast differentiation and activation

2.12.1 Optimisation of OPG

Human recombinant OPG (Catalogue number SRP3132, Sigma Aldrich) was reconstituted in 5 mM Tris (pH 7.5) to a concentration of 1 mg/ml, and stored at -80°C. Following OPG preparation an osteoclastogenesis assay was conducted as described in section (section 2.9), however prior to exposing the monocytes to the conditioned media collected from the serum starved cells (NOF, CAF and S-NOF), recombinant OPG was added to the media samples at graded concentrations (1 ng/ml, 10 ng/ml, 50 ng/ml, 100 ng/ml and 200 ng/ml) to evaluate the optimal dose needed for optimal blockade of osteoclast generation. Conditioned media from serum starved cells (NOF, CAF, S-NOF) was the positive control, while monocytes in alpha MEM media served as a negative control.

After 7 days of repeated change of media with or without OPG, TRAP staining was performed as previously described (section 2.9.1-2.9.3). The number of positive cells were counted and compared to the equivalent positive control. The dose of OPG showing the highest reduction in monocyte differentiation to osteoclasts was utilised. Optimal human recombinant OPG dose was determined to be 100 ng/ml.

2.12.2 Investigating the role of OPG in antagonising RANKL expression

To confirm the significance of RANKL in OSCC bone invasion, OPG, RANKL decoy receptor and antagonist was studied. An osteoclastogenesis assay was conducted (section 2.9), monocytes were exposed to EV or conditioned media collected from serum starved NOF, experimentally induced CAF (NOF treated with 5 ng/ml recombinant human TGFβ1), CAF (isolated from human OSCC tissue), and senescent fibroblasts (exposed to 500 μM H_2O_2). Samples were treated with OPG (100 ng/ml) prior to exposure to monocytes. Monocytes exposed to CAF conditioned, and monocytes in alpha MEM media supplemented with OPG served as controls (Figure 2.7).

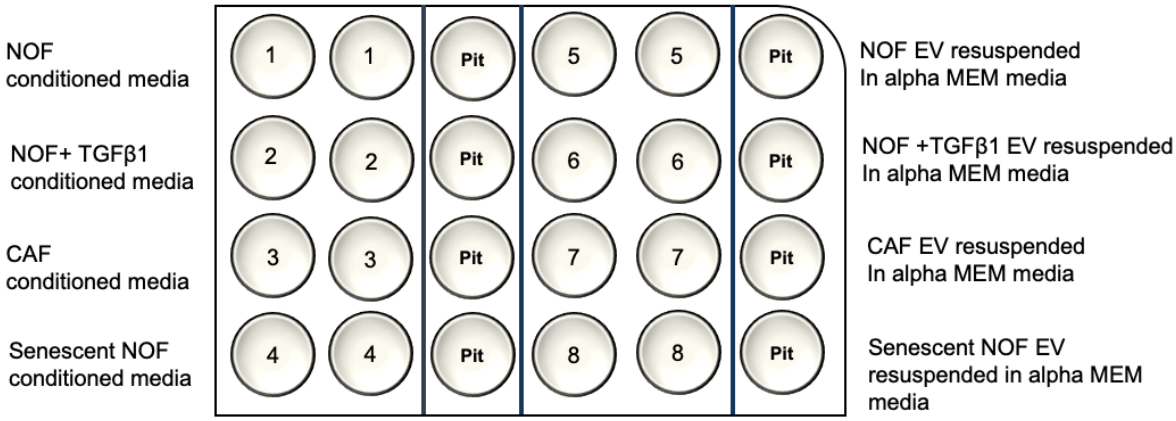

Figure 2.7: The effect of OPG on osteoclastogenesis. Corning osteo surface 24 well plate seeded with 20,000 RAW 264.7 monocyte/macrophage cells (passage 5). Cells were subjected to a daily alpha MEM conditioned media change for 7 days. Samples included 1. Conditioned media from serum starved NOF (NOF803). 2. Conditioned media from serum starved NOF (NOF803) treated with TGFβ1. 3. Conditioned media from serum starved CAF (CAF003). 4. Conditioned media from serum starved senescent fibroblasts (NOF803 exposed to H_2O_2). 5. EV isolated from conditioned media from serum starved NOF (NOF803).6. EV isolated from conditioned media from serum starved NOF (NOF803) treated with TGFβ1. 7. EV isolated from conditioned media from serum starved CAF (CAF003). 8. EV isolated from conditioned media from serum starved senescent fibroblasts (NOF803 exposed to H_2O_2). Negative control, monocytes in serum free alpha MEM media. Two wells were designated for TRAP staining, and the third well was left to dry after day 7 to observe pit formation. The experiment was performed in triplicate.

Following 7 days of media change, TRAP staining, pit formation, and cell nucleation was assessed (2.10.1 - 2.10.3).

2.13 Statistical analyses

Data was reported as mean ± standard deviation (mean ± STDV). ANOVA and Student's t-test was utilised to verify the statistical significance of findings as indicated in individual figure legends. A p-value of less than 0.05 was considered significant. All experiments were conducted in triplicate and repeated three times.

Chapter 3

The role of myofibroblastic CAF in the tumour microenvironment of bone invasive OSCC

3.1 Introduction

The tumour microenvironment, also termed the tumour stroma, is composed of diverse non-malignant cells such as inflammatory cells, mesenchymal stem cells, pericytes, bone marrow derived cells, haematopoietic and vascular endothelial cells, nerves and lipocytes, and fibroblasts, integrated in a complex extracellular matrix (Joyce and Pollard, 2009). The cross talk between neoplastic cells and surrounding stroma is constantly maintained, enabling tumour cell stimulation of the microenvironment, which as a result actively transmits paracrine signals increasing tumour cell proliferation and invasion. Historically bone invasive OSCC was thought to be related to tumour size as a result of direct pressure related resorption. However, due to the close proximity of these tumours to bone, there is increasing evidence that the surrounding tumour stroma including bone cells play a key role in tumour progression. In current literature, the TME has become a major focus of cancer and in particular OSCC research. αSMA, a myofibroblastic marker has been frequently reported to be expressed by CAF in the tumour stroma in several solid tumours (Radisky et a., 2007; Xing et al., 2010; Shiga et al., 2015). The myofibroblastic differentiation of CAF from resting fibroblasts, circulating fibrocytes, pericytes, and mesenchymal cells has been described to be mainly triggered by TGFβ1 signalling (Bierie and Moses, 2006; Xu et al., 2009). CAF have also been reported to be involved in regional lymph node metastasis, local recurrence and poor patient outcome in OSCC (Kellermann et al., 2007; Vered et al., 2010; Lin et al., 2017). In addition, *in vitro* experiments have shown that CAF can significantly prompt tumour cell proliferation and dissemination (Kellermann et al., 2008; Daly et al., 2008), however, little is known of the role of CAF in bone invasion in OSCC.

Several reports have suggested that CAF may be a potential target in treating cancer, due to their genetic stability, and phenotypic similarities of stromal fibroblasts across various cancers (Kalluri et al., 2006; Santos et al. 2009; Shiga et al., 2015; LeBleu and Kalluri, 2018), suggesting that depletion of CAF could be a potentially effective therapeutic approach. This chapter investigates the expression and role of myofibroblastic CAF in OSCC progression and bone invasion.

3.1.1 Aim

To investigate the expression and role of myofibroblastic CAF in bone invasion and remodelling in OSCC.

3.1.2 Experimental approach

1. OSCC cases with bone involvement (from 1994 to 2017) were retrieved from the unit archive and reports reviewed for clinicopathological parameters.
2. IHC was performed on a smaller cohort to investigate αSMA, RANKL and OPG expression in incisional OSCC biopsies of cases undergoing bone resection at a later date to compare expression of myofibroblastic marker αSMA and bone turnover markers RANKL and OPG.
3. Double IHC on tissue from OSCC bone resection specimens were conducted to investigate the co-expression of αSMA and RANKL in CAF.
4. Human primary osteoblasts (HOB) were indirectly co cultured with conditioned media from OSCC cells and CAF, and changes in RANKL and OPG mRNA was assessed using qPCR.
5. Primary normal fibroblasts (NOF) were exposed to TGFβ1 to induce a myofibroblastic phenotype and αSMA expression determined through

immunofluorescence and further quantified on a transcript level by qPCR.

6. Soluble RANKL protein secretion was also examined in both NOF and CAF using an ELISA.

7. An osteoclastogenesis assay was performed by culturing murine monocytes (RAW 264.7) with OSCC, NOF, NOF exposed to TGFβ1 and CAF conditioned media. TRAP staining, pit formation and nucleation assays will be conducted to confirm osteoclastic differentiation.

3.2 Clinicopathological data

To study the clinical parameters involved in bone invasive OSCC, reports of 407 diagnosed OSCC cases (1994 to 2017) with maxillary or mandibular bone resections were reviewed using the pathology database of the unit of Oral and Maxillofacial Pathology, University of Sheffield and different clinicopathological parameters such as gender, age, site, tumour grade, bone invasion, and metastasis were analysed.

3.2.1 Gender and Site

The bone resection cases included a broad age range (38 to 91 years), with an average age of 67 years, the average age in males and females was 64.8 and 72.6 years with an age range of 38 to 91, and 48 to 87 years respectively. Sixty-three per cent (n=260) of the cases were from male patients while 36.11% (n=147) were from females, with a male to female ratio (1.76:1) (Figure 3.1).

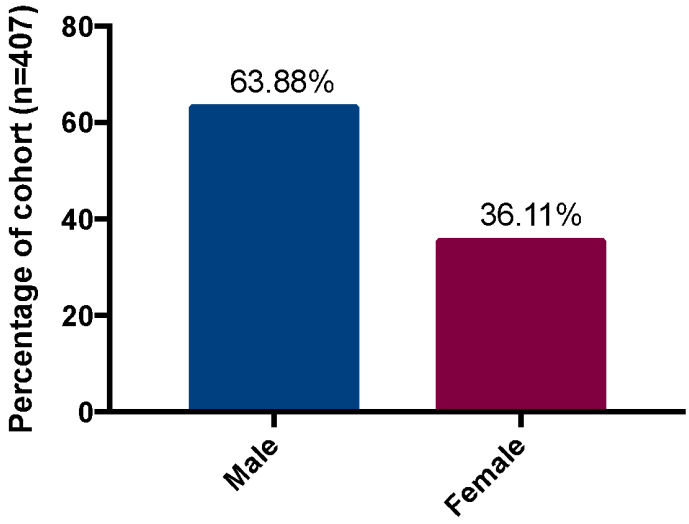

Figure 3.1: Gender distribution in 407 bone invasive OSCC cases, 63.88% (n=260) were male, while 36.11% (n=147) were female patients.

The majority of the cohort (71.49%, n=291) involved mandible resections whereas 28.5% (n=116) were maxillary bone resections (Figure 3.2).

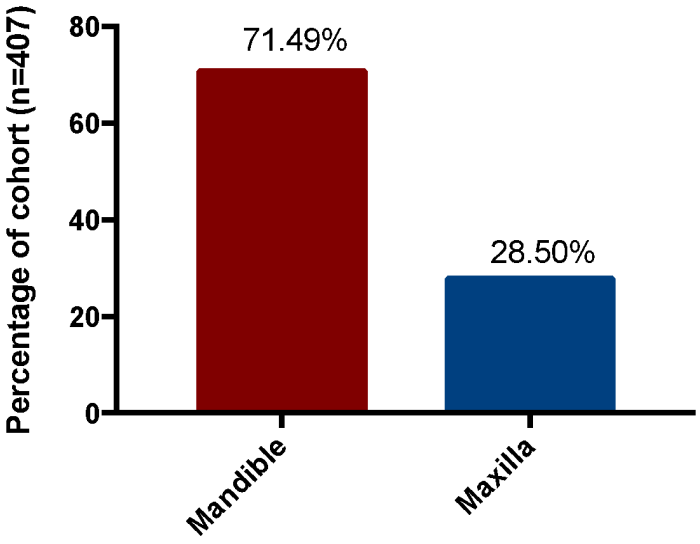

Figure 3.2: Site distribution of 407 bone invasive OSCC cases. 71.49% (n=291) were mandibular, while 28.50% (n=116) were maxillary resections.

3.2.2 OSCC histological grade

A predominance of moderately differentiated tumours were observed in the cohort (54.79%, n=223), while 27.27% (n=111), and 17.93% (n=73) were well and poorly differentiated SCCs (Figure 3.3).

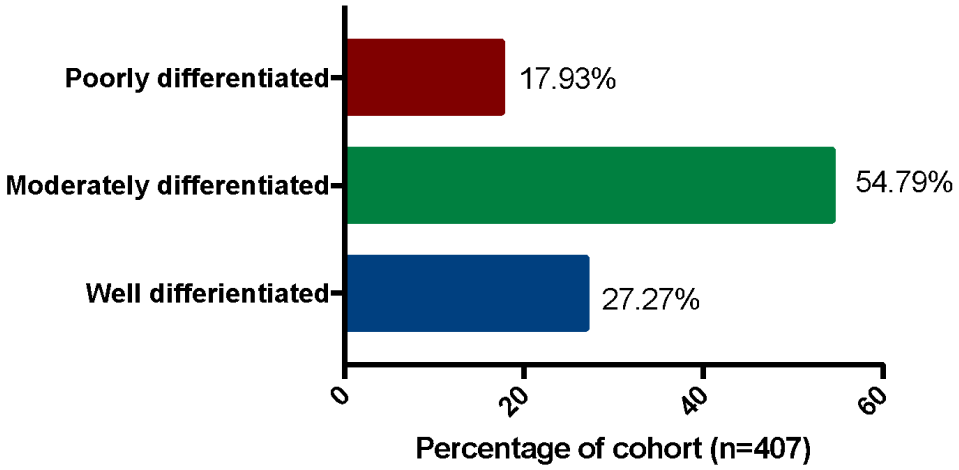

Figure 3.3: Grade of primary OSCC tumour. Out of the 407 OSCC cases with bone resection reviewed, the majority of tumours were moderately differentiated (54.79%, n=223). 27.27% (n=111) of tumours were well differentiated and 17.93% (n=73) poorly differentiated SCCs.

3.2.3 Bone involvement

The involvement and extent of OSCC bone invasion was also examined. OSCC bone involvement was defined in accordance to pathology report to superficial cortical bone resorption and cancellous bone involvement, the latter categorised as true bone invasion (Frederick et al., 2002). Approximately half of the cohort (50.98%, n=207) exhibited some degree of bone involvement. 22.24% (n=90) of the cases presented with superficial cortical bone resorption (not true bone invasion), while 28.74% (n=117) displayed frank cancellous bone invasion (Figure 3.4 and 3.5).

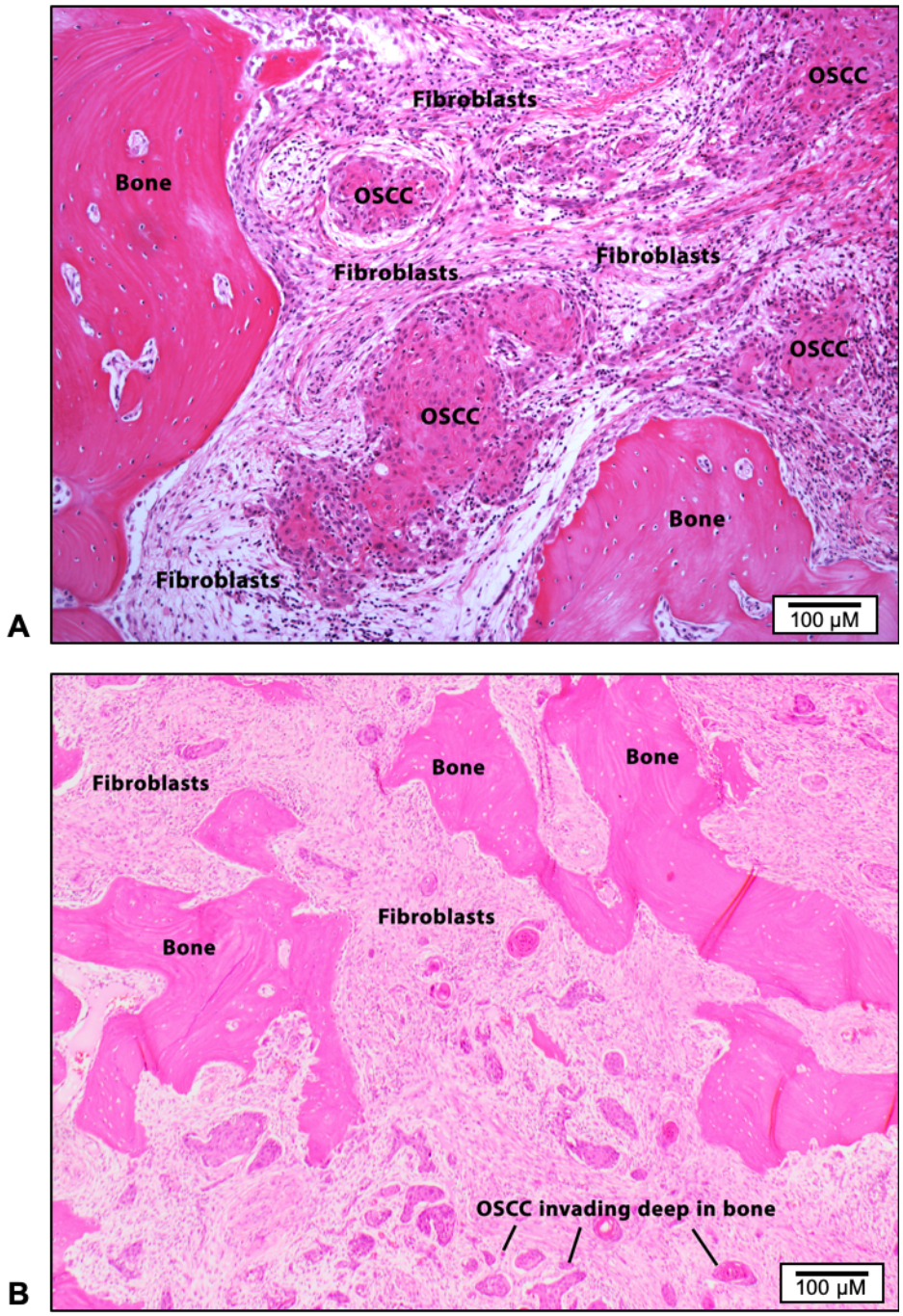

Figure 3.4: Representative photomicrograph showing bone involvement distribution in OSCC cases with bone resection. (A) Superficial cortical resorption. (B) Cancellous bone invasion. (magnification x20)

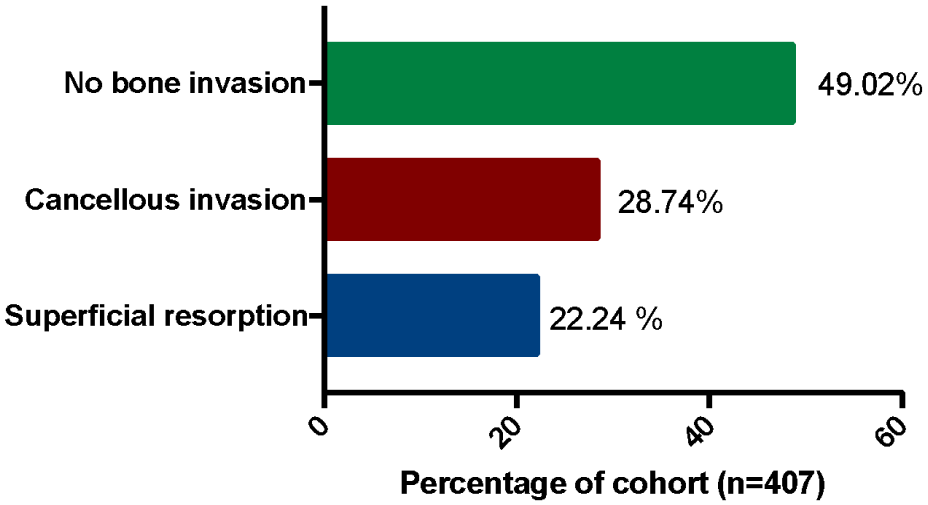

Figure 3.5: Bone involvement distribution in 407 OSCC cases with bone resection. 28.74% (n=117) showed true cancellous bone invasion, while 22.24% (n=90) superficial cortical bone resorption, and 49.02% (n=200) showed no evidence of tumour in close proximity of bone.

3.2.4 Metastasis

The OSCC cohort was further investigated for the presence or absence of metastasis using the archived pathology reports. Metastasis was evident in 36.6% (n=149) (Figure 3.6). 30.7% (n=36/117) of SCCs with cancellous bone invasion, and 8.8% (n=8/90) with superficial cortical resorption showed regional metastasis.

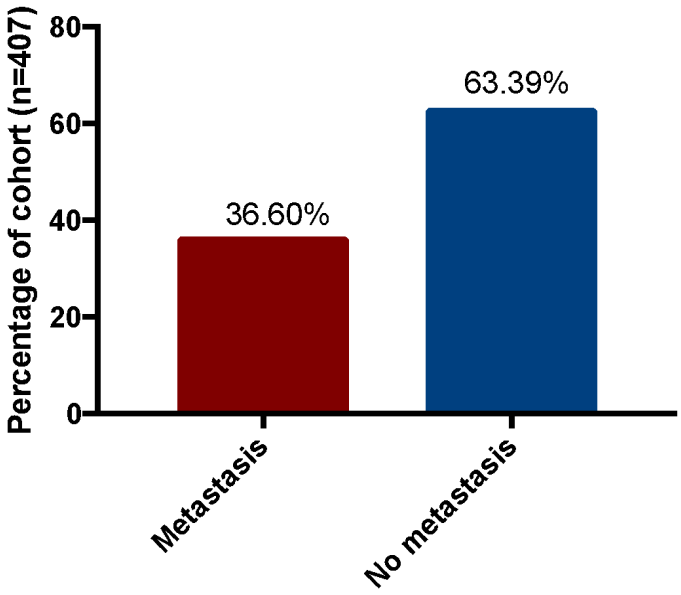

Figure 3.6: Distribution of metastasis in 407 OSCC samples with bone resection. 63.39% (n=258) had no metastasis, while 36.60% (n=149) showed neck lymph node metastases.

3.3 Evaluation of stromal marker αSMA and bone turnover markers RANKL and OPG expression in OSCC tissue away from bone

Ten incisional biopsies of patients with OSSC (5 cases cortical/superficial, and 5 cases cancellous bone involvement) matched with bone resections previously examined (Elmusrati et al., 2017, data from masters thesis) were selected for analysis, to investigate the expression of αSMA, RANKL and OPG in OSCC CAF, and to correlate whether the intensity of expression of these markers could be used to predict bone invasion. IHC was conducted to examine the abundance of the CAF marker αSMA, as well as the expression of bone turnover markers RANKL and OPG in tumour and surrounding stroma. Following staining, the samples were scanned, and staining intensity was evaluated using HistoQuest software.

3.3.1 Expression of αSMA in tumour microenvironment away from bone

In our previous data (Elmusrati et al., 2017) in over 90% of our cohort (n=10, 5 deep bone invasion, 5 superficial bone resorption), αSMA positive fibrous stroma was seen invading bone ahead of the invasive front of the tumour. In an attempt to investigate whether tumour stroma away from bone expressed αSMA, and to assess whether αSMA abundance can be used to predict bone invasion on resections, incisional biopsies from cases with OSCC bone invasion were assessed. Although the expression of αSMA was evident, it was weakly detected in fibroblasts in 60% of cases, surrounding the main tumour mass, and in smooth muscle cells of blood vessels (Figure 3.7). The average expression of αSMA positive cells in incisional biopsy cases that later demonstrated superficial cortical resorption was 30.71 ± 10.56 (mean ± STDV), while the average αSMA expression intensity was 37.47 ± 3.19. In cases with cancellous bone involvement, the average expression of αSMA positive cells in incisional biopsies was 42.82 ± 5.04, while the average expression intensity was 41.57 ± 1.58, The highest expression of αSMA positive cells was 48.82% detected in the TME of OSCC cancellous bone invasion, however there was no significant difference in αSMA expression (p=0.67) in incisional biopsy of superficial cortical bone resorption or cancellous bone invasive OSCC (Figure 3.8).

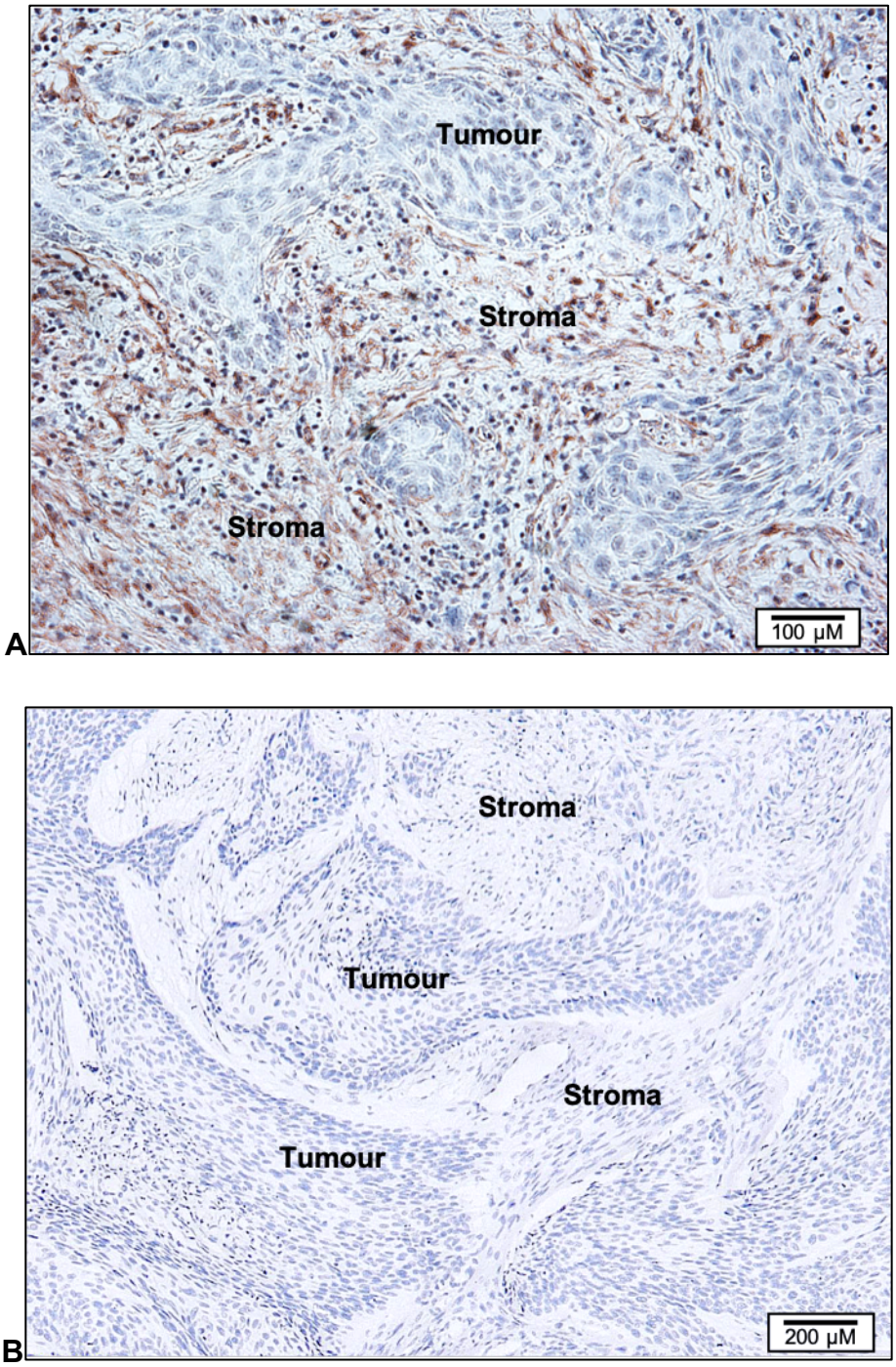

Figure 3.7: Representative photomicrographs showing IHC localisation of αSMA in incisional biopsies away from bone. (A) Strong αSMA (antibody dilution 1:100) expression in myofibroblastic stroma at the invasive tumour front. (B) Negative control (magnification x 20).

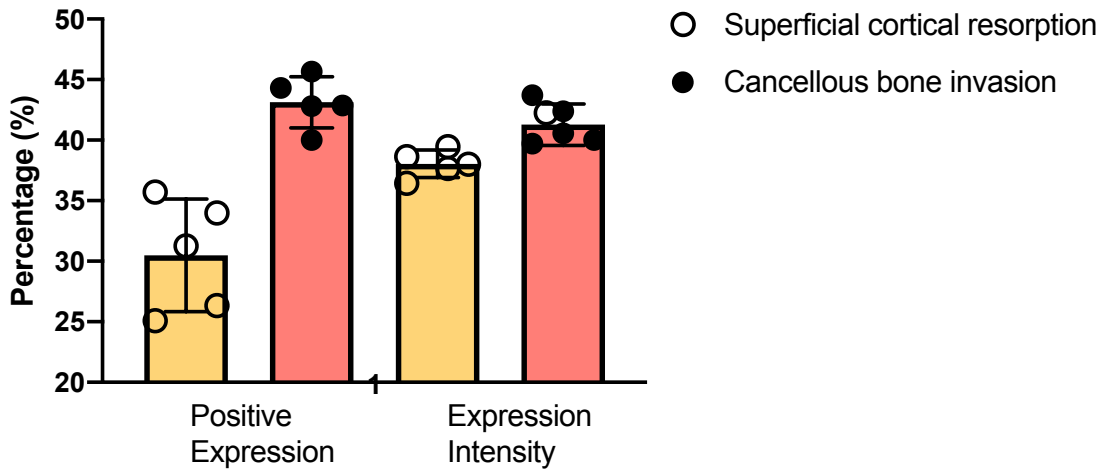

Figure 3.8: Quantification of αSMA expression in OSCC biopsy sections away from bone interface in selected cohort (n=10, 5 superficial cortical resorption and 5 cancellous bone involvement). The average expression of αSMA positive cells in cases that presented with superficial cortical bone resorption was 30.71 ± 10.56 (mean ± STDV), while the average αSMA expression intensity was 37.47 ± 3.19. In cases with cancellous bone involvement the average expression of αSMA positive cells was 42.82 ± 5.04, while the average expression intensity was 41.57 ± 1.58. Error bar = STDV.

3.3.2 RANKL and OPG expression

Bone turnover markers RANKL and OPG were also evaluated in biopsies of tumour away from the bone interface. Our previous results showed readily detectable expression in tumour cells and fibroblasts adjacent to bone (Elmusrati et al., 2017). In the incisional biopsies, RANKL expression varied, as in cases with cancellous bone invasion the expression of RANKL positive cells 43.42 ± 21.60 (mean ± STDV), and RANKL expression intensity (15.98 ± 4.07) was evident in tumour and stroma. This expression was weaker in comparison to cases with superficial cortical resorption 54.76 ± 12.30, 17.95 ± 1.17 respectively (p=1.01) (Figure 3.9). Moreover, OPG was also weakly detected or absent in 75% (n=8) of the samples (Figure 3.10). In cases with cancellous bone invasion the expression of OPG positive cells (58.67 ± 9.14 (mean ± STDV) was higher when

compared to cases with superficial cortical resorption (42.33 ± 5.3), however, these differences were not significant (p=0.98) (Figure 3.11 to 3.14).

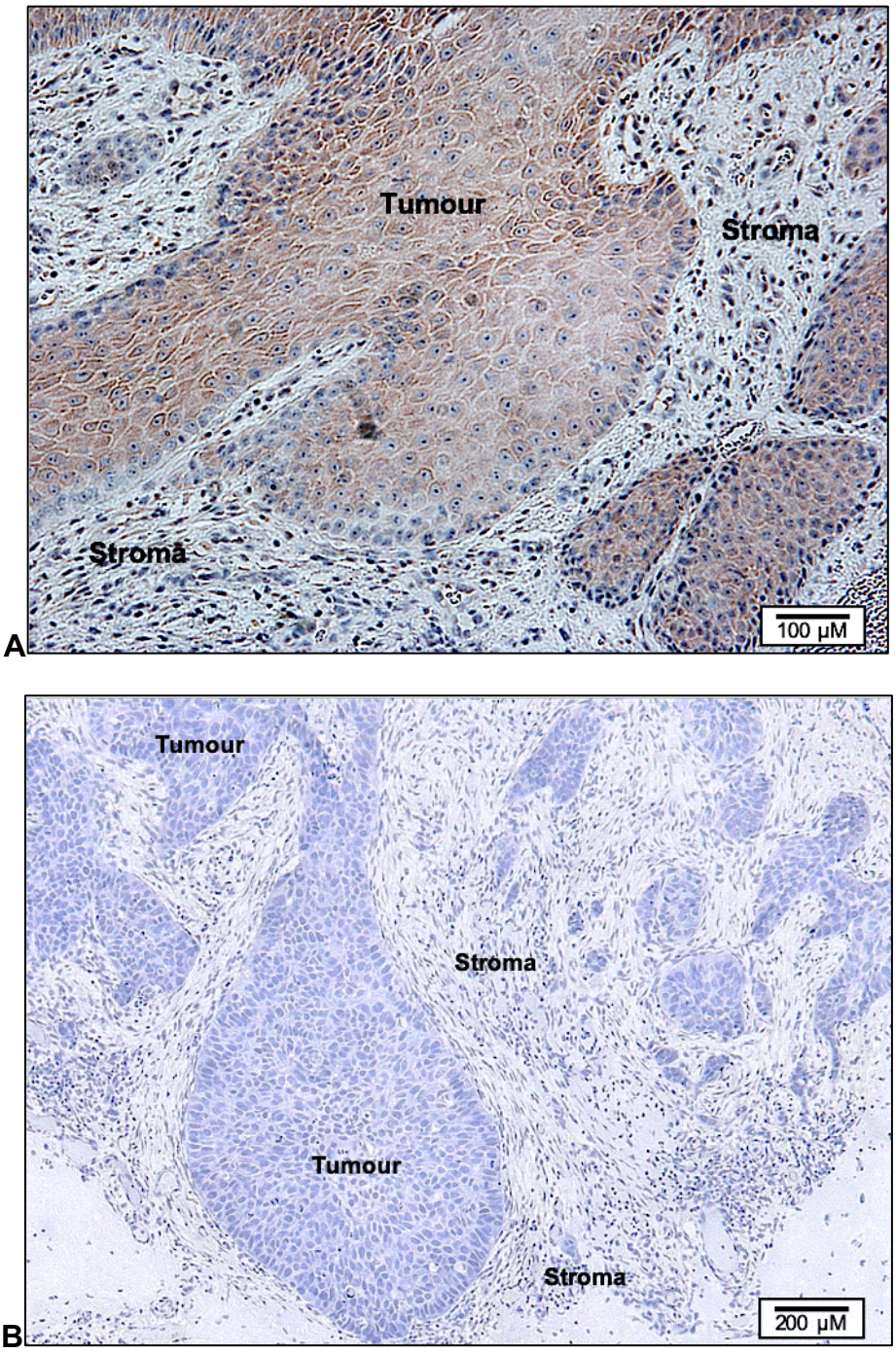

Figure 3.9: Representative photomicrographs showing IHC localisation of RANKL in incisional biopsies away from bone. (A) RANKL staining evident in OSCC and surrounding fibrous stroma. (B) Negative control (magnification x 20).

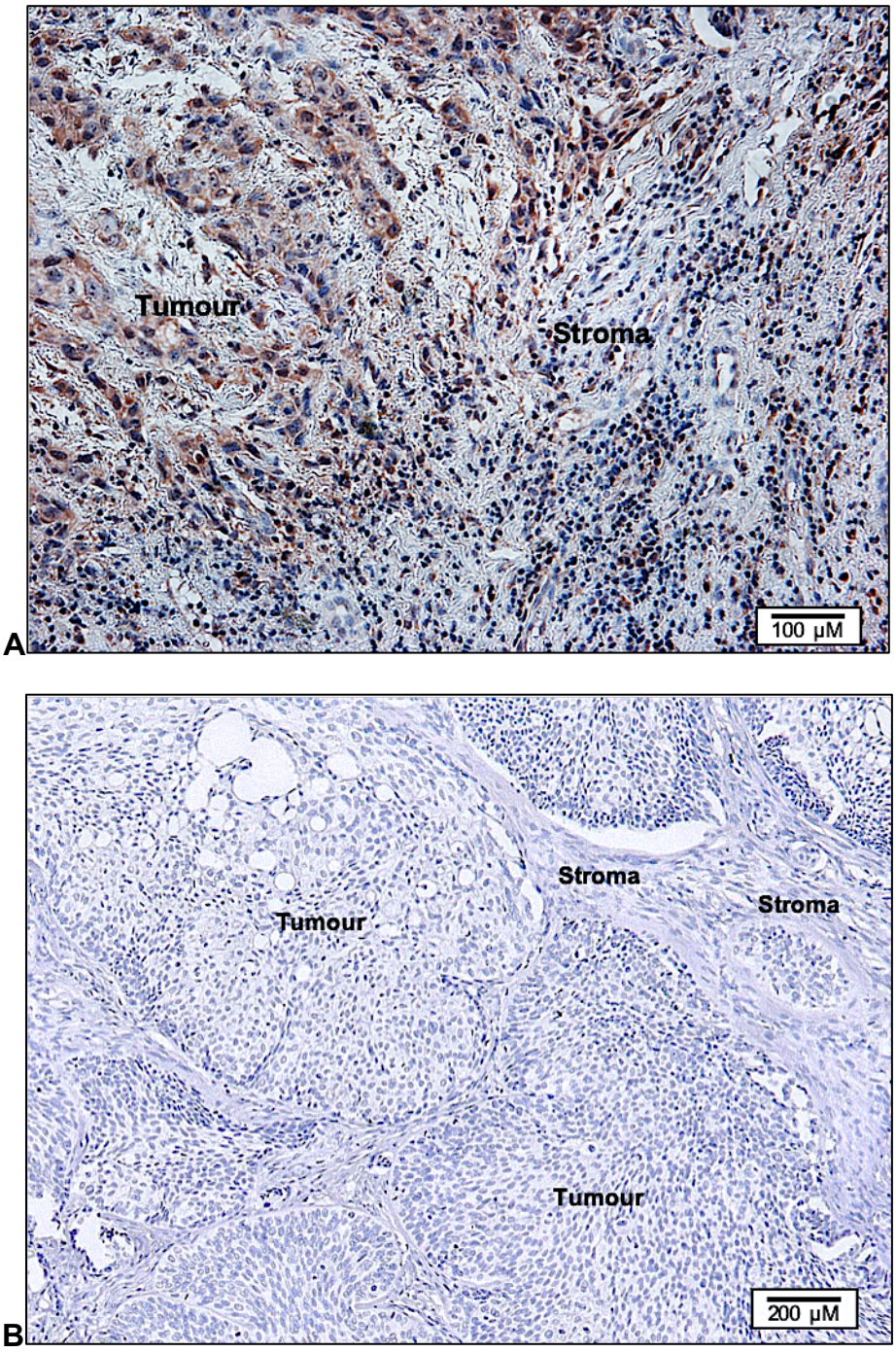

Figure 3.10: Representative photomicrographs showing IHC localisation of OPG in incisional biopsies away from bone. (A) Weak OPG staining in tumour and stroma. (B) Negative control (magnification x 20).

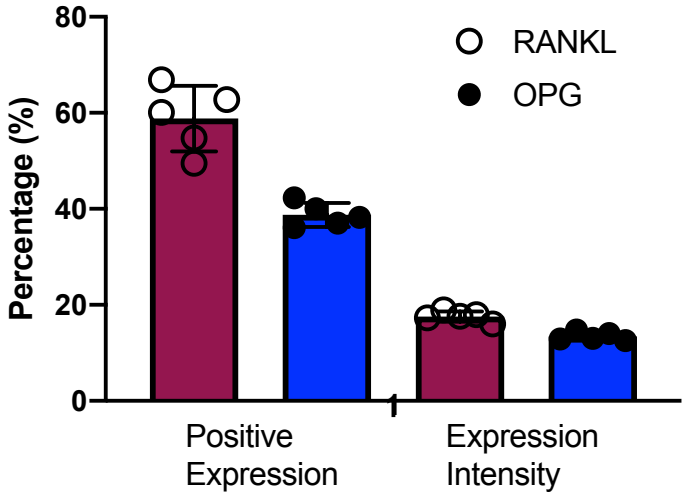

Figure 3.11: Expression of RANKL and OPG in biopsies of tumour (away from bone interface) with superficial cortical bone resorption (n=5). The average expression of RANKL positive cells in biopsies of tumours with superficial cortical resorption was 58.76 ± 12.30 (mean ± STDV), while the average RANKL expression intensity was 17.95 ± 1.17. Average expression of OPG positive tumour cells was 42.33 ± 5.38, while the average expression intensity was 14.74 ± 1.97. Error bar = STDV.

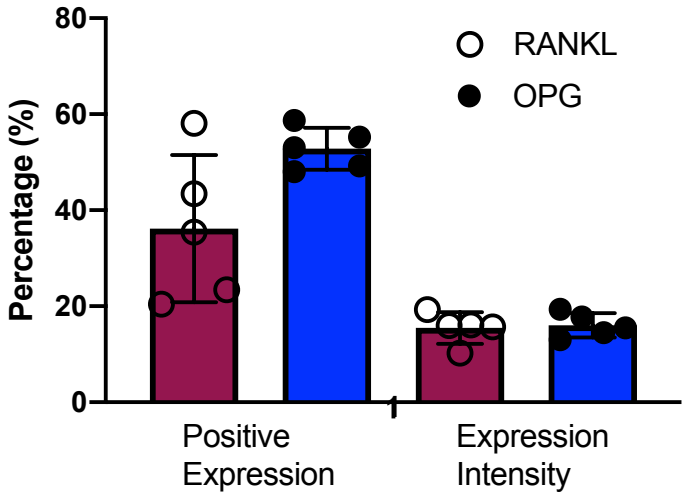

Figure 3.12: Expression of RANKL and OPG in tumour biopsies (away from bone interface) with cancellous bone involvement (n=5). The average expression of RANKL positive tumour cells in biopsies of tumours with definite cancellous bone involvement was 37.42 ± 21.60 (mean ± STDV) while the average RANKL expression intensity was 15.98 ± 4.07. Average expression of OPG positive tumour cells was 58.67 ± 9.14, while the average expression intensity was 15.51 ± 4.35. Error bar = STDV.

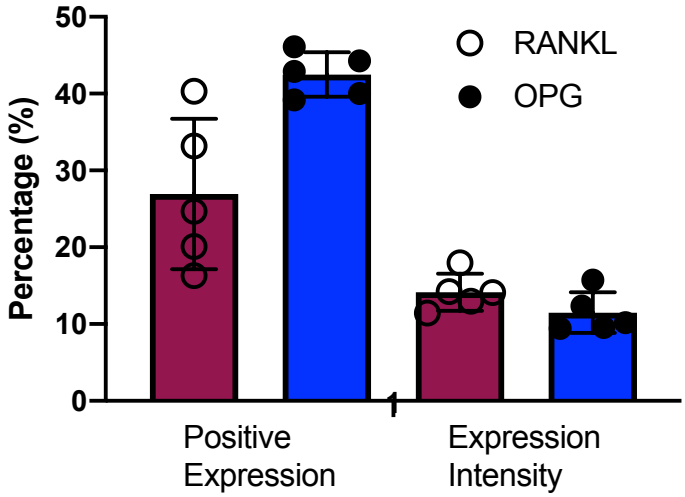

Figure 3.13: Expression of RANKL and OPG in stroma of OSCC (biopsies-away from bone interface) with superficial cortical bone resorption(n=5). The average expression of RANKL positive stromal cells in biopsies of cases with superficial cortical bone resorption was 26.70 ± 16.27 (mean ± STDV), while the average RANKL expression intensity was 12.23 ± 3.62. Average expression of OPG positive cells was 42.91 ± 3.68, while the average OPG expression intensity was 11.35 ± 3.68. Error bar = STDV.

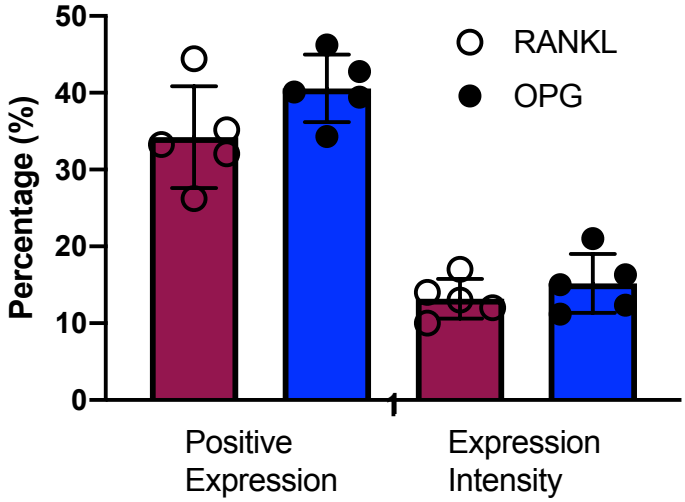

Figure 3.14: Expression of RANKL and OPG in stroma of OSCC biopsies (away from bone interface) with cancellous bone invasion (n=5). The average expression of RANKL positive stromal cells in initial biopsies of cases with cancellous bone involvement was 32.85 ± 12.77 (mean ± STDV), while the average RANKL expression intensity was 13.00 ± 4.08. Average expression of OPG positive stromal cells was 39.77 ± 4.58, while the average OPG expression intensity was 13.87 ± 3.48. Error bar = STDV.

3.4 Double αSMA and RANKL expression in OSCC microenvironment

We have previously shown that OSCC stroma expresses the myofibroblastic marker（αSMA) and bone turnover marker RANKL in bone resections (Elmusrati et al., 2017). To further confirm the co-localisation of both markers in fibroblastic tumour stroma, a double immunohistochemical analysis of αSMA and RANKL was performed. Matching cases (n=10, 5 cortical/superficial bone resorption, and 5 cancellous bone invasion) of OSCC with bone were selected and investigated. Our data shows that OSCC cells express RANKL, and co-localisation of αSMA and RANKL was expressed in fibroblastic stroma surrounding OSCC cells, confirming that αSMA positive CAF express RANKL (Figure 3.15).

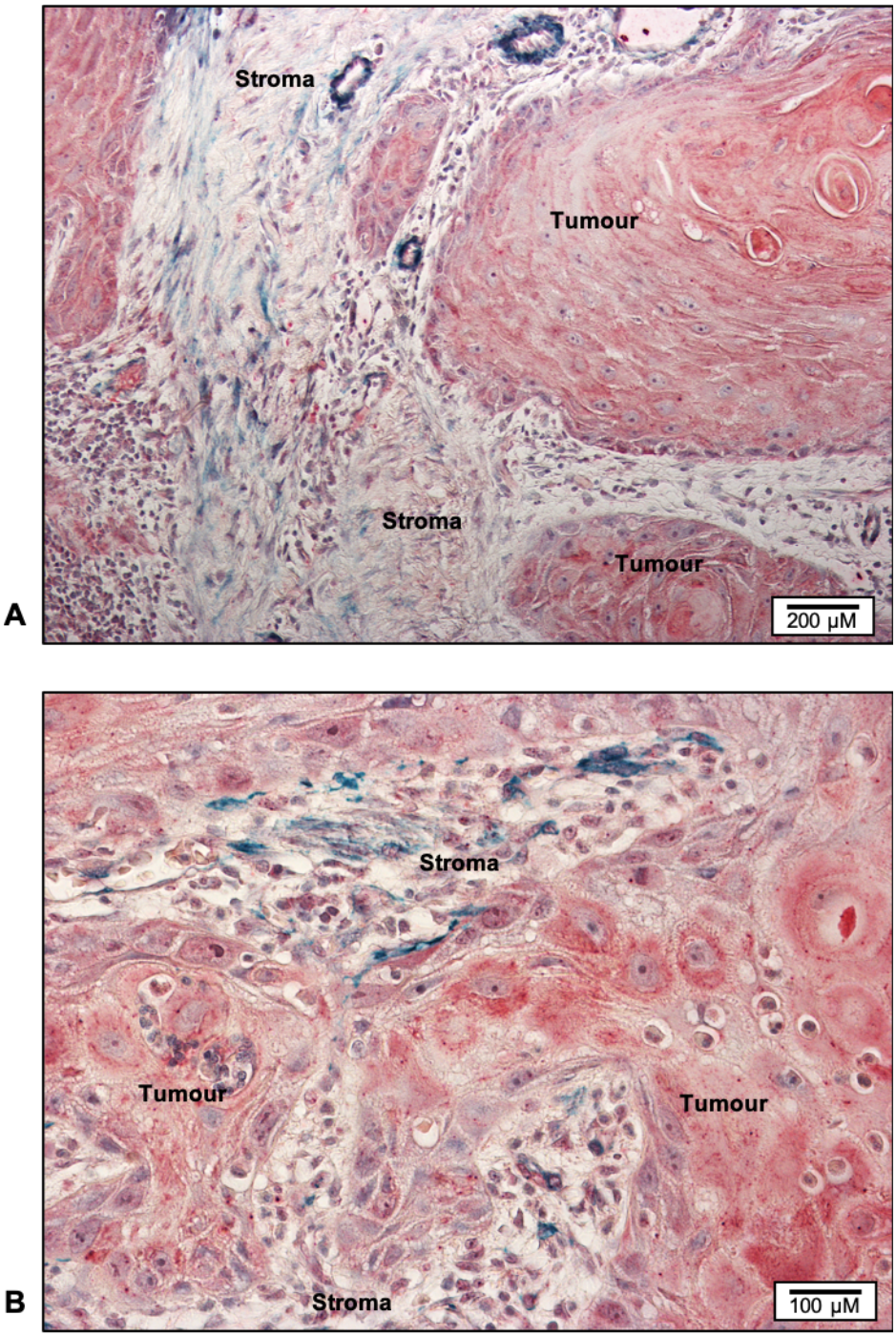

Figure 3.15: Representative photomicrographs showing IHC co-localisation of αSMA and RANKL. αSMA (antibody dilution 1:100) expression (green stain) in myofibroblastic stroma. RANKL expression (red) in tumour as well as SMA positive cells in OSCC stroma. Co-localization of αSMA and RANKL was evident in fibrous tumour stroma (blue). (A) Magnification x 10. (B) Higher magnification (x 20).

3.5 Experimentally induced CAF and primary CAF isolated from OSCC express stromal marker αSMA

We have previously shown abundant expression of αSMA in stroma ahead of OSCC invasive front in tissue from bone resections (Elmusrati et a., 2017). To begin to explore the mechanisms underlying this observation, αSMA expression was examined in an *in vitro* model of CAF formation from normal fibroblasts and in OSCC-derived CAF.

To generate an *in vitro* model of CAF development, primary oral fibroblasts (NOF003, NOF804, and NOF822) were seeded on coverslips, serum starved (24 h), and treated with recombinant TGFβ1 (5 ng/ml), as previously described (Elmusrati et al., 2017; Mellone et al., 2017; Melling et al., 2018). After 24 h, fibroblasts were fixed, and αSMA expression and localisation examined by immunocytochemistry. Primary CAF isolated from fresh human OSCC tissue were also examined for αSMA. Primary normal oral fibroblasts, in serum free media, served as the negative control (Figure 3.16).

The myofibroblastic marker αSMA was readily detected in NOF following TGFβ1 exposure. Staining was observed as discrete fibres spanning the cell cytoplasm (Figure 3.16). αSMA staining was also evident, in a similar pattern to TGFβ1-treated NOF in CAF isolated from OSSC tissue and its localisation is in keeping with previous reports showing αSMA association with contractile stress fibres in myofibroblasts (Serini and Gabbiani, 1999; Lewis et al., 2004; Hinsley et al., 2012). However, minimal αSMA expression was seen in NOF not exposed to TGFβ1 (Figure 3.16).

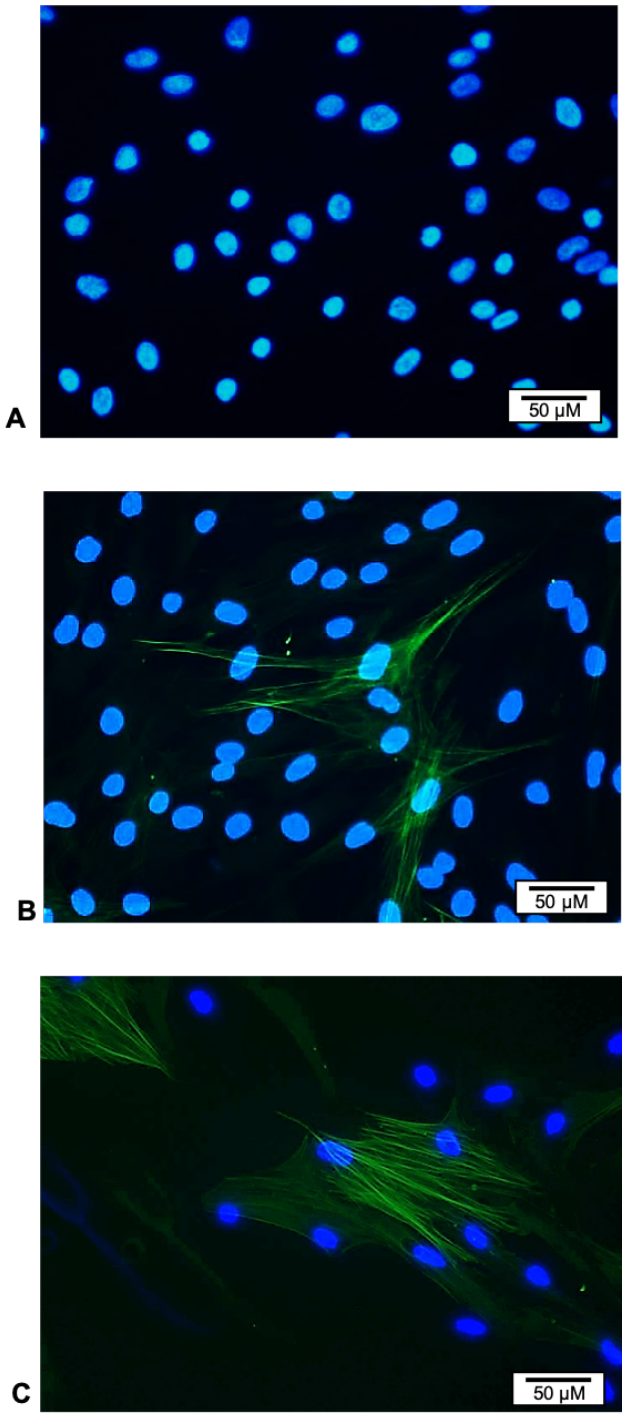

Figure 3.16: Representative photomicrographs showing cytoplasmic αSMA expression in fibroblasts using immunofluorescence (A) Negative control, oral fibroblasts in serum free media. (B) Normal human oral fibroblasts following TGF-β1 (5 ng/ml) treatment (24 h) in serum free media. (C) CAF isolated from human OSCC tissue. Myofibroblastic differentiation is evident by αSMA staining in contractile stress fibres (magnification x40).

To assess αSMA mRNA expression, RNA extracted from NOF exposed to TGFβ1, CAF isolated from human OSCC tissue, and untreated NOF (negative control) were subjected to qPCR analysis. αSMA transcript expression was significantly higher in CAF, and in NOF following TGFβ1 treatment (by 44.21 ± 2.91, and 39.13 ± 1.60 (mean fold change ± STDV) respectively) while the expression was undetectable in unstimulated NOF (Figure 3.17).

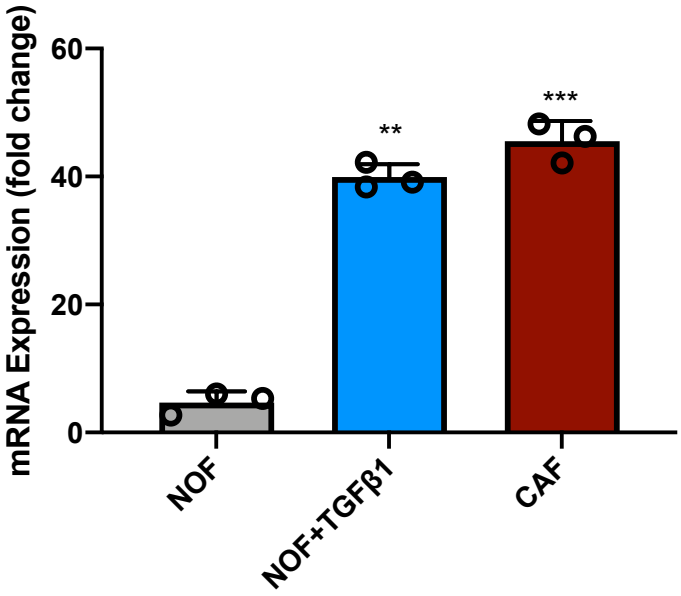

Figure 3.17: Relative expression of αSMA mRNA in normal oral fibroblasts following TGFβ1 treatment and CAF isolated from OSCC. NOF (250,000 cells/ well) were seeded in 6 well plates, serum starved (24 h), then treated with TGFβ1 (5 ng/ml) for 24 h. CAF isolated from human OSCC tissue (250,000 cells/ well) were seeded in 6 well plates, serum starved (24 h). A significant increase in αSMA mRNA was expressed with an average of 39.13 ± 1.60 (mean fold change ± STDV) following TGFβ1 exposure. αSMA expression in CAF was 44.21 ± 2.91. NOF in serum free media served as the negative control. Error bars= STDV. ** p≤0.01 and **p≤0.001, following a Student's t-test. The graph represents combined results of multiple assays. Experiment performed three times in triplicate.

3.6 OSCC derived CAF express soluble RANKL protein

We have previously shown that myofibroblasts and NOF exposed to TGFβ1 show significantly higher RANKL expression on a transcript and protein level (Elmusrati et al., 2017). To further investigate whether OSCC-derived CAF express soluble RANKL protein, CAF and NOF were serum starved (24 h), conditioned media was collected and RANKL detected by ELISA. RANKL protein expression (mean ρg/ml ± STDV) was significantly up regulated in conditioned media collected from CAF and myofibroblasts (NOF exposed to TGFβ1) (430.90 ± 13.6, p=0.004 and 323.33 ± 34.9, p=0.0008 respectively) when compared to NOF (161.04 ± 9.9) (Figure 3.18).

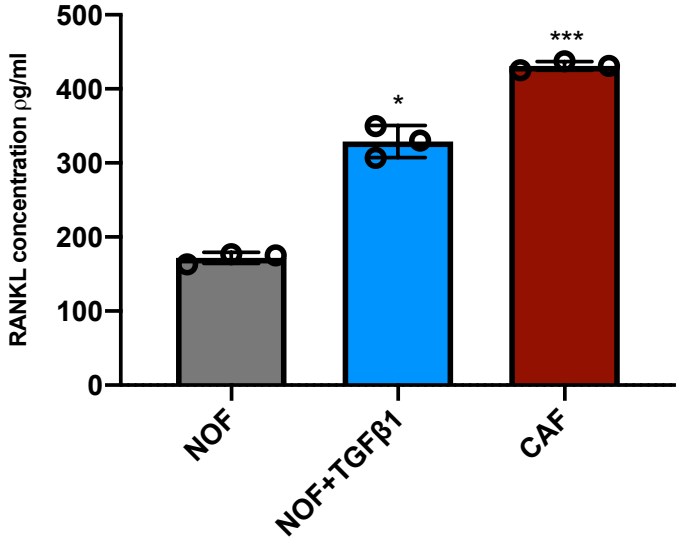

Figure 3.18: Soluble RANKL protein expression in CAF and NOF. CAF isolated from human tissue express significantly higher RANKL than NOF. 250,000 cell/ well of NOF (803, 804, and 822), and (CAF 002, 003, and 004) were seeded into 6 well plates, allowed to settle overnight, and serum starved (24 h). Conditioned media was collected and subjected to an ELISA. Error bar=STDV. The experiment was performed three times in triplicate. The increased concentration of RANKL was significantly expressed (mean ρg/ml ± STDV) in CAF (430.90 ± 13.6), myofibroblasts (323.33 ± 34.9) when compared to NOF (161.04 ± 9.9). The graph represents combined results of multiple assays. Error bars= STDV. * p≤0.05, following a Student's t-test. Experiment performed three times in triplicate.

3.7 Expression of RANKL and OPG mRNA in primary human osteoblasts

Bone remodelling is regulated by RANKL, its receptor RANK found on osteoclast precursors and the antagonist receptor OPG expressed by osteoblast. RANKL is the main marker of osteoclast activation, and only in the presence of RANKL in the tumour and surrounding microenvironment will bone destruction commence. We have previously demonstrated (Elmusrati et al., 2017) that human primary osteoblasts show significantly amplified RANKL and reduced OPG mRNA when exposed to conditioned media isolated from CAF compared to NOF.

3.7.1 CAF increase RANKL and reduce OPG expression in human primary osteoblasts on a transcript level

To evaluate the influence of human OSCC cells and CAF on RANKL and OPG expression in human primary osteoblasts, OSCC cell line H357 and primary CAF were serum starved for 24 h, followed by conditioned media treatment (24 h) of serum-starved primary osteoblasts (HOB) for 24 h. RANKL and OPG expression was quantified using a TaqMan real time qPCR assay. Media collected from primary osteoblasts in serum free DMEM, served as the negative control (Figure 3.19).

As exhibited in Figure 3.19, exposure of HOB to OSCC and CAF-derived conditioned media significantly amplified RANKL mRNA expression in primary osteoblasts. Conversely, OPG expression was significantly reduced in comparison with control. The greatest increase in RANKL (4.35 ± 1.02) (mean fold change ± STDV) ($p< 0.009$) and decrease in OPG expression (-0.21 ± 0.13) ($p<0.004$) in HOB was seen following exposure to primary CAF (conditioned

media. H357 conditioned media also increased RANKL expression (3.18 ± 0.77, p< 0.008), and reduced OPG expression (-0.37 ± 0.39, p< 0.006) in HOB

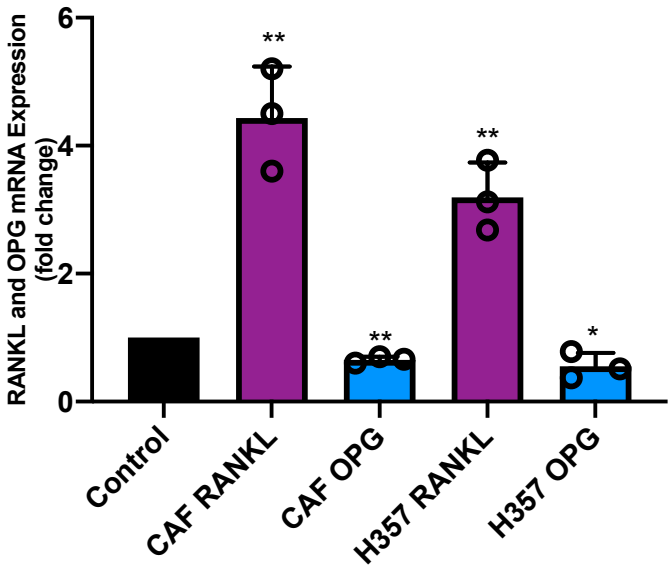

Figure 3.19: Relative expression of RANKL and OPG mRNA in HOB when cultured with CAF, and OSCC conditioned media. HOB (5 X 10^5) were indirectly co-cultured with conditioned media collected from serum starved (24 h) CAF (CAF 002, CAF 003 and CAF 004) and H357 cells. A significant increase in RANKL mRNA expression was seen when HOB were indirectly co-cultured with conditioned media from CAF (4.35 ± 1.02) (mean ± STDV) compared to control (HOB in serum free media). A significant increase was also seen following exposure of HOB to H357 conditioned media (3.18 ± 0.77) OPG mRNA expression was significantly reduced in CAF (-0.21 ± 0.13), and H357 conditioned media (-0.37 ± 0.39). Values= mean ± SD. Error bar = STDV. The graph represents combined results of multiple assays. The experiments were performed thrice in triplicates. *p<0.05 was considered significant, following a Student's t-test.

3.8 OSCC cells, experimentally induced CAF, and CAF isolated from human OSCC tissue induce osteoclastogenesis

Osteoclasts develop from the fusion of monocytic haematopoietic cells. For the differentiation of haematopoietic cells to osteoclasts the cytokines RANKL and M-CSF1 are essential. M-CSF1 promotes osteoclastogenesis by stimulating the proliferation of osteoclast precursors, while RANKL is vital for promoting differentiation of osteoclast precursors to functional osteoclasts (Teitelbaum 2000). In the presence of macrophage survival and proliferation cytokine M-CSF1, monocytes fuse to form a pre-osteoclast and in the presence of RANKL results the quiescent pre-osteoclast becoming an active osteoclast that exhibits TRAP activity and the ability to form pits in bone substrates. In this study, osteoclasts were generated from the murine macrophage cell line RAW 264.7. The advantage of using RAW 264.7 cell is that they express both M-CSF1 and its receptor c-fms, and no treatment with M-CSF1 is required (Marino et al., 2014)

After demonstrating that myofibroblastic CAF express RANKL *ex vivo* and *in vitro,* an experiment was conducted to investigate whether this expression was sufficient to initiate osteoclastogenesis.

Monocytes were seeded in Corning Osseo plates, which contain a synthetic bone substrate, serum starved, then treated with conditioned media collected from serum starved H357 cells, NOF, experimentally induced CAF (NOF treated with TGFβ1 (5 ng/ml), and primary CAF isolated from OSCC tissue, in separate wells. Media was changed daily. After 7 days, TRAP staining, pit formation assay, and nucleation, was studied (Figure 3.20).

As previously reported (Elmusrati et al., 2017), H357 cells induced osteoclastogenesis (mean number of TRAP positive cells/well ± STDV) (22.61 ± 2.30), CAF showed a significantly higher increase on osteoclast generation (51.16 ± 4.5) compared to NOF exposed to TGFβ1 (21 ± 1.35).These results were also reflected in pit forming assays (mean number of pits/ 3 high power fields ± STDV) (13 ± 3), (24 ± 3), and (14 ± 2) (Table 3.1). Multi-nucleation was also indicative of osteoclastogenesis (Figure 3.21).

Table 3.1: Osteoclastogenesis assay: quantification of TRAP positive cells and pits formed.

Sample	Total no. of TRAP positive cells (mean ± STDV, p value)	No. of pits per 3 high power fields (mean ± STDV, p value)
Negative control	0.0 ± 0.0	0.0 ± 0.0
NOF	0.0 ± 0.0	0.0 ± 0.0
NOF + TGFβ1	21 ± 1.35, p=0.0008	14 ± 3, p=0.00006
Primary CAF	51.16 ± 4.5, p=0.0001	24 ± 3, p=0.00003
H357	22.61 ± 2.30, p=0.00003	13 ± 2, p=0.00002
RANKL	33.05 ± 1.8, p=0.00007	18.2 ± 4.0, p=0.00004

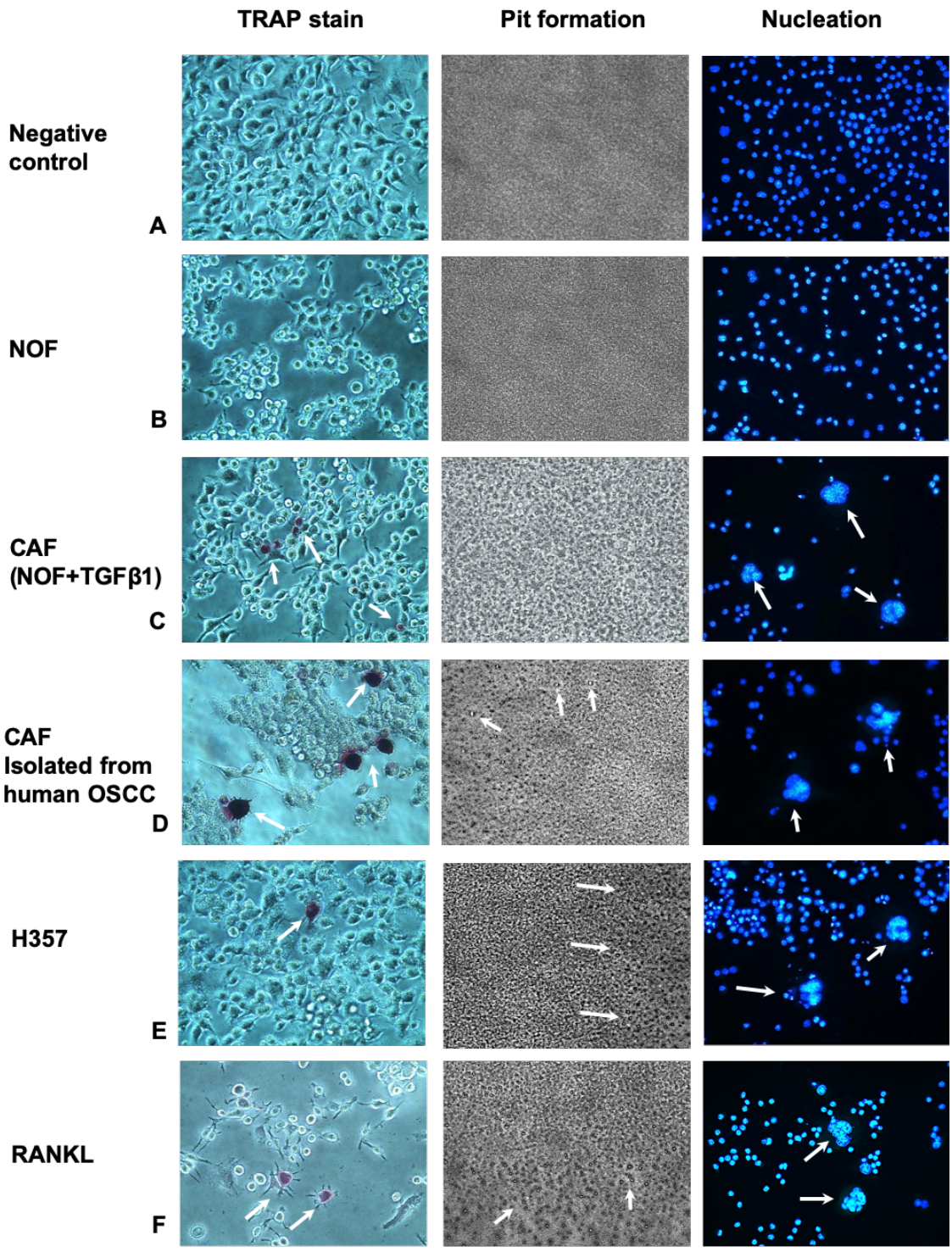
TRAP stain
Pit formation
Nucleation
Negative control
A
NOF
B
CAF (NOF+TGFβ1)
C
CAF Isolated from human OSCC
D
H357
E
RANKL
F

Figure 3.20: Osteoclastogenesis assay. Monocytes (RAW 264.7) were seeded in Osteo Assay surface 24 well plates at a density of 20,000 per well. (A) Negative control; cells were grown in serum free alpha MEM media. TRAP staining was negative, pit formation was not evident, and DAPI staining showed no multinucleated cells (B) NOF; cells were treated with conditioned media collected from serum starved NOF cells in alpha MEM media. TRAP staining was negative, pit formation was not evident, and DAPI staining showed no multinucleated cells. (C) Experimentally induced CAF; cells were treated with conditioned media collected from serum starved NOF treated with TGFβ1 (5 ng/ml) in serum free alpha MEM media. TRAP staining was observed positively staining osteoclasts, pit formation was evident, and DAPI staining showed multinucleated cells. (D) CAF isolated from human tissue; cells were treated with conditioned media collected from serum starved CAF cells in alpha MEM media. TRAP staining was observed positively staining osteoclasts, pit formation was evident, and DAPI staining showed multinucleated cells. (E) H357; Cells were treated with conditioned media collected from serum starved H357 cells in alpha MEM media. TRAP staining was observed positively staining osteoclasts, pit formation was evident, and DAPI staining showed multinucleated cells. (F) Positive control; Cells were treated with rRANKL (50 ng/ml) in serum free alpha MEM media. TRAP staining was observed positively staining osteoclasts, pit formation was evident, and DAPI nucleation showed multi-nucleated cells. Media was changed daily for 7 days. The experiment was performed three times in duplicate. Magnification x40.

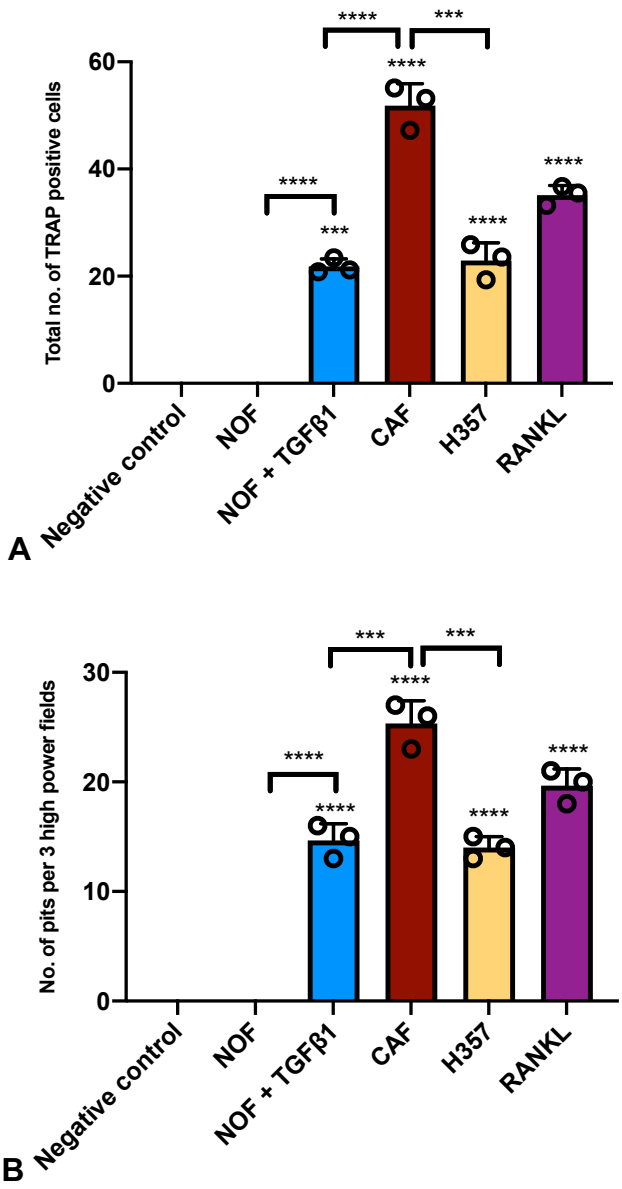

Figure 3.21: Osteoclast and pit formation quantification. The number of TRAP positive cells was counted, and the average number of osteoclasts generated were plotted. The number of pits formed due to osteoclasts in three high power fields were counted, and the average number of pits was plotted. The highest number of osteoclast (mean ± STDV) (51.16 ± 4.5) and resorption pits (24 ± 3), was noticed when conditioned media from CAF were exposed to monocytes. H357 cells induced osteoclastogenesis (22.61 ± 2.30), as well as NOF exposed to TGFβ1 (21 ± 1.35). These results were also reflected in pit forming assays (mean pits ± STDV) (14 ± 3), and (13 ± 2). Error bar = STDV. Graphs represent combined results of multiple assays. *p<0.05 was considered significant, following a Student's t-test.

3.9 Discussion

In this chapter, the mechanism of OSCC bone invasion was investigated, with particular focus on whether stromal fibroblasts cross talk with proximal bone. OSCC is heterogeneous in nature and has a tendency to invade regional anatomical structures. Due to proximity of maxillofacial bones to oral mucosa, OSCC has a high tendency to invade these structures (Nomara et al., 2005).

Marsh et al. (2011) highlighted that the presence of a myofibroblastic αSMA positive stroma in OSCC is a more sensitive predictor of disease progression and prognosis than other long standing and well-known parameters such as TNM stage (including tumour size, regional and distant metastasis), perineural or lymphovascular invasion and depth/pattern of invasion. Despite these recent findings showing the importance of stroma in OSCC, its role in bone invasive OSCC remains largely unexplored. We have previously reported that over 90% of bone invasive OSCC cases do not demonstrate direct contact between tumour cells and bone, and that αSMA positive myofibroblastic CAF are seen intervening, and infiltrating bone ahead of the tumour invasive front (Elmusrati et al., 2017). The expression of bone turnover markers (RANKL and OPG) in bone invasive OSCC and associated stroma was further investigated. Interestingly, these markers were highly expressed in both tumour and stroma in close proximity to bone suggesting a potential role of CAF in OSCC bone invasion and bone turnover.

In the current study, we aimed to determine whether there is a difference in αSMA expression, indicative of the presence of CAF, in OSCC stroma, and RANKL/OPG expression adjacent to and away from bone and whether initial diagnostic biopsies from these cases can be used to predict bone invasion. In the

cohort, αSMA expression was consistently evident in all OSCC cases, in agreement with other studies showing high prevalence of αSMA-positive CAF (Kellermann et al., 2007; Rao et al., 2014; Bussard et al., 2016). RANKL was expressed was evident in tumour cells and surrounding stroma whereas OPG staining was either weak or absent. There was no significant difference in αSMA, RANKL or OPG expression between incisional diagnostic biopsies taken from tumours with cortical resorption or cancellous bone invasion. However, this may be due to the small cohort size. Expanding the sample size to include variations in histological pattern, tumour site (maxilla / mandible), size, and overall OSCC stage, and to examine whether the intensity of expression or the location of expression whether adjacent or away from bone is of more importance, is worth exploring further.

Double IHC for bone destruction marker RANKL and myofibroblastic marker αSMA was further conducted on OSCC bone resections, to investigate whether αSMA-positive CAF express RANKL. RANKL staining was seen in fibrous stroma as well as in tumour cells in vicinity of bone. RANKL expression in OSCC stroma (Ishikuro et al., 2018) and OSCC cells (Tada et al., 2005; Kayamori et al., 2010) have been reported. These findings suggest that RANKL expression in tumour cells is related to proximity of invasive front, and the possibility that CAF adjacent to OSCC cells may be facilitating this expression.

Osteoblast regulation of osteoclastogenesis by RANKL expression is a key modulator of bone remodelling (Simonet et al., 1997). In the current study, OSCC cells were shown to upregulate RANKL and down regulate OPG in HOB (Elmusrati et al., 2017), and these results are in agreement with previous reports (Ishikuro et al., 2008). However, following identification of αSMA positive CAF

express of bone turnover markers OPG and RANKL in OSCC stroma in bone resection tissue samples, the influence of CAF on mRNA expression of bone turnover markers RANKL and OPG in primary human osteoblasts after indirect co-culture was further investigated. CAF-derived factors induced significant RANKL amplification and OPG downregulation in primary human osteoblasts. These findings show for the first time that primary CAF isolated from human OSCC, and experimentally induced myofibroblasts influence similar responses to osteoblasts, playing a functional role, promoting a more aggressive TME susceptible to bone invasion (Elmusrati et al., 2017).

Bone destruction and OSCC invasion requires complex interactions with diverse cell types, including osteoclasts, multinucleated bone resorbing cell, originating from monocyte/macrophage lineage haematopoietic precursors. It has been previously reported that the murine macrophage cell line RAW 264.7, upon exposure to RANKL, readily triggers osteoclastogenesis (Vincent et al., 2009). After demonstrating that CAF express RANKL *in vitro* and *ex vivo*, a functional assay was conducted to evaluate whether this expression was sufficient to induce osteoclastogenesis in the absence of OSCC cell or osteoblast derived RANKL. In the current study, highest osteoclast generation was noted when RAW 264.7 cells were exposed to CAF-derived conditioned media, further highlighting a possible role CAF play in OSCC bone invasion. These results were also reflected in the pit forming assay

In conclusion, this data provides novel evidence that myofibroblastic CAF play a role in bone invasion in OSCC through a RANKL-dependent pathway. The mechanistic evidence presented here provides support to the *ex vivo* observations that myofibroblastic CAF may play a role in bone invasion of OSCC,

raising the possibility that targeting CAF may be an opportunity for therapeutic intervention.

Chapter 4

Exploring the role of fibroblast senescence in bone invasion in OSCC

4.1 Introduction

Cellular senescence is a consequence of an accumulation in DNA damage whether due to replicative stress caused my telomeres shortening, or independent of telomeres length induced by exposure to elevated levels of oxidative or genotoxic stress. In spite of these cells being vital and metabolically functional, they are non-dividing cells that fail to proliferate following considerable cell division. The irreversible state of growth arrest (at G1 phase) is termed senescence, characterised by distinctive chromatin and secretome alterations, and distinctive to myofibroblasts, as senescent fibroblasts express up-regulated levels of tumour suppressor gene p16INK4a and p21 (Prime et al., 2016).

Various stimulants are responsible for fibroblasts to undergo permanent DNA damage induced as a result of oxidative stress from mitochondrial malfunction, chemo and radiotherapy as well as exhaustive mitotic activity (Di Micco et al., 2006). Senescence can be induced *in vitro* through treatment with hydrogen peroxide, anticancer therapeutics such as cisplatin, exposure to irradiation and replicative exhaustion (Rodier and Campisi, 2011; Kabir et al., 2016).

In normal physiology, senescent cells and their SASP have recently been indicated to have beneficial roles in tissue remodeling and wound healing (Storer et al., 2013; Demaria et al., 2014). However, in carcinomas, irreversible damage in cell recovery, or over exhausted DNA, results in senescence, which acts as an effective tumour suppressor. Counter-intuitively, when senescent cells accumulate in cancer, they are considered as tumour promoters, through their enhancement of neoplastic proliferation, invasion, metastasis and therapeutic resistance (Prime et al., 2016). Senescent fibroblasts express a vast range of pro-tumorigenic secretory proteins, which are jointly termed SASP (Kuilman and

Peeper, 2009; Pazolli et al., 2009). Senescence has been reported in CAF, having the ability to promote dysplastic and neoplastic cell proliferation and tumorigenesis in carcinomas (Krtolica et al., 2011; Cirri and Chiarugia, 2011; Kabir et al., 2016)

Recently, a number of senotherapeutics have emerged specifically targeting pro-apoptotic pathways eliminating senescent cell burden, these agents are called senolytics or senomorphics, which suppress SASP expression. Several recent studies have used senolytics, not to target senescent cells but due to their pro apoptotic capabilities (Zhu et al., 2015; Mertens et al., 2017) Senolytics, which target pro-survival pathways as p53/p21, Bcl-2/Bcl-XL, and PI3K/AKT or ROS-protective anti-apoptotic pathways, HSP90, when blocked result in senescent cell apoptosis. However, the inhibition of senescent cell SASP secretome can be targeted by using IɣB Kinase or JAK inhibitors as metformin and rapamycin (Niedernhofer and Robbins, 2018). Prospective concerns about the side effects and long-term consequences of senolytics must be raised. However, due to the intermittent delivery of drug, as senescent cells take a considerable amount of time to re-accumulation following clearance these concerns are diminished. In contrast, this argument cannot be made for senomorphics, which are administered in continuous levels to maintain SASP suppression.

CAF are heterogenous population of cells comprising different phenotypes (LeBleu and Kallurri, 2018; Liu et al., 2019). Previous findings in our lab have shown that a subgroup αSMA positive OSCC derived CAF show senescent characteristics (Mellone et al., 2017). In this study we sought to identify senescence in OSCC microenvironment, understand the possible contribution of

senescent CAF to bone invasion. This is of particular interest due to the number of emerging drugs targeting senescent cells.

4.1.1 Aims

To examine the different subsets of CAF, in particular the impact of senescence in tumour microenvironment of bone invasive OSCC.

4.1.2 Experimental approach

1. IHC was performed to investigate the expression of senescence markers p16INK4a, and DPP4 (CD26) in OSCC bone resections.
2. Double IHC in OSCC bone resections was conducted to investigate the co-expression of αSMA and p16INK4a.
3. Senescence was induced *in vitro*, by exposing low passage NOF to oxidative stress H_2O_2 (S-NOF^{H2O2}), chemotherapeutic drug cisplatin (S-NOF^{Cis}), and replicative stress (S-NOF^{Rep}). SA-β-Gal assays was conducted to monitor senescence.
4. Lipofuscin has been reported to accumulate in senescence cells. Histochemical stain SBB, known to react towards lipofuscin was utilised to confirm senescence induction in NOF.
5. Expression of myofibroblastic marker αSMA was determined *in vitro* using immunofluorescence.
6. CAF isolated from human OSCC tissue, and S-NOF^{H2O2}, S-NOF^{Cis}, S-NOF^{Rep} was assessed on a transcript level for senescence marker p16INK4a, SASP factor IL6, and bone turnover markers RANKL and OPG.
7. Soluble RANKL protein was examined in CAF, NOF, S-NOF^{H2O2}, S-NOF^{Cis}, and S-NOF^{Rep} using an ELISA.
8. An osteoclastogenesis assay was performed by culturing murine

monocytes (RAW 264.7) with OSCC, NOF, S-NOF^{H2O2}, S-NOF^{Cis}, S-NOF^{Rep}, and CAF conditioned media. TRAP staining, pit formation and nucleation assays was conducted to confirm osteoclastic differentiation.

9. Senescent fibroblasts were targeted by using senotherapeutics, and the impact of senolytics drugs (Alvespimycin (17-DMAG) and Navitoclax (ABT263)) on osteoclast generation was also studied.

4.2 Evaluation of senescence marker p16INK4a and DPP4 expression in *ex vivo* OSCC bone resections at tumour bone interface

Ten bone resection samples of patients with bone invasive OSSC (5 cases cortical/superficial bone resorption, and 5 cases cancellous bone involvement) were selected from the Unit archive and analysed using IHC to examine expression of senescence markers p16INK4a, and the recently described DPP4 (CD26). Following staining, the samples were scanned, and staining intensity was evaluated using HistoQuest software.

4.2.1 Expression of tumour suppressor gene p16INK4a in tumour microenvironment proximal to bone

We have previously reported that αSMA expressing cells are seen invading bone ahead of OSCC islands in over 90% of cases (Elmusrati et al., 2017). Given the recent findings from our lab that αSMA positive fibroblasts frequently show characteristics of senescence (Mellone et al., 2017), we sought to determine whether a subpopulation of the fibrous stroma was senescent.

Expression of the well-characterised senescence marker p16INK4a was first investigated. Readily detectable p16INK4a was noticed in OSCC cells, stromal cells adjacent to bone, and surrounding osteoclasts in bone resorptive areas, and

osteoblasts. The percentage of expression of positive cells ranged from 26.8% to 71.3% (Figure 4.1 and 4.2).

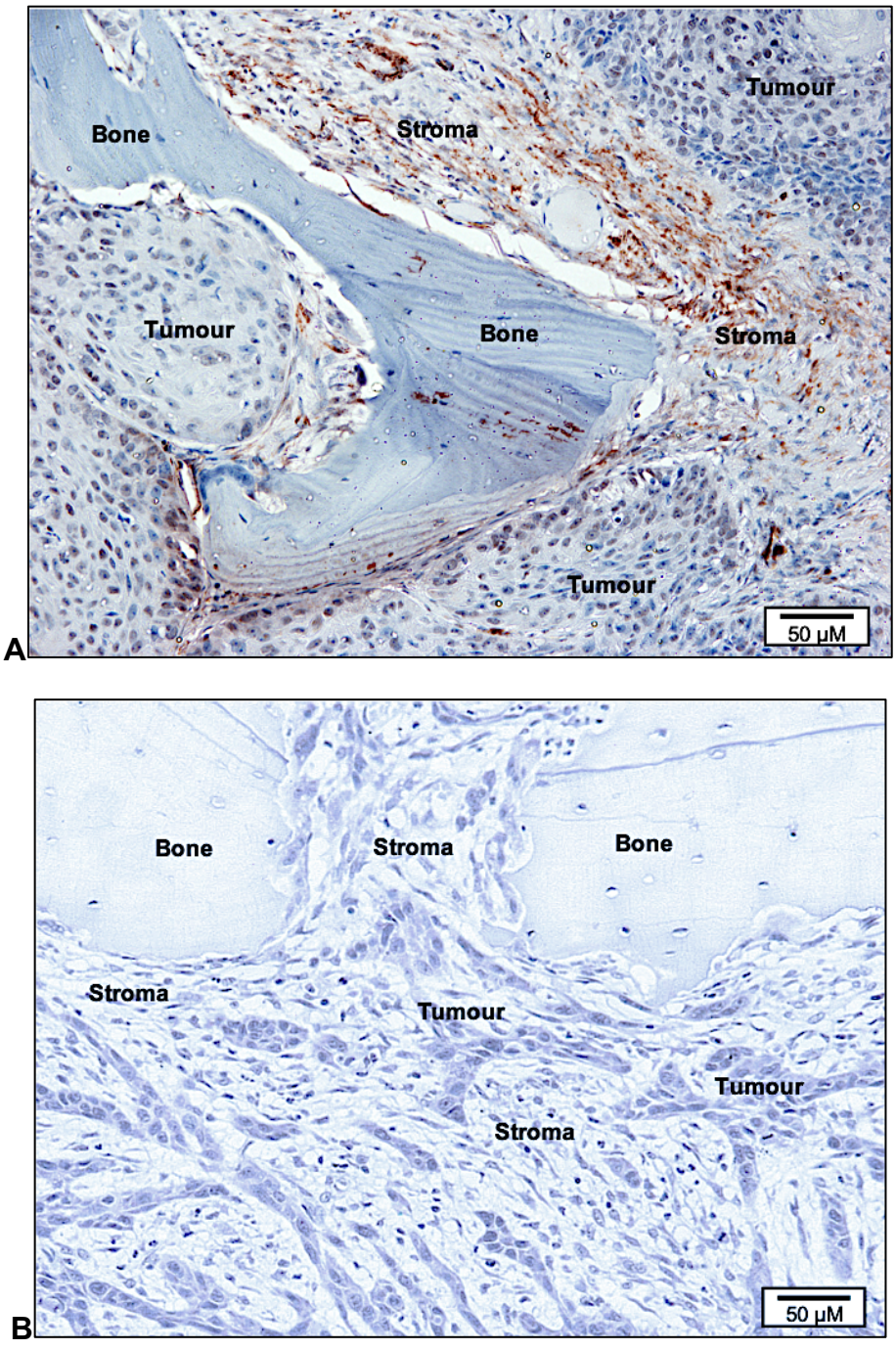

Figure 4.1: Representative photomicrographs showing IHC localisation of p16INK4a. (A) Strong p16INK4a (antibody dilution 1:100) expression in myofibroblastic stroma at the invasive tumour front (magnification x40). (B) Negative control.

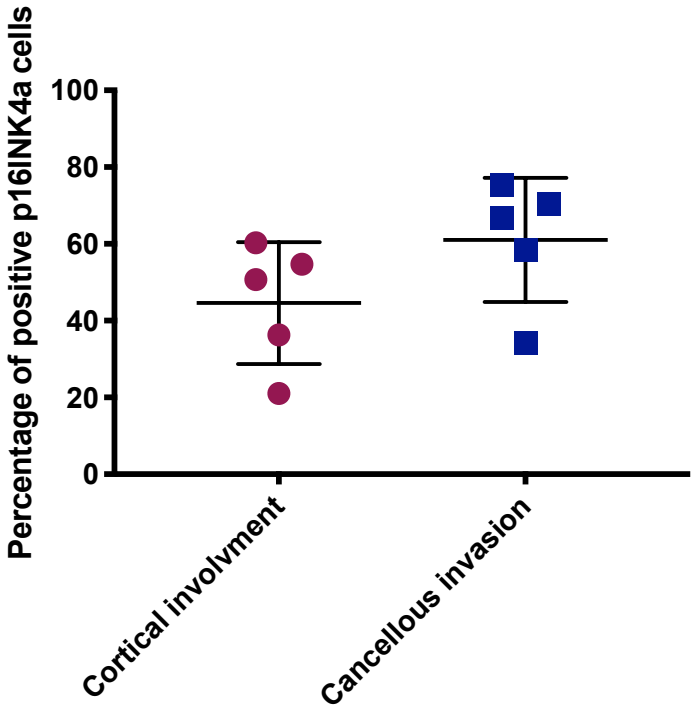

Figure 4.2: Quantification of p16INK4a expression in stromal cells of OSCC bone resections. (n=10, 5 superficial cortical resorption and 5 cancellous bone involvement). The average percentage of p16INK4a positive cells in cases with superficial bone resorption was (45.22 ± 18.96) and (60.48 ± 26.21) in cancellous invasion (mean ± STDV). Error bar = STDV.

4.2.2 Expression of senescence marker DPP4 (CD26) in tumour microenvironment proximal to bone

To further confirm the presence of senescent cells in the microenvironment of tumour bone interface an additional cell surface senescent marker, DPP4, was also examined. Recently, following mass spectrometry analysis of senescent fibroblasts, DPP4 was reported to be expressed by senescent but not proliferating fibroblasts (Kim et al., 2017).

DPP4 expression was observed in OSCC cells and fibroblasts near bone resorptive sites. The percentage of cells expressing DPP4 ranged from 21.7%, with the highest percentage of positive expressing cells being 64.05%, and a mean expression of 48.31% (Figure 4.3 and 4.4).

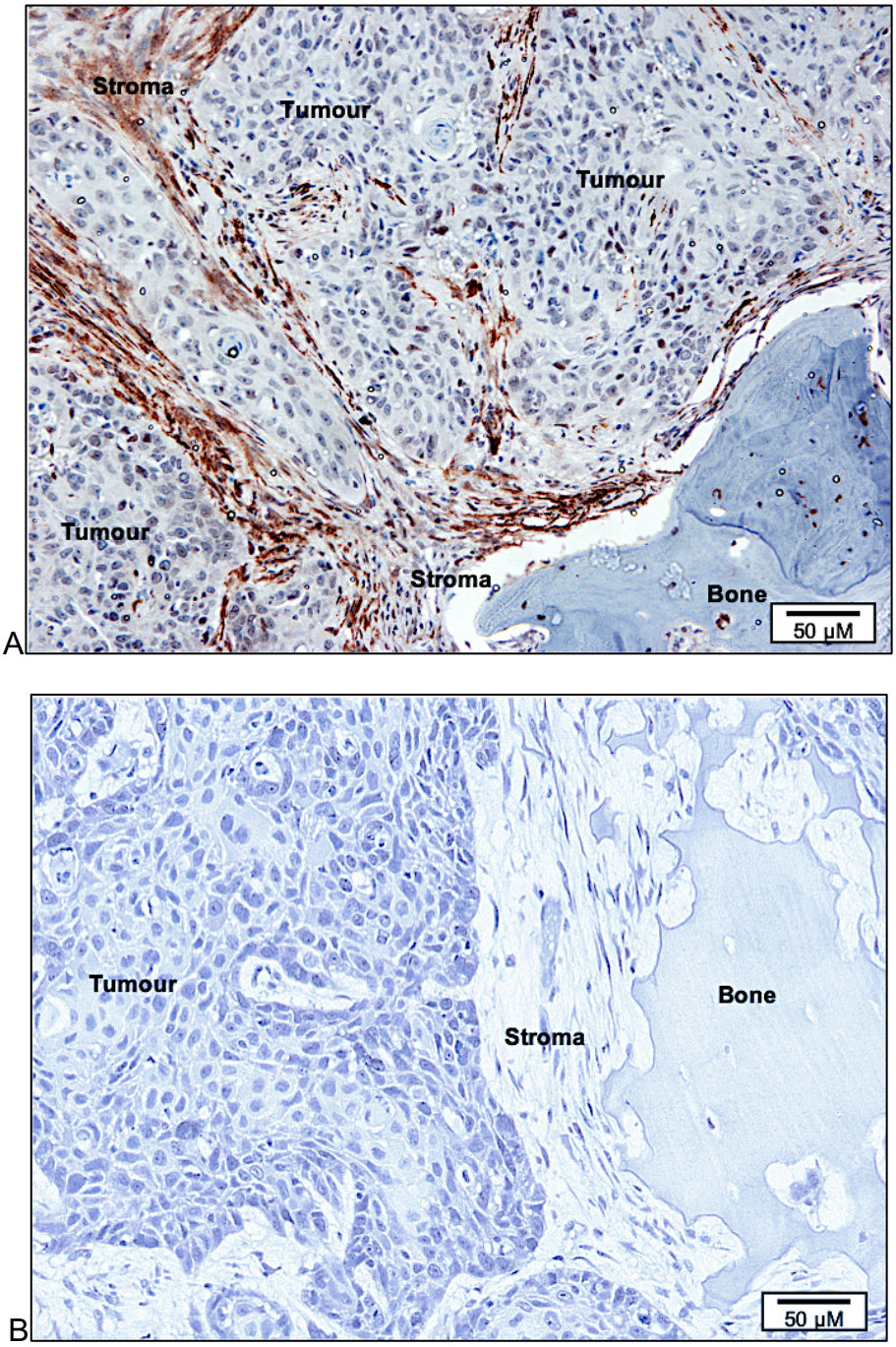

Figure 4.3: Representative photomicrographs showing IHC localisation of DPP4. (A) Strong DPP4 (antibody dilution 1:100) expression in myofibroblastic stroma at the invasive tumour front (magnification x 40). (B) Negative control.

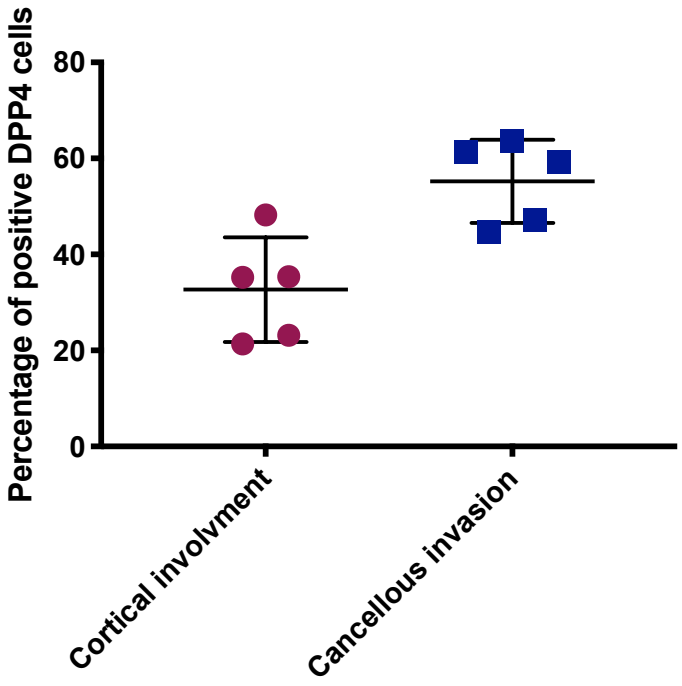

Figure 4.4: Quantification of DPP4 expression in stromal cells in OSCC bone resections (n=10, 5 superficial cortical resorption and 5 cancellous bone involvement). The average percentage DPP4 positive cells in cases with superficial cortical bone resorption was (33.22 ± 18.96) and (57.48 ± 26.21) in cancellous invasion (mean ± STDV). Error bar = STDV.

4.3 Senescent fibroblasts exhibit contractility features through the expression of αSMA in tumour microenvironment proximal to bone

Following identification that CAF in OSCC fibrous stroma express myofibroblastic marker αSMA and senescence by p16INK4a expression through single staining IHC, double immunohistochemical analyses of αSMA and senescent marker p16INK4a was carried out to assess whether myofibroblastic CAF are also senescent. Matching cases of OSCC with bone involvement were selected as described previously. Our data shows that a large proportion of myofibroblastic CAF also show senescent characteristics. Senescence was also evident in tumour cells (Figure 4.5).

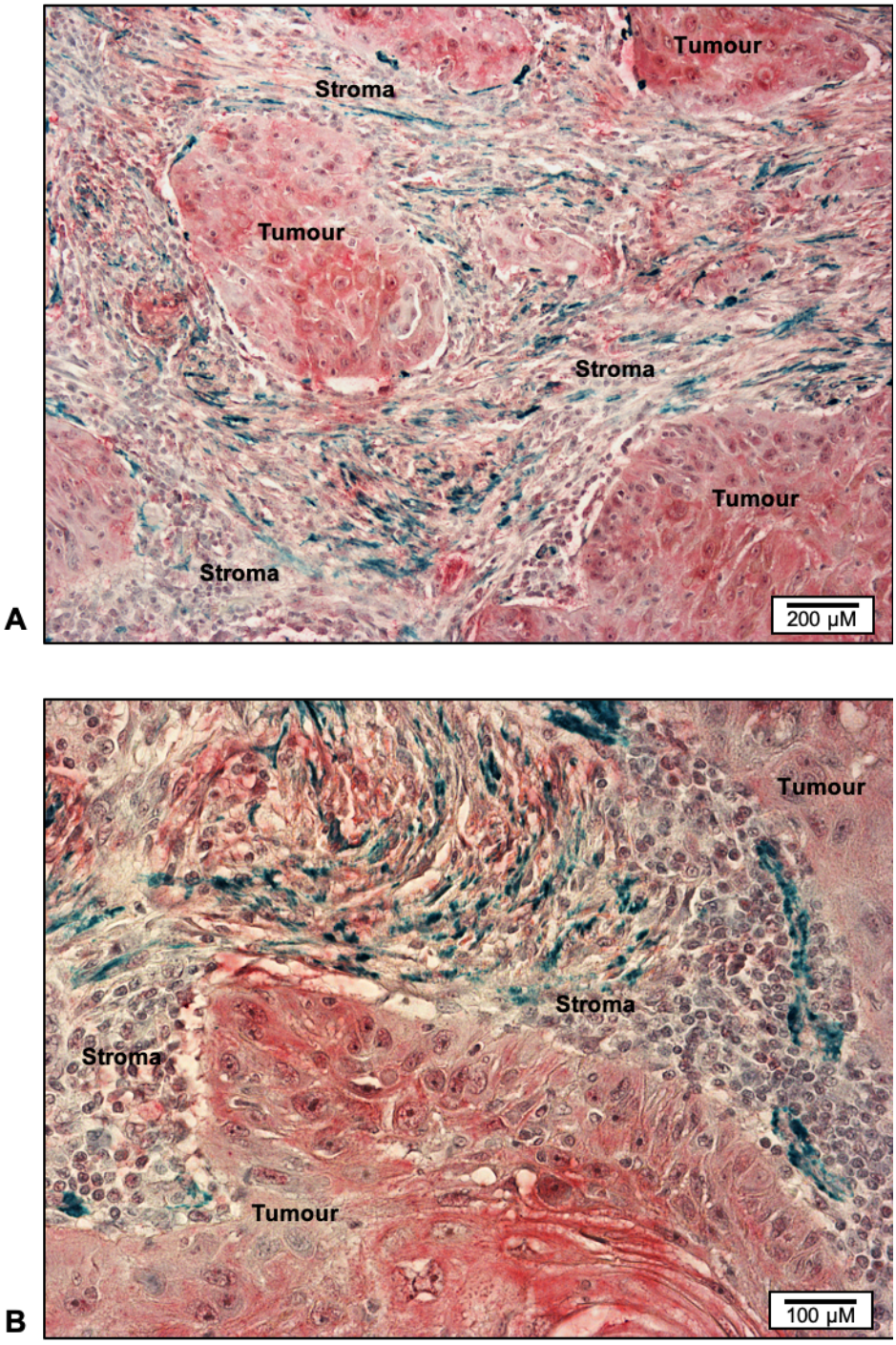

Figure 4.5: Representative photomicrographs showing IHC co-localisation of αSMA (Green) and p16INK4a (Red). αSMA (antibody dilution 1:100) expression (green stain) in myofibroblastic stroma at the invasive tumour front. p16INK4a expression (red) in tumour as well as SMA positive cells in tumour stroma. Co-localization of αSMA and p16INK4a was evident in fibrous tumour stroma (blue).

4.4 Characterisation of induction of senescence *in vitro*

Following identification that stromal cells in bone invasive OSCC tissue express senescent characteristics ex vivo, senescence induction in NOF was conducted *in vitro* to investigate the potential functionality of senescent CAF in OSCC bone invasion. This assay was performed to verify whether senescence could be induced in oral fibroblasts (DENF 316, NOF803, NOF804, NOF822) subjected to oxidative stress, exposed to chemotherapeutic drugs or replicative mitotic exhaustion, by utilising β-galactosidase as a biomarker. The following abbreviations will be used (S-NOF^{H2O2}, S-NOF^{Cis}, and S-NOF^{Rep}) to denote the associated conditions (Table 4.1).

Table 4.1: Abbreviations used for different senescence induction methods

Types of senescence induction	Abbreviation
Exposure of NOF to oxidative stress (500 μM H_2O_2 for 2 h)	S-NOF^{H2O2}
Exposure of NOF to genotoxic stress (10 μM cisplatin for 24 h)	S-NOF^{Cis}
Exposure of NOF to replicative stress (passage 25)	S-NOF^{Rep}

Cells were seeded (10,000/well) in a 12 well plate and stained with X-gal solution. A blue precipitate was evident in senescent fibroblasts following the overnight incubation (Figure 4.6). The percentage of blue stained cells resulting from lysosomal galactosidase cleavage of X-gal chromogenic substrate was quantified. The highest percentage of senescent cells was detected in S-NOF^{Rep} (78.04 ± 8.3, p=0.00003), followed by S-NOF^{H2O2} (64.21 ± 5.6,

p=0.00005), S-NOF^{Cis} (57.03 ± 3.8, p=0.00007), and CAF (31.89 ± 7.9, p=0.00009) (mean ± STDV) (Figure 4.7).

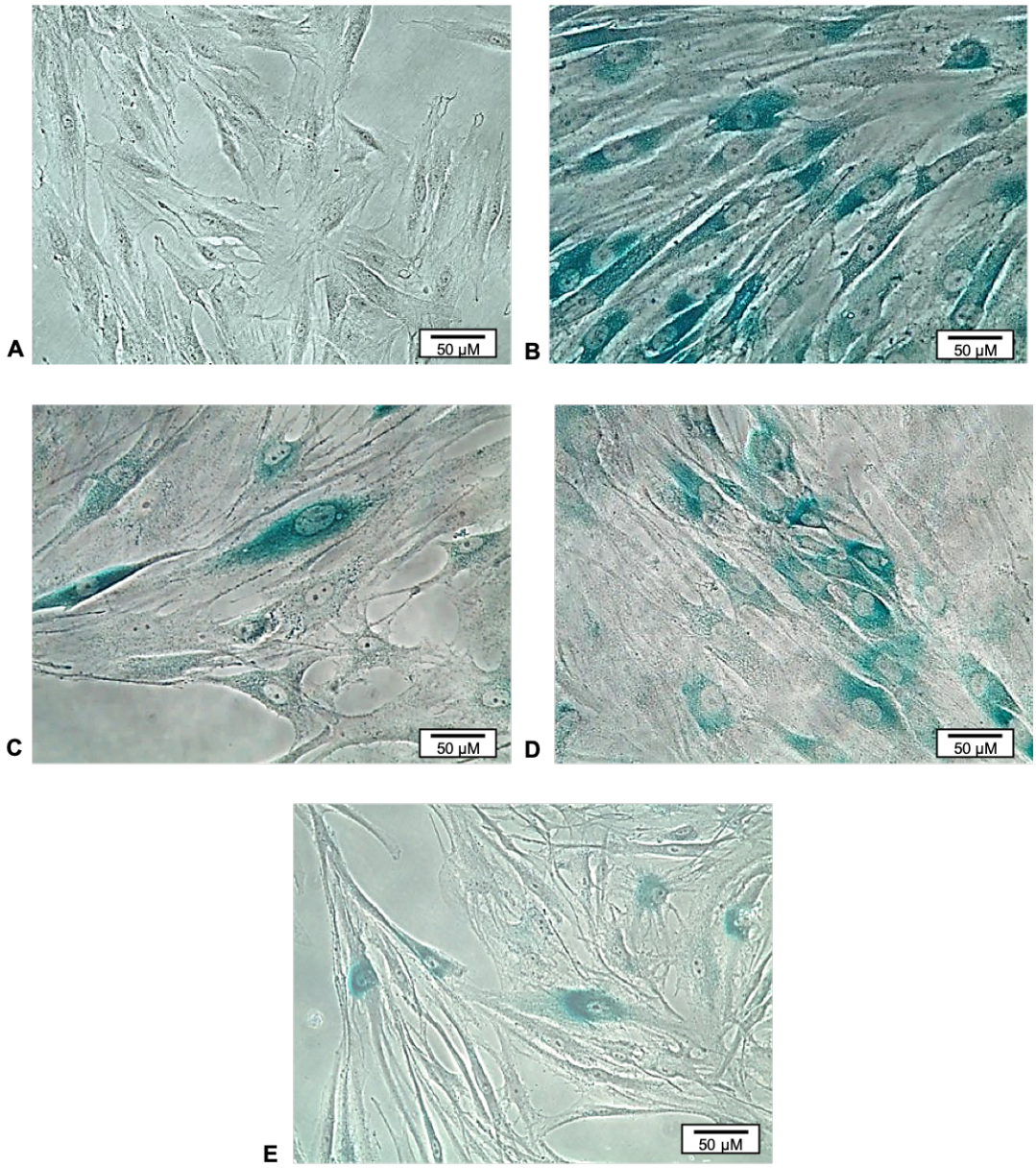

Figure 4.6: Representative photomicrographs of SA-β-Gal detection in NOF following exposure to different senescence inducers. Primary oral fibroblasts exposed to H_2O_2, cisplatin or replicative mitotic exhaustion were seeded into a 12 well plate at a density of 10,000 cells/well. On the following day, cells were rinsed in PBS, fixated, and stained with X-gal staining solution (24 h). (A) NOF (803, 804 and 822) not subjected to oxidative stress served as a negative control (magnification x20). (B) Senescent fibroblasts following H_2O_2 exposure produced a blue/turquoise precipitate. (C) Senescent fibroblasts following cisplatin exposure. (D) Senescent fibroblasts following replicative exhaustion. (E) Primary CAF (002, 003, and 004) isolated from human tumour tissue also showed senescence.

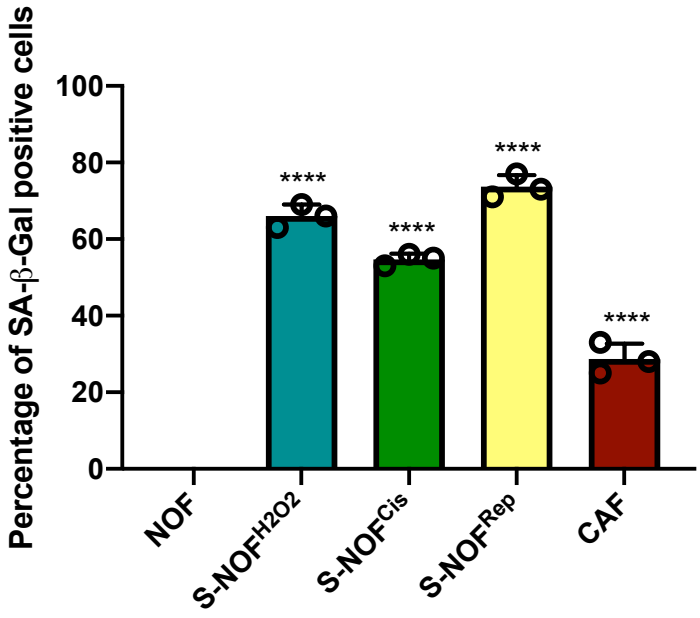

Figure 4.7: Quantification of SA-β-Gal positive cells. The number of stained cells (blue precipitate) in 3 high power fields (magnification x40) after SA-β-Gal assay was conducted. The highest percentage of senescence was seen when NOF were subjected to replicative exhaustion (passage 25) S-NOF^{Rep} (78.04 ± 8.3), followed by S-NOF^{H2O2} (64.21 ± 5.6), S-NOF^{Cis} (57.03 ± 3.8), and CAF (31.89 ± 7.9) (mean ± STDV). Experiment conducted three times in triplicate. *p<0.05 was considered significant, following a Student's t-test. Error bar = STDV.

4.5 Primary oral fibroblasts express Sudan B Black *in vitro* after experimental senescence induction

Sudan B Black has been recently identified as a biomarker of senescence, specifically staining lipofuscin, which distinctively accumulates in senescent cells (Georgakopoulou et al., 2013). As there is no single specific marker to detect senescence, Sudan B Black histochemical staining was performed to further support the findings from the SA-β Gal assay (Figure 4.8). The percentage of SBB stained (black deposits) cells was quantified. The highest percentage of positive cells was noticed in S-NOF^{H2O2} (61.66 ± 3.4, p=0.00009), followed by S-NOF^{Cis} (54.21 ± 6.0, p=0.00076), and CAF (28.97 ± 8.3, p=0.00083) (mean ± STDV, p value) (Figure 4.9).

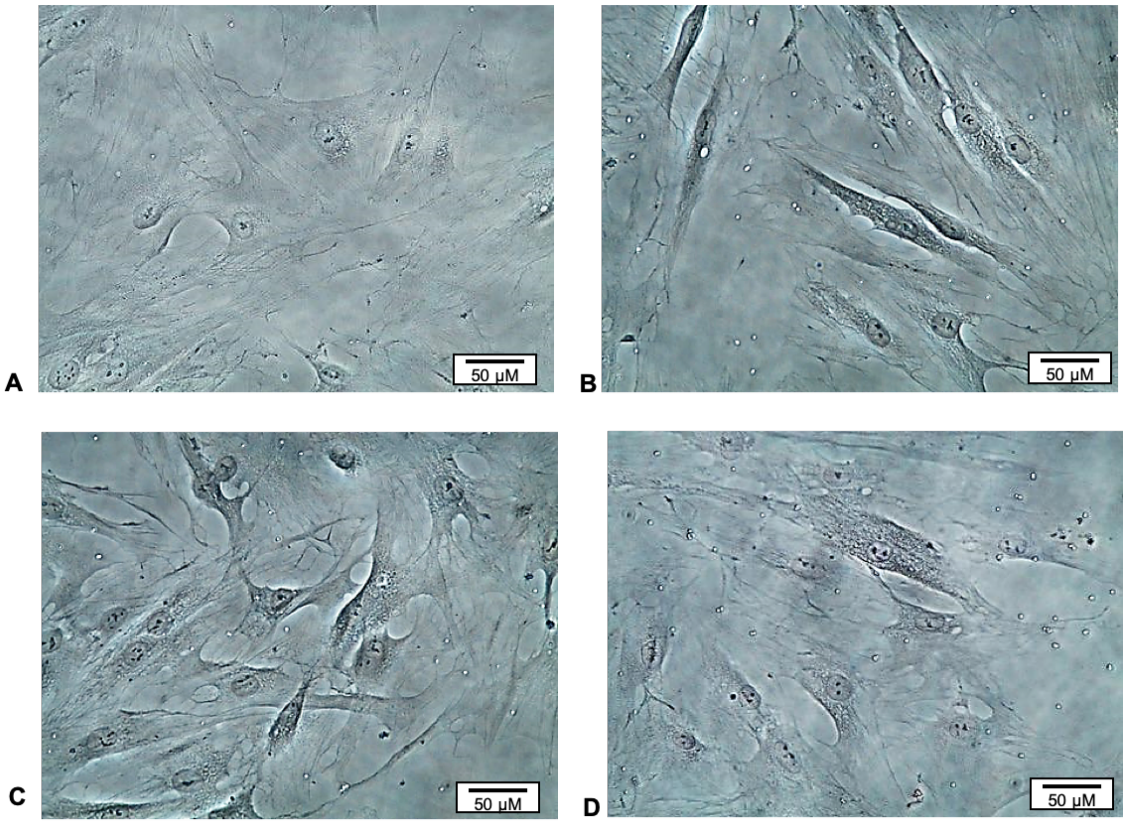

Figure 4.8: Representative photomicrographs showing Sudan B Black histochemical staining in response to different senescence inducers. Primary oral fibroblasts exposed to H_2O_2, cisplatin or replicative mitotic exhaustion were seeded into a 12 well plate at a density of 10,000 cells/well. On the following day, cells were rinsed in PBS, fixated, and stained Sudan B Black stain (2 h). (A) NOF (803, 804, and 822) not subjected to oxidative stress served as a negative control (magnification x20). (B) NOF following H_2O_2 exposure produced a black granular precipitate. (C) NOF following cisplatin exposure. (D) Primary CAF (002, 003, and 004) isolated from human tumour tissue showing evidence of senescence. This experiment was performed three times in triplicate. (magnification x40).

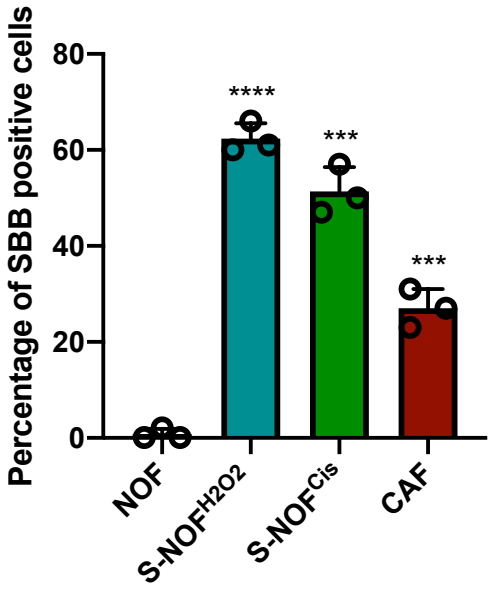

Figure 4.9: Quantification of SSB positive cells. The number of stained cells (black precipitate) in 3 high power fields (magnification x40) was counted and the percentage of stained cells calculated following Sudan B Black staining. The highest percentage of positive cells was noticed in S-NOF^{H2O2} (61.66 ± 3.4, p=0.00009), followed by S-NOF^{Cis} (54.21 ± 6.0, p=0.00076), and CAF (28.97 ± 8.3, p=0.00083) (mean ± STDV, p value) Error bar = STDV. *p<0.05 was considered significant, following a Student's t-test. Experiment conducted three times in triplicate.

4.6 mRNA expression of p16INK4a and SASP factor IL6 is significantly higher in senescent fibroblasts

Senescent fibroblasts S-NOF^{H2O2}, S-NOF^{Cis}, S-NOF^{Rep} and primary CAF were tested for their expression of p16INK4a, and IL6. qPCR analysis of p16INK4a and IL6 was performed to detect and quantify senescence on a transcript level. These results were compared to primary normal oral fibroblasts, which served as a negative control. Significant amplification in senescent marker p16INK4a and IL6 expression was observed in senescent fibroblasts, and CAF. The increased fold change of p16INK4a was observed as follows, S-NOF^{H2O2} (4.1 ± 2.04, p=0.006), S-NOF^{Cis} (6.30 ± 0.13, p=0.0008), S-NOF^{Rep} (7.43 ± 1.88, p=0.0004), and CAF (3.14 ± 1.7, p=0.005) (mean ± STDV, p value) (Figure 4.10 A). Moreover, IL6 expression was S-NOF^{H2O2} (15.3 ± 2.08, p=0.03), S-NOF^{Cis} (24.5 ± 3.52, p=0.002), S-NOF^{Rep} (24.43 ± 1.88, p=0.0006), and CAF (22.56 ± 2.7, p=0.00034) (Figure 4.10 B).

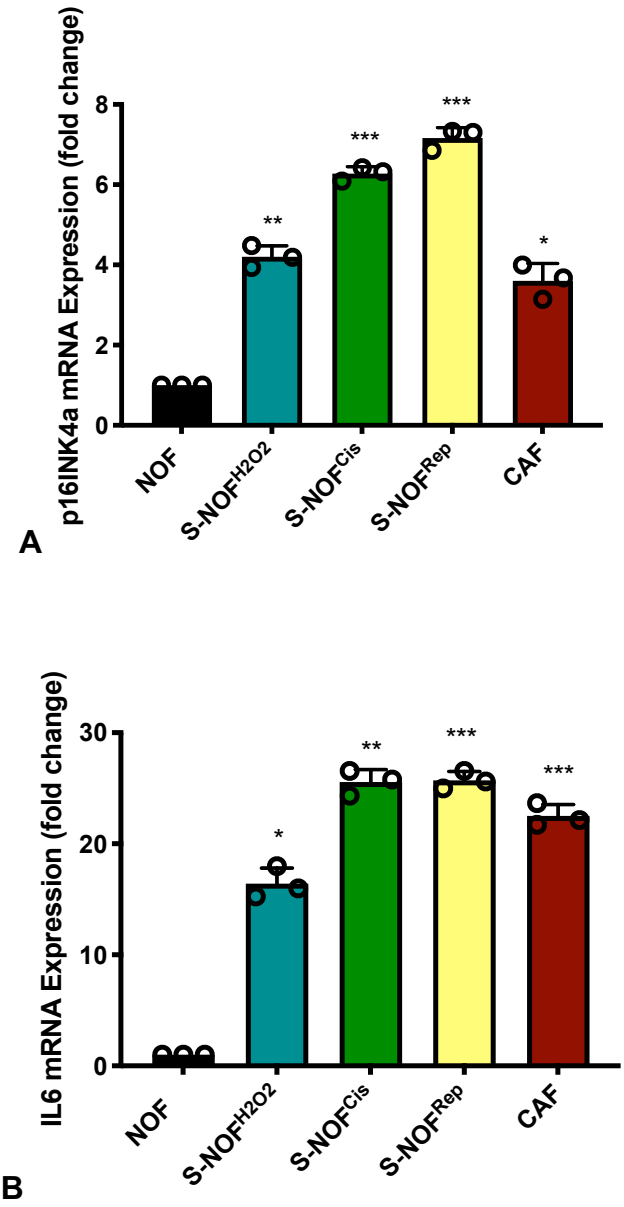

Figure 4.10: Relative expression of p16INK4a and IL6 mRNA in senescent oral fibroblasts. mRNA expression of senescent marker (A) p16INK4a and (B) IL6 in senescent NOF (NOF803, NOF804, and NOF822) was significantly amplified, following exposure of low passage NOF (passage 5) to H_2O_2 (500 μM) for 2 h, cisplatin (10 μM) for 24 h, or exposure to replicative mitotic exhaustion (passage 25). (A) The increased fold change of p16INK4a was observed as follows, S-NOF^{H2O2} (4.1 ± 2.04, p=0.006), S-NOF^{Cis} (6.30 ± 0.13, p=0.0008), S-NOF^{Rep} (7.43 ± 1.88, p=0.0004), and CAF (3.14 ± 1.7, p=0.005) (mean ± STDV, p value). (B) IL6 expression, S-NOF^{H2O2} (15.3 ± 2.08, p=0.03), S-NOF^{Cis} (24.5 ± 3.52, p=0.002), S-NOF^{Rep} (24.43 ± 1.88, p=0.0006), and CAF (22.56 ± 2.7, p=0.00034) Data represented n=3, ± STDV *p<0.05 was considered significant, following a Student's t-test. Error bar = STDV.

4.7 Experimentally induced senescent fibroblasts express stromal marker αSMA

Following SA-β-Gal and SBB staining, and senescent marker p16INK4a expression confirming senescent induction, senescent oral fibroblasts S-NOF^{H2O2}, and S-NOF^{Cis}, were seeded on coverslips and analysed for intracellular αSMA (dilution 1:100) expression using a FITC-conjugated antibody. These results show that senescent fibroblasts also exhibit myofibroblastic characteristics as αSMA expression was evident in contractile stress fibres (Figure 4.11 A and B). These findings were further compared to experimentally induced myofibroblasts following TGFβ1 stimulation (Figure 4.11 C), and primary oral CAF isolated from human tissue (Figure 4.11 D) which showed similar results. Expression in proliferating normal oral fibroblasts was not detectable (Figure 4.11 E).

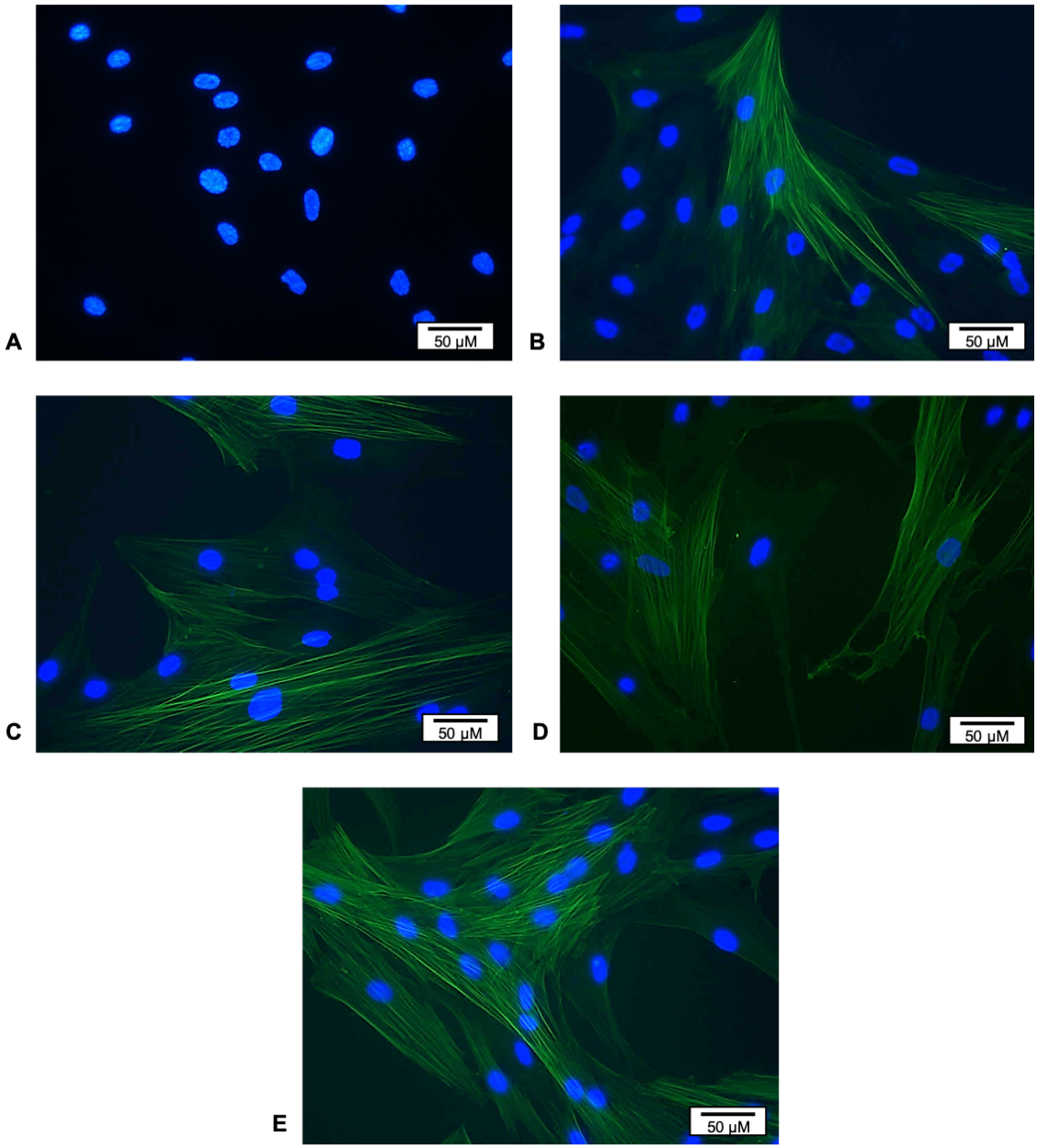

Figure 4.11: Representative photomicrographs showing immunofluorescence detection of αSMA (1:100) αSMA evident staining in contractile stress fibres in normal human oral fibroblasts following (A) Negative control, oral fibroblasts (NOF 803, 804) in serum free media. (B) NOF (803, 804) exposure to H_2O_2 (500µM, 2 h) (C) NOF (803, 804) exposure to cisplatin (10 µM, 24 h) (D) TGFβ1 (5 ng/ml) treatment (24 h) in serum free media. (E) CAF (003) isolated from human OSCC tissue. (magnification x40).

4.8 Senescent oral fibroblasts express RANKL a transcript and protein

We have previously demonstrated that myofibroblasts (NOF exposed to TGFβ1) and primary CAF isolated from human tumour tissue express significantly higher levels of the bone turnover marker RANKL compared to primary NOF (Elmusrati et al., 2017).

To investigate whether experimentally induced senescent fibroblasts produce bone turnover marker RANKL and OPG on a transcript level and soluble RANKL protein level in culture, senescent fibroblasts S-NOF^{H2O2}, S-NOF^{Cis}, S-NOF^{Rep} and primary CAF were examined. RANKL mRNA was significantly amplified (S-NOF^{H2O2} (5.8 ± 1.14, p=0.01), S-NOF^{Cis} (3.70 ± 1.83, p=0.013), S-NOF^{Rep} (5.87 ± 1.23, p=0.001), and CAF (8.84 ± 0.97, p=0.00051) (mean ± STDV, p value) (Figure 4.12 A), while a significant downregulation of RANKL decoy receptor OPG was observed (S-NOF^{H2O2} (-0.5 ± 0.64, p=0.017), S-NOF^{Cis} (-0.30 ± 0.15, p=0.0042), S-NOF^{Rep} (-0.53 ± 0.48, p=0.0055), and CAF (-0.42 ± 0.7, p=0.0044) (Figure 4.12 B).

For soluble RANKL protein detection, on day 5, 10 and 15 following treatment, S-NOF^{H2O2} and S-NOF^{Cis} were serum starved (24 h), conditioned media was collected and subjected to an ELISA. RANKL expression in S-NOF^{Rep} (passage 25) was also examined. RANKL protein expression was significantly up regulated in conditioned media collected from S-NOF^{H2O2} after 5 days, and this expression increased following 10 and 15 days (220 ± 3.10, p=0.05, 311 ± 4.2, p=0.002, and 356 ± 4.01, p=0.0006 respectively) (mean ρg/ml ± STDV, p value). However, for S-NOF^{Cis} a significant RANKL expression was only noticed following 15 day of cisplatin exposure (338 ± 2.02, p=0.002). Moreover, primary CAF and S-NOF^{Rep}

demonstrated a significant RANKL expression (497 ± 8.03, p=0.0002 and 366 ± 4.11, p=0.00011 respectively) when compared to NOF media (Figure 4.13).

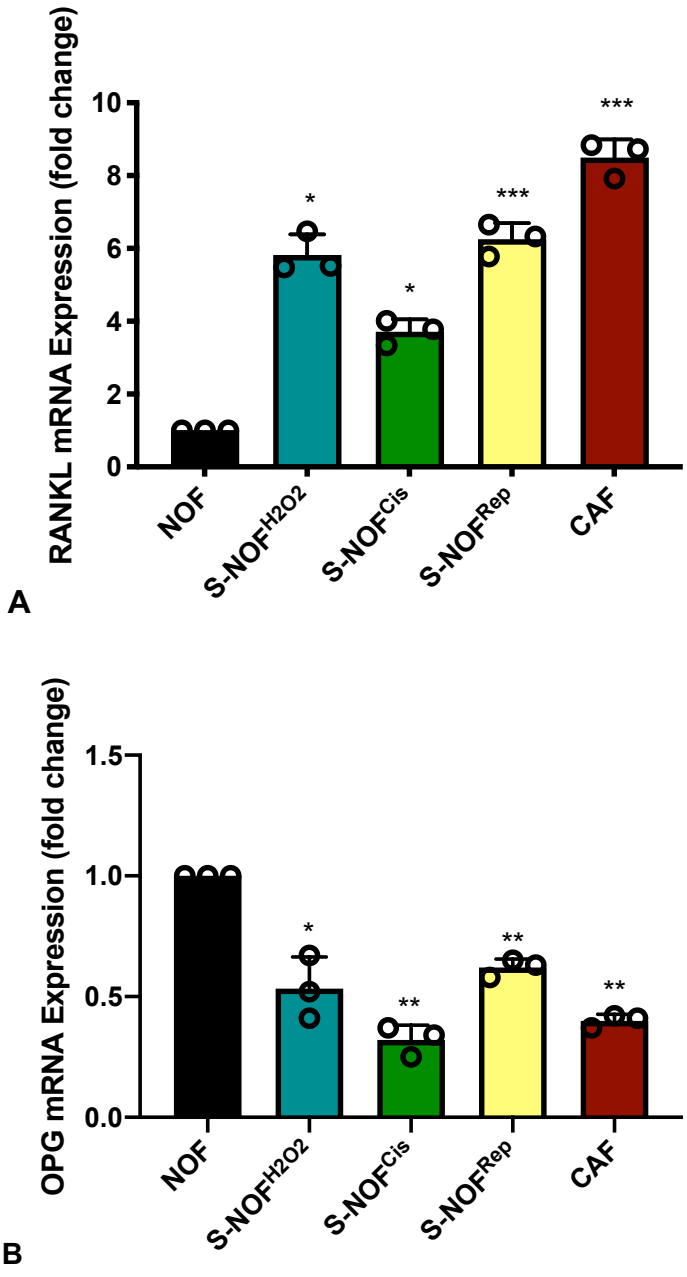

Figure 4.12: Expression of mRNA RANKL and OPG in senescent oral fibroblasts. mRNA expression of bone turnover markers (A) Significant RANKL and (B) Significant OPG downregulation was observed in senescent NOF (NOF803, NOF804, and NOF822), which was significantly increased, following exposure of low passage NOF (passage 5) to H_2O_2 (500 μM) for 2 h, cisplatin (10 μM) for 24 h, or exposure to replicative mitotic exhaustion (passage 25). Data represented n=3, ±SD *p<0.05 was considered significant, following a Student's t- test. Error bar = STDV.

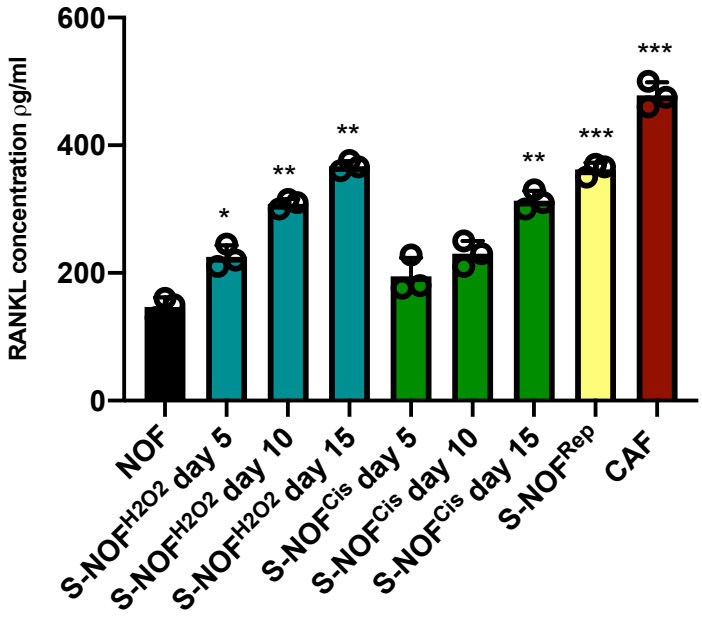

Figure 4.13: Expression of soluble RANKL protein in senescent oral fibroblasts. Senescent oral fibroblasts express significantly higher RANKL protein than unstimulated NOF. Highest levels of RANKL seen following 15 days of genotoxic exposure, and in non-proliferative NOF (passage 25). 500,000 senescent fibroblasts were seeded in T75 plates and allowed to settle overnight. The fibroblasts were subjected to oxidative stress by treating the cells with H_2O_2 (500 μM) for 2 h or exposure to chemotherapeutic agent cisplatin (10 μM) for 24 h. Conditioned media (day 5, 10 and 15 respectively) was collected from serum starved fibroblasts (24 h) and subjected to an ELISA. RANKL expression in replicative mitotic exhausted oral fibroblasts (passage 25) was also examined. Conditioned media from serum starved (24 h) NOF served as a negative control. A significant amplification in RANKL expression was noticed after day 10. Data represent n=3 ± SD. *$p<0.05$ was considered significant, following a Student's t-test. Error bar = STDV. Experiment conducted three times in triplicate. The graph represents combined results of multiple assays.

4.9 Senescent oral fibroblasts induce osteoclastogenesis

Following induction and assessment of senescence and demonstrating that senescent fibroblasts secrete elevated levels of RANKL protein compared to proliferating cells, an osteoclastogenesis assay was performed to study whether these cells had the ability to initiate osteoclast generation. RAW 264.7 cells were seeded on Corning Osseo plates, serum starved, then treated with conditioned media collected from serum starved S-NOF^{H2O2}, S-NOF^{Cis}, S-NOF^{Rep}, OSCC-derived CAF, and NOF, in separate wells. Media was changed daily. After 7 days, TRAP staining, pit formation, and nucleation was studied (Figure 4.14).

Following exposure of monocytes to conditioned media collected from senescent oral fibroblasts and primary CAF isolated from human OSCC tissue, TRAP staining was positive S-NOF^{H2O2} (32 ± 2, p=0.0002), S-NOF^{Cis} (26 ± 3, p=0.004), S-NOF^{Rep} (34 ± 5, p=0001) and CAF (37 ± 2, p=0.00006) (mean ± STDV, p value), the ability of the cells to form resorptive pits S-NOF^{H2O2} (18 ± 4, p=0.008), S-NOF^{Cis} (13 ± 3, p=0.0005), S-NOF^{Rep} (16 ± 4, p=0.0002) and CAF (21 ± 6, p=0.0001) (Table 4.2) in the bone scaffold lining , as well as multinucleation was also evident further confirming osteoclast formation. However, when monocytes were exposed to conditioned media collected from serum starved NOF, osteoclastogenesis was not seen, in keeping with data in Chapter 3 (section 3.8). Monocytes in serum free alpha MEM media served as a negative control (Figure 4.15).

Table 4.2: Quantification of TRAP positive cells and pits formed.

Sample	Total no. of TRAP positive cells (mean ± STDV, p value)	No. of pits per 3 high power fields (mean ± STDV, p value)
Negative control	0.0 ± 0.0	0.0 ± 0.0
NOF	0.0 ± 0.0	0.0 ± 0.0
S-NOF^{H2O2}	32 ± 2, p=0.0002	18 ± 4, p=0.008
S-NOF^{Cis}	26 ± 3, p=0.004	13 ± 3, p=0.0005
S-NOF^{Rep}	34 ± 5, p=0001	16 ± 4, p=0.0002
CAF	37 ± 2, p=0.00006	21 ± 6, p=0.0001

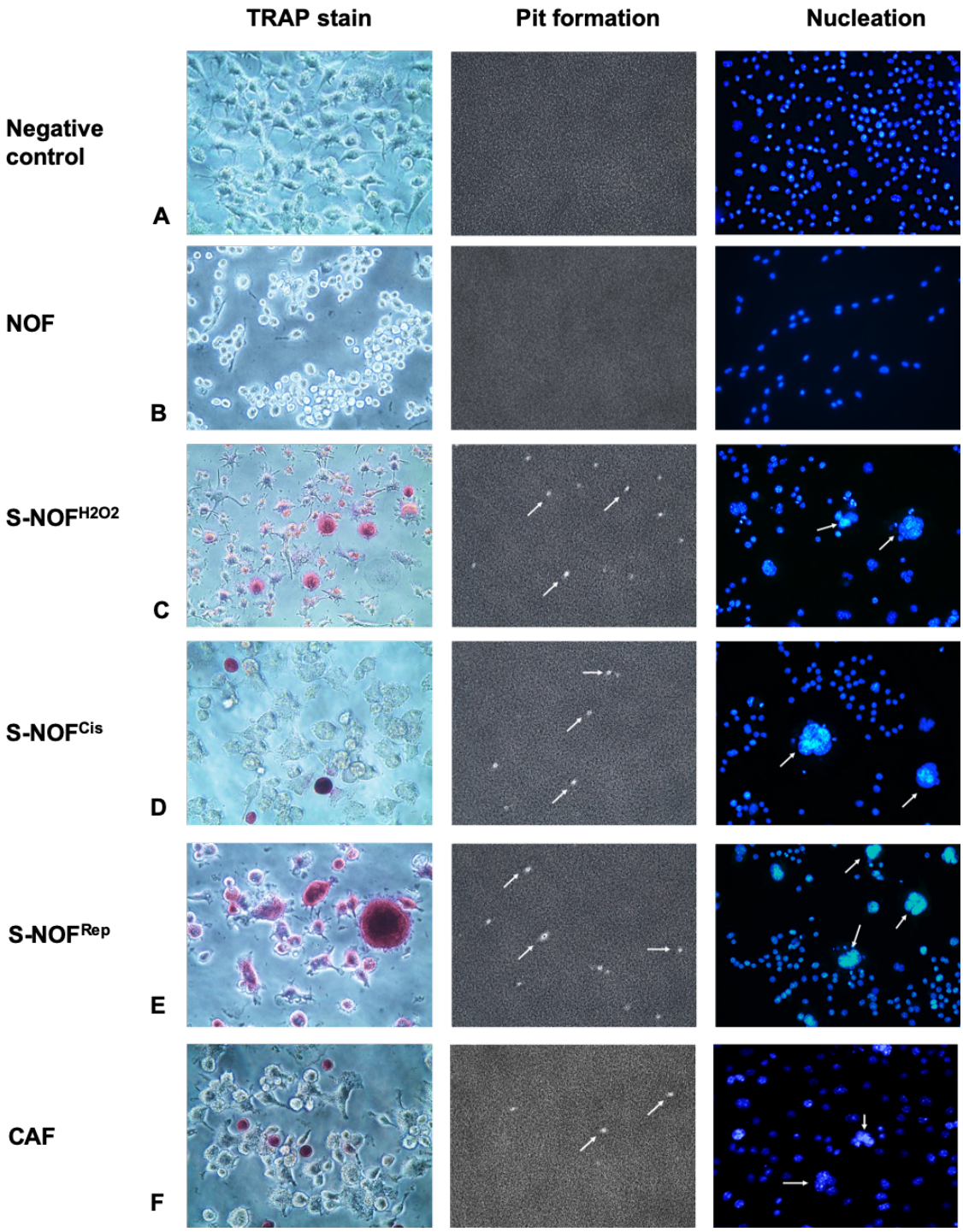
TRAP stain
Pit formation
Nucleation
Negative control
A
NOF
B
S-NOF^{H2O2}
C
S-NOF^{Cis}
D
S-NOF^{Rep}
E
CAF
F

Figure 4.14: Osteoclastogenesis assay. Monocytes (RAW 264.7) were seeded in Osteo Assay surface 24 well plates at a density of 20,000 per well. Cell were serum starved in alpha MEM media, media was collected every 24 h and monocytes were exposed to a daily change of fresh conditioned media for 7 days (A) Negative control; cells were grown in serum free alpha MEM media. TRAP staining was negative, pit formation was not evident, and DAPI staining showed no multinucleated cells (B) NOF; cells were treated with conditioned media collected from serum starved NOF cells. TRAP staining was negative, pit formation was not evident, and DAPI staining showed no multinucleated cells. Conditioned media collected from (C) S-NOF^{H2O2}; H_2O_2 (500 μM for 2 h), (D) S-NOF^{Cis}; cisplatin (10 μM for 24 h), and (E) S-NOF^{Rep}; replicative exhaustion (passage 25) cells. TRAP staining was observed in osteoclasts, pit formation was evident, and DAPI staining showed multinucleated cells. (F) CAF; cells were treated with conditioned media collected from primary human CAF isolated from OSCC tissue. TRAP staining was observed in osteoclasts, pit formation was evident, and DAPI staining showed multi-nucleated cells. The experiment was performed three times in duplicate. Magnification x40.

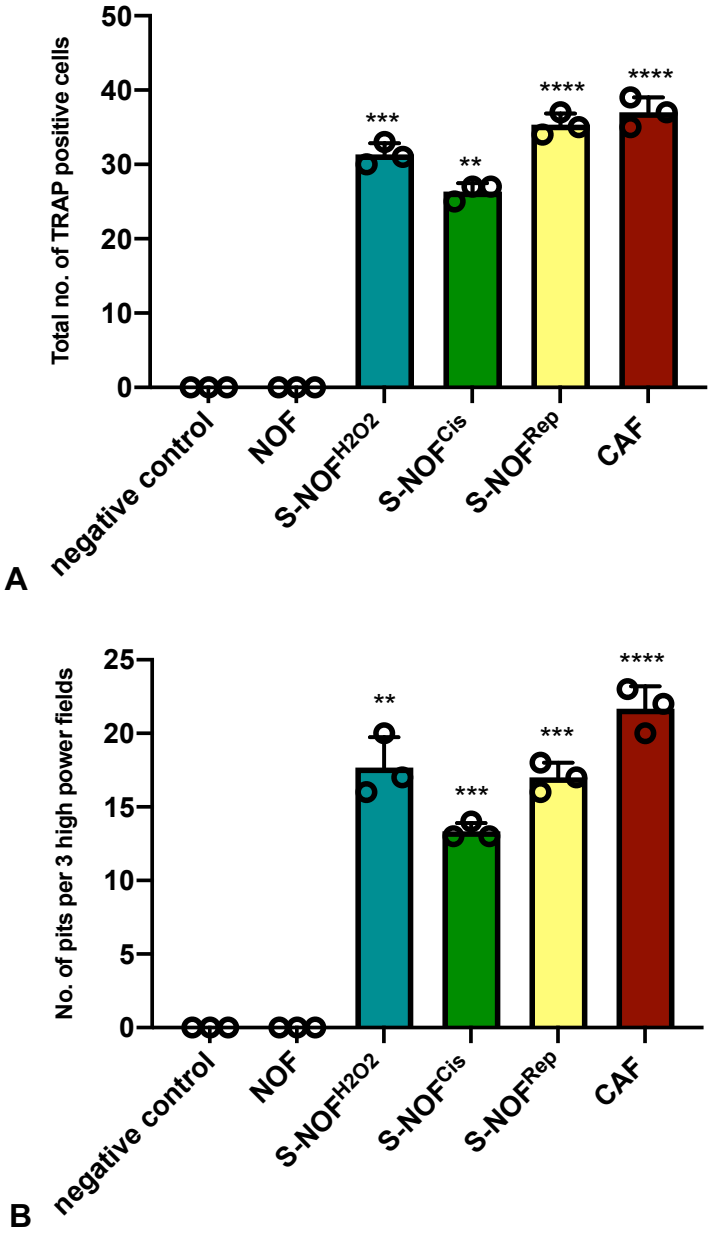

Figure 4.15: Senescent oral fibroblasts induce osteoclastogenesis. 15 days after NOF (803, 804, and 822) were exposed to H_2O_2, cisplatin or replicative exhaustion (passage 25), RAW 264.7 monocytes were seeded in a 24 well plate at a density of 20,000 cells/well. Senescent cells were serum starved in alpha MEM media, and monocytes were treated daily with the conditioned media for 7 days. (A) The number of TRAP positive cells was counted positive S-NOF^{H2O2} (32 ± 2, p=0.0002), S-NOF^{Cis} (26 ± 3, p=0.004), and S-NOF^{Rep} (34 ± 5, p=0001). The highest stimulation of osteoclastogenesis was noticed when monocytes were exposed to conditioned media from primary CAF (37 ± 2, p=0.00006). (B) Pit formation quantification. The number of pits formed due to osteoclasts actively was counted S-NOF^{H2O2} (18 ± 4, p=0.008), S-NOF^{Cis} (13 ± 3, p=0.0005), S-NOF^{Rep} (16 ± 4, p=0.0002). The highest significant differentiation of osteoclasts was seen when monocytes were exposed to conditioned media from primary CAF 21 ± 6, p=0.0001. Error bar = STDV. *p<0.05 was considered significant, following a Student's t-test.

4.10 Senolytic drugs impede tumour progression and bone invasion, giving promising therapeutic benefits

We have identified that senescent CAF are present in the microenvironment of bone-invasive OSCC. We have also provided evidence, *in vitro*, that senescent fibroblasts and CAF are able to induce osteoclastogenesis, suggesting that CAF senescence may play a functional role in bone invasion, and therefore represent a potential novel therapeutic target.

Alvespimycin and Navitoclax have recently been described as 'senolytics' due to their ability to selectively promote apoptosis of senescent cells, decreasing their pro-tumourgenic burden (Chen et al., 2016; Saini et al., 2018). These two drugs were chosen to examine their influence on senescent fibroblast-induced bone invasion as they target different pro-apoptotic pathways.

4.10.1 The effect of senolytics Alvespimycin (17-DMAG) and Navitoclax (ABT263) on NOF viability

Normal oral fibroblasts were exposed to a range of concentrations of Alvespimycin or Navitoclax, to determine the optimum dose to deplete senescent, but not proliferating, fibroblasts. NOF and S-NOF^{H2O2}, and S-NOF^{Cis} were exposed to senolytic drugs Alvespimycin (17-DMAG), and Navitoclax (ABT263) of various doses, and the dose with minimal effect on proliferative cells was selected 500 nM for Alvespimycin (17-DMAG), and 3 μM Navitoclax (ABT263) (Figure 4.16 A and B).

A

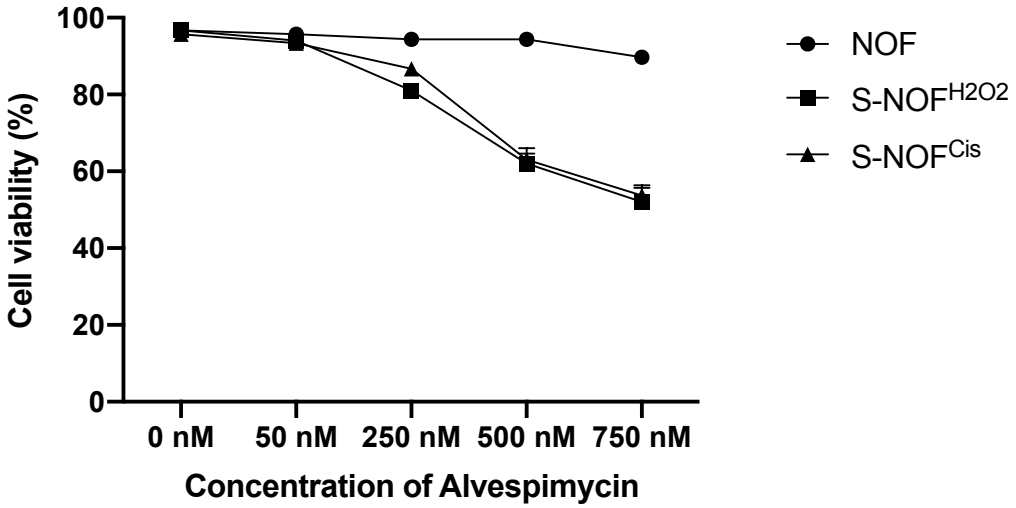

B

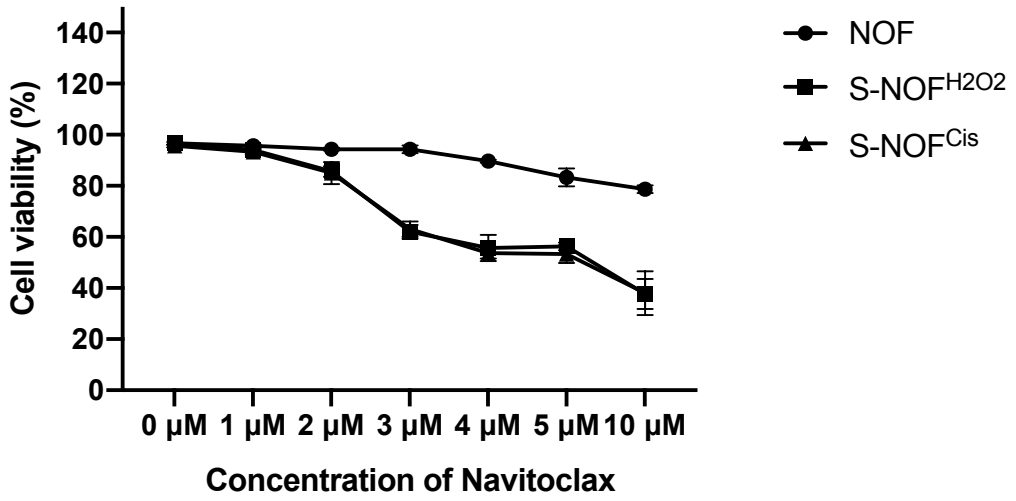

Figure 4.16: Effect of senolytics on NOF viability. NOF (803, 804 and 822), S-NOF^{H2O2} , and S-NOF^{Cis} were subjected to different concentrations of (A) Alvespimycin (50 nM, 250 nM, 500 nM and 750 nM), or (B) Navitoclax (1 µM, 2 µM, 3 µM, 4 µM, 5 µM and 10 µM) in separate wells of a 24 well plate seeded with 20,000 NOF (803, 804 and 822). Cell viability was measured at 24 h. Cell viability (%) was plotted against different senolytic drug concentrations. Experiment conducted three times in triplicate. Error bar = STDV.

4.10.2 Senotherapeutics Alvespimycin (17-DMAG) and Navitoclax (ABT263) target senescence.

SA-β-Gal assays were conducted to investigate the effect of senolytic drugs Alvespimycin and Navitoclax on senescent fibroblasts (Figure 4.17 and 4.18). A significant decrease in senescent cell number was noted. Navitoclax (3 μM) reduced senescence by a range of 58-63% ($p=0.0005$), while Alvespimycin's (500 nM) effect was more potent reducing the senescence by 66-75% ($p=0.00021$) (Figure 4.19).

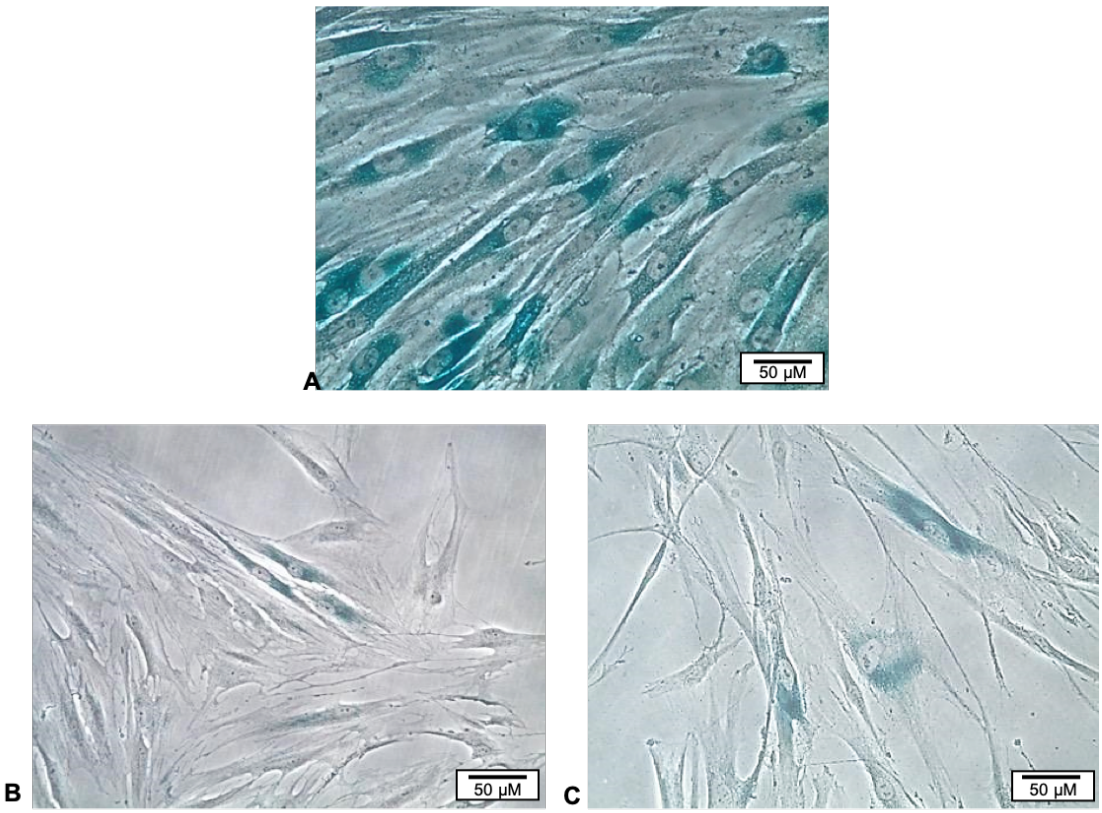

Figure 4.17: Representative photomicrographs showing the effect of senolytics on S-NOF^{H2O2}. Oral fibroblasts (NOF803, NOF804and NOF822) exposed to H_2O_2 (500 µM) were seeded into a 12 well plate at a density of 10,000 cells/well. On the following day, these cells were exposed to senolytic drugs Alvespimycin (500 nM) or Navitoclax (3 µM). After 24 h, cells were rinsed in PBS, fixed, and stained with X-gal staining solution (24 h). (A) Senescent fibroblasts induced by exposure to H_2O_2 produced a blue/turquoise precipitate. (B) Senescent fibroblasts following exposure to Alevspimycin (500 nM). (C) Senescent fibroblasts following exposure to Navitoclax (3 µM). (magnification x20). The experiment was performed three times in triplicate.

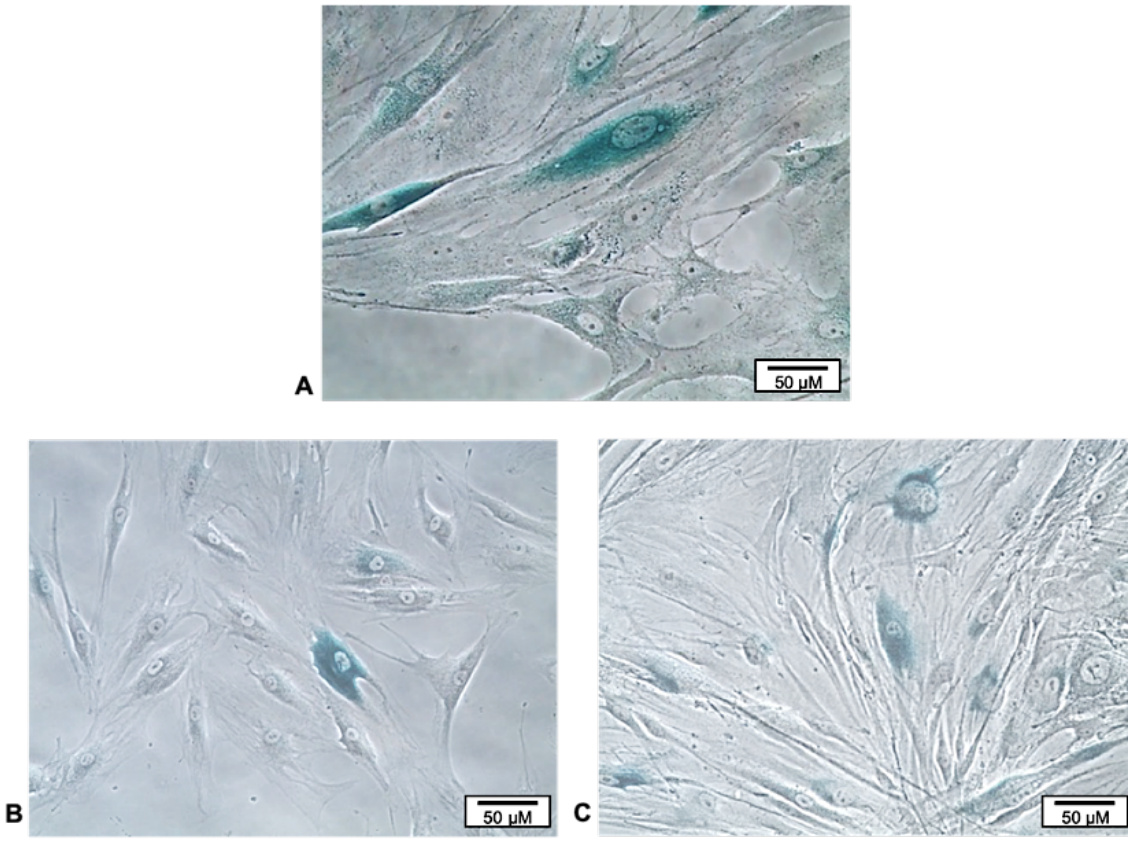

Figure 4.18: Representative photomicrographs showing the effect of senolytics on S-NOF^{Cis}. NOF (803, 804 and 822) exposed to cisplatin (10 µM) were seeded into a 12 well plate at a density of 10,000 cell/well. On the following day, these cells were exposed to Alvespimycin (500 nM) or Navitoclax (3 µM). After 24 h, cells were rinsed in PBS, fixed, and stained with X-gal staining solution (24 h). (A) Senescent NOF induced by exposure to chemotherapeutic cisplatin produced a blue/turquoise precipitate, and a reduction in positive cells was seen following treatment with senolytics. (B) Senescent fibroblasts following exposure to Alespimycin (500 nM). (C) Senescent fibroblasts following exposure to Navitoclax (3 µM). (magnification x20). The experiment was performed three times in triplicate.

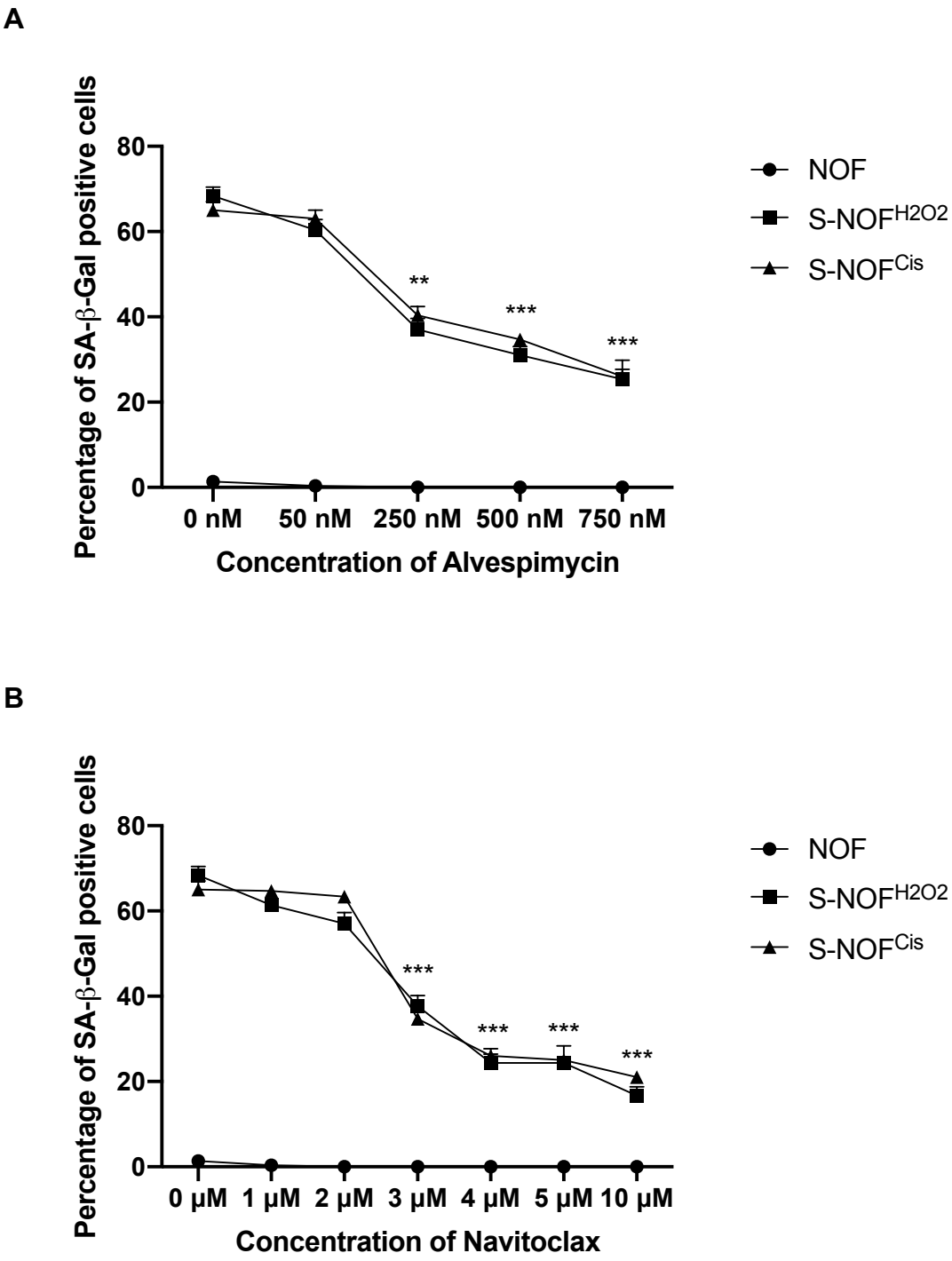

Figure 4.19: Evaluation of senescence following exposure to senolytics. NOF (803, 822), S-NOF^{H2O2}, and S-NOF^{Cis} were exposed to senolytic drugs. The percentage of SA-β-Gal positive cells following 24 h treatment with (A) Alvespimycin (50 nM, 250 nM, 500 nM, and 750 nM). (B) Navitoclax (1 μM, 2 μM, 3 μM, 4 μM, 5 μM, 10 μM) was assessed. The graph represents combined results of multiple assays. Experiment conducted three times in triplicate. *p<0.05 was considered significant, following a Student's t-test. Error bar = STDV.

4.10.3 Senolytic drugs limit bone invasion by reducing osteoclast generation

The influence of Alvespimycin, and Navitoclax on osteoclastogenesis was next studied. Murine monocytes (RAW 264.7) were seeded in 24 well Osteo assay surface plates, and treated with conditioned media from serum starved experimentally induced senescent fibroblasts S-NOF^{H2O2}, S-NOF^{Cis}, S-NOF^{H2O2} and S-NOF^{Cis} exposed to Alvespimycin (500 nM) or Navitoclax (3 μM), and conditioned media from serum starved CAF. After 7 days, TRAP staining, pit formation and nucleation was evaluated. RAW 264.7 cells cultured in NOF conditioned media served as the negative control. The number of osteoclasts generated were significantly less following Alvespimycin and Navitoclax exposure, S-NOF^{H2O2} (33 ± 4, 7 ± 2 after Alvespimycin exposure, and 12 ± 4 Navitoclax), S-NOF^{Cis} (24 ± 4, 3 ± 1 Alvespimycin, and 5 ± 3 Navitoclax), CAF (38 ± 3, 13 ± 2 Alvespimycin, and 21 ± 3 Navitoclax) (mean ± STDV). These results were also reflected in the pit forming (S-NOF^{H2O2} (17 ± 2, 4 ± 1 after Alvespimycin treatment, and 7 ± 1 Navitoclax), S-NOF^{Cis} (14 ± 3, 2 ± 1 Alvespimycin, and 5 ± 1 Navitoclax), CAF (19.1 ± 3.8, 6.9 ± 1.5 Alvespimycin, and 10 ± 2 Navitoclax), and nucleation assays (Table 4.3). Throughout the samples Alvespimycin exposure had a more potent effect on osteoclastogenesis and pit formation reduction compared to Navitoclax (Figure 4.20 and 4.21).

Table 4.3: Quantification of TRAP positive cells and pits formed following senolytic drug exposure

Sample	Total no. of TRAP positive cells (mean ± STDV, p value)	No. of pits per 3 high power fields (mean ± STDV, p value)
Negative control	0.0 ± 0.0	0.0 ± 0.0
NOF	0.0 ± 0.0	0.0 ± 0.0
S-NOF^{H2O2}	33 ± 4, p=0.001	17 ± 2, p=0.0001
S-NOF^{H2O2}+ Alvespimycin	7 ± 2, p=0.00006	4 ± 1, p=0.00002
S-NOF^{H2O2} + Navitoclax	12 ± 4, p=0.0001	7 ± 1, p=0.001
S-NOF^{Cis}	24 ± 3, p=0.00003	14 ± 3, p=0.0001
S-NOF^{Cis} + Alvespimycin	3 ± 1, p=0.00005	2 ± 1, p=0.00008
S-NOF^{Cis} + Navitoclax	5 ± 3, p=0.001	5 ± 1, p=0.0008
CAF	38 ± 2, p=0.00002	19.1 ± 3.8, p=0.00002
CAF + Alvespimycin	13 ± 2, p=0.0005	6.9 ± 1.5, p=0.0007
CAF + Navitoclax	21 ± 3, p=0.003	10.01 ± 2, p=0.0006

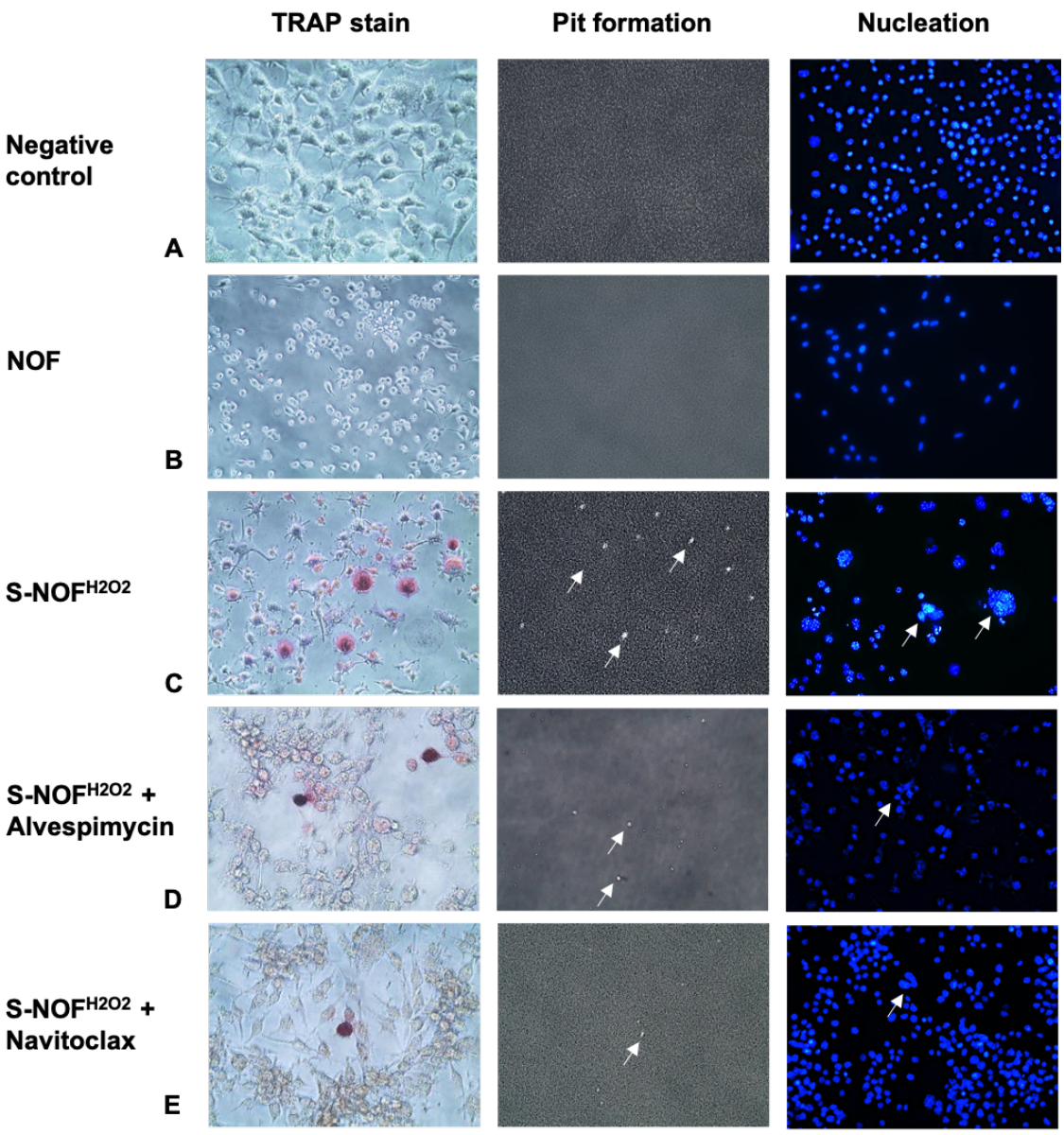
TRAP stain
Pit formation
Nucleation
Negative control
A
NOF
B
S-NOF^{H2O2}
C
S-NOF^{H2O2} + Alvespimycin
D
S-NOF^{H2O2} + Navitoclax
E

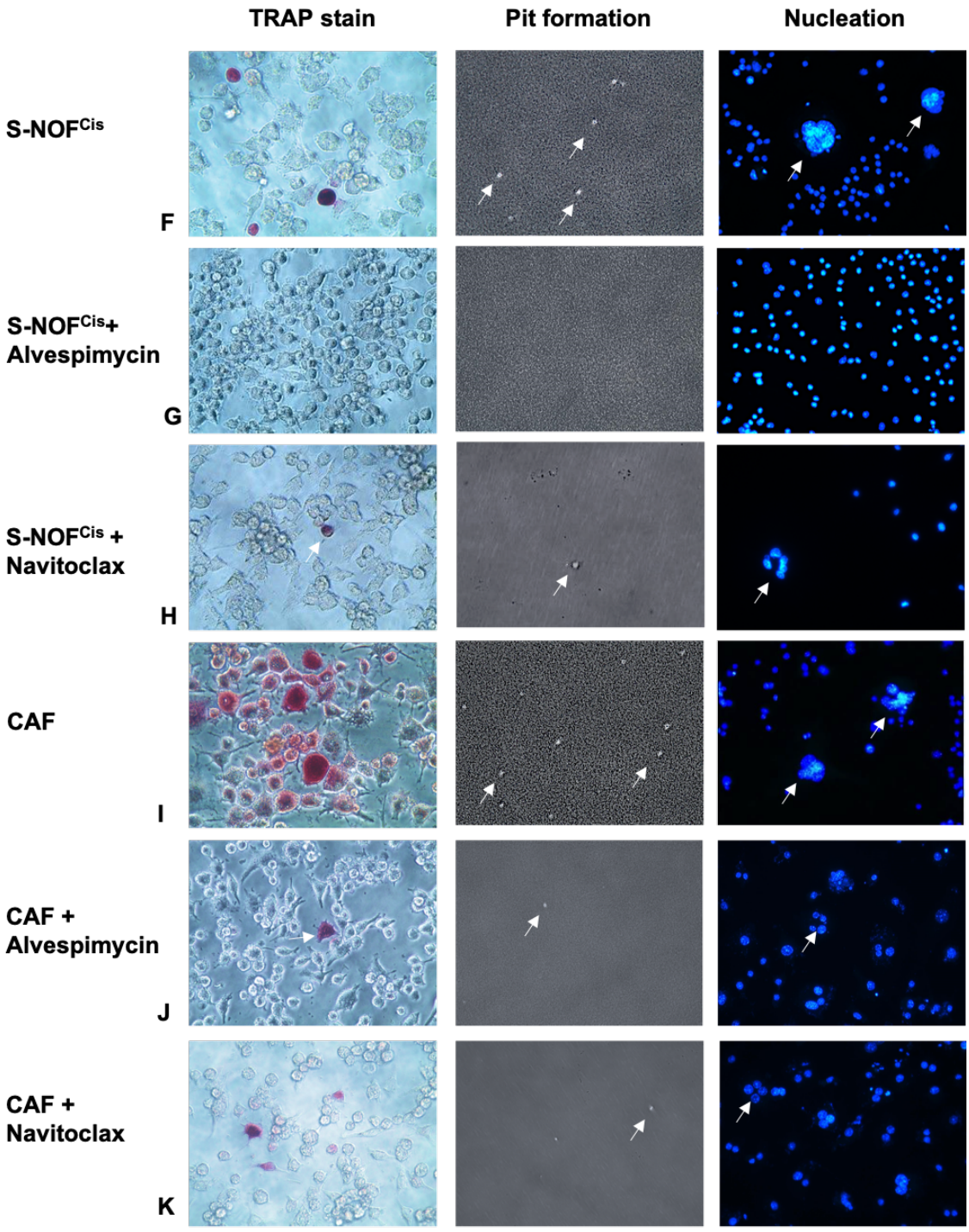
TRAP stain
Pit formation
Nucleation
S-NOF^{Cis}
F
S-NOF^{Cis}+ Alvespimycin
G
S-NOF^{Cis} + Navitoclax
H
CAF
I
CAF + Alvespimycin
J
CAF + Navitoclax
K

Figure 4.20: Osteoclastogenesis assay, the effect of senolytics on osteoclast generation. RAW 264.7 monocytes (20,000 cells/well) were seeded in Osteo Assay surface 24 well plates. Cell were serum starved in alpha MEM media. Monocytes were exposed to the collected media. Media was changed daily for 7 days (A) Negative control; cells were grown in serum free alpha MEM media. TRAP staining was negative, pit formation was not evident, and DAPI staining showed no multinucleated cells (B) NOF; cells were treated with conditioned media collected from serum starved NOF cells. TRAP staining was negative, pit formation was not evident, and DAPI staining showed no multinucleated cells. (C) S-NOF^{H2O2}; cells were treated with conditioned media collected from serum starved NOF treated with H_2O_2 (500 μM for 2 h). TRAP staining was observed was observed in osteoclasts, pit formation was evident, and DAPI staining showed multinucleated cells. (D) S-NOF^{H2O2} treated with Alvespimycin; cells were treated with conditioned media collected from serum starved S-NOF^{H2O2} following exposure to Alvespimycin (500 nM for 24 h) and (E) S-NOF^{H2O2} treated with Navitoclax; S-NOF^{H2O2} following exposure to Navitoclax (3 μM for 24 h). A significant reduction of TRAP staining osteoclasts, pit formation, and multinucleated cells DAPI staining was observed. (F) S-NOF^{Cis}; cells were treated with conditioned media collected from serum starved NOF treated with cisplatin (10 μM for 24 h). TRAP staining was observed positively staining osteoclasts, pit formation was evident, and DAPI staining showed multinucleated cells. (G) S-NOF^{Cis} treated with Alvespimycin; cells were treated with conditioned media collected from serum starved S-NOF^{H2O2} following exposure to Alvespimycin, and (H) S-NOF^{Cis} treated with Navitoclax; S-NOF^{H2O2} following exposure to Navitoclax. A significant reduction of TRAP positive osteoclasts, pit formation, and multinucleated cells with DAPI staining were observed. (I) CAF; cells were treated with conditioned media collected from primary CAF isolated from OSCC tissue. TRAP staining was observed in osteoclasts, the ability for the activated osteoclast to form pits in the bone scaffold was evident, and DAPI nucleation showed multi-nucleated cells. (J) CAF treated with Alvespimycin; cells were treated with conditioned media collected from serum starved primary CAF following exposure to Alvespimycin, and (K) CAF treated with Navitoclax; primary CAF following exposure to Navitoclax. The number of TRAP positive osteoclasts, pit formation, and multinucleated cell DAPI staining significantly decreased. The experiment was performed three times in duplicate. Magnification x40.

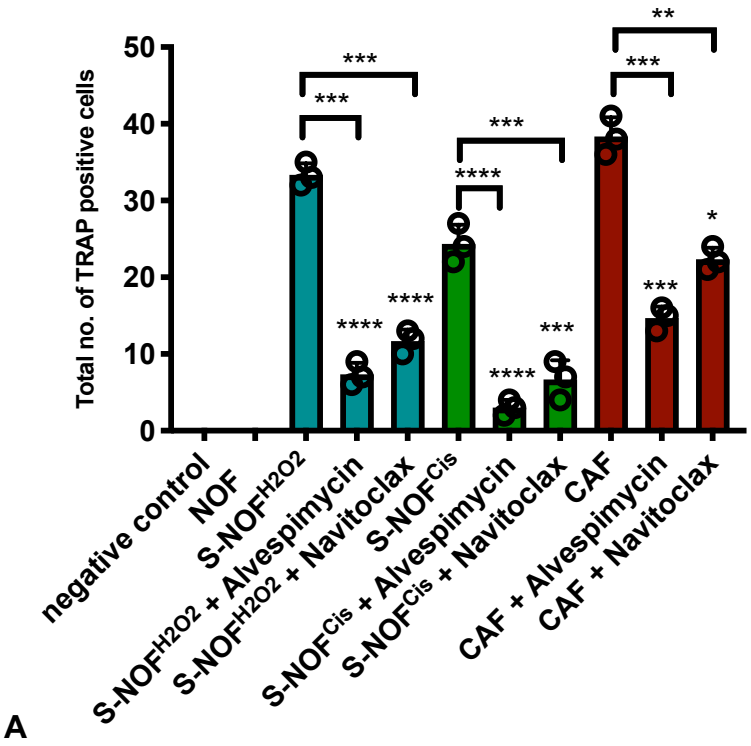
Total no. of TRAP positive cells
50
40
30
20
10
0
negative control
NOF
S-NOF^{H2O2}
S-NOF^{H2O2} + Alvespimycin
S-NOF^{H2O2} + Navitoclax
S-NOF^{Cis}
S-NOF^{Cis} + Alvespimycin
S-NOF^{Cis} + Navitoclax
CAF
CAF + Alvespimycin
CAF + Navitoclax

A

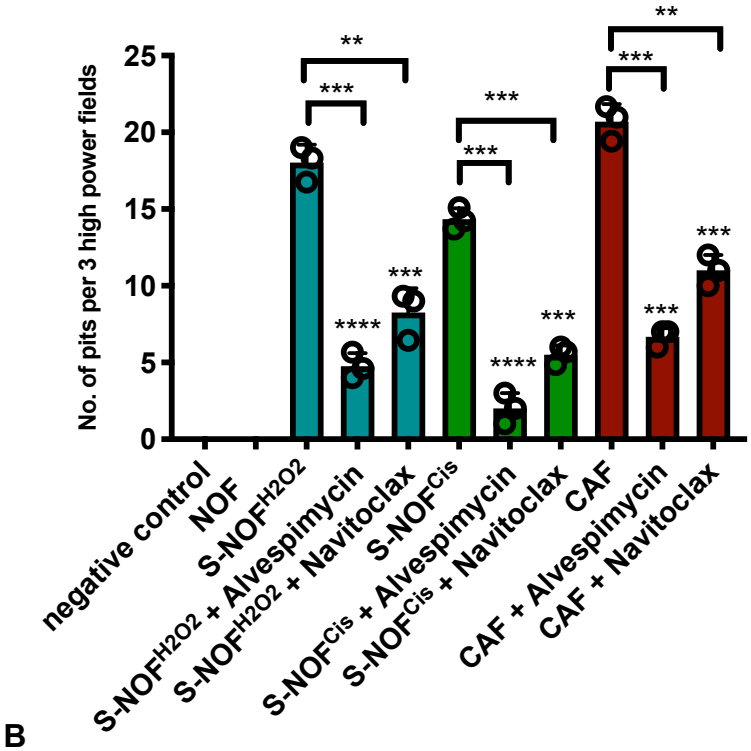
No. of pits per 3 high power fields
25
20
15
10
5
0
negative control
NOF
S-NOF^{H2O2}
S-NOF^{H2O2} + Alvespimycin
S-NOF^{H2O2} + Navitoclax
S-NOF^{Cis}
S-NOF^{Cis} + Alvespimycin
S-NOF^{Cis} + Navitoclax
CAF
CAF + Alvespimycin
CAF + Navitoclax

B

Figure 4.21: Senolytics reduce osteoclast generation. 15 days after fibroblasts (NOF803, NOF804, NOF822) were exposed to H_2O_2, or cisplatin, senescent fibroblasts were treated with Alvespimycin (500 nM) or Navitoclax (3 μM) for 24 h. RAW 264.7 monocytes were seeded in a 24 well plate at a density of 20,000 cells/ well. Senescent cells before and after exposure with senolytic drugs were serum starved in alpha MEM media, and monocytes were treated daily with the conditioned media for 7 days. (A) Osteoclast generation quantification. The number of TRAP positive cells was counted. The number of osteoclasts generated were significantly less following Alvespimycin and Navitoclax exposure, S-NOF^{H2O2} (33 ± 4, 7 ± 2 after Alvespimycin exposure, and 12 ± 4 Navitoclax), S-NOF^{Cis} (24 ± 4, 3 ± 1 Alvespimycin, and 5 ± 3 Navitoclax), CAF (38 ± 3, 13 ± 2 Alvespimycin, and 21 ± 3 Navitoclax) (mean ± STDV). (B) Pit formation quantification. These results were also reflected in the pit forming (S-NOF^{H2O2} (17 ± 2, 4 ± 1 after Alvespimycin treatment, and 7 ± 1 Navitoclax), S-NOF^{Cis} (14 ± 3, 2 ± 1 Alvespimycin, and 5 ± 1 Navitoclax), CAF (19.1 ± 3.8, 6.9 ± 1.5 Alvespimycin, and 10 ± 2 Navitoclax), The experiment was performed three times in duplicate. Error bar = STDV. **p<0.01was considered significant, following a Student's t-test.

4.11 Discussion

The TME plays a critical role in cancer progression and invasion. A considerable amount of research has focused on αSMA-expressing myofibroblastic CAF in the TME. However, recent reports have provided evidence that CAF represent a heterogeneous population, and one sub-population of CAF, which are senescent fibroblasts have been described. Senescent fibroblasts are evident in premalignant lesions (Costea et al., 2013; Procopio et al., 2015) as well as OSCC stroma (Hassona et al., 2013). Campisi et al. (2007), reported that the characteristic features of senescent cells including elevated levels of cytokines and growth factors which have a pro tumourgenic effect in cancers.

In oral cancer, senescent cells have been described to be evident through the elevated expression of p16INK4a (Parkinson, 2010; Hassona et al., 2013; Kabir et al., 2016; Mellone et al., 2017). However, in the current study, cell surface protein DPP4 (CD26), reported by Kim et al. (2017), which is specifically expressed in senescent cells was investigated for the first time in OSCC to further support the expression of the well-recognised senescent marker p16INK4a. Tissue from OSCC bone resections was examined for the presence of senescent cells in tumour stroma. Senescent markers p16INK4a and DPP4 were analysed and the percentage of positive stromal cells at the tumour bone interface ranged from 21% to 73%. These findings identify that senescence is evident in OSCC cells and surrounding stroma, suggesting an active role in bone invasion.

To study senescence *in vitro*, normal oral fibroblasts at a low passage were exposed to DNA damaging agents H_2O_2, cisplatin or replicative exhaustion to induce senescence. Following five days of H_2O_2 or cisplatin treatment, and replicative mitotic exhaustion (passage 25) the majority of the fibroblasts were

positive for SA-β-Gal, further confirming senescence transformation of resting oral fibroblasts. These results are in agreement with previous studies (Kabir et al., 2016).

Senescent fibroblasts were investigated on a transcript level for senescence marker p16INK4a, and SASP factor IL6, and a significant amplification was noted when compared to NOF. Bone turnover markers RANKL and antagonist or decoy receptor OPG were further examined and a significant up-regulation in RANKL was observed, while OPG mRNA expression was down-regulated consistently, compared to control NOF. Conditioned media collected at different time intervals was also subjected to an ELISA to investigate whether senescent fibroblasts secreted RANKL protein. Senescent fibroblasts produced significantly more soluble RANKL protein in comparison to untreated NOF. These findings are in further agreement that RANKL expression is activated in senescence and may be considered a novel SASP factor (Kim et al., 2017)

To further evaluate these findings, exposure of RAW 264.7 monocytes to conditioned media from senescent fibroblasts resulted in osteoclast generation. These findings suggest that the TME in OSCC comprises CAF as well as senescent fibroblasts and both could potentially contribute to OSCC-mediated bone destruction.

Following confirmation that senescent fibroblasts play a key role in the initiation of osteoclastogenesis, senolytics were investigated to assess whether a reduction in senescence can reduce the paracrine effects promoting osteoclastogenesis. Fuhrmann-Stroissnigg et al. 2017 first introduced Alvespimycin as a novel senolytic agent able to promote apoptosis in senescent

fibroblasts. In addition, in recent studies, Navitoclax has been reported to promote apoptosis in senescent cells as human lung fibroblasts, human umbilical vein epithelial cells, and mouse embryonic fibroblasts (Zhu et al., 2015). Moreover, navitoclax decreased senescence fibroblast burden in the liver leading to a reduction in fibrosis (Moncsek et al., 2018). Furthermore, Chen et al. (2016), demonstrated the pro apoptotic functionality of Navitoclax in targeting CAF in hepatocellular carcinoma, however senescence was never examined.

The current study is the first to specifically target senescent CAF with senolytics. Drugs were optimised, and dose selected targeting senescent fibroblasts but having minimal effect on proliferative cells, 500 nM for Alvespimycin (17-DMAG), and 3 μM Navitoclax (ABT263). Significant reduction in osteoclast generation was recorded following exposure to both senolytics. These results suggest a potential clinical application for senolytic drugs as an adjunct therapy in the treatment of bone invasive oral cancer, reducing the pro-tumourigenic burden of senescence cells.

Chapter 5

Extracellular vesicles: communicators in the OSCC microenvironment

5.1 Introduction

EV have been gaining interest as a novel mode of cellular communication in biomedical research. Increasing evidence shows that cancer-derived EV play important roles in tumour progression (Kahlert and Kalluri, 2013). EV transport nucleic acids and proteins to recipient cells, influencing tumour growth, advancement, metastasis and therapeutic resistance (Vader et al., 2014; Minciacchi et al., 2015; Becker et al., 2016). EV derived from malignant cells are capable of inducing dysplastic transformation in normal cells. Abd Elmageed et al. (2014), found that adipose-derived stem cells became malignant when exposed to EV isolated from prostate cancer. Similar results have also been reported in breast cancer, where miRNA containing EV silenced mRNA in non-neoplastic cells, resulting in transcriptome reprogramming and malignant transformation (Melo et al., 2014).

Cancer derived EV have a significant impact on the TME by encouraging tumour angiogenesis, immune cell infiltration, and activation of resting fibroblasts to CAF, facilitating tumour progression. Webber et al. (2010), reported that prostate cancer EV expressed TGFβ, and actively triggered myofibroblastic differentiation of normal fibroblasts in tumour microenvironment promoting tumour growth. These results are in further agreement where cancer EV stimulated the differentiation of mesenchymal cells to CAF in gastric (Gu et al., 2012) and breast cancer (Cho et al., 2012).

In bone, EV have also been reported to regulate osteoclast-osteoblast communication, where EV derived from osteoblasts were described to promote osteoclastogenesis (Deng et al., 2015). Moreover, Huynh et al. (2016) observed that osteoclasts expressed EV inhibited osteoclast generation. As one of the

main objectives of this study, we sought to investigate the role of EV and CAF in OSCC microenvironment and examine their influence on bone invasion.

5.1.1 Aims

To examine OSCC and different subsets of CAF derived EV and assess whether these EV influence bone invasion in oral cancer.

5.1.2 Experimental approach

1. EV were isolated from NOF, OSCC, CAF and senescent fibroblasts by graded centrifugation and size exclusion chromatography, quantified using nano particle tracking.
2. Assessment of enrichment of the EV markers CD9, CD63 and CD81 was used to confirm EV isolation.
3. Soluble RANKL protein was also examined in EV isolated from OSCC, NOF, CAF, and senescent fibroblasts with an ELISA.
4. An osteoclastogenesis assay was performed by culturing murine monocytes (RAW 264.7) with OSCC, NOF, CAF, and senescent fibroblasts conditioned media as well as EV isolated from these samples. TRAP staining, pit formation and nucleation assays was conducted to confirm osteoclastic differentiation.
5. The ability of OPG, a RANKL decoy receptor, to influence the functions of EV was assessed through an osteoclastogenesis assay, following exposing monocytes to conditioned media or EV treated with OPG.

5.2 EV isolation from OSCC, NOF, CAF, myofibroblasts and senescent oral fibroblasts

5.2.1 Collection of EV from oral cancer and stromal cells

Cells were grown in culture media (DMEM) in tissue culture treated surface flasks. Once 70-80% confluence was reached, cells were rinsed twice with PBS, and serum starved in DMEM for 72 h. Conditioned media was collected ready for EV isolation by graded centrifugation and SEC. A cell count of 18 million cells was sufficient for optimal EV isolation and downstream analyses.

5.2.2 Quantification and size distribution of EV

A ZetaView (ZetaView Basic NTA- Nanoparticle Tracking Video Microscope PMX-120, Particle Matrix) was used to analyse the concentration and size of EV. Following EV isolation, a small quantity (3 ml) of the isolate was used for nanoparticle tracking analysis.

EV from NOF, myofibroblasts (NOF exposed to TGFβ1), CAF, S-NOF^{H2O2} and S-NOF^{Cis}, and H357 were loaded into the ZetaView. The samples were scanned at 11 positions (in triplicate), and particles were tracked by Brownian motion to obtain an average measurement. The number of EV produced per cell was calculated by multiplying the dilution factor of the sample used with the particle concentration and divided by the total number of cells at the time of conditioned media collection (Figure 5.1 and 5.2).

The average number of particles (mean ± STDV) and majority of the particle size range were observed as follows, NOF (84.12 ± 7.53, and 105 to 165 nm), myofibroblasts (NOF + TGFβ1) (127.15 ± 2.2, and 105 to 225 nm). CAF (142.51 ± 6.26, and 75 to 195 nm), S-NOF^{H2O2} (182.58 ± 5.39, and 105 to 225 nm), S-

NOF^{Cis} (166.34 ± 3.33, and 75 to 165 nm), and H357 (280.5 ± 2.7, and 75 to 255 nm). The data showed significant differences ($p<0.0001$) in average particle number between samples following a one-way ANOVA statistical test.

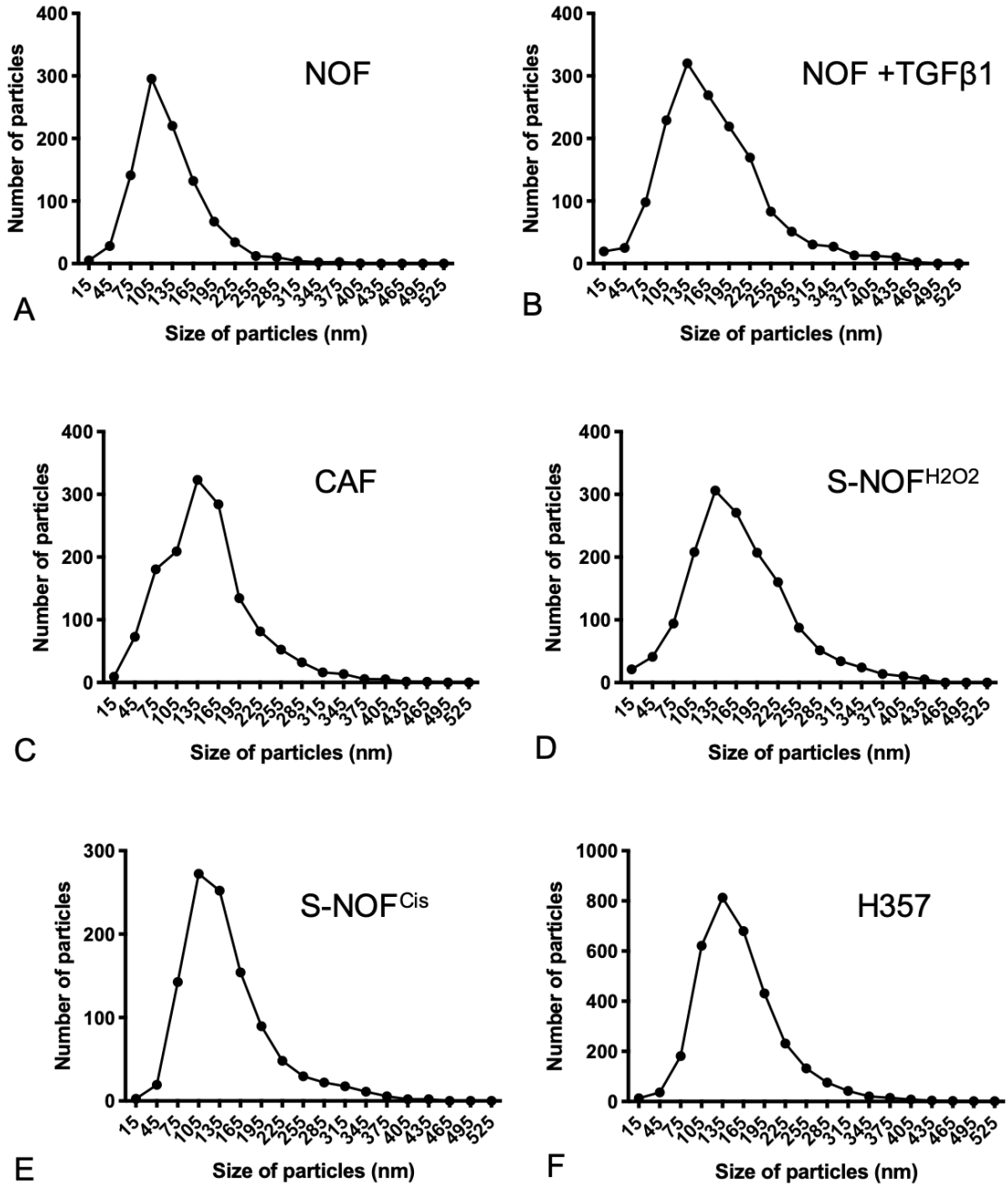

Figure 5.1: EV size distribution analysis by nanoparticle tracking using ZetaView instrument. Cells were serum starved (72 h), following EV isolation by SEC, EV were tracked by Brownian motion to obtain and average measurement. (A) Representative distribution of EV size distribution profile in NOF (803, 804, and 822). (B) Representative distribution of EV size in myofibroblasts, NOF (803, 804, and 822) treated with TGFβ1 (5 ng/ml). (C) Representative distribution of EV size in CAF (002, 003, and 004). (D) Representative distribution of EV size in senescent oral fibroblasts (NOF803, 804, and 822) induced by exposure to H_2O_2 (500 μM). (E) Representative distribution of EV size in senescent oral fibroblasts (NOF803, 804, and 822) induced by exposure to cisplatin (10 μM). (F) Size distribution of EV in OSCC cell line H357. p value of 0.0001 following a one-way ANOVA statistical test. All samples were run in triplicate (3 biological and experimental repeats). Histograms plotted using GraphPad Prism 8 software.

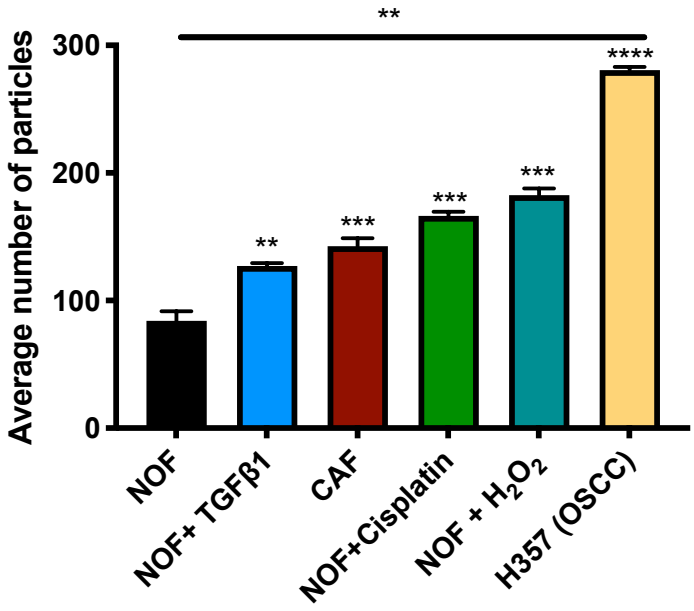

Figure 5.2: Average number of EV produced by different cell types. The ZetaView instrument was utilised to calculate the mean number of EV produced, NOF (84.12 ± 7.53), myofibroblasts NOF exposed to TGFβ1 (5 ng/ml) (127.15 ± 2.2), CAF isolated from human tissue (142.51 ± 6.26), senescent oral fibroblasts NOF exposed to H_2O_2 (500 µM) (182.58 ± 5.39), senescent oral fibroblasts NOF treated with cisplatin (10 µM) (166.34 ± 3.33), and OSCC cell line H357 (280.5 ± 2.7). Values are expressed as (mean ± SD). Error bar = STDV. Experiment was conducted in triplicate. *p<0.05 was considered significant, following a Student's t-test. **p value of 0.0013 following a one-way ANOVA statistical test.

5.3 Characterisation of EV expressed by oral cancer cells and NOF

Following EV isolation and particle profile analysis conducted through ZetaView nanoparticle tracking, further investigation was required to confirm the enrichment of EV, and exclude the presence of non-EV lipoproteins, salt aggregates, or other contaminants as isolation/profile analyses only detect nanoparticles but do not provide definitive evidence that these particles are EV. An ExoView R100 was utilised using affinity-based technology to characterise EV

isolated from OSCC cell line H357, and primary NOF from conditioned media of serum starved cells (72 h), through graded centrifugation and SEC. EV samples were probed with widely reported EV markers tetraspanins CD9, CD63, and CD8 (Théry et al., 2018). Murine IgG acted as a negative control.

As previously described (section 2.11.5) samples were diluted in ExoView Incubation Solution. 35ul of sample was incubated on ExoView Tetraspanin Chips (placed in a 24 well plate for 16h RT) to allow EV marker-specific binding. Following incubation, fluorophore secondary antibody labelling with anti-CD81 Alexa-555, anti-CD63 Alexa-647 and anti-CD9 Alexa-488 was further applied, specifically binding to tetraspanins expressed on EV membrane. Both H357 and NOF samples were positive for tetraspanin markers CD9, CD63, and CD8, and expression of multiple markers was also observed (Figure 5.3 and 5.4).

Furthermore, in addition to characterisation, EV size distribution profiling was also conducted. In both NOF and H357 cells, the largest group of EV was between 45-70 nm, with slight discrepancy between tetraspanin expression. The average size of NOF derived EV in accordance with tetraspanin marker expression was as follows CD9 (63.4 nm) (Figure 5.3 A), CD63 (67.7 nm) (Figure 5.3 B), and CD81 (63.1 nm) (Figure 5.3 C) , while H357 EV profile was CD9 (65.6 nm) (Figure 5.4 A), CD63 (65.1 nm) (Figure 5.4 B), and CD81 (65.9 nm) (Figure 5.4 C). The particle count however was distinctly different. H357 cells (Figure 5.4 E) produced 10 times more EV in comparison with NOF derived EV (Figure 5.4 E). These results are in agreement with the data generated following EV quantification using the ZetaView nanoparticle tracking instrument (section 5.2.2).

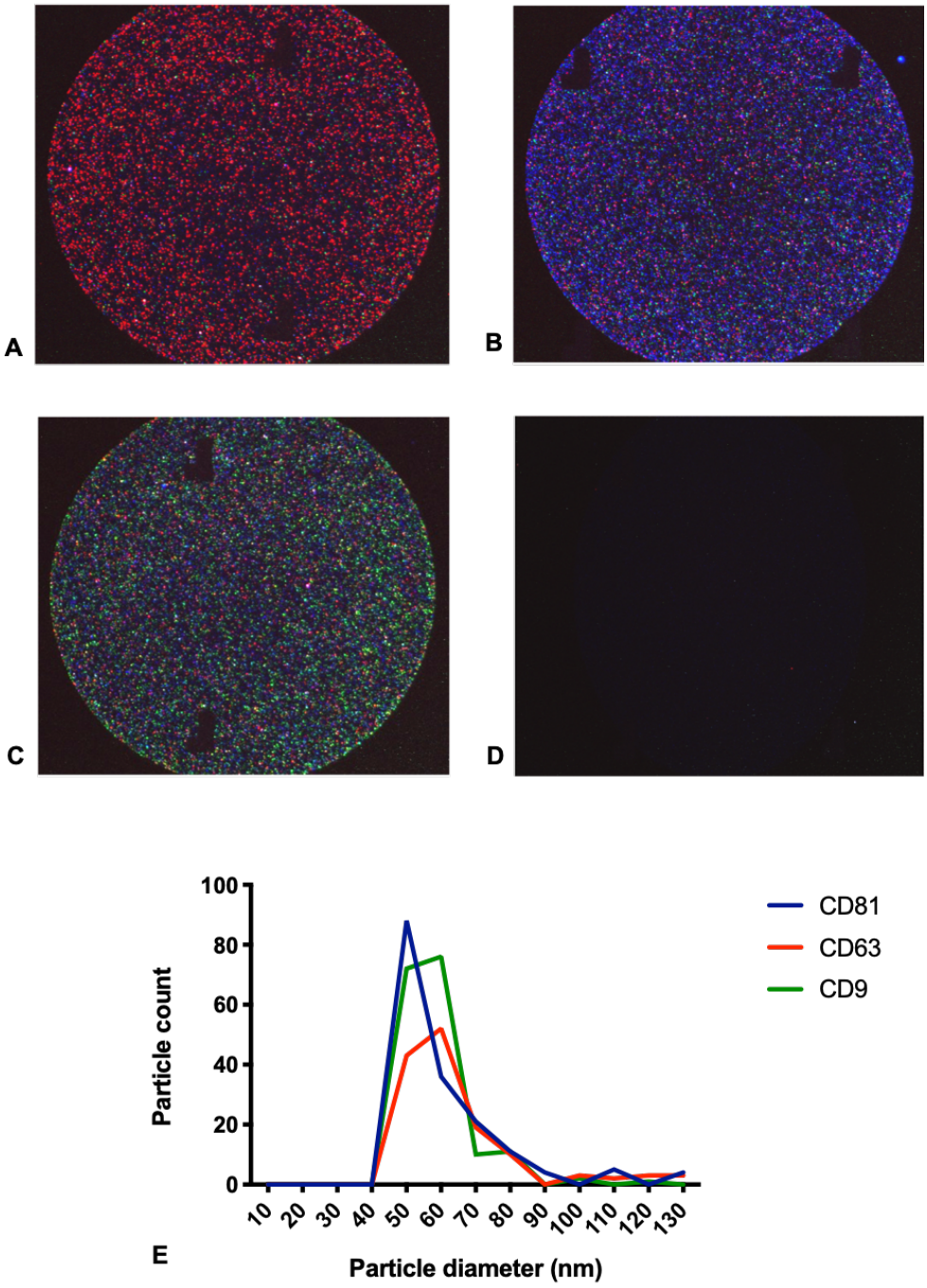

Figure 5.3. Characterisation of EV derived from primary NOF. Exoview R100 was utilised for affinity-based technology for EV characterisation. EV tetraspanin markers (A) CD63 (red), (B) CD81 (blue), and (C) CD9 (green) were selected, and antibodies against the specific tetraspanin antigen were labelled with fluorophores to detect the presence of EV. EV expression of more than one marker exhibited a mixed colour of fluorophore probes. SEC isolated NOF samples were diluted (1:600). (D) Murine IgG negative control. (E) EV population size distribution showed an amplified expression in EV with a size range of 45 to 70 nm, with a specific EV profile of CD9 (63.4 nm), CD63 (67.7 nm), and CD81 (63.1 nm).

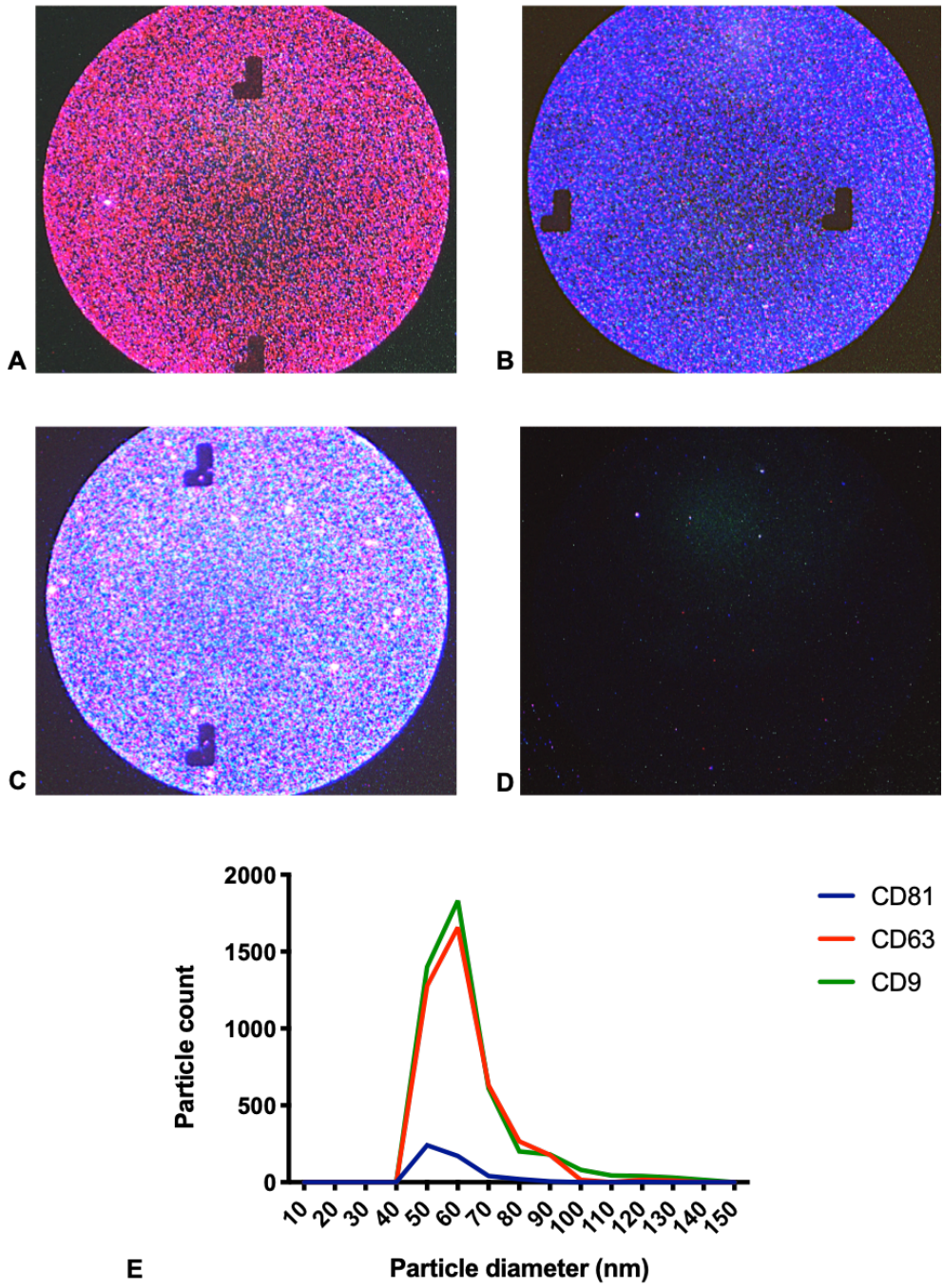

Figure 5.4. Characterisation of EV derived from OSCC cell line H357. Exoview R100 was utilised for affinity-based technology for EV characterisation. EV tetraspanin markers (A) CD63 (red), (B) CD81(blue), and (C) CD9 (green) were selected, and antibodies against the specific tetraspanin antigen were labelled with fluorophores to detect the presence of EV. EV expression of more than one marker exhibited a mixed colour of fluorophore probes. SEC isolated H357 samples were diluted (1:600). (D) Murine IgG negative contro. (E) EV population size distribution showed an amplified expression in EV with a size range of 45 to 70 nm, with a specific EV profile of CD9 (65.6 nm), CD63 (65.1 nm), and CD81 (65.9 nm).

5.4 EV isolated from OSCC, CAF and senescent fibroblasts express bone resorption marker RANKL

EV can carry different cargo as growth factors. RANKL has been reported to be carried in osteoblast derived EV playing a functional role in osteoclast formation (Deng et al., 2015). After identifying that RANKL expression is significantly increased in H357, myofibroblasts, CAF (section 3.6 and 3.7), and S-NOF (section 4.8) and had the ability to promote osteoclastogenesis , the presence of RANKL in EV derived from H357, OSCC-derived CAF , NOF, myofibroblasts (NOF treated with 5 ng/ml TGFβ1), and S-NOF^{H2O2} and S-NOF^{Cis} was investigated. Cells were serum starved (72 h), conditioned media was collected and EV isolated by SEC were subjected to ELISA for RANKL. Secreted RANKL protein was significantly increased in conditioned media collected from H357, CAF and senescent oral fibroblasts compared to NOF. Concentration (ρg/ml) of soluble RANKL protein was recorded as follows (mean ρg/ml ± SD, p value) , NOF (102.01 ± 9.04, p=0.012), myofibroblasts (NOF + TGFβ1) (155.6 ± 8.3, p=0.0008), senescent EV S-NOF^{H2O2} (198.76 ± 7.16, p=0.0004), senescent EV S-NOF^{Cis} (177.37 ± 7.83, p=0.013), CAF EV (183.85 ± 9.11, p=0.011), and H357 EV (267.48 ± 2.60, p=0.00077). (Figure 5.5).

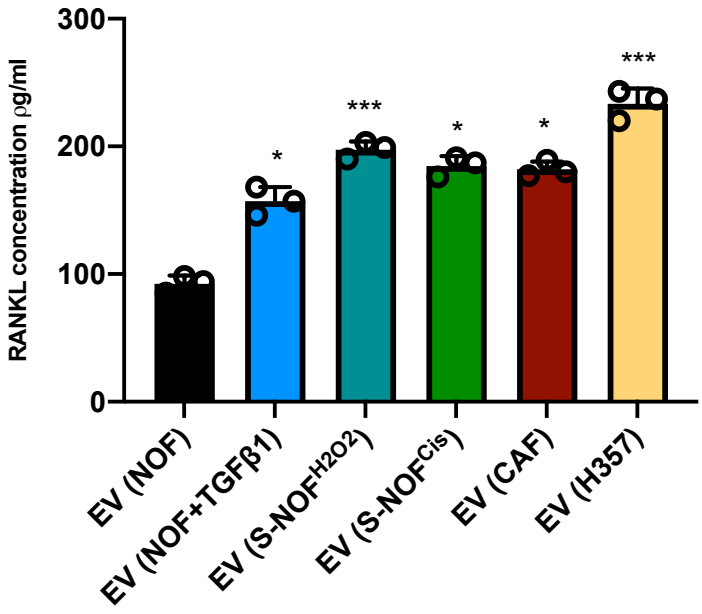

Figure 5.5: Soluble RANKL protein expression in EV isolated from OSCC, CAF, myofibroblasts and senescent oral fibroblast. OSCC cell line H357, primary CAF isolated from human tissue (CAF 002, 003, and 004), senescent oral fibroblasts senescent oral fibroblasts induced by exposure of NOF (803, 804 and 822) to H_2O_2 (500 μM) or cisplatin (10 μM) following 15 days of senescence induction, myofibroblasts (NOF 803, 804, and 822 treated with 5 ng/ml TGFβ1), and primary normal oral fibroblasts (NOF 803, 804, and 822) were propagated in T175 flasks (3 flasks) until 80% confluence (8 million cells/flask). Cells were then serum starved (72 h), conditioned media was collected and EV isolated by SEC. EV resuspended in PBS were subjected to an ELISA. Error bar=STDV. *$p<0.05$ was considered significant, following a Student's t-test. The graph represents combined results of multiple assays. Experiment was conducted in triplicate.

5.5 EV isolated from OSCC, CAF and senescent fibroblasts EV are instrumental in promoting bone invasion in OSCC

After demonstrating that EV isolated from H357, CAF, and S-NOF^{H2O2} or S-NOF^{Cis} express RANKL *in vitro*, an experiment was conducted to investigate whether this expression was sufficient to initiate osteoclastogenesis.

As previously mentioned (section 2.9) monocytes (RAW 264.7, which express MCSF-1) were seeded in Corning Osseo plates, serum starved, then treated with EV isolated from conditioned media collected from serum starved (72 h) cells (20 million cells), H357, NOF, experimentally induced myofibroblasts (NOF treated with TGFβ1, primary CAF, and senescent oral fibroblasts in separate wells. EV isolated from 18 million cells were resuspended in alpha MEM media, and media was changed daily. After 7 days, TRAP staining, pit formation assay, and nucleation, was examined as described (section 2.9) (Figure 5.6).

Osteoclast generation (Figure 5.7 A) and pit formation (Figure 5.7 B) was evident following exposure of monocytes to EV derived from NOF +TGFβ1 (25 ± 1.54, p=0.0003 and 18 ± 2.9, p=0.0004, respectively), S-NOF^{H2O2} (30 ± 2.35, p=0.0005 and 20 ± 3.77, p=0.0003) , S-NOF^{Cis} (25 ± 3.01, p=0.00007 and 15 ± 2.40, p=0.0009), CAF (34 ± 1.06, p=0.0001 and 20 ± 1.73, p=0.00008), and H357 (36 ± 2.77, p=0.00004 and 22 ± 3.03, p=0.00002) compared to NOF (Table 5.1).

Table 5.1: Number of TRAP positive cells and pits formed following EV exposure

Sample	Total no. of TRAP positive cells (mean ± STDV, p value)	No. of pits per 3 high power fields (mean ± STDV, p value)
EV NOF	0.0 ± 0.0	0.0 ± 0.0
EV NOF + TGFβ1	25 ± 1.54, p=0.0003	18 ± 2.9, p=0.0004
EV S-NOF^{H2O2}	30 ± 2.35, p=0.0005	20 ± 3.77, p=0.0003
EV S-NOF^{Cis}	25 ± 3.01, p=0.00007	15 ± 2.40, p=0.0009
EV CAF	34 ± 1.06, p=0.0001	20 ± 1.73, p=0.00008
EV H357	36 ± 2.77, p=0.00004	22 ± 3.03, p=0.00002
CAF	41.83 ± 2.7, p=0.0001	36.2 ± 2.7, p=0.00001

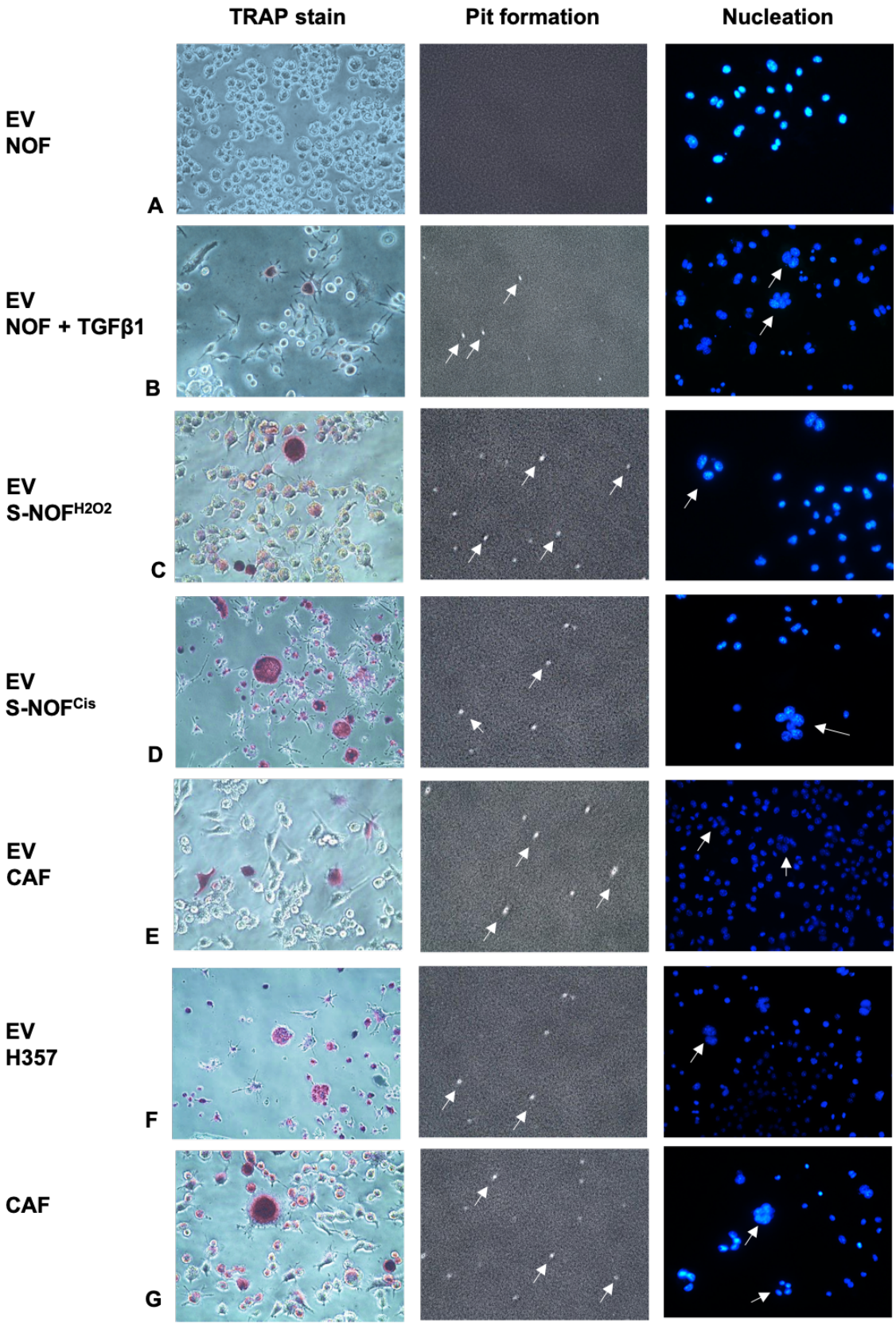
TRAP stain
Pit formation
Nucleation
EV
NOF
A
EV
NOF + TGFβ1
B
EV
S-NOF^{H2O2}
C
EV
S-NOF^{Cis}
D
EV
CAF
E
EV
H357
F
CAF
G

Figure 5.6: Osteoclastogenesis assay with EV isolated from conditioned media. Monocytes (RAW 264.7) were seeded in Osteo Assay surface 24 well plates at a density of 20,000 per well. RAW 264.7 cells were exposed to EV isolated (graded centrifugation and SEC) from conditioned media collected from serum starved (72 h) cells (18, 000,000 cells) in alpha MEM media. (A) NOF (803, 822) EV; TRAP staining negative, no pit formation or multinucleation observed. (B) NOF + TGFβ1 (803, 822) EV (C) S-NOF^{H2O2} (803, 822) EV (D) S-NOF^{Cis} (803, 822) EV; (E) CAF (003, 004) EV (F) H357 EV TRAP positive osteoclasts, pit formation and multinucleated cells observed. (G) CAF (003, 004) conditioned media; media was collected from serum starved CAF and monocytes were exposed to this media. This sample served as a positive control. Osteoclasts stained positive for TRAP, pit formation and multinucleated cells were evident. Error bar=STDV. *$p<0.05$ was considered significant. The graph represents combined results of multiple assays. Experiment was conducted in triplicate. Magnification x40.

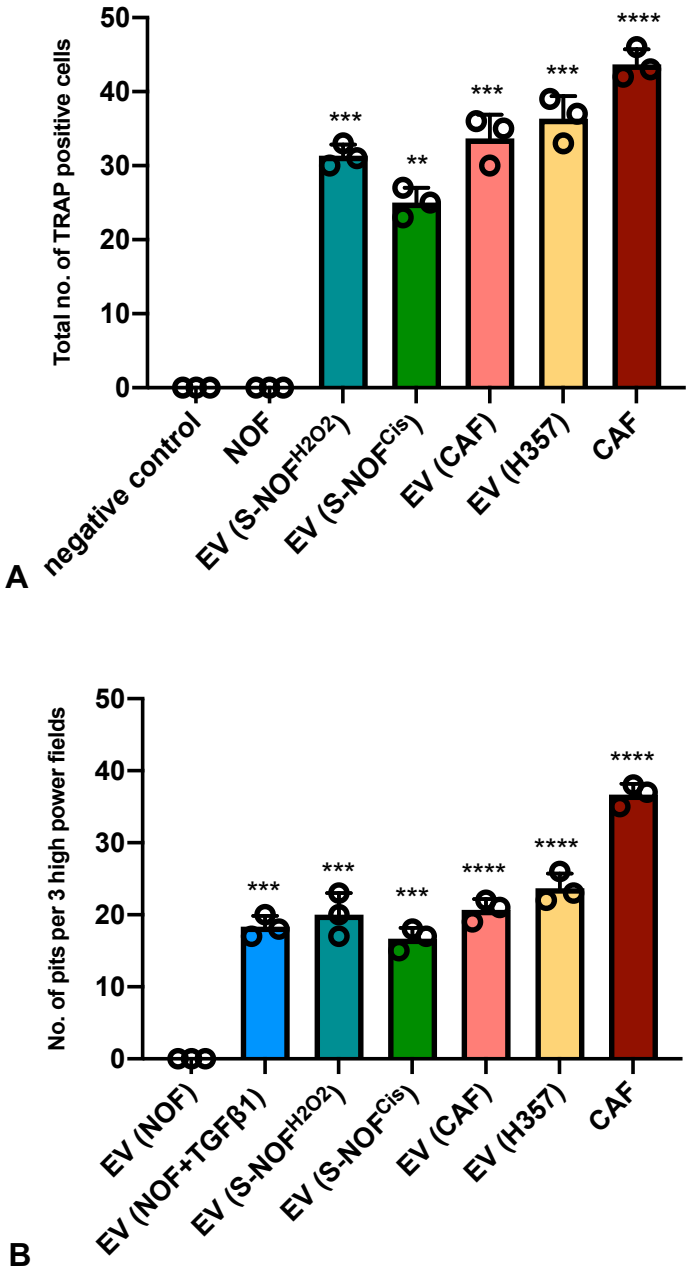

Figure 5.7: EV produced by OSCC, CAF, and senescent oral fibroblasts induce osteoclastogenesis. RAW 264.7 monocytes were seeded in a 24 well plate at a density of 20,000 cells/ well. OSCC cell line H357, CAF (003, and 004), senescent oral fibroblasts (NOF 803, and 822 exposed to H_2O_2 (500 µM) or treated with cisplatin (10 µM) were serum starved in alpha MEM media. EV were isolated by SEC, and monocytes were treated daily with EV isolated from conditioned media for 7 days. (A) The number of TRAP positive cells was counted. EV derived from NOF +TGFβ1 (25 ± 1.54), S-NOF^{H2O2} (30 ± 2.35), S-NOF^{Cis} (25 ± 3.01), CAF (34 ± 1.06), and H357 (36 ± 2.77) (B) Pit formation quantification. The number of pits formed by EV derived from NOF +TGFβ1 (18 ± 2.9), S-NOF^{H2O2} (20 ± 3.77) , S-NOF^{Cis} (15 ± 2.40), CAF (20 ± 1.73), and H357 (22 ± 3.03). Error bar=STDV. *p<0.05 was considered significant, following a Student's t-test. The graph represents combined results of multiple assays. Experiment was conducted in triplicate.

5.6 OPG antagonises RANKL production by EV isolated from OSCC, CAF and senescent fibroblasts and impedes bone invasion in OSCC

The major factors responsible for bone homeostasis are RANK, RANKL and its antagonist OPG. The RANK/RANKL signalling cascade facilitates differentiation of bone lining cells, osteocytes and osteoblasts to osteoclasts, along with M-CSF while OPG suppresses these signals. Alterations in functional equilibrium of these cytokines will either result in osteogenesis, favoured by elevated OPG expression or osteolysis, promoted by elevated RANKL levels.

OPG acts as a signal for bone deposition, and limitation of bone resorption. This experiment was conducted to study the importance of RANKL in bone invasive OSCC and evaluate if blocking RANKL with its decoy receptor OPG, affects osteoclast generation.

5.6.1 Optimisation of RANKL antagonist OPG

Following OPG preparation (section 2.12.1) an osteoclastogenesis assay was conducted as described before (section 2.9). However, unlike the osteoclastogenesis assay previously described, NOF, H357, CAF and S-NOF were treated with OPG at graded concentrations (1 ng/ml, 10 ng/ml, 50 ng/ml, 100 ng/ml and 200 ng/ml) in serum free media. Following 24 h for OPG treatment, monocytes were exposed to the conditioned media and EV collected from the treated cells, and the optimal dose needed for maximum hindering of osteoclast generation was analysed. Conditioned media from serum starved cells (H357, CAF, senescent fibroblasts) served as the positive control, while monocytes in alpha MEM media acted as the negative control. An osteoclastogenesis assay was conducted, and the optimal dose of OPG with the highest reduction in

monocyte differentiation to osteoclast was analysed. A significant reduction (mean ± STDV) in osteoclast numbers was observed following exposure OPG (100ng/ml) exposure. S-NOF^{H2O2} (24.6 ± 2.5, and 3 ± 1.4, p=0.003), CAF (33.92 ± 4.21, and 5 ± 2.2, p=0.00082), H357 (41.77 ± 3.44, and 6 ± 2.55, p=0.00003) (Figure 5.8).

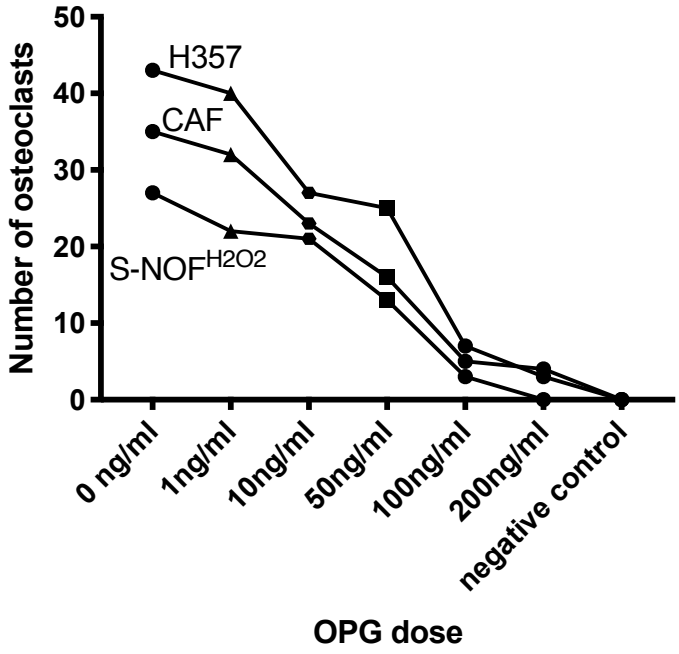

Figure 5.8: Optimisation of cell treatments with recombinant human OPG. NOF, CAF, H357, and senescent oral fibroblasts were serum starved for 24 h and subjected to different concentrations of recombinant human OPG (1ng/ml, 10 ng/ml, 50 ng/ml, 100 ng/ml, and 200ng/ml), prior to exposure to monocytes RAW 264.7, with a daily media change for 7 days. The relative reduction of osteoclast generated following OPG treatment was plotted against dose. Monocytes in serum free alpha MEM media served as the negative control. Experiment was conducted three times in duplicate.

5.6.2 OPG significantly reduces osteoclast generation

To confirm the significance of RANKL in OSCC bone invasion, an osteoclastogenesis assay was conducted (section 2.9), monocytes were exposed to conditioned media and EV collected from serum starved NOF, experimentally induced myofibroblasts (NOF exposed to TGFβ1), CAF (isolated from human OSCC tissue), and S-NOF^{H2O2} treated with OPG (100 ng/ml) (Figure 5.9). The number of TRAP positive cells generated (Figure 5.10 A) and pits formed (Figure 5.10 B) following OPG exposure to conditioned media and EV samples were quantified, and these results were compared to conditioned media not supplemented with OPG, and negative controls (RAW 264.7 in serum free alpha MEM media). A significant reduction in osteoclasts was observed (Table 5.2).

Table 5.2: Number of TRAP positive cells and pits formed following OPG exposure

Sample	Total no. of TRAP positive cells (mean ± STDV, p value)	No. of pits per 3 high power fields (mean ± STDV, p value)
Negative control	0.0 ± 0.0	0.0 ± 0.0
NOF	0.0 ± 0.0	0.0 ± 0.0
NOF + TGFβ1	27.2 ± 3.6, p=0.001	15.3 ± 2.25, p=0.001
NOF + TGFβ1 + OPG	5.05 ± 2.1, p=0.00038	4.7 ± 1.5, p=0.04
EV (NOF + TGFβ1) + OPG	1 ± 1.2, p=0.008	2 ± 1.5, p=0.02
S-NOF^{H2O2}	24.7 ± 3.4, p=0.0007	30.1 ± 5.4, p=0.00003
S-NOF^{H2O2} + OPG	11.83 ± 2.7, p=0.0009	6.8 ± 2.7, p=0.002
EV (S-NOF^{H2O2} + OPG)	3.05 ± 1.8, p=0.0079	2.2 ± 1.3, p=0.04
H357	36.7 ± 4.2, p=0.00004	33.1 ± 4.6, p=0.0002
H357 + OPG	15.01 ± 3.82, p=0.0005	17.02 ± 2.88, p=0.0031
EV (H357) + OPG	7.0 ± 2.8, p=0.006	5.1 ± 3.8, p=0.019
CAF	37.03 ± 3.85, p=0.00003	32.95 ± 7.35, p=0.00007
CAF + OPG	13.04 ± 1.28, p=0.0002	16.01 ± 2.28, p=0.018
EV (CAF) + OPG	5.01 ± 3.39, p=0.008	2.03 ± 1.7, p=0.05

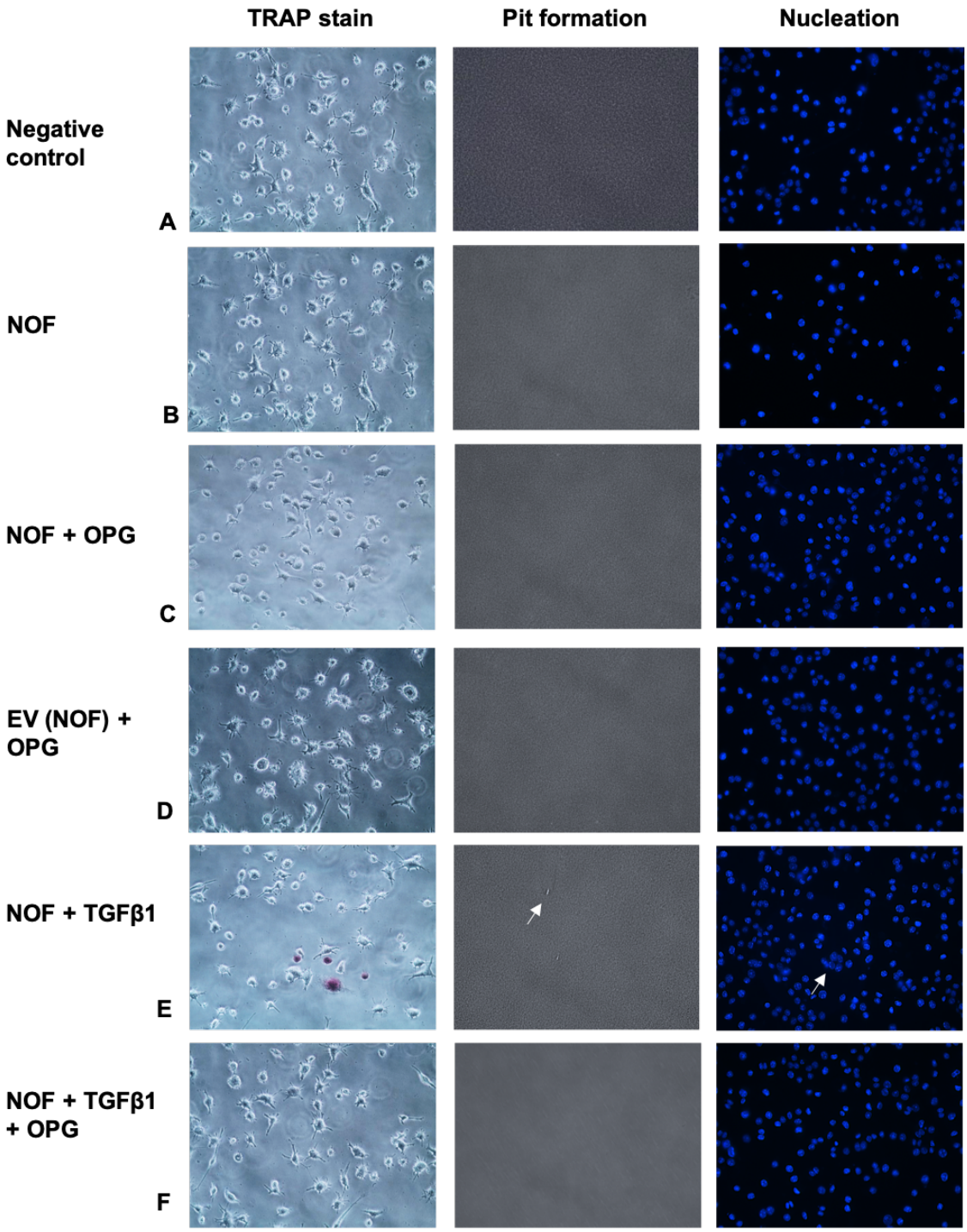
TRAP stain
Pit formation
Nucleation
Negative control
A
NOF
B
NOF + OPG
C
EV (NOF) + OPG
D
NOF + TGFβ1
E
NOF + TGFβ1 + OPG
F

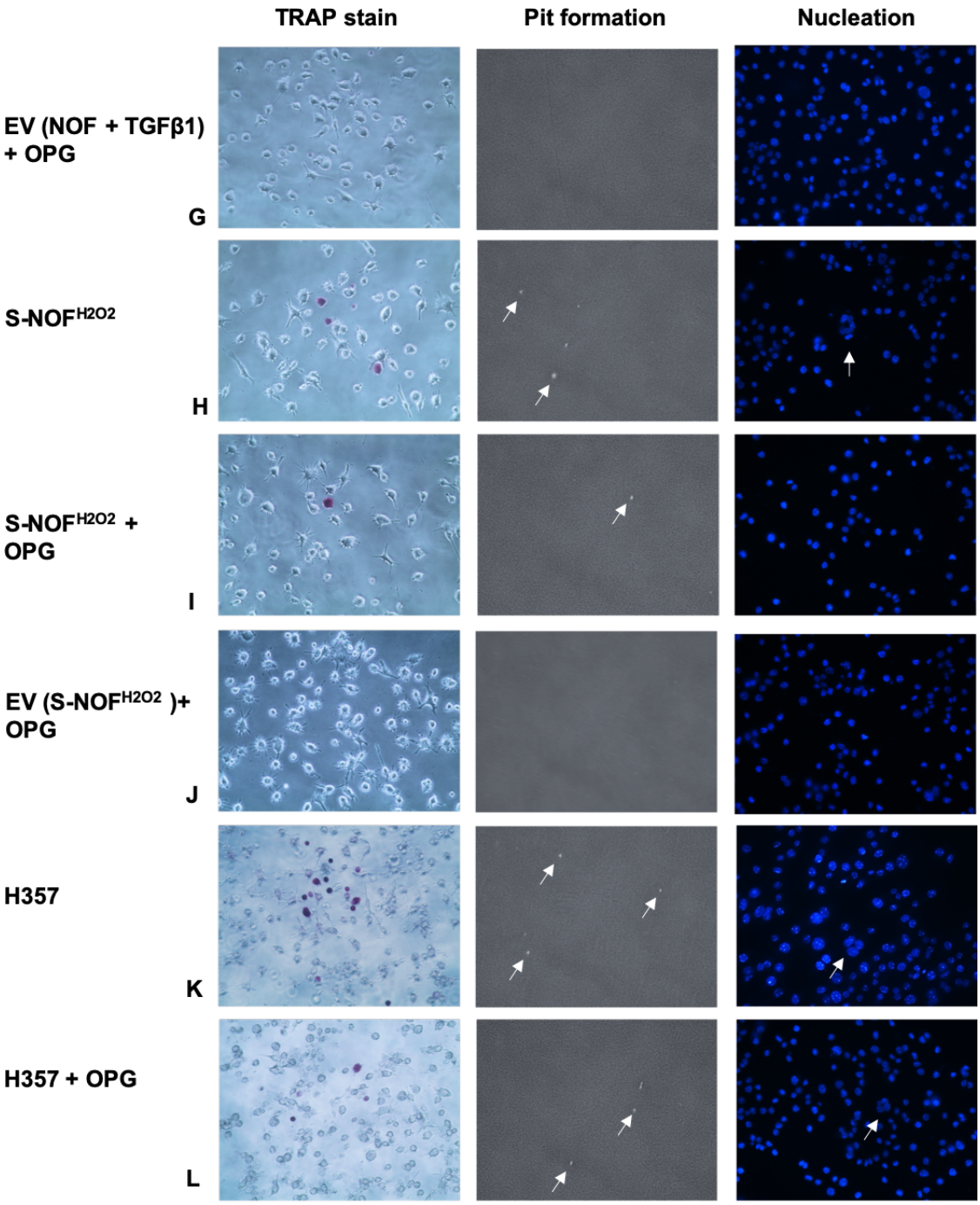
TRAP stain
Pit formation
Nucleation
EV (NOF + TGFβ1) + OPG
G
S-NOF^{H2O2}
H
S-NOF^{H2O2} + OPG
I
EV (S-NOF^{H2O2})+ OPG
J
H357
K
H357 + OPG
L

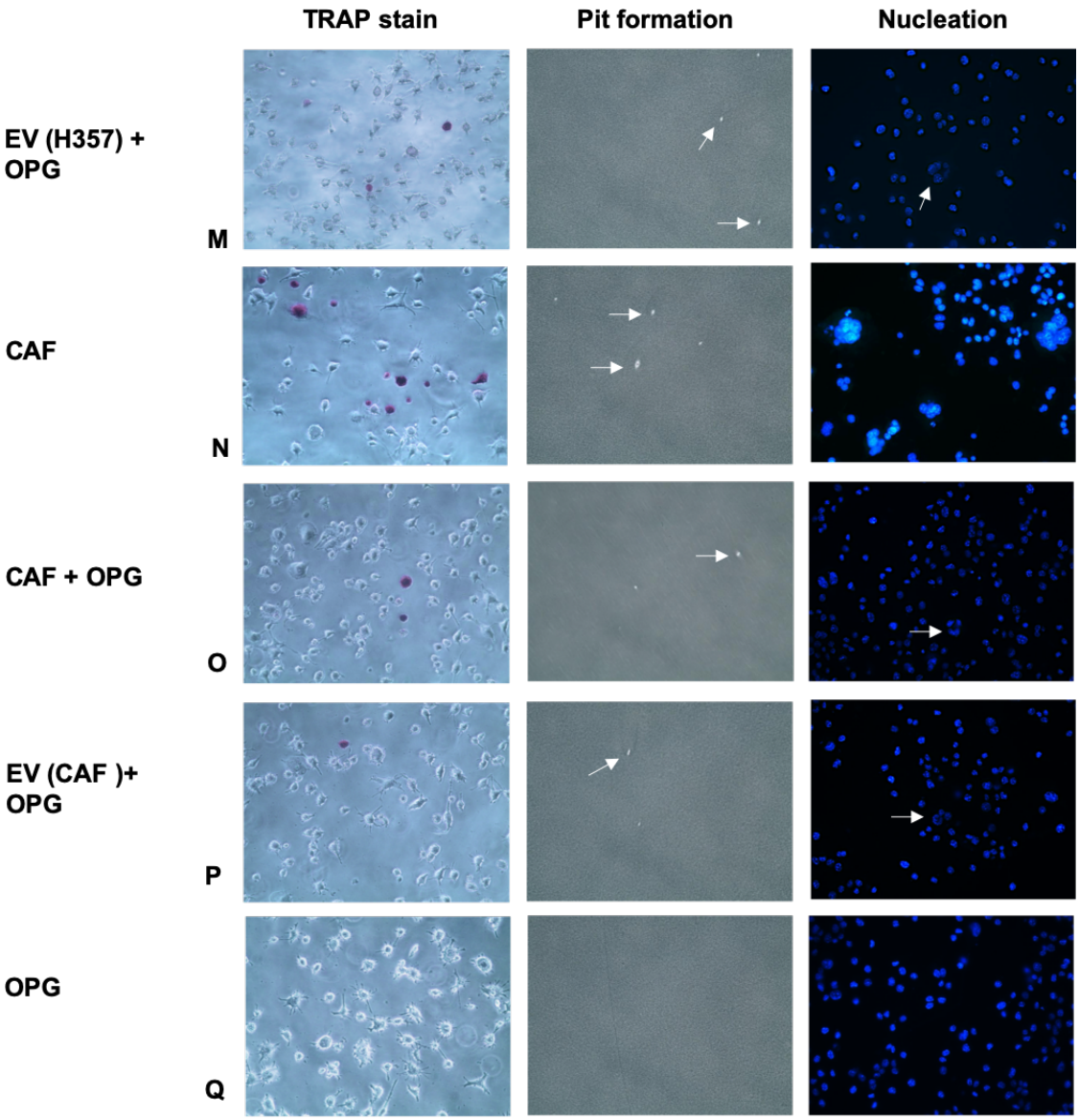
TRAP stain
Pit formation
Nucleation
EV (H357) + OPG
M
CAF
N
CAF + OPG
O
EV (CAF)+ OPG
P
OPG
Q

Figure 5.9: Osteoclastogenesis assay with OPG treatment. Monocytes (RAW 264.7) were seeded in Osteo Assay surface 24 well plates at a density of 20,000 per well. RAW 264.7 cells were exposed to conditioned media or EV isolated (graded centrifugation and SEC) from conditioned media collected from serum starved (72 h) cells (18, 000,000 cells) in alpha MEM media. Samples were then treated with OPG (100 ng/ml) prior to being exposed to monocytes. Media was changed daily for 7 days. (A) Negative control; RAW 264.7 exposed to serum free alpha MEM media. TRAP staining negative, no pit formations or DAPI multinucleation. In samples (B) NOF, (C) NOF conditioned media treated with OPG, and (D) NOF EV treated with OPG, TRAP staining, pit formation and multinucleation was not evident. (E) Experimentally induced CAF/myofibroblasts (NOF treated with 5 ng/ml TGFβ1) conditioned media. TRAP staining was seen in osteoclasts, pit formation was evident, and DAPI staining showed multinucleated cells. (F) Experimentally induced myofibroblasts conditioned media and (G) EV treated with OPG. TRAP positive cells, pit formation and multinucleated cells reduced in number. (H) S-NOF^{H2O2}, NOF803 conditioned media exposed to H_2O_2 (500μM) initiated osteoclast generation, pit formation and multinucleation. (I) S-NOF^{H2O2} media treated with OPG. RAW 264.7 cells were exposed to OPG (100 ng/ml) treated conditioned media collected from serum starved S-NOF^{H2O2}, reduction of osteoclast generation, pit formation and multinucleated cells. (J) S-NOF^{H2O2} EV treated with OPG. TRAP staining was negative, pit formation was absent, and DAPI staining showed no multinucleated cells. (K) H357 conditioned media, TRAP staining was observed positively staining osteoclasts, pit formation was evident, and DAPI staining showed multinucleated cells. (L) H357 conditioned media and (M) EV treated with OPG. A reduction in TRAP staining, pit formation was evident, as well as DAPI stained multinucleated cells. (N) CAF conditioned media. TRAP staining was observed in osteoclasts, pit formation was evident, and DAPI staining showed multinucleated cells. (O) CAF conditioned media and (P) EV treated with OPG. TRAP positive cells, pit formation and multinucleated cells were evident but less in number. (Q) OPG diluted in alpha MEM media. Monocytes were exposed to OPG (100 ng/ml) in alpha MEM media. TRAP staining was negative, pit formation was absent, and DAPI staining showed no multinucleated cells. The experiment was performed three times in duplicate. Magnification x40.

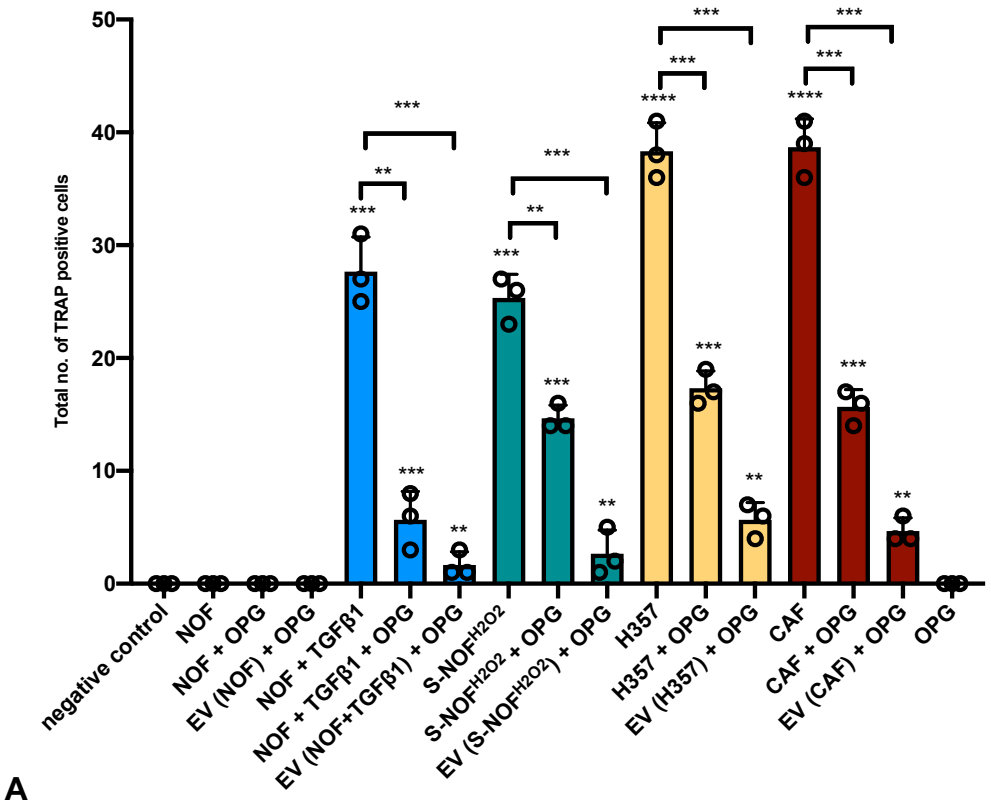
Total no. of TRAP positive cells
50
40
30
20
10
0
negative control
NOF
NOF + OPG
EV (NOF) + OPG
NOF + TGFβ1
NOF + TGFβ1 + OPG
EV (NOF+TGFβ1) + OPG
S-NOF^{H2O2}
S-NOF^{H2O2} + OPG
EV (S-NOF^{H2O2}) + OPG
H357
H357 + OPG
EV (H357) + OPG
CAF
CAF + OPG
EV (CAF) + OPG
OPG

A

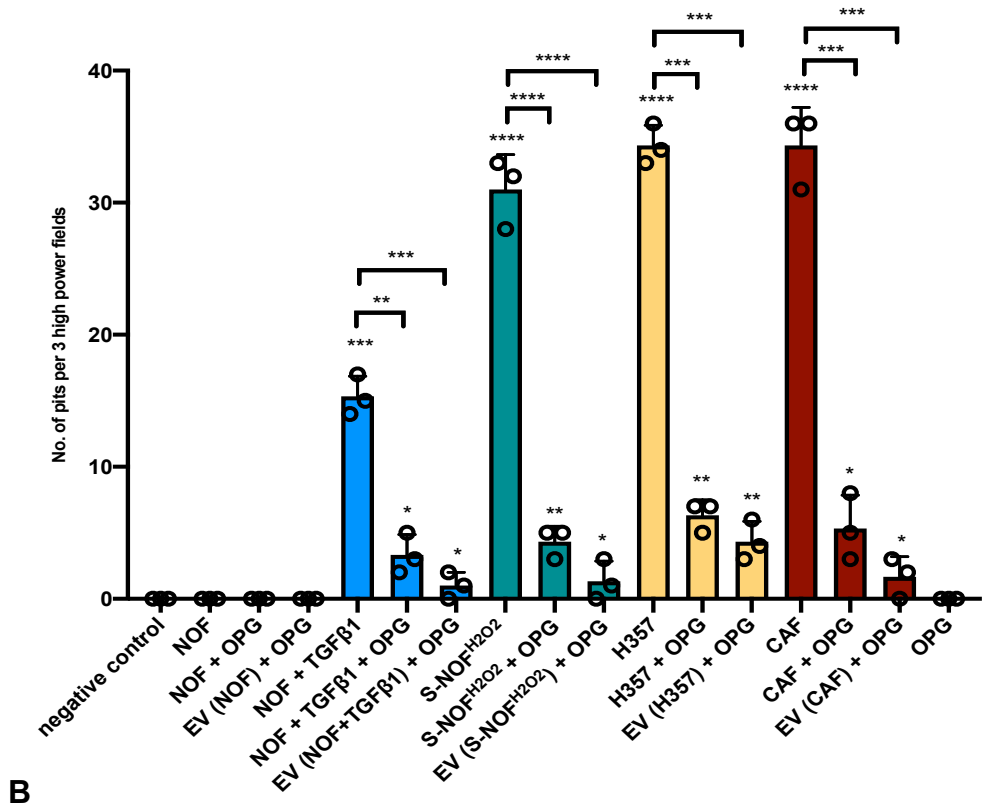
No. of pits per 3 high power fields
40
30
20
10
0
negative control
NOF
NOF + OPG
EV (NOF) + OPG
NOF + TGFβ1
NOF + TGFβ1 + OPG
EV (NOF+TGFβ1) + OPG
S-NOF^{H2O2}
S-NOF^{H2O2} + OPG
EV (S-NOF^{H2O2}) + OPG
H357
H357 + OPG
EV (H357) + OPG
CAF
CAF + OPG
EV (CAF) + OPG
OPG

B

Figure 5.10: OPG significantly reduced osteoclast generation caused by H357, CAF, and senescent oral fibroblasts and derived EV. RAW 264.7 monocytes were seeded in a 24 well plate at a density of 20,000 cells/ well. Normal oral fibroblasts (NOF803), myofibroblast (NOF exposed to TGFβ1, 5 ng/ml), OSCC cell line H357, CAF (003), senescent oral fibroblasts (NOF 803 exposed to H_2O_2 500 μM) or treated with cisplatin (10 μM) were serum starved in alpha MEM media. EV were isolated by SEC, and monocytes were treated daily with conditioned media or EV isolated from conditioned media. A media change was conducted daily, OPG (100 ng/ml) was added to the conditioned media/EV for 7 days. Monocytes exposed to CAF conditioned media served as a positive control, while monocytes treated with OPG diluted in alpha MEM media was a negative (A) The number of TRAP positive cells was counted. A reduction in osteoclastogenesis was significantly noticed throughout the samples. NOF + TGFβ1 (27.2 ± 3.6), NOF + TGFβ1 + OPG (5.05 ± 2.1), EV (NOF + TGFβ1) + OPG (1 ± 1.2), S-NOF^{H2O2} (24.7 ± 3.4), S-NOF^{H2O2} + OPG (11.83 ± 2.7), EV (S-NOF^{H2O2} + OPG) (3.05 ± 1.8), H357 (36.7 ± 4.2), H357 + OPG (15.01 ± 3.82), EV (EV (H357) + OPG) (7.0 ± 2.8), CAF (37.03 ± 3.85), CAF + OPG (13.04 ± 1.28), and EV (CAF) + OPG (5.01 ± 3.39). (B) Pit formation quantification. The number of pits formed due to osteoclasts was counted. NOF + TGFβ1 (15.3 ± 2.25), NOF + TGFβ1 + OPG (4.7 ± 1.5), EV (NOF + TGFβ1) + OPG (2 ± 1.5), S-NOF^{H2O2} (30.1 ± 5.4), S-NOF^{H2O2} + OPG (6.8 ± 2.7), EV (S-NOF^{H2O2} + OPG) (2.2 ± 1.3), H357 (33.1 ± 4.6), H357 + OPG (17.02 ± 2.88), EV (EV (H357) + OPG) (5.1 ± 3.8), CAF (32.95 ± 7.35), CAF + OPG (16.01 ± 2.28), and EV (CAF) + OPG (2.03 ± 1.7). Error bar=STDV. *$p<0.05$ was considered significant, following a Student's t-test. The experiment was performed three times in triplicate.

5.7 Discussion.

In the previous chapters CAF were observed to play a significant role in bone remodelling and OSCC bone invasion. To further investigate the role of EV as communicators in TME, in this chapter, cancer and CAF derived EV were isolated from conditioned media, characterised and examined to determine whether they play a role in bone invasion in oral cancer.

Cancer derived EV have a significant impact on the TME by encouraging tumour angiogenesis, immune cell infiltration, and activation of resting fibroblasts to CAF, mediating tumour progression. Webber et al. (2010), reported that prostate cancer carried TGFβ on the EV surface and actively triggered myofibroblastic differentiation of normal fibroblasts in the TME, which promoted tumour growth. These results are in agreement with findings subsequently reported in gastric (Gu et al., 2012), and breast cancer (Cho et al., 2012). Stromal derived EV have also been suggested to promote invasion and metastasis in breast cancer (Luga et al., 2012). Hence, EV communication between cancer and surrounding stromal fibroblasts may add another dimension to the complexity of TME and contribute to tumour progression. This chapter showed for the first time OSCC communication with the surrounding fibroblastic stroma, and the communication between non-malignant cell of the TME. In particular, the role of EV released by OSCC, CAF, myofibroblasts, and senescent oral fibroblasts in bone remodelling.

In this study, EV were isolated from OSCC cell line H357, CAF, NOF, myofibroblasts (NOF exposed to TGFβ1), and senescent oral fibroblasts (induced by H_2O_2 or cisplatin exposure). Size profiling, and quantification was performed by ZetaView nanoparticle tracking analysis. It is important to highlight that although nanoparticle analysis is commonly used for EV profiling, this technique

has its limitations. The ZetaView lacks specificity in detecting the purity of the sample to be examined, as it records any particles that can be tracked (Bachurski et al., 2019).

To further confirm EV isolation, ExoView analysis which employs affinity-based system on a multiplex microarray chip was conducted to further supplement the data generated by NanoView nanoparticle tracking. In ExoView, tetraspanin CD81, CD63, and CD9 are immuno captured on the chip and observed for each single EV, and the co-expression of a maximum three EV surface proteins can be assessed. Furthermore, EV of a size as small at 50 nM can accurately be detected (Bachurski et al., 2019). Our samples demonstrated an EV size population ranging between 45-70 nm. Tetraspanin marker CD9, CD63, and CD81 were significantly expressed throughout the samples.

The international Society of Extracellular Vesicles has recommended the assessment of EV markers by western blot in EV research (Lötvall et al., 2014). However, in this study several attempts were made but unfortunately due to the low yield of EV quantities and isolated protein, immunoblotting was unsuccessful.

To evaluate the role of EV in bone invasion, the presence or absence of bone resorptive soluble RANKL protein in EV was analysed. EV isolated from conditioned media were subjected to ELISA. RANKL protein expression was significantly increased in EV isolated from H357, CAF and senescent oral fibroblasts compared to NOF. To further evaluate these findings and assess the functionality of RANKL, a functional osteoclastogenesis assay was conducted. RAW 264.7 monocytes were exposed to EV isolates extracted from H357, primary CAF isolated from human OSCC tissue, experimentally induced CAF

(NOF exposed to TGFβ1), S-NOF^{H2O2}. Osteoclast generation was significantly amplified when compared primary human NOF.

Following confirmation that H357, CAF, myofibroblasts, and senescent oral fibroblasts, and derived EV carry RANKL, and play a key role in the initiation of osteoclastogenesis, the ability of recombinant human OPG to block the observed effects was assessed. It has previously been reported that OPG inhibits osteoclast differentiation from murine haematopoietic precursors *in vitro* (Simonet et al., 1996; Lacey et al., 1998). Significant reduction in osteoclast generation was observed following exposure of OPG to both conditioned media and EV, suggesting that bone invasion in OSCC is mainly manipulated through a RANKL dependent pathway.

In conclusion, these results show for the first time that cancer and CAF derived EV carry RANKL, and significantly promote osteoclast generation. On blocking this signal with OPG, osteoclastogenesis was significantly reduced. These results suggest that RANKL expressing EV are involved in cell to cell communication between CAF and osteoclast progenitor cells, and OPG decreases osteoclast formation by interrupting this signal.

Chapter 6

Discussion

6.1 Introduction

Oral squamous cell carcinoma (OSCC) comprises 95% of all neoplasia of the oral cavity, and approximately 30% of head and neck malignancies (Haddad and Shin, 2008). It is the eleventh most common cancer worldwide, with over half a million new patients diagnosed annually, and is the 8th most frequent cause of cancer-related mortality (Warnakulasuriya, 2009). In the United Kingdom alone, more than 11,900 new cases of head and neck cancers were reported in 2016, with an increase in incidence of over 33% for new patients diagnosed with oral cancer in the last decade, and over 4000 oral cancer-related deaths reported annually (Cancer Research UK, 2019).

In the past decade, accumulating evidence has emerged supporting a role for the tumour stroma in cancer progression (Radisky et al., 2007; De Wever et al., 2008; Xu et al., 2009; Marsh et al., 2011; Dourado et al., 2019). Pietras and Ostman, (2010) described the pro-tumourgenic stromal remodelling that occurs due to altered paracrine signalling from neoplastic epithelial cells, generating a more permissible environment promoting tumour progression and spread. Cancer associated fibroblasts (CAF), frequently the predominant cell type in the tumour microenvironment, have been shown to regulate various aspects of tumour advancement, such as the infiltration of immune cells, angiogenesis, and ECM remodelling promoting neoplastic cell migration and metastasis. In addition, the presence of CAF is considered a strong predictor of poor prognosis in OSCC (Surowiak et al., 2007; Kellermann et al., 2007; Marsh et al., 2011; Dourado et al, 2019).

In this study, the contribution of CAF to OSCC bone invasion was investigated. Ebrahimi et al. (2011) reported the frequent complication of bone invasive OSCC,

significantly increasing recurrence, morbidity and mortality rates. Owing to the proximity of maxillofacial bones, OSCC has a high tendency to invade bone (Nomara et al., 2005). However, the precise mechanisms by which OSCC invades bone remains unclear. Invasion of bone by OSCC has traditionally been ascribed to tumour size and a consequence of pressure related resorption (Slootweg and Müller, 1989). However, recent studies suggest that the process is not as simple as originally thought and small tumours can be highly infiltrative with evidence of bone invasion (Fives et al., 2017). This suggests the existence of more complex interactions between tumour, and possibly cells of the TME, and bone.

In our previous study, over 90% of our cohort presented with stroma intervening between tumour front and proximal bone with absence of direct contact between OSCC cells and bone (Elmusrati et al., 2017, masters thesis). These findings suggested that the stroma in OSCC, which predominantly comprises CAF, may play a role in bone invasion. Therefore, in this current study we set out to further investigate interactions between CAF and bone invasion.

CAF are heterogeneous in nature as they differentiate from various cell types and can also be divided into different sub populations (LeBleu and Kallurri, 2018; Liu et al., 2019). Of these different CAF phenotypes, a senescent CAF subgroup has previously been identified (Kabir et al., 2016; Mellone et al., 2017).

This current study is the first to report that CAF, whether isolated from human OSCC tissue, experimentally induced *in vitro* by treatment of human primary NOF with TGFβ1 (myofibroblastic phenotype) or exposed to oxidative (H_2O_2), genotoxic stress (cisplatin) and replicative exhaustion (senescent phenotype)

have a functional role in up regulation of bone turnover markers and promotion of osteoclast generation and activation. Furthermore, we demonstrate a role for CAF-derived RANKL, a key mediator of bone destruction, in this process and provide evidence that extracellular vesicles may act as mediators of these effects. Interestingly, our data indicates that the pro-bone invasive effects of CAF may be ameliorated by a new class of drugs, senolytics, currently entering clinical trials for other indications.

CAF, unlike cancer cells, are genetically stable, making them unlikely to develop resistance, and limiting side effects that are reported with available cancer cell targeted treatments, amplifying their therapeutic potential. Targeting these cells with senolytics may be a promising therapeutic approach to limit tumour spread and bone involvement.

6.2 Myofibroblastic stroma in OSCC

A great deal of attention has been focussed in recent years on studying tumour cell interaction with 'myofibroblastic' CAF in tumour growth and invasion (De Wever et al., 2008). Myofibroblasts were first described in healing wounds, and due to their contractile characteristics, facilitate healing by increasing proximity of wound edges (Majno et al., 1971). These fibroblasts differentiate from multiple cell types and can be divided into different subpopulations. Besides their contribution to wound healing, myofibroblast-like fibroblasts are present in the TME and play a key role in cancer cell proliferation and invasion (Marsh et al., 2011; Elmusrati et al., 2017).

Although there is no specific marker for CAF, αSMA, expressed in myofibroblasts, is the most reliable and frequently used marker to identify CAF histopathologically

(Pietras and Östman, 2010; Dourado et al., 2018). Marsh et al. (2011) highlighted that the presence of a myofibroblastic αSMA positive stroma in OSCC is a more sensitive predictor of disease progression and prognosis than other long standing and well-known parameters such as TNM stage (including tumour size and metastasis), perineural or lymphovascular invasion and depth and pattern of invasion. Despite these recent findings showing the importance of CAF in OSCC, its role in bone invasive OSCC remains largely unexplored. Ishikuro et al. (2008) reported the presence of intervening fibrous stroma that expressed RANK and RANKL in OSCC mandibular bone resections. Moreover, following co-culture of human OSCC cell lines with mouse osteoblasts, an up regulation in RANKL and RANK mRNA expression was reported. We have previously shown that over 90% of our bone invasive OSCC cases did not demonstrate direct contact between tumour cells and bone, and that αSMA positive myofibroblastic CAF were seen intervening, and infiltrating bone ahead of the tumour invasive front. We further investigated the expression of bone turnover markers (RANKL and OPG) in bone invasive OSCC and associated stroma. Interestingly, the bone destructive marker RANKL was highly expressed in both tumour and stroma in close proximity to bone suggesting a potential role of CAF in OSCC bone invasion and bone turnover (Elmusrati et al., 2017).

In our current study, we set out to determine whether there is a difference in αSMA-expression in OSCC stroma, and RANKL/OPG expression adjacent to and away from bone and whether initial staging biopsies from these cases can be used to predict bone invasion. RANKL expression was expressed in tumour cells and surrounding stroma in a number of our samples. On reviewing the histology of resection specimens from these cases, the tumour appeared to be in close

proximity to bone. However, OPG staining was either weak or absent. These findings are quite similar to previous studies in the context of tumour and bone cells (Kayamori et al., 2010; Ishikuro et al., 2005; Tada et al., 2005) and show that RANKL expression is more prominent near bone, suggesting that RANKL plays a key role in promoting bone invasion

Chuang et al. (2009) compared the IHC expression of osteoclastogenesis markers RANKL and OPG in OSCC samples with and without bone involvement. Amplified RANKL, and reduced OPG staining was evident in OSCC cells in both groups. This expression may be due to the proximity of underlying bone to tumour front, and the capability of both OSCC groups to initiate bone invasion. This study also reported positive RANKL expression in normal oral mucosa (control group), which is unusual and highlights the need for further investigations to determine the validity of these findings.

Osteoblasts express RANKL and are necessary in promotion of osteoclast generation and activation (Kular et al., 2012). To further investigate the effect of H357 and CAF on RANKL and OPG mRNA expression in primary human osteoblasts, an indirect co-culture method was employed. A significant amplification of RANKL and down regulation of OPG on a transcript level was consistently noted in HOB after exposure to H357 and CAF conditioned media following 24 h compared to controls (human primary osteoblasts in serum free media). Our findings are in agreement with previous research where an indirect co-culture of murine osteoblast with OSCC (BHY) conditioned media show an upregulation in mRNA RANKL (Ishikuro et al., 2008). This is also in keeping with previous studies that have reported mRNA OPG down regulation when BHY (human OSCC cell line) cells were cultured with primary murine osteoblasts (Jimi

et al., 2011). Interestingly, these RANKL expressing BHY cells, when inoculated into mice, developed a highly invasive tumour but were unable to initiate osteoclast differentiation from murine haematopoietic cells. However, this study did not consider investigating any other tumour microenvironment variables, and only focused on the effect of cancer cells on mouse osteoblasts. In our study, we demonstrate for the first time the effect of CAF-derived factors on RANKL and OPG expression in primary human osteoblasts.

Previous studies have demonstrated that OSCC cell lines can promote myofibroblastic transdifferentiation of oral fibroblasts by conditioned media treatments through TGFβ1 signalling (Lewis et al., 2004; Marsh et al., 2011; Webber et al., 2018). In culture, exposure of fibroblasts to recombinant TGFβ1 is sufficient to induce a myofibroblastic phenotype (Sobral et al., 2011). In the current study, primary NOF isolated from human gingival tissue were treated with an optimal dose (5 ng/ml) of recombinant TGFβ1 for 24 h to trigger the transition of resting NOF to a myofibroblastic, CAF-like phenotype (Elmusrati et al., 2017; Melling et al., 2018). Following TGFβ1 stimulation, αSMA is integrated in actin stress fibres, increasing the contractility of normal fibroblasts (Serini and Gabbiani, 1999; Lewis et al., 2004; Hinsley et al., 2011). In keeping with these, αSMA expression was observed in contractile stress fibres through immunofluorescence and was significantly amplified on a transcript level in experimentally induced CAF as well as CAF isolated from human tissue compared to controls. CAF isolated from human OSCC tissue and experimentally induced CAF share common characteristics, however, it is now known that myofibroblastic CAF induced through TGFβ1 signalling pathway represent only a subpopulation of CAF (Lewis et al., 2004; Kellermann et al., 2008; Mellone et al.,

2017). Other subpopulations, such as those displaying a senescent phenotype through the expression of both αSMA and senescent marker p16INK4a have been reported as a CAF subset (Mellone et al., 2017).

Bone invasion in OSCC is mainly regulated by the differentiation and activation of osteoclasts from hematopoietic precursors (Jimi et al., 2010). It has previously been proposed that stromal cells and osteoblasts are required in osteoclast generation through a process involving cell-to-cell communication with osteoclast precursors. This assumption was further confirmed by the discovery of TNF ligand RANKL (Suda et al., 1999; Boyle et al., 2003). Osteoclastogenesis is a complex mechanism regulated by three necessary molecules, RANKL expressed by osteoblasts, stromal and cancer cells and osteoblasts, its receptor RANK found on osteoclasts, and decoy RANKL antagonist OPG regulated by osteoblasts. RANKL and M-CSF have been reported to promote osteoclastogenesis in the absence of osteoblasts highlighting the importance of these markers in osteoclast differentiation and survival (Suda et al., 1999; Ross and Teitelbaum, 2005). In the current study, osteoclasts were generated from the murine macrophage cell line RAW 264.7. It has been previously reported that the murine macrophage cell line RAW 264.7, upon exposure to RANKL readily triggers osteoclastogenesis (Vincent et al., 2009). The advantage of using RAW 264.7 cell is that they express both M-CSF and its receptor c-fms, and no treatment with M-CSF is required (Marino et al., 2014). RAW 264.7 monocytes were exposed to conditioned media collected from experimentally induced myofibroblastic CAF, and CAF isolated from human OSCC tissue. In our study, we observed morphological transdifferentiation of RAW 264.7 cells to large multinucleated cells after five days, and TRAP positive osteoclasts within seven

days of RANKL treatment. In addition, osteoclast functionality was evaluated by observing resorption pit formation on osteo-surface wells. Although H357 cells induced osteoclastogenesis, CAF showed the highest influence on osteoclast generation and these results were also reflected in pit forming assays showing multi-nucleation indicative of osteoclastogenesis. This is the first evidence that CAF are able to influence osteoclastogenesis, suggesting they may play a role in bone invasion.

6.3 Senescence promotes OSCC bone invasion

A considerable amount of research has focused on the role of αSMA-expressed myofibroblasts or CAF in tumour microenvironment. However, in recent years it has become evident that CAF represent a heterogeneous population with different fibroblastic phenotypes, suggesting that these distinct activated fibroblasts may have discrete roles in cancer progression (Shiga et al., 2015; Prime et al., 2017; Puram et al., 2017). A subpopulation of CAF that show characteristics of senescence are also evident in premalignant lesions (Costea et al., 2013; Procopio et al., 2015) as well as OSCC stroma (Hassona et al., 2013). Laberge et al. (2015), reported the characteristic features of senescent cells comprising a state of irreversible growth arrest, whilst maintaining metabolic activity, and expressing elevated levels of cytokines, growth factors and extracellular matrix components. This altered secretome is referred to as senescence associated secretory phenotype (SASP).

Two separate types of CAF have been isolated from genetically stable (GS-OSCC) and unstable (GU-OSCC) oral cancers. In this study, OSCC characterisation was based on the expression of p53 and p16INK4a mutations. The research group reported that CAF extracted from GU-OSCC were senescent

due to their loss of p53 and p16INK4a, while in contrast CAF isolated from GS-OSCC exhibited wild type p53 and p16INK4a (Lim et al., 2011). Hassona et al. (2013) further contemplated that the development of the senescent CAF phenotype was caused by amplified levels of ROS related to TGFβ1, and TGFβ2, resulting in oxidative DNA damage. However, not all CAF in this model were senescent, further confirming CAF heterogeneity in OSCC.

In the current study, senescent CAF were identified through immunohistochemical analysis of tissue from OSCC bone resections. Staining for senescence markers p16INK4a and DPP4/CD26, a recently discovered marker, reported to specifically be expressed on senescent cells following mass spectrometry analysis (Kim et al., 2017), was seen in stromal CAF proximal to invading bone.

Mellone et al. (2017) analysed the two CAF subtypes, αSMA positive myofibroblasts and senescent fibroblasts. They showed that senescent CAF predominantly expressed αSMA in vivo, and that following senescence induction *in vitro* (irradiation, exposure to H_2O_2, cisplatin and replicative exhaustion) developed molecular and morphological features similar to myofibroblasts induced through the TGFβ1 signalling pathway. Co-expression of p16INK4a and αSMA in senescent fibroblasts was also confirmed using dual IF staining. In our study, double immunostaining on OSCC bone resections was conducted to examine whether a subpopulation of senescent CAF was present within the αSMA positive population. Co-localisation of senescence marker p16INK4a in αSMA positive CAF was evident in our cohort confirming the presence of senescent CAF in bone invasive OSCC stroma. These findings were in

agreement with previous studies (Hassona et al., 2013; Mellone et al., 2017; Dourado et al., 2019).

Senescence induction can be induced *in vitro* by DNA damaging stimulants as exposure to H_2O_2, cisplatin, replicative exhaustion or irradiation (Prime et al., 2017, Mellone et al., 2017). In this study, to examine mechanistically whether senescent oral fibroblasts could influence bone remodelling, senescence was induced in normal oral fibroblasts at a low passage. Following five days of H_2O_2 or cisplatin treatment, and after being cultured to replicative exhaustion (passage 25), the majority of the fibroblasts exhibited a flattened and expanded morphology (Wagner et al., 2008), and were significantly positive for SA-β-Gal, indicative of senescence induction in agreement with previous studies (Kabir et al., 2016).

Due to the lack of one specific marker to identify cellular senescence, and SA-β-Gal becoming the most reliable and widely used senescence biomarker, a panel of indicators was required to confirm senescence induction. Sudan B Black (SBB), a histochemical stain for lipofuscin, which accumulates in aging cells, has recently been reported to identify senescent cells (Georgakopoulou et al., 2013). Therefore, to support the SA-β-Gal and p16INK4a data, SBB abundance was analysed in fibroblasts in culture. Black granular deposits of SBB were evident, further confirming senescence in primary CAF isolated from human OSCC, and experimentally induced senescent CAF (S-NOF^{H2O2}, S-NOF^{Cis}, and S-NOF^{Rep}).. These results are in agreement with the cytological staining reported by Georgakopoulou et al. (2013). However, the SBB staining in FFPE tissue sections reported by the group was somewhat unreliable and controversial, as staining did

not appear specific. In the current study, SBB was also attempted in tissue from FFPE OSCC bone reactions however staining appeared variable and not specific to senescent cells. The lack of specificity in staining lipofuscin in paraffin embedded section may be due to elimination of these lipoproteins in the process of tissue preservation and deparaffinisation, making senescence difficult to identify in archived, fixed, tissue. The lack of a reliable marker of senescence in fixed tissue remains a problem for the field; however, in this thesis we observed specific staining of stromal cells for DPP4, a recently described marker of senescent cells, suggesting this may be a good senescence indicator in FFPE tissue.

Senescent CAF have been reported to express αSMA (Mellone et al., 2017), and αSMA positivity in OSCC stroma has been reported to be linked to poor survival (Kellermann et al., 2007). In this study. CAF isolated from human OSCC and senescent CAF induced *in vitro* (S-NOF^{H2O2}, S-NOF^{Cis}, and S-NOF^{Rep}) exhibited apparent αSMA positive stress fibres when compared to unstimulated primary NOF, following immunofluorescence. These findings suggest that senescent CAF may represent a population of αSMA positive CAF identified in OSCC, and these cells must be considered when investigating prognosis and potentially CAF-targeting therapy.

In bone, cellular senescence accumulating at pathological sites has a detrimental effect on bone mass (Kim et al., 2017; Farr et al., 2019). Chen et al., (2013), reported that an increased cellular senescence in bone resulted in an upregulation of SASP components such as IL6, TNFα, and NF-kB ligand (RANKL), and a decrease in OPG protein, leading to an unbalanced RANKL to OPG ratio promoting osteoclastogenesis and favouring bone destruction.

In this study, further analysis of senescence marker p16INK4a, IL6 and bone turnover RANKL and OPG in senescent CAF revealed a significant increase in p16INK4a, IL6 and RANKL, while OPG expression was downregulated on a transcript level throughout our cohort when compared to NOF. The prime bone destruction marker RANKL is expressed in both membrane bound and secreted soluble forms (Ikeda et al., 2001). Based on the evidence that NF-kB signalling is activated in senescence (Chen et al., 2013; Kim et al., 2017) and SASP develop with time (Kabir et al., 2016; Ohtani, 2019) an ELISA was conducted to investigate the expression of soluble RANKL protein at different time intervals following senescence induction *in vitro*. RANKL expression was significantly up-regulated in S-NOF^{H2O2}, S-NOF^{Cis}, and S-NOF^{Rep} following 5 days, 15 days of senescence induction and at passage 25 respectively. These findings provide direct evidence that senescent oral fibroblasts can synthesise and secrete elevated levels of RANKL, and the kinetics are similar to those of the well-established SASP component IL6, indicating that RANKL may be considered a novel component of SASP.

Exposure of RAW 264.7 monocytes to conditioned media collected from senescent fibroblasts resulted in osteoclast generation. These findings suggest that the TME composed of senescent and myofibroblastic CAF could potentially contribute to OSCC-mediated bone destruction.

6.4 Senolytics, a promising therapeutic application in limiting bone invasion in OSCC

The common modality for treatment of OSCC with bone involvement is surgery with bone resection followed by chemo and/or radiotherapy. Unfortunately, the available chemotherapeutic drugs are cytotoxic for both normal and cancerous cells. In addition, exposure of the tumour and surrounding normal tissue to genotoxic stress caused by chemotherapeutic drugs such as cisplatin or high doses of radiation may further complicate treatment by triggering senescence induction.

Senolytic drugs have recently been shown to selectively promote apoptosis in senescent cells, decreasing their pro-tumourgenic burden (Short et al., 2019). Several senolytics have been developed targeting different pro-apoptotic pathways. In this study, Navitoclax (ABT263) - an inhibitor of BCL-2 family - was used. Navitoclax has been reported to trigger senescent cell death in some but not all human and mouse cells (Chang et al., 2016; Zhu et al., 2016; Moncsek et al., 2018), however, toxicity has been reported due to weak cell selectivity exhibited with BCL-2 senolytics (Garland et al., 2013). Nonetheless, since the development of navitoclax as a senolytic it has been substantially used as a tool to study senescence (Chang et al., 2016; Kim et al., 2017; Zhu et al., 2017). Kim et al., (2017) recently reported an increase in apoptosis of bone marrow stromal cells following treatment with navitoclax in aged mouse models. This depletion in senescent cell burden in bone microenvironment resulted in a significant decrease in RANKL expression, further impeding osteoclast formation.

More recently, HSP90 inhibitors (17-DMAG) have been identified as a novel group of senolytic drugs (Fuhrmann-Stroissnigg et al., 2017). HSP stabilizing proteins have been reported to be associated with tumour cell proliferation in several cancers, making it a potential drug target (Taipale et al., 2010). Numerous current and previous clinical trials have explored the use of HSP90 solely or in adjunction with chemo or radiotherapy (Trepel et al., 2010; Jhaveri et al., 2012; Shah et al., 2018). HSP90 inhibitors are not only expressed in pathology,but have important physiological roles in cellular processes.It is probably for these reasons that there are still no FDA approved HSP90 inhibitors available for cancer treatment.

Following demonstration that senescent fibroblasts are able to promote osteoclastogenesis, we next assessed whether the removal of senescent fibroblasts would reduce the paracrine effects promoting osteoclastogenesis. Previous reports have demonstrated the pro apoptotic functionality of senolytics in targeting CAF in hepatocellular carcinoma, nonetheless senescence was never examined (Chen et al., 2016). However, this current study is the first to specifically target senescent CAF with senolytics. Doses were selected targeting senescent fibroblasts but having minimal effect on proliferative cells. Significant reduction in osteoclast generation was recorded following exposure of senescent fibroblasts to both senolytics. Although the reduction in osteoclastogenesis was significant when CAF were exposed to Alvespimycin and Navitoclax, this reduction was less compared to experimentally induced S-NOF. These findings may be due to the heterogeneous nature of primary CAF isolated from OSCC, comprising different phenotypes.

6.5 Cell to cell communications in the tumour microenvironment are mediated by secreted EV

In the past decade, a role has been established for EV in cell-to-cell communication. In the context of cancer, the cross talk between tumour and associated microenvironment is crucial to support cancer development and invasion. EV are involved in diverse mechanisms that sustain tumour advancement including angiogenesis, inflammation, EMT transition, cell proliferation as well as migration subsequently leading to invasion and metastasis (Becker et al., 2016; Xu et al., 2018).

Unfortunately, the literature is lacking in research on oral cancer/OSCC derived EV. Most of the published studies have focused on investigating oral cancer biomarkers in EV isolated from saliva (Tanaka et al., 2013; Winck et al., 2015; Iwai et al., 2016; Kawahara et al., 2016) highlighting its diagnostic and prognostic potential in oral cancer. More recently, Dourado et al. (2019) reported that CAF-derived EV secreted in the tumour microenvironment promoted OSCC cell proliferation and invasion. This research group highlighted the heterogeneous nature of five primary CAF cultures isolated from well differentiated OSCC of the lateral border of the tongue or floor of mouth. All the primary CAF exhibited myofibroblastic features, and senescent phenotypes were also detected in these cultures (approximately 20% of the CAF population). Moreover, CAF-derived EV showed an increased proteolytic profile and loss of cell adhesion factors when compared to EV isolated from NOF following proteomic analysis, explaining the migratory phenotype of CAF, and on further exposure of OSCC cell lines to CAF-EV, an increase in OSCC cell migration was reported.

To date, the role of EV in bone invasion hasn't been studied. However, recent reports have investigated the role of EV in bone remodelling, providing evidence that EV play a functional role in the dynamics of bone synthesis and resorption (Deng et al., 2015; Yin et al., 2017; Tao and Guo, 2019). These findings provided rationale to investigate the role of EV in bone invasive OSCC.

In the current study, EV were isolated from OSCC cell line (H357), primary NOF and CAF, experimentally induced CAF (NOF exposed to TGFβ1) and senescent fibroblasts (S-NOF^{H2O2}, S-NOF^{Cis}). To enhance purity and decrease contaminants, graded centrifugation followed by SEC was chosen as an optimal method in isolating EV from cell culture supernatants (Gardiner et al., 2016).

Following EV extraction, size profiling and quantification, characterisation was conducted to confirm EV isolation. Well-established EV 'markers' CD9, CD63, and CD81 were examined, and were significantly observed throughout our samples confirming EV isolation.

To investigate the potential of EV to communicate with osteoclast precursors and initiate osteoclastogenesis, RANKL expression was examined through an ELISA and the soluble RANKL protein was significantly increased in EV isolated from conditioned media collected from H357, CAF and senescent oral fibroblasts compared to NOF.

To further evaluate these findings and assess the functionality of RANKL, RAW 264.7 monocytes were exposed to EV isolates extracted from H357, primary CAF from human OSCC tissue, experimentally induced CAF (NOF exposed to TGFβ1), S-NOF^{H2O2}, S-NOF^{Cis}, and compared to primary human NOF, in an attempt to study the influence of EV derived from these cells on osteoclastogenesis,

Osteoclast generation and activation was evident throughout the samples, suggesting a significant contribution of RANKL expressed EV in bone invasive OSCC. Previous reports have implicated EV in bone remodelling (Deng et al., 2015; Yin et al., 2017; Tao and Guo, 2019). However, this data is the first to show the effect of cancer cell and CAF-derived EV, and the first to directly demonstrate association of RANKL with EV in OSCC related bone invasion.

OPG, a decoy receptor of RANKL has been reported to limit bone resorption by inhibiting osteoclast formation (Simonet et al., 1997). Several studies have shown that following administration of OPG, cancer cell invasion or metastasis to bone was inhibited (Canon et al., 2008; Armstrong et al., 2008; Tada et al., 2013). These results suggest that RANKL is the key modulator of bone involvement in cancer. Tada et al. (2013), demonstrated that by treating a co-culture of OSCC cells and murine osteoblasts with OPG, osteoclastogenesis was inhibited. Furthermore, in a recent study, RANKL expression in OSCC cells was inhibited following OPG exposure, and conditioned media collected from OSCC cells following RANKL knockout decreased osteoclast generation and bone resorption (Sambandan et al., 2017).

In this current study, and previously published data (Elmusrati et al., 2017) RANKL expression was seen in tissue OSCC bone resections with staining seen in carcinoma cells and CAF invading bone ahead of tumour using IHC. Moreover, following the observation that OPG expression was down regulated in H357, primary CAF, experimentally induced myofibroblasts, and S-NOF, while increased levels of RANKL in H357, CAF, myofibroblasts, and senescent oral fibroblasts, and EV derived from these cells was observed *in vitro*. This further suggests that RANKL play a key role in bone invasive OSCC.

Recombinant human OPG, was used to target RANKL/RANK signalling cascade. Significant reduction in osteoclast generation was recorded following exposure of both conditioned media and EV to OPG. These findings suggest that obstructing RANKL/RANK interaction with OPG can impede osteoclastogenesis and inhibit bone invasion in oral cancer.

6.6 Prospective implications in improvement of cancer therapies

Bone destruction associated with OSCC invasion is a devastating sequel leading to a poor prognosis. Numerous studies have focused on understanding the pathway by which carcinoma cells invade bone in oral cancer, however, the molecular mechanism associated with how CAF promote tumour advancement is not fully understood. CAF, unlike cancer cells, are generally thought to be genetically stable and therefore make good therapeutic targets as resistance is unlikely to develop.

Amongst the heterogeneous subpopulations of CAF in oral carcinomas, the myofibroblastic and senescent phenotypes are the most characterised. The introduction of senolytic drugs that target CAF in anti-cancer therapies is an expanding and particularly promising specialty of contemporary research for modern cancer treatments. However, this study is the first to utilise senolytic drugs to target senescent CAF and derived EV. Alvespimycin and Navitoclax demonstrated a significant reduction in senescent CAF burden, and further reducing OSCC bone destruction by osteoclastogenesis impediment.

The perspective of EV targeted cancer therapies has also recently emerged. EV have low immunogenicity, biocompatible and are naturally capable of

communicating with target cells. They can carry cargo of vast oncogenic proteins, and also have potential for drug delivery as well (Samanta et al., 2018). The growing focus on EV in cancer, however, brings about new challenges as isolation and quantification, and whether current technologies are efficient in detecting minimal EV levels remains controversial. Regardless of these obstacles, unlike protein biomarkers, EV contain RNA which can be promptly amplified and profiled, providing advanced opportunities for the development of diagnostic biomarkers in cancer. Moreover, EV also have the ability to transmit messages raising the possibility that senescent cells may potentially have systemic effects on the body.

6.7 Conclusions

I. αSMA-positive CAF intervening between tumour and underlying bone appear to play a role in bone invasive OSCC.

II. RANKL and OPG expression *ex vivo* correlates to proximity of tumour to bone. The expression of both RANKL and OPG is higher in cases with frank OSCC bone invasion.

III. Indirect co-culture of human primary osteoblasts with conditioned media from human OSCC and human isolated CAF significantly amplify RANKL and reduce OPG mRNA expression *in vitro*.

IV. Treatment of normal oral fibroblasts with recombinant TGFβ1 induces transdifferentiation of resting fibroblasts to a αSMA positive CAF phenotype, significantly increasing RANKL expression on a transcript and protein level, and further promoting osteoclastogenesis.

V. Senescent fibroblasts can be experimentally induced by exposure to oxidative (H_2O_2), genotoxic stress (cisplatin) and replicative exhaustion.

VI. Conditioned media collected from primary CAF isolated from fresh human oral tissue, and experimentally induced senescent fibroblasts (S-NOF^{H2O2}, S-NOF^{Cis}, and S-NOF^{Rep}) and derived EV, show significantly higher expression of soluble RANKL protein compared to NOF.

VII. EV isolated from H357, primary CAF, experimentally induced myofibroblasts (NOF exposed to TGFβ1), S-NOF^{H2O2}, S-NOF^{Cis} produce significantly more RANKL protein compared to NOF derived EV.

VIII. CAF isolated from human tissue, experimentally induced myofibroblasts (NOF exposed to TGFβ1) and experimentally induced senescent fibroblasts (S-NOF) all show a significant increase in osteoclast generation.

IX. Senolytics Alvespimycin and Navitoclax, significantly promote death in senescent fibroblasts, and reduce osteoclast formation.

X. Recombinant OPG blocks RANKL expression in CAF and senescent fibroblasts and derived EV, and reduces osteoclastogenesis

To summarise, this study shows that CAF play a key role in bone invasive OSCC providing an opportunity for therapeutic intervention.

6.8 Future work

I. Our restricted ethical approval limited the extent of the clinical data to be analysed. We would further like to expand and correlate all the OSCC bone invasive clinical reports for 5-year disease free survival rate and prognostic evaluation.

II. Examining a larger histological and IHC bone invasive cohort, and further increasing the control group as well.

III. Further verify the presence of CAF in tumour microenvironment but studying other myofibroblastic IHC markers as FAP and FSP.

IV. Examine other components of the tumour environment as inflammatory cells, through IHC staining for lymphocytes, macrophages and endothelial cells and correlate with bone invasion.

V. Further examine the role of CAF and senescent oral fibroblasts on osteoclastogenesis *in vivo*.

VI. Investigate the efficacy of senolytics or senomorphics on OSCC bone invasion *in vivo.*

References

Abd Elmageed, Z., Yang, Y., Thomas, R., Ranjan, M., Mondal, D., Moroz, K., Fang, Z., Rezk, B., Moparty, K., Sikka, S., Sartor, O. and Abdel-Mageed A. (2014). Neoplastic reprogramming of patient-derived adipose stem cells by prostate cancer cell-associated exosomes. Stem Cells, 32(4), pp.983-997.

Allan, E., Hausler, K., Wei, T., Gooi, J., Quinn, J., Irwin, B., Pompolo, S., Sims, N., Gillespie, M., Onyia, J. and Martin, T. (2008). EphrinB2 regulation by parathyroid hormone (PTH) and PTHrP revealed by molecular profiling in differentiating osteoblasts. Journal of Bone Mineral Research. 23, pp.1170–81.

Allen, M. and Louise Jones, J. (2011). Jekyll and Hyde: the role of the microenvironment on the progression of cancer. Journal of Pathology, 223.2, pp.163-177.

Alspach, E., Flanagan, K., Luo, X., Ruhland, M., Huang, H., Pazolli, E., Donlin, M., Marsh, T., Piwnica-Worms, D., Monahan, J., Novack, D., McAllister, S. and Stewart, S. (2014). p38MAPK plays a crucial role in stromal-mediated tumorigenesis. Cancer Discovery, 4(6), pp.716-729.

Andaloussi, S., Mäger, I., Breakefield, X. and Wood, M. (2013). Extracellular vesicles: biology and emerging therapeutic opportunities. Nature Reviews Drug Discovery, 12(5), p.347.

Anderberg, C. and Pietras, K., (2009). On the origin of cancer-associated fibroblasts. Cell Cycle, 8(10), pp.1461-1465.

Armstrong, A., Miller, R., Jones, J., Zhang, J., Keller, E. and Dougall, W. (2008). RANKL acts directly on RANK-expressing prostate tumour cells and mediates migration and expression of tumour metastasis genes. Prostate. 68, pp.92-104.

Augsten, M. (2014). Cancer-associated fibroblasts as another polarized cell type of the tumor microenvironment. Frontiers in Oncology, 4, p.62.

Bachurski, D., Schuldner, M., Nguyen, P., Malz, A., Reiners, K., Grenzi, P., Babatz, F., Schauss, A., Hansen, H., Hallek, M. and Pogge von Strandmann, E. (2019). Extracellular vesicle measurements with nanoparticle tracking analysis–An accuracy and repeatability comparison between NanoSight NS300 and ZetaView. Journal of Extracellular Vesicles, 8(1), p.1596016.

Baietti, M., Zhang, Z., Mortier, E., Melchior, A., Degeest, G., Geeraerts, A., Ivarsson, Y., Depoortere, F., Coomans, C., Vermeiren, E., Zimmermann, P. and David, G. (2012). Syndecan–syntenin–ALIX regulates the biogenesis of exosomes. Nature Cell Biology, 14(7), p.677.

Banito, A. and Lowe, S. (2013). A new development in senescence. *Cell*, *155*(5), pp.977-978.

Barth, P., Zu Schweinsberg, T., Ramaswamy, A. and Moll, R. (2004). CD34+ fibrocytes, α-smooth muscle antigen-positive myofibroblasts, and CD117 expression in the stroma of invasive squamous cell carcinomas of the oral cavity, pharynx, and larynx. Virchows

Archive, 444(3), pp.231-234.

Becker, A., Thakur, B., Weiss, J., Kim, H., Peinado, H. and Lyden, D. (2016). Extracellular vesicles in cancer: cell-to-cell mediators of metastasis. Cancer Cell, 30(6), pp.836-848.

Bhowmick, N., Chytil, A., Plieth, D., Gorska, A., Dumont, N., Shappell, S., Washington, M., Neilson, E. and Moses, H. (2004). TGF-ß signaling in fibroblasts modulates the oncogenic potential of adjacent epithelia. Science, 303(5659), pp.848-851.

Bierie, B. and Moses, H. (2006). Tumour microenvironment: TGFβ: the molecular Jekyll and Hyde of cancer. Nature Reviews Cancer, 6(7), p.506.

Bingle, L., Brown, N. and Lewis, C. (2002). The role of tumour-associated macrophages in tumour progression: implications for new anticancer therapies. The Journal of Pathology, 196(3), pp.254-265.

Bissell, M., Hall, H. and Parry, G. (1982). How does the extracellular matrix direct gene expression? Journal of Theoretical Biology, 99(1), pp.31-68.

Boelens, M., Wu, T., Nabet, B., Xu, B., Qiu, Y., Yoon, T., Azzam, D., Twyman-Saint Victor, C., Wiemann, B., Ishwaran, H., Ter Brugge, P., Jonkers, J, Slingerland, J. and Minn, A. (2014). Exosome transfer from stromal to breast cancer cells regulates therapy resistance pathways. Cell, 159(3), pp.499-513.

Boy, J. (2002). The extracellular matrix of animals. In Alberts. B., Johnson, A., J., Martin, and Roberts, K. The Molecular Biology of the Cell (4th Ed.). Garland Science.

Boyle, W., Simonet, W. and Lacey, D. (2003). Osteoclast differentiation and activation. Nature, 423(6937), p.337.

Brailo, V., Vucicevic-Boras, V., Lukac, J., Biocina-Lukenda, D., Zilic-Alajbeg, I., Milenovic, A. and Balija, M. (2012). Salivary and serum interleukin 1 beta, interleukin 6 and tumor necrosis factor alpha in patients with leukoplakia and oral cancer. Medicina Oral Patologia Oral Cirugia Bucal, 17(1), pp.e10-e15.

Bryne, M., Koppang, H., Lilleng, R., Stene, T., Bang, G. and Dabelsteen, E. (1989). New malignancy grading is a better prognostic indicator than Broders' grading in oral squamous cell carcinomas. Journal of Oral Pathology & Medicine, 18(8), pp.432-437.

Bryne, M., Thrane, P. and Dabelsteen, E. (1991). Loss of expression of blood group antigen H is associated with cellular invasion and spread of oral squamous cell carcinomas. Cancer, 67(3), pp.613-618.

Bussard, K., Mutkus, L., Stumpf, K., Gomez-Manzano, C. and Marini, F.C. (2016). Tumor-associated stromal cells as key contributors to the tumor microenvironment. Breast Cancer Research, 18(1), p.84.

Calon, A., Tauriello, D. and Batlle, E. (2014). TGF-beta in CAF-mediated tumor growth and metastasis. In Seminars in Cancer Biology (25), pp.15-22. Academic Press.

Campisi, J. and di Fagagna, F. (2007). Cellular senescence: when bad things happen to

good cells. Nature Reviews Molecular Cell Biology, 8(9), p.729.

Cancer Research UK, (2019), Cancer Research UK. [online] Available at: http://www.cancerresearchuk.org/[Accessed 3 May 2019.

Canning, M., Postovit, L., Clarke, S. and Graham, C. (2001). Oxygen-mediated regulation of gelatinase and tissue inhibitor of metalloproteinases-1 expression by invasive cells. Experimental Cell Research, 267(1), pp.88-94.

Cardone, M., Salvesen, G., Widmann, C., Johnson, G. and Frisch, S. (1997). The regulation of anoikis: MEKK-1 activation requires cleavage by caspases. Cell, 90(2), pp.315-323.

Carmeliet, P. and Jain, R. (2000). Angiogenesis in cancer and other diseases. Nature, 407(6801), pp.249-257.

Carmeliet, P., Dor, Y., Herbert, J., Fukumura, D., Brusselmans, K., Dewerchin, M., Neeman, M., Bono, F., Abramovitch, R., Maxwell, P., Koch, C., Ratcliffe, P., Moons, L., Jain, R., Collen, D. and Keshet, E. (1998). Role of HIF-1α in hypoxia-mediated apoptosis, cell proliferation and tumour angiogenesis. Nature, 394(6692), pp.485-490.

Centrella, M., McCarthy, T. and Canalis, E. (1991). Transforming growth factor-beta and remodeling of bone. Journal of Bone Joint Surgery American. 73, pp.1418–28.

Chalmin, F., Ladoire, S., Mignot, G., Vincent, J., Bruchard, M., Remy-Martin, J., Boireau, W., Rouleau, A., Simon, B., Lanneau, D., De Thonel, A., Multhoff, G, Hamman, A., Martin, B., Solary, E., Zitvogel, L., Garrido, C., Ryffel, B., Borg, C., Apetoh, L., Rebe, C. and Ghiringhelli, F. (2010). Membrane-associated Hsp72 from tumor-derived exosomes mediates STAT3-dependent immunosuppressive function of mouse and human myeloid-derived suppressor cells. The Journal of Clinical Investigation, 120(2), pp.457-471.

Chang, J., Wang, Y., Shao, L., Laberge, R., Demaria, M., Campisi, J., Janakiraman, K., Sharpless, N., Ding, S., Feng, W., Luo, Y., Wang, X., Aykin-Burns, N., Krager, K., Ponnappan, U., Hauer-Jensen, M., Meng, A., and Zhou, D. (2016). Clearance of senescent cells by ABT263 rejuvenates aged hematopoietic stem cells in mice. Nature Medicine, 22(1), p.78.

Chen, B., Wang, Z., Sun, J., Song, Q., He, B., Zhang, H., Wang, X., Dai, W. and Zhang, Q. (2016). A tenascin C targeted nanoliposome with navitoclax for specifically eradicating of cancer-associated fibroblasts. Nanomedicine: Nanotechnology, Biology and Medicine, 12(1), pp.131-141.

Chen, C., Chu, J., Su, W., Huang, S. and Lee, W. (2010). Hypoxia and metabolic phenotypes during breast carcinogenesis: expression of HIF-1α, GLUT1, and CAIX. Virchows Archive, 457(1), pp.53-61.

Chen, Q., Liu, K., Robinson, A., Clauson, C., Blair, H., Robbins, P., Niedernhofer, L.and Ouyang, H. (2013). DNA damage drives accelerated bone aging via an NF-κB–dependent mechanism. Journal of Bone and Mineral Research, 28(5), pp.1214-1228.

Chen, Y., Kuo, S., Fang, K. and Hao, S. (2011). Prognostic impact of marginal

mandibulectomy in the presence of superficial bone invasion and the nononcologic outcome. Head Neck. 33(5), pp.708–713.

Cheng, Y., Rees, T. and Wright, J. (2014). A review of research on salivary biomarkers for oral cancer detection. Clinical and Translational Medicine, 3(1), p.1.

Chikatsu. N., Takeuchi, Y., Tamura, Y., Fukumoto, S., Yano, K., Tsuda, E., Ogata, E. and Fujita, T. (2000). Interactions between cancer and bone marrow cells induce osteoclast differentiation factor expression and osteoclast-like cell formation in vitro. Biochemical biophysical research. Communications. 267, pp.632–637.

Cho, J., Park, H., Lim, E. and Lee, K. (2012). Exosomes from breast cancer cells can convert adipose tissue-derived mesenchymal stem cells into myofibroblast-like cells. International Journal of Oncology, 40(1), pp.130-138.

Chuang, F., Hsue, S., Wu, C. and Chen, Y. (2009). Immunohistochemical expression of RANKL, RANK, and OPG in human oral squamous cell carcinoma. Journal of Oral Pathology and Medicine. 38, pp.753-759.

Cirillo, N., Hassona, Y., Celentano, A., Lim, K., Manchella, S., Parkinson, E. and Prime, S. (2016). Cancer-associated fibroblasts regulate keratinocyte cell–cell adhesion via TGF-β-dependent pathways in genotype-specific oral cancer. Carcinogenesis, p.113.

Cirri, P. and Chiarugi, P. (2011). Cancer associated fibroblasts: the dark side of the coin. American Journal of Cancer Research, 1(4), p.482.

Clarke, B., (2008). Normal bone anatomy and physiology. Clinical journal of the american society of nephrology, 3(Supplement 3), pp.S131-S139.

Cleary, C., Leeman, J., Higginson, D., Katabi, N., Sherman, E., Morris, L., McBride, S., Lee, N. and Riaz, N. (2016). Biological features of human papillomavirus-related head and neck cancers contributing to improved response. Clinical Oncology, 28(7), pp.467-474.

Colella, G., Gaeta, G., Moscariello, A. and Angelillo, I. (2008). Oral cancer and dentists: knowledge, attitudes, and practices in Italy. Oral Oncology, 44(4), pp.393-399.

Colombo, M., Moita, C., van Niel, G., Kowal, J., Vigneron, J., Benaroch, P., Manel, N., Moita, L.F., Théry, C. and Raposo, G. (2013). Analysis of ESCRT functions in exosome biogenesis, composition and secretion highlights the heterogeneity of extracellular vesicles. Journal of Cell Science, 126(24), pp.5553-5565.

Colotta, F., Allavena, P., Sica, A., Garlanda, C. and Mantovani, A. (2009). Cancer-related inflammation, the seventh hallmark of cancer: links to genetic instability. Carcinogenesis, 30(7), pp.1073-1081.

Coppé, J., Patil, C., Rodier, F., Sun, Y., Muñoz, D., Goldstein, J., Nelson, P.S., Desprez, P. and Campisi, J. (2008). Senescence-associated secretory phenotypes reveal cell-nonautonomous functions of oncogenic RAS and the p53 tumor suppressor. PLOS Biology, 6(12), e301.

Corcoran, C., Friel, A., Duffy, M., Crown, J. and O'Driscoll, L. (2011). Intracellular and

extracellular microRNAs in breast cancer. Clinical Chemistry, 57(1), pp.18-32.

Costea, D., Hills, A., Osman, A., Thurlow, J., Kalna, G., Huang, X., Murillo, C.P., Parajuli, H., Suliman, S., Kulasekara, K., Johannessen, A. and Partridge, M. (2013). Identification of two distinct carcinoma-associated fibroblast subtypes with differential tumor-promoting abilities in oral squamous cell carcinoma. Cancer Research, 73(13), pp.3888-3901.

Costea, D., Kulasekara, K., Neppelberg, E., Johannessen, A. and Vintermyr, O. (2006). Species-specific fibroblasts required for triggering invasiveness of partially transformed oral keratinocytes. The American Journal of Pathology, 168(6), pp.1889-1897.

Crawford, S., Stellmach, V., Murphy-Ullrich, J., Ribeiro, S., Lawler, J., Hynes, R., Boivin, G. and Bouck, N., (1998). Thrombospondin-1 is a major activator of TGF-β1 in vivo. Cell, 93(7), pp.1159-1170.

Daly, A., McIlreavey, L. and Irwin, C. (2008). Regulation of HGF and SDF-1 expression by oral fibroblasts–implications for invasion of oral cancer. Oral Oncology, 44(7), pp.646-651.

Davies, M., Prime, S., Stone, A., Huntley, S., Eveson, J., and Paterson, I. (2000). Endogenous TGF-beta1 inhibits the growth and metastatic dissemination of rat oral carcinoma cell lines but enhances local bone resorption. Journal of Oral Pathology & Medicine, 29(5), pp.232–240.

De Toro, J., Herschlik, L., Waldner, C. and Mongini, C. (2015). Emerging roles of exosomes in normal and pathological conditions: new insights for diagnosis and therapeutic applications. Frontiers in Immunology, 6, p.203.

De Wever, O., Demetter, P. and Mareel, M. (2008). Stromal myofibroblasts are drivers of invasive cancer growth. International Journal of Cancer, 123, pp.2229 – 2238.

Demaria, M., Ohtani, N., Youssef, S., Rodier, F., Toussaint, W., Mitchell, J., Laberge, R., Vijg, J., Van Steeg, H., Dollé, M., Hoeijmakers, J., Bruin, A., Hara, E. and Campisi, J. (2014). An essential role for senescent cells in optimal wound healing through secretion of PDGF-AA. Developmental Cell, 31(6), pp.722-733.

Demehri, S., Turkoz, A. and Kopan, R. (2009). Epidermal Notch1 loss promotes skin tumorigenesis by impacting the stromal microenvironment. Cancer Cell, 16(1), pp.55-66.

Deng, L., Peng, Y., Jiang, Y., Wu, Y., Ding, Y., Wang, Y., Xu, D. and Fu, Q. (2017). Imipramine protects against bone loss by inhibition of osteoblast-derived microvesicles. International Journal of Molecular Sciences, 18(5), p.1013.

Deng, L., Wang, Y., Peng, Y., Wu, Y., Ding, Y., Jiang, Y., Shen, Z. and Fu, Q. (2015). Osteoblast-derived microvesicles: a novel mechanism for communication between osteoblasts and osteoclasts. Bone, 79, pp.37-42.

Dental Health Organisation (2019), The state of mouth cancer reports UK 2018/2019. (online). Accessed by https://www.dentalhealth.org/Pages/Category/mouth-cancer-action-month 3 October 2019.

Derynck, R. and Feng, X. (1997). TGF-β receptor signaling. Biochimica et Biophysica Acta (BBA). Reviews on Cancer, 1333(2), pp.F105-F150.

Derynck, R., Akhurst, R. and Balmain, A. (2001). TGF-β signaling in tumor suppression and cancer progression. Nature Genetics, 29(2), pp.117-129.

Desmouliere, A., Guyot, C. and Gabbiani, G. (2004). The stroma reaction myofibroblast: a key player in the control of tumor cell behavior. International Journal of Developmental Biology, 48(5-6), pp.509-517.

Dewhirst, F., Stashenko, P., Mole, J. and Tsurumachi, T. (1985). Purification and partial sequence of human osteoclast- activating factor: identity with interleukin 1 beta. Journal of Immunology. 135(4), pp.2562–2568.

Di Micco, R., Fumagalli, M., Cicalese, A., Piccinin, S., Gasparini, P., Luise, C., Schurra, C., Nuciforo, P., Bensimon, A., Maestro, R., Pelicci, P. and Fagagna, F. (2006). Oncogene-induced senescence is a DNA damage response triggered by DNA hyper-replication. Nature, 444(7119), pp.638-642.

Dimri, G., Lee, X., Basile, G., Acosta, M., Scott, G., Roskelley, C., Medrano, E., Linskens, M., Rubelj, I. and Pereira-Smith, O. (1995). A biomarker that identifies senescent human cells in culture and in aging skin in vivo. Proceedings of the National Academy of Sciences, 92(20), pp.9363-9367.

Direkze, N., Jeffery, R., Hodivala-Dilke, K., Hunt, T., Playford, R., Elia, G., Poulsom, R., Wright, N. and Alison, M. (2006). Bone Marrow–Derived Stromal Cells Express Lineage-Related Messenger RNA Species. Cancer Research, 66(3), pp.1265-1269.

Dourado, M., Guerra, E., Salo, T., Lambert, D. and Coletta, R. (2018). Prognostic value of the immunohistochemical detection of cancer-associated fibroblasts in oral cancer: A systematic review and meta-analysis. Journal of Oral Pathology & Medicine, 47(5), pp.443-453.

Dourado, M., Korvala, J., Åström, P., De Oliveira, C., Cervigne, N., Mofatto, L., Campanella Bastos, D., Pereira Messetti, A., Graner, E., Paes Leme, A., Coletta, R. and Salo, T. (2019). Extracellular vesicles derived from cancer-associated fibroblasts induce the migration and invasion of oral squamous cell carcinoma. Journal of Extracellular Vesicles, 8(1), p.1578525.

Ebrahimi, A., Murali, R., Gao, K., Elliott, M. and Clark, J. (2011). The prognostic and staging implications of bone invasion in oral squamous cell carcinoma. Cancer, 117(19), pp.4460–4467.

Emmanouilidou, E., Melachroinou, K., Roumeliotis, T., Garbis, S., Ntzouni, M., Margaritis, L., Stefanis, L. and Vekrellis, K. (2010). Cell-produced α-synuclein is secreted in a calcium-dependent manner by exosomes and impacts neuronal survival. Journal of Neuroscience, 30(20), pp.6838-6851.

Esteban, M., Tran, M., Harten, S., Hill, P., Castellanos, M., Chandra, A., Raval, R., O'Brien, T. and Maxwell, P. (2006). Regulation of E-cadherin expression by VHL and hypoxia-inducible factor. Cancer Research, 66(7), pp.3567-3575.

Farr, J., Xu, M., Weivoda, M., Monroe, D., Fraser, D., Onken, J., Negley, B., Sfeir, J., Ogrodnik, M., Hachfeld, C., LeBrasseur, N., Drake, M., Pignolo, R., Pirtskhalava, T., Tchkonia, T., Oursler, M., Kirkland, J. and Khosla, S. (2017). Targeting cellular senescence prevents age-related bone loss in mice. Nature Medicine, 23(9), p.1072.

Fives, C., Nae, A., Roche, P., O'Leary, G., Fitzgerald, B., Feeley, L. and Sheahan, P. (2017). Impact of mandibular invasion on prognosis in oral squamous cell carcinoma four centimeters or less in size. The Laryngoscope, 127(4), pp.849-854.

Frederick, L., Page, D., Fleming, I., Fritz, A., Balch, C., Haller, D. and Morrow, M. (2002). AJCC Cancer Staging Manual (Vol. 1). Springer Science & Business Media.

Fuhrmann-Stroissnigg, H., Ling, Y., Zhao, J., McGowan, S., Zhu, Y., Brooks, R., Grassi, D., Gregg, S., Stripay, J., Dorronsoro, A., Corbo, L., Tang, P., Bukata, C., Ring, N., Giacca, M., Li, X., Tchkonia, T., Kirkland, J., Niedernhofer, L. and Robbins, P. (2017). Identification of HSP90 inhibitors as a novel class of senolytics. Nature Communications, 8(1), p.422.

Fukumura, D., Xu, L., Chen, Y., Gohongi, T., Seed, B. and Jain, R. (2001). Hypoxia and acidosis independently up-regulate vascular endothelial growth factor transcription in brain tumors in vivo. Cancer Research, 61(16), pp.6020-6024.

Gabbiani, G. (1994). Modulation of fibroblastic cytoskeletal features during wound healing and fibrosis. Pathology-Research and Practice, 190(9), pp.851-853.

Gaggioli, C., Hooper, S., Hidalgo-Carcedo, C., Grosse, R., Marshall, J., Harrington, K. and Sahai, E. (2007). Fibroblast-led collective invasion of carcinoma cells with differing roles for RhoGTPases in leading and following cells. Nature Cell Biology, 9(12), pp.1392-1400.

Gardiner, C., Vizio, D., Sahoo, S., Théry, C., Witwer, K., Wauben, M. and Hill, A. (2016). Techniques used for the isolation and characterization of extracellular vesicles: results of a worldwide survey. Journal of Extracellular Vesicles, 5(1), p.32945.

Garland, W., Benezra, R. and Chaudhary, J. (2013). Targeting Protein–Protein Interactions to Treat Cancer—Recent Progress and Future Directions. In Annual Reports in Medicinal Chemistry, vol. 48, pp. 227-245. Academic Press.

Ge, M., Ke, R., Cai, T., Yang, J. and Mu, X. (2015). Identification and proteomic analysis of osteoblast-derived exosomes. Biochemical and Biophysical Research Communications, 467(1), pp.27-32.

Georgakopoulou, E., Tsimaratou, K., Evangelou, K., Fernandez, M., Zoumpourlis, V., Trougakos, I., Kletsas, D., Bartek, J., Serrano, M. and Gorgoulis, V. (2013). Specific lipofuscin staining as a novel biomarker to detect replicative and stress-induced senescence. A method applicable in cryo-preserved and archival tissues. Aging (Albany NY), 5(1), p.37.

Glenn, D. (2004). Cytokines in cancer pathogenesis and cancer therapy. Nature Reviews Cancer. 4, pp.11-22.

Greco, V., Hannus, M. and Eaton, S. (2001). Argosomes: a potential vehicle for the spread of morphogens through epithelia. Cell, 106(5), pp.633-645.

Gu, J., Qian, H., Shen, L., Zhang, X., Zhu, W., Huang, L., Yan, Y., Mao, F., Zhao, C., Shi, Y. and Xu, W. (2012). Gastric cancer exosomes trigger differentiation of umbilical cord derived mesenchymal stem cells to carcinoma-associated fibroblasts through TGF-β/Smad pathway. PLOS One, 7(12), p.e52465.

Gutiérrez-Fernández, A., Fueyo, A., Folgueras, A., Garabaya, C., Pennington, C., Pilgrim, S., Edwards, D., Holliday, D., Jones, J., Span, P., Sweep, F., Puente, X. and Lopez-Otin, C. (2008). Matrix metalloproteinase-8 functions as a metastasis suppressor through modulation of tumor cell adhesion and invasion. Cancer Research, 68(8), pp.2755-2763.

Haddad, R. and Shin, D. (2008). Recent advances in head and neck cancer. National English Journal of Medicine, 359, pp.1143-1154.

Harris, S., Harris, M., Mahy, P., Wozney, J., Feng, J. and Mundy, G. (1994). Expression of bone morphogenetic protein messenger RNAs by normal rat and human prostate and prostate cancer cells. Prostate, 24, pp.204–11.

Hassona, Y., Cirillo, N., Heesom, K., Parkinson, E. and Prime, S. (2014). Senescent cancer-associated fibroblasts secrete active MMP-2 that promotes keratinocyte dis-cohesion and invasion. British Journal of Cancer, 111(6), pp.1230-1237.

Hassona, Y., Cirillo, N., Lim, K., Herman, A., Mellone, M., Thomas, G., Pitiyage, G., Parkinson, E. and Prime, S. (2013). Progression of genotype-specific oral cancer leads to senescence of cancer-associated fibroblasts and is mediated by oxidative stress and TGF-β. Carcinogenesis, p35.

Hearnden, V., Lomas, H., MacNeil, S., Thornhill, M., Murdoch, C., Lewis, A., Madsen, J., Blanazs, A., Armes, S. and Battaglia, G. (2009). Diffusion studies of nanometer polymersomes across tissue engineered human oral mucosa. Pharmaceutical Research, 26(7), pp.1718-1728.

Hill, M. and Mackenzie, I. (1984). The influence of differing connective tissue substrates on the maintenance of adult stratified squamous epithelia. Cell and Tissue Research, 237(3), pp.473-478.

Hinsley, E., Hunt, S., Hunter, K., Whawell, S. and Lambert, D. (2012) Endothelin-1 stimulates motility of head and neck squamous carcinoma cells by promoting stromal–epithelial interactions. International Journal of Cancer 130(1), pp.40-47.

Hinz, B., Phan, S., Thannickal, V., Galli, A., Bochaton-Piallat, M. and Gabbiani, G. (2007). The myofibroblast: one function, multiple origins. The American Journal of Pathology, 170(6), pp.1807-1816.

Houghton, A., Grisolano, J., Baumann, M., Kobayashi, D., Hautamaki, R., Nehring, L., Cornelius, L. and Shapiro, SR (2006). Macrophage elastase (matrix metalloproteinase-12) suppresses growth of lung metastases. Cancer research, 66(12), pp.6149-6155.

Hsu, C., Morohashi, Y., Yoshimura, S., Manrique-Hoyos, N., Jung, S., Lauterbach, M., Bakhti, M., Grønborg, M., Möbius, W., Rhee, J., Barr, F. and Simons, M. (2010). Regulation of exosome secretion by Rab35 and its GTPase-activating proteins TBC1D10A–C. The Journal of Cell Biology, 189(2), pp.223-232.

Hsu, H., Shan, Y., Lai, M. and Lin, P. (2010). Osteopontin-positive infiltrating tumor-associated macrophages in bulky ampullary cancer predict survival. Cancer Biology & Therapy, 10(2), pp.144-154.

Hu, G., Drescher, K. and Chen, X. (2012). Exosomal miRNAs: biological properties and therapeutic potential. Frontiers in Genetics, 3, p.56.

Huang, L., Cheng, Y., Chow, L., Zheng, M. and Kumta, S. (2002). Tumour cells produce receptor activator of NF-kB ligand (RANKL) in skeletal metastases. Journal of Clinical Pathology, 55, pp.877 – 878.

Huynh, N., VonMoss, L., Smith, D., Rahman, I., Felemban, M., Zuo, J., Rody Jr, W., McHugh, K. and Holliday, L. (2016). Characterization of regulatory extracellular vesicles from osteoclasts. Journal of Dental Research, 95(6), pp.673-679.

Hwang, Y., Park, K. and Chung, W. (2014). Stromal transforming factor-beta 1 is crucial for reinforcing the invasive potential of low invasive cancer. Oral Biology, 59, pp.687-694.

Hwang, Y.S., Lee, S.K., Park, K.K. and Chung, W.Y., (2012). Secretion of IL-6 and IL-8 from lysophosphatidic acid-stimulated oral squamous cell carcinoma promotes osteoclastogenesis and bone resorption. Oral oncology, 48(1), pp.40-48.

Ikeda, T., Kasai, M., Utsuyama, M. and Hirokawa, K. (2001). Determination of Three Isoforms of the Receptor Activator of Nuclear Factor-κB Ligand and Their Differential Expression in Bone and Thymus. Endocrinology, 142(4), pp.1419-1426.

Ishikuro, M., Sakamoto, K., Kayamori, K., Akashi, T., Kanda, H., Izumo, T. and Yamaguchi, A. (2008). Significance of the fibrous stroma in bone invasion by human gingival squamous cell carcinomas. Bone, 43, pp.621–627.

Ito, T., Williams, J., Fraser, D. and Phillips, A. (2004). Hyaluronan regulates transforming growth factor-β1 receptor compartmentalization. Journal of Biological Chemistry, 279(24), pp.25326-25332.

Itoh, S., Itoh, F., Goumans, M. and ten Dijke, P. (2000). Signaling of transforming growth factor-β family members through Smad proteins. European Journal of Biochemistry, 267(24), pp.6954-6967.

Iwai, K., Minamisawa, T., Suga, K., Yajima, Y. and Shiba, K. (2016). Isolation of human salivary extracellular vesicles by iodixanol density gradient ultracentrifugation and their characterizations. Journal of Extracellular Vesicles, 5(1), p.30829.

Jhaveri, K., Taldone, T., Modi, S. and Chiosis, G. (2012). Advances in the clinical development of heat shock protein 90 (Hsp90) inhibitors in cancers. Biochimica et Biophysica Acta (BBA)-Molecular Cell Research, 1823(3), pp.742-755.

Jimi, E., Furuta, H., Matsuo, K., Tominaga, K., Takahashi, T. and Nakanishi, O. (2011). The cellular and molecular mechanisms of bone invasion by oral squamous cell carcinoma. Oral Disease. 17, pp.462-468.

Jimi, E., Shin, M., Furuta, H., Tada, Y. and Kusukawa, J. (2013). The RANKL/RANK system as a therapeutic target for bone invasion by oral squamous cell carcinoma (Review). International Journal of Oncology, 42, pp.803-809

Johansson, A., Ansell, A., Jerhammar, F., Lindh, M., Grénman, R., Munck-Wikland, E., Östman, A. and Roberg, K. (2012). Cancer-Associated Fibroblasts Induce Matrix Metalloproteinase–Mediated Cetuximab Resistance in Head and Neck Squamous Cell Carcinoma Cells. Molecular Cancer Research, 10(9), pp.1158-1168.

Joyce, J. and Pollard, J. (2009). Microenvironmental regulation of metastasis. Nature Reviews Cancer, 9(4), pp.239-252.

Kabir, T., Leigh, R., Tasena, H., Mellone, M., Coletta, R., Parkinson, E., Prime, S., Thomas, G., Paterson, I., Zhou, D., McCall, J., Speight, P. and Lambert, D. (2016). A miR-335/COX-2/PTEN axis regulates the secretory phenotype of senescent cancer-associated fibroblasts. Aging (Albany NY), 8(8), p.1608.

Kagan, H. and Li, W. (2003). Lysyl oxidase: properties, specificity, and biological roles inside and outside of the cell. Journal of Cellular Biochemistry, 88(4), pp.660-672.

Kahlert, C. and Kalluri, R. (2013). Exosomes in tumor microenvironment influence cancer progression and metastasis. Journal of Molecular Medicine, 91(4), pp.431-437.

Kalluri, R. and Zeisberg, M. (2006). Fibroblasts in cancer. Nature Reviews Cancer, 6(5), pp.392-401.

Kaneda, A., Wakazono, K., Tsukamoto, T., Watanabe, N., Yagi, Y., Tatematsu, M., Kaminishi, M., Sugimura, T. and Ushijima, T. (2004). Lysyl oxidase is a tumor suppressor gene inactivated by methylation and loss of heterozygosity in human gastric cancers. Cancer Research, 64(18), pp.6410-6415.

Kawahara, R., Bollinger, J., Rivera, C., Ribeiro, A., Brandão, T., Leme, A. and MacCoss, M. (2016). A targeted proteomic strategy for the measurement of oral cancer candidate biomarkers in human saliva. Proteomics, 16(1), pp.159-173.

Kawashiri, S., Tanaka, A., Noguchi, N., Hase, T., Nakaya, H., Ohara, T., Kato, K. and Yamamoto, E. (2009). Significance of stromal desmoplasia and myofibroblast appearance at the invasive front in squamous cell carcinoma of the oral cavity. Head & Neck, 31(10), pp.1346-1353.

Kayamori, K., Sakamoto, K. and Nakashima, T. (2010). Roles of interleukin-6 and parathyroid hormone-related peptide in osteoclast formation associated with oral cancers: significance of interleukin-6 synthesized by stromal cells in response to cancer cells. American Journal of Pathology. 176, pp.968–980.

Kellermann, M., Sobral, L., Da Silva, S., Zecchin, K., Graner, E., Lopes, M., Nishimoto, I., Kowalski, L. and Coletta, R. (2007). Myofibroblasts in the stroma of oral squamous

cell carcinoma are associated with poor prognosis. Histopathology, 51(6), pp.849-853.

Kessenbrock, K., Plaks, V. and Werb, Z. (2010). Matrix metalloproteinases: regulators of the tumor microenvironment. Cell. 141(1), pp.52–67.

Kim, H., Chang, J., Shao, L., Han, L., Iyer, S., Manolagas, S., O'Brien, C., Jilka, R., Zhou, D. and Almeida, M. (2017). DNA damage and senescence in osteoprogenitors expressing Osx1 may cause their decrease with age. Aging Cell, 16(4), pp.693-703.

Kim, K., Noh, J., Bodogai, M., Martindale, J., Yang, X., Indig, F., Basu, S., Ohnuma, K., Morimoto, C., Johnson, P., Biragyn, A., Abdelmohsen, K. and Gorospe, M. (2017). Identification of senescent cell surface targetable protein DPP4. Genes & Development, 31(15), pp.1529-1534.

Kim, S., Turnbull, J. and Guimond, S. (2011). Extracellular matrix and cell signalling: the dynamic cooperation of integrin, proteoglycan and growth factor receptor. Journal of Endocrinology, 209(2), pp.139-151.

Kinugasa, Y., Matsui, T. and Takakura, N. (2014). CD44 Expressed on Cancer-Associated Fibroblasts Is a Functional Molecule Supporting the Stemness and Drug Resistance of Malignant Cancer Cells in the Tumor Microenvironment. Stem Cells, 32(1), pp.145-156.

Kowal, J., Tkach, M. and Théry, C. (2014). Biogenesis and secretion of exosomes. Current Opinion in Cell Biology, 29, pp.116-125.

Krane, S. and Inada, M. (2008). Matrix metalloproteinases and bone. Bone. 43(1), pp.7–18.

Krtolica, A., Parrinello, S., Lockett, S., Desprez, P. and Campisi, J. (2001). Senescent fibroblasts promote epithelial cell growth and tumorigenesis: a link between cancer and aging. Proceedings of the National Academy of Sciences, 98(21), pp.12072-12077.

Kuilman, T. and Peeper, D.S. (2009). Senescence-messaging secretome: SMS-ing cellular stress. Nature Reviews Cancer, 9(2), pp.81-94.

Kukita, T., Wada, N., Kukita, A., Kakimoto, T., Sandra, F. and Toh, K. (2004). RANKL-induced DC-STAMP is essential for osteoclastogenesis. Journal of Experimental Medicine. 200, pp.941–6.

Kular, J., Tickner, J., Chim, S. and Xu, J. (2012). An overview of the regulation of bone remodelling at the cellular level. Clinical Biochemistry, 45(12), pp.863-873.

Laberge, R., Sun, Y., Orjalo, A., Patil, C., Freund, A., Zhou, L., Curran, S., Davalos, A., Wilson-Edell, K., Liu, S., Limbad, C., Demaria, M., Li, P., Hubbard, G., Ikeno, Y., Javors, M., Desprez, P., Benz, C., Kapahi, P., Nelson, P. and Campisi, J. (2015). MTOR regulates the pro-tumorigenic senescence-associated secretory phenotype by promoting IL1A translation. Nature Cell Biology, 17(8), pp.1049-1061.

Lacey, D., Timms, E., Tan, H., Kelley, M., Dunstan, C., Burgess, T., Elliott, R., Colombero, A., Elliott, G., Scully, S., Hsu, H., Sullivamn, J., Hawkins, N., Davy, E., Capparelli, C., Eli, A., Qian, Y., Kaufman, S., Sarosi, I., Shalhoub, V., Senaldi, G.,

Delaney, J. and Boyle, W. (1998). Osteoprotegerin ligand is a cytokine that regulates osteoclast differentiation and activation. Cell, 93(2), pp.165-176.

Laoui, D., Movahedi, K., Van Overmeire, E., Van den Bossche, J., Schouppe, E., Mommer, C., Nikolaou, A., Morias, Y., De Baetselier, P. and Van Ginderachter, J. (2011). Tumor-associated macrophages in breast cancer: distinct subsets, distinct functions. International Journal of Developmental Biology, 55(7-8-9), pp.861-867.

Lässer, C., Alikhani, V., Ekström, K., Eldh, M., Paredes, P., Bossios, A., Sjöstrand, M., Gabrielsson, S., Lötvall, J. and Valadi, H. (2011). Human saliva, plasma and breast milk exosomes contain RNA: uptake by macrophages. Journal of Translational Medicine, 9(1), p.9.

LeBleu, V. and Kalluri, R. (2018). A peek into cancer-associated fibroblasts: origins, functions and translational impact. Disease models & mechanisms, 11(4), p.dmm029447.

Lee, S., Rho, J., Jeong, D., Sul, J., Kim, T. and Kim, N. (2006). v-ATPase V0 subunit d2-deficient mice exhibit impaired osteoclast fusion and increased bone formation. Nature Medicine. 12, pp.1403–9.

Levental, K., Yu, H., Kass, L., Lakins, J., Egeblad, M., Erler, J., Fong, S., Csiszar, K., Giaccia, A., Weninger, W., Yamauchi, M., Gasser, D. and Weaver, V. (2009). Matrix crosslinking forces tumor progression by enhancing integrin signaling. Cell, 139(5), pp.891-906.

Lewis, C. and Pollard, J (2006). Distinct role of macrophages in different tumor microenvironments. Cancer Research, 66(2), pp.605-612.

Lewis, J., Landers, R., Underwood, J., Harris, A. and Lewis, C. (2000). Expression of vascular endothelial growth factor by macrophages is up-regulated in poorly vascularized areas of breast carcinomas. The Journal of Pathology, 192(2), pp.150-158.

Lewis, M., Lygoe, K., Nystrom, M., Anderson, W., Speight, P., Marshall, J. and Thomas, G. (2004). Tumour-derived TGF-b1 modulates myofibroblast differentiation and promotes HGF/SF-dependent invasion of squamous carcinoma cells. British Journal of Cancer. 90(4), pp.822 – 832.

Li, Y., Samuvel, D., Sundararaj, K., Lopes-Virella, M. and Huang, Y. (2010). IL-6 and high glucose synergistically upregulate MMP-1 expression by U937 mononuclear phagocytes via ERK1/2 and JNK pathways and c-Jun. Journal of Cellular Biochemistry. 110, pp.248–259.

Lim, K., Cirillo, N., Hassona, Y., Wei, W., Thurlow, J., Cheong, S., Pitiyage, G., Parkinson, E. and Prime, S. (2011). Fibroblast gene expression profile reflects the stage of tumour progression in oral squamous cell carcinoma. The Journal of pathology, 223(4), pp.459-469.

Lin, N., Wang, P., Zhao, D., Zhang, F., Yang, K. and Chen, R. (2017). Significance of oral cancer-associated fibroblasts in angiogenesis, lymphangiogenesis, and tumor invasion in oral squamous cell carcinoma. Journal of Oral Pathology & Medicine, 46(1),

pp.21-30.

Liu, T., Zhou, L., Li, D., Andl, T. and Zhang, Y. (2019). Cancer-Associated Fibroblasts Build and Secure the Tumor Microenvironment. Frontiers in cell and developmental biology, 7.

Livak, K. and Schmittgen, T. (2001). Analysis of relative gene expression data using real-time quantitative PCR and the 2− ΔΔCT method. Methods, 25(4), pp.402-408.

Lötvall, J., Hill, A., Hochberg, F., Buzás, E., Di Vizio, D., Gardiner, C., Gho, Y., Kurochkin, I., Mathivanan, S., Quesenberry, P., Sahoo, S., Tahara, H., Wauben, M., Witwer, K. and Thery, C. (2014). Minimal experimental requirements for definition of extracellular vesicles and their functions: a position statement from the International Society for Extracellular Vesicles.

Luga, V., Zhang, L., Viloria-Petit, A., Ogunjimi, A., Inanlou, M., Chiu, E., Buchanan, M., Hosein, A., Basik, M. and Wrana, J. (2012). Exosomes mediate stromal mobilization of autocrine Wnt-PCP signaling in breast cancer cell migration. Cell, 151(7), pp.1542-1556.

Lygoe, K., Wall, I., Stephens, P. and Lewis, M. (2007). Role of vitronectin and fibronectin receptors in oral mucosal and dermal myofibroblast differentiation. Biology of the cell, 99(11), pp.601-614.

Mackenzie, I. and Dabelsteen, E. (1987). Connective tissue influences on the expression of epithelial cell-surface antigens. Cell and Tissue Research, 248(1), pp.137-141.

Majno, G., Gabbiani, G., Hirschel, B., Ryan, G. and Statkov, P. (1971). Contraction of granulation tissue in vitro: similarity to smooth muscle. Science, 173(3996), pp.548-550.

Mantovani, A., Marchesi, F., Malesci, A., Laghi, L. and Allavena, P. (2017). Tumour-associated macrophages as treatment targets in oncology. Nature Reviews Clinical Oncology.

Mantovani, A., Schioppa, T., Porta, C., Allavena, P. and Sica, A. (2006). Role of tumor-associated macrophages in tumor progression and invasion. Cancer and Metastasis Reviews, 25(3), pp.315-322.

Mantovani, A., Sica, A., Sozzani, S., Allavena, P., Vecchi, A. and Locati, M. (2004). The chemokine system in diverse forms of macrophage activation and polarization. Trends in Immunology, 25(12), pp.677-686.

Mao, Y., Keller, E., Garfield, D.H., Shen, K. and Wang, J. (2013). Stromal cells in tumor microenvironment and breast cancer. Cancer and Metastasis Reviews, 32(1-2), pp.303-315.

Marino, S., Logan, J., Mellis, D. and Capulli, M. (2014). Generation and culture of osteoclasts. BoneKEy reports, 3.

Marleau, A., Chen, C., Joyce, J. and Tullis, R. (2012). Exosome removal as a therapeutic adjuvant in cancer. Journal of Translational Medicine, 10(1), p.134.

Marsh, D., Suchak, K., Moutasim, K., Vallath, S., Hopper, C., Jerjes, W., Upile, T.,

Kalavrezos, N., Violette, S., Weinreb, P., Chester,K., Chana, J., Marshall, J., Hart, I., Hackshaw, A., Piper, K. and Thomas, G. (2011). Stromal features are predictive of disease mortality in oral cancer patients. Journal of Pathology. 223, pp.470–481.

Martin, L. and Boyd, N. (2008). Mammographic density. Potential mechanisms of breast cancer risk associated with mammographic density: hypotheses based on epidemiological evidence. Breast Cancer Research, 10(1), p.1.

Massagué, J. (1998). TGF-β signal transduction. Annual Review of Biochemistry, 67(1), pp.753-791.

Massagué, J., Blain, S. and Lo, R. (2000). TGFβ signaling in growth control, cancer, and heritable disorders. Cell, 103(2), pp.295-309.

Matrisian, L. and Hogan, B. (1990). 8 Growth Factor-Regulated Proteases and Extracellular Matrix Remodeling during Mammalian Development. Current Topics in Developmental Biology, 24, pp.219-259.

Matsuo, K. and Irie, N. (2008). Osteoclast-osteoblast communication. Archives of Biochemistry and Biophysics, 473(2), pp.201–209.

McAnulty, R. (2007). Fibroblasts and myofibroblasts: their source, function and role in disease. The International Journal of Biochemistry & Cell Biology, 39(4), pp.666-671.

McClung, M., Grauer, A., Boonen, S., Bolognese, M., Brown, J., Diez-Perez, A., Langdahl, B., Reginster, J., Zanchetta, J., Wasserman, S., Katz, L., Maddox, J., Yang, Y., Libanati, C. and Bone, H. (2014). Romosozumab in postmenopausal women with low bone mineral density. New England Journal of Medicine, 370(5), pp.412-420.

Melling, G., Flannery, S., Abidin, S., Clemmens, H., Prajapati, P., Hinsley, E., Hunt, S., Catto, J., Coletta, R., Mellone, M., Thomas, G., Parkinson, E., Prime, S., Paterson, I., Buttle, D. and Lambert, D. (2018). A miRNA-145/TGF-β1 negative feedback loop regulates the cancer-associated fibroblast phenotype. Carcinogenesis, 39(6), pp.798-807.

Melo, S., Luecke, L., Kahlert, C., Fernandez, A., Gammon, S., Kaye, J., LeBleu, V., Mittendorf, E., Weitz, J., Rahbari, N., Reissfelder, C., Pilarsky, C., Fraga, M., Piwnica-Worms, D. and Kalluri, R. (2015). Glypican-1 identifies cancer exosomes and detects early pancreatic cancer. Nature, 523(7559), p.177.

Melo, S., Sugimoto, H., O'Connell, J., Kato, N., Villanueva, A., Vidal, A., Qiu, L., Vitkin, E., Perelman, L., Melo, C., Lucci, A. Ivan, A., Calin, G. and Kalluri, R. (2014). Cancer exosomes perform cell-independent microRNA biogenesis and promote tumorigenesis. Cancer cell, 26(5), pp.707-721.

Mellone, M., Hanley, C., Thirdborough, S., Mellows, T., Garcia, E., Woo, J., Tod, J., Frampton, S., Jenei, V., Moutasim, K., Kabir, T., Brennan, P., Venturi, G., Ford, K., Herranz, N., Lim, K., Clarke, J., Lambert, D., Prime, S., Underwood, T., Vijayanand, P., Eliceiri, K., Woelk, C., King, E., Gil, J., Ottensmeier, C. and Thomas, G. (2017). Induction of fibroblast senescence generates a non-fibrogenic myofibroblast phenotype that differentially impacts on cancer prognosis. Aging (Albany NY), 9(1), p.114.

Minciacchi, V., Freeman, M. and Di Vizio, D. (2015). Extracellular vesicles in cancer: exosomes, microvesicles and the emerging role of large oncosomes. In Seminars in Cell & Developmental Biology, 40, pp. 41-51. Academic Press.

Mohan, S. and Baylink, D. (1991). Bone growth factors. Clinical Orthopaedics and Related Research, pp.30–48.

Moncsek, A., Al-Suraih, M., Trussoni, C., O'hara, S., Splinter, P., Zuber, C., Patsenker, E., Valli, P., Fingas, C., Weber, A., Zhu, Y., Tchkonia, T., Kirkland, J., Gores, G., Mullhaupt, B., LaRusso, N. and Mertens, J. (2018). Targeting senescent cholangiocytes and activated fibroblasts with B-cell lymphoma-extra large inhibitors ameliorates fibrosis in multidrug resistance 2 gene knockout (Mdr2−/−) mice. Hepatology, 67(1), pp.247-259.

Morello, M., Minciacchi, V., De Candia, P., Yang, J., Posadas, E., Kim, H., Griffiths, D., Bhowmick, N., Chung, L., Gandellini, P., Freeman, M., Demichelis, F. and DiVizio, D. (2013). Large oncosomes mediate intercellular transfer of functional microRNA. Cell Cycle, 12(22), pp.3526-3536.

Mosser, D. and Edwards, J. (2008). Exploring the full spectrum of macrophage activation. Nature Reviews Immunology, 8(12), pp.958-969.

Mueller, L., Goumas, F., Affeldt, M., Sandtner, S., Gehling, U., Brilloff, S., Walter, J., Karnatz, N., Lamszus, K., Rogiers, X. and Broering, D. (2007). Stromal fibroblasts in colorectal liver metastases originate from resident fibroblasts and generate an inflammatory microenvironment. The American Journal of Pathology, 171(5), pp.1608-1618.

Mulcahy, L., Pink, R. and Carter, D. (2014). Routes and mechanisms of extracellular vesicle uptake. Journal of Extracellular Vesicles, 3(1), p.24641.

Müller, H. and Slootweg, P. (1990). Mandibular invasion by oral squamous cell carcinoma. Clinical aspects. Journal of Craniomaxillofacial Surgery, 18, pp.80-84.

Munger, J., Huang, X., Kawakatsu, H., Griffiths, M., Dalton, S., Wu, J., Pittet, J., Kaminski, N., Garat, C., Matthay, M., Rifkin, D. and Sheppard, D. (1999). A mechanism for regulating pulmonary inflammation and fibrosis: the integrin αvβ6 binds and activates latent TGF β1. Cell, 96(3), pp.319-328.

Murdoch, C., Muthana, M., Coffelt, S. and Lewis, C. (2008). The role of myeloid cells in the promotion of tumour angiogenesis. Nature Reviews Cancer, 8(8), pp.618-631.

Nagasaki, T, Hara, M., Nakanishi, H., Takahashi, H., Sato, M. and Takeyama, H. (2013). Interleukin-6 released by colon cancer-associated fibroblasts is critical for tumour angiogenesis: anti-interleukin-6 receptor antibody suppressed angiogenesis and inhibited tumour–stroma interaction. British Journal of Cancer, 110, pp.469–478.

Nanci, A. (2017). Ten Cate's Oral Histology: Development, Structure, and Function. Elsevier. 9th Ed.

Niedernhofer, L. and Robbins, P. (2018). Senotherapeutics for healthy ageing. Nature Reviews Drug Discovery, 17(5), p.377.

Nilsson, J., Skog, J., Nordstrand, A., Baranov, V., Mincheva-Nilsson, L., Breakefield, X.O. and Widmark, A. (2009). Prostate cancer-derived urine exosomes: a novel approach to biomarkers for prostate cancer. British Journal of Cancer, 100(10), p.1603.

Nomura, T., Shibahara, T., Cui, N.H. and Noma, H. (2005). Patterns of mandibular invasion by gingival squamous cell carcinoma. Journal of oral and maxillofacial surgery, 63(10), pp.1489-1493.

O'Brien, C., Gubrij, I., Lin, S., Saylors, R. and Manolagas, S. (1999). STAT3 activation in stromal/osteoblastic cells is required for induction of the receptor activator of NF-jB ligand and stimulation of osteoclastogenesis by gp130- utilizing cytokines or interleukin-1 but not 1,25-di- hydroxyvitamin D3 or parathyroid hormone. Journal of Biological Chemistry, 274, pp.19301–19308.

O'Sullivan, C., Lewis, C. and Harris, A. (1993). Secretion of epidermal growth factor by macrophages associated with breast carcinoma. Lancet, 342: pp.148–149.

Office for National Statistics. (2017) Cancer Registration Statistics, England- Office for National Statistics, [online] Available at: https://ons.gov.uk/peoplepopulationandcommunity/healthandsocialcare/conditionsanddiseases/bulletins/cancerregistrationstatisticsengland/2014 [Accessed 8 Jan, 2017].

Ojalvo, L., Whittaker, C., Condeelis, J. and Pollard, J. (2010). Gene expression analysis of macrophages that facilitate tumor invasion supports a role for Wnt-signaling in mediating their activity in primary mammary tumors. The Journal of Immunology, 184(2), pp.702-712.

Paget, S. (1889). The distribution of secondary growths in cancer of the breast. The Lancet, 133(3421), pp.571-573.

Papetti, M. and Herman, I. (2002). Mechanisms of normal and tumor-derived angiogenesis. American Journal of Physiology-Cell Physiology, 282(5), pp.C947-C970.

Parkinson, E.K. (2010). Senescence as a modulator of oral squamous cell carcinoma development. Oral Oncology, 46(12), pp.840-853.

Parolini, I., Federici, C., Raggi, C., Lugini, L., Palleschi, S., De Milito, A., Coscia, C., Iessi, E., Logozzi, M., Molinari, A., Colone, M., Tatti, M., Sargiacoma, M. and Fais, S. (2009). Microenvironmental pH is a key factor for exosome traffic in tumor cells. Journal of Biological Chemistry, 284(49), pp.34211-34222.

Pascucci, L., Coccè, V., Bonomi, A., Ami, D., Ceccarelli, P., Ciusani, E., Viganò, L., Locatelli, A., Sisto, F., Doglia, S., Parati, E., Bernardo, M., Muraca, M., Alessandri, G., Bondiolotti, G. and Pessina, A. (2014). Paclitaxel is incorporated by mesenchymal stromal cells and released in exosomes that inhibit in vitro tumor growth: a new approach for drug delivery. Journal of Controlled Release, 192, pp.262-270.

Pazolli, E., Luo, X., Brehm, S., Carbery, K., Chung, J., Prior, J., Doherty, J., Demehri, S., Salavaggione, L., Piwnica-Worms, D. and Stewart, S. (2009). Senescent stromal-derived osteopontin promotes preneoplastic cell growth. Cancer Research, 69(3), pp.1230-1239.

Peacock, B., Rigby, A., Bradford, J., Pink, R., Hunter, K., Lambert, D. and Hunt, S. (2018). Extracellular vesicle micro RNA cargo is correlated with HPV status in oropharyngeal carcinoma. Journal of Oral Pathology & Medicine, 47(10), pp.954-963.

Pfeilschifter, J. and Mundy, G. (1987). Modulation of transforming growth factor b activity in bone cultures by osteotrophic hormones. Proceedings of National Academy of Science USA. 84, pp.2024-2028.

Pickup, M., Novitskiy, S. and Moses, H. (2013). The roles of TGFβ in the tumour microenvironment. Nature Review Cancer. 13, pp.788–799.

Piek, E., Heldin, C. and Ten Dijke. (1999). Specificity, diversity, and regulation in TGF-β superfamily signaling. The FASEB Journal, 13(15), pp.2105-2124.

Pietras, K. and Östman, A. (2010). Hallmarks of cancer: interactions with the tumor stroma. Experimental Cell Research, 316(8), pp.1324-1331.

Pitt, J., Charrier, M., Viaud, S., André, F., Besse, B., Chaput, N. and Zitvogel, L. (2014). Dendritic cell–derived exosomes as immunotherapies in the fight against cancer. The Journal of Immunology, 193(3), pp.1006-1011.

Prideaux, M., Findlay, D. and Atkins, G. (2016). Osteocytes: the master cells in bone remodelling. Current Opinion in Pharmacology, 28, pp.24-30.

Prime, S., Cirillo, N., Hassona, Y., Lambert, D., Paterson, I., Mellone, M., Thomas, G., James, E. and Parkinson, E. (2016). Fibroblast activation and senescence in oral cancer. Journal of Oral Pathology & Medicine.

Procopio, M., Laszlo, C., Al Labban, D., Kim, D., Bordignon, P., Jo, S., Goruppi, S., Menietti, E., Ostano, P., Ala, U., Provero, P., Hoetzenecker, W., Neel, V., Kilarski, W., Swartz, M., Brisken, C., Lefort, K. and Dotto, G. (2015). Combined CSL and p53 downregulation promotes cancer-associated fibroblast activation. Nature Cell Biology.

Puram, S., Tirosh, I., Parikh, A., Patel, A., Yizhak, K., Gillespie, S., Rodman, C., Luo, C., Mroz, E., Emerick, K., Deschler, D., Varvares, M., Mylvagnam, R., Rozenblatt-Rosen, O., Rocco, J., Faquin, W., Lin, D., Regev, A and Bernstien, B. (2017). Single-cell transcriptomic analysis of primary and metastatic tumor ecosystems in head and neck cancer. Cell, 171(7), pp.1611-1624.

Qiao, B., Johnson, N. and Gao, J. (2010). Epithelial-mesenchymal transition in oral squamous cell carcinoma triggered by trans- forming growth factor-beta1 is Snail family-dependent and correlates with matrix metalloproteinase-2 and -9 expressions. International Journal of Oncology. 37, pp.663–668.

Qin, Y., Peng, Y., Zhao, W., Pan, J., Ksiezak-Reding, H., Cardozo, C., Wu, Y., Pajevic, P., Bonewald, L., Bauman, W. and Qin, W. (2017). Myostatin inhibits osteoblastic differentiation by suppressing osteocyte-derived exosomal microRNA-218: A novel mechanism in muscle-bone communication. Journal of Biological Chemistry, 292(26), pp.11021-11033.

Quan, J., Elhousiny, M., Johnson, N. and Gao, J. (2013). Transforming growth factor-b1

treatment of oral cancer induces epithelial-mesenchymal transition and promotes bone invasion via enhanced activity of osteoclasts. Clinical Experimental Metastasis. 30, pp.659–670.

Quan, J., Johnson, N., Zhou, J., Zhou, G., Parsons, P., Boyle, G. and Gao, J. (2012). Potential molecular targets for inhibiting bone invasion by oral squamous cell carcinoma: a review of mechanisms. Cancer Metastasis Review 31, pp.209–219.

Radisky, E. and Radisky, D. (2007). Stromal induction of breast cancer: inflammation and invasion. Reviews in Endocrine and Metabolic Disorders, 8(3), pp.279-287.

Rao, B., Malathi, N., Narashiman, S. and Rajan, S. (2014). Evaluation of myofibroblasts by expression of alpha smooth muscle actin: a marker in fibrosis, dysplasia and carcinoma. Journal of Clinical and Diagnostic Research, *8*(4).

Raposo, G. and Stoorvogel, W. (2013). Extracellular vesicles: exosomes, microvesicles, and friends. Journal of Cell Biology, 200(4), pp.373-383.

Recker, R., Benson, C., Matsumoto, T., Bolognese, M., Robins, D., Alam, J., Chiang, A., Hu, L., Krege, J., Sowa, H., Mitlak, B. and Myers, S. (2015). A randomized, double-blind phase 2 clinical trial of blosozumab, a sclerostin antibody, in postmenopausal women with low bone mineral density. Journal of Bone and Mineral Research, 30(2), pp.216-224.

Rodemann, H. and Müller, G. (1991). Characterization of human renal fibroblasts in health and disease: II. In vitro growth, differentiation, and collagen synthesis of fibroblasts from kidneys with interstitial fibrosis. American Journal of Kidney Diseases, 17(6), pp.684-686.

Rodier, F. and Campisi, J., (2011). Four faces of cellular senescence. The Journal of Cell Biology, 192(4), pp.547-556.

Rodrigues, P., Da Costa Miguel, M. De Aquino, S., Fonseca, F., Dos Santos Silva, A., Paes Leme, A. and Coletta, R. (2015). Stromal myofibroblasts in potentially malignant and malignant lesions of the oral cavity. Oncology letters, 9(2), pp.667-670.

Rønnov-Jessen, L. and Bissell, M. (2009). Breast cancer by proxy: can the microenvironment be both the cause and consequence? Trends in Molecular Medicine, 15(1), pp.5-13.

Roos, C., Zhang, B., Palmer, A., Ogrodnik, M., Pirtskhalava, T., Thalji, N., Hagler, M., Jurk, D., Smith, L., Casaclang-Verzosa, G., Zhu, Y. Schafer, M., Tchkonia, T., Kirkland, J. and Miller, J. (2016). Chronic senolytic treatment alleviates established vasomotor dysfunction in aged or atherosclerotic mice. Aging Cell, 15(5), pp.973-977.

Saini, J. and Sharma, P.K., 2018. Clinical, prognostic and therapeutic significance of heat shock proteins in cancer. *Current drug targets*, *19*(13), pp.1478-1490.

Samanta, S., Rajasingh, S., Drosos, N., Zhou, Z., Dawn, B. and Rajasingh, J. (2018). Exosomes: new molecular targets of diseases. Acta Pharmacologica Sinica, 39(4), p.501.

Santos, A., Jung, J., Aziz, N., Kissil, J. and Puré, E. (2009). Targeting fibroblast activation protein inhibits tumor stromagenesis and growth in mice. The Journal of Clinical Investigation, 119(12), pp.3613-3625.

Sato, M., Suzuki, T., Kawano, M. and Tamura, M. (2017). Circulating osteocyte derived exosomes contain miRNAs which are enriched in exosomes from MLO-Y4 cells. Biomedical Reports, 6(2), pp.223-231.

Savina, A., Furlán, M., Vidal, M. and Colombo, M. (2003). Exosome release is regulated by a calcium-dependent mechanism in K562 cells. Journal of Biological Chemistry, 278(22), pp.20083-20090.

Schmid, C., Schlapfer, I., Futo, E., Waldvogel, M., Schwander, J. and Zapf, J. (1992). Triiodothyronine (T3) stimulates insulin-like growth factor (IGF)-1 and IGF binding protein (IGFBP)-2 production by rat osteoblasts in vitro. Acta Endocrinologica. (Copenhagen), 126, pp.467–73.

Schultz-Cherry, S. and Murphy-Ullrich, J.E., (1993). Thrombospondin causes activation of latent transforming growth factor-beta secreted by endothelial cells by a novel mechanism. The Journal of Cell Biology, 122(4), pp.923-932.

Serini, G. and Gabbiani, G. (1999). Mechanisms of myofibroblast activity and phenotypic modulation. Experimental Cell Research, 250(2), pp.273-283.

Shah, J. and Lydiatt, W. (1999). Buccal mucosa, alveolus, retromolar trigone, floor of mouth, hard palate, and tongue tumors. In: Comprehensive Management of Head and Neck Tumors. Thawley SE. 2nd edition. WB Saunders, Philadelphia, PA, pp.686-693.

Shah, J. and Gil, Z. (2009). Current concepts in management of oral cancer–surgery. Oral oncology, 45(4), pp.394-401.

Shah, S., Luke, J., Jacene, H., Chen, T., Giobbie-Hurder, A., Ibrahim, N., Buchbinder, E., McDermott, D., Flaherty, K., Sullivan, R., Lawrence, D., Ott, P., and Hodi, S. (2018). Results from phase II trial of HSP90 inhibitor, STA-9090 (ganetespib), in metastatic uveal melanoma. Melanoma Research, 28(6), pp.605-610.

Shibahara, T., Nomura, T., Cui, N. and Noma, H. (2005). A study of osteoclast-related cytokines in mandibular invasion by squamous cell carcinoma. International Journal of Oral Maxillofacial Surgery. 34, pp.789–93.

Shiga, K., Hara, M., Nagasaki, T., Sato, T., Takahashi, H. and Takeyama, H. (2015). Cancer-associated fibroblasts: their characteristics and their roles in tumor growth. Cancers, 7(4), pp.2443-2458.

Shimo, T., Kanyama, M., Wu, C., Sugito, H., Billings, P., Abrams, W., Rosenbloom, J., Iwamoto, M., Pacifici, M. and Koyama, E. (2004). Expression and roles of connective tissue growth factor in Meckel's cartilage development. Developmental Dynamics, 231(1), pp.136-147.

Shimo, T., Kubota, S., Goda, T., Yoshihama, Y., Kurio, N. and Nishida, T. (2008). Clinical significance and pathogenic function of connective tissue growth factor (CTGF/CCN2) in

osteolytic mandibular squamous cell carcinoma. Anticancer Research. 28(4C), pp.2343–2348.

Shin, M., Matsuo, K. and Tada, T. (2011). The inhibition of RANKL/RANK signaling by osteoprotegerin suppresses bone invasion by oral squamous cell carcinoma cells. Carcinogenesis, 32, pp.1634-1640.

Short, S., Fielder, E., Miwa, S. and von Zglinicki, T., 2019. Senolytics and senostatics as adjuvant tumour therapy. *EBioMedicine*.

Sica, A., Saccani, A., Bottazzi, B., Polentarutti, N., Vecchi, A., Van Damme, J. and Mantovani, A. (2000). Autocrine production of IL-10 mediates defective IL-12 production and NF-κB activation in tumor-associated macrophages. The Journal of Immunology, 164(2), pp.762-767.

Siegel, P. and Massagué, J. (2003). Cytostatic and apoptotic actions of TGF-β in homeostasis and cancer. Nature Reviews Cancer, 3(11), pp.807-820.

Simonet, W., Lacey, D., Dunstan, C., Kelley, M., Chang, M., Lüthy, R., Nguyen, H., Wooden, S., Bennett, L., Boone, T., Shimamoto, G., DeRose, M., Elliot, R., Colombero, A., Tan, H., Trail, G., Sullivan, J., Cavy, E., Bucay, N., Renshaw-Gegg, L., Hughes, T., Hill.,D., Pattison, W., Campbell., P. Sander, S., Van, G., Tarpley, J., Derby, P., Lee, R. and Boyle, W. (1997). Osteoprotegerin: a novel secreted protein involved in the regulation of bone density. Cell, 89(2), pp.309-319.

Sims, N. and Gooi, J. (2008). Bone remodeling: Multiple cellular interactions required for coupling of bone formation and resorption. Seminars of Cell Development Biology. 19, pp.444–451.

Sinevici, N. and O'sullivan, J. (2016). Oral cancer: Deregulated molecular events and their use as biomarkers. Oral Oncology, 61, pp.12-18.

Slootweg, P. and Müller, H. (1989). Mandibular invasion by oral squamous cell carcinoma. Journal of Cranio-Maxillofacial Surgery, 17(2), pp.69-74.

Smitha, A., Rao, K., Umadevi, H., Smitha, T., Sheethal, H. and Vidya, M. (2019). Immunohistochemical study of α-smooth muscle actin expression in oral leukoplakia and oral squamous cell carcinoma. Journal of oral and maxillofacial pathology: JOMFP, 23(1), p.59.

Sobral, L., Montan, P., Zecchin, K., Martelli-Junior, H., Vargas, P., Graner, E. and Coletta, R. (2011). Smad7 Blocks Transforming Growth Factor-β1–Induced Gingival Fibroblast–Myofibroblast Transition via Inhibitory Regulation of Smad2 and Connective Tissue Growth Factor. Journal of Periodontology, 82(4), pp.642-651.

Stein, J. and Luzio, J. (1991). Ectocytosis caused by sublytic autologous complement attack on human neutrophils. The sorting of endogenous plasma-membrane proteins and lipids into shed vesicles. Biochemical Journal, 274(2), pp.381-386.

Storer, M., Mas, A., Robert-Moreno, A., Pecoraro, M., Ortells, M., Di Giacomo, V., Yosef, R., Pilpel, N., Krizhanovsky, V., Sharpe, J. and Keyes, W. (2013). Senescence is a

developmental mechanism that contributes to embryonic growth and patterning. Cell, 155(5), pp.1119-1130.

Suda, T., Takahashi, N., Udagawa, N., Jimi, E., Gillespie, M. and Martin, T. (1999). Modulation of osteoclast differentiation and function by the new members of the tumor necrosis factor receptor and ligand families. Endocrine Reviews, 20(3), pp.345-357.

Sutherland, M., Geoghegan, J., Yu, C., Turcott, E., Skonier, J. and Winkler, D. (2004). Sclerostin promotes the apoptosis of human osteoblastic cells: a novel regulation of bone formation. Bone, 35, pp.828–35.

Tada, T., Jimi, E., Okamoto, M., Ozeki, S. and Okabe, K. (2005). Oral squamous cell carcinoma cells induce osteoclast differentiation by suppression of osteoprotegerin expression in osteoblasts. International Journal of Cancer, 116, pp.253-262.

Tada, T., Shin, M., Fukushima, H., Okabe, K., Ozeki, S., Okamoto, M. and Jimi, E. (2009). Oral squamous cell carcinoma cells modulate osteoclast function by RANKL-dependent and independent mechanisms. Cancer Letters, 274, pp.126-131.

Taipale, M., Jarosz, D. and Lindquist, S. (2010). HSP90 at the hub of protein homeostasis: emerging mechanistic insights. Nature Reviews Molecular Cell Biology, 11(7), p.515.

Tan, A., De La Peña, H. and Seifalian, A. (2010). The application of exosomes as a nanoscale cancer vaccine. International Journal of Nanomedicine, 5, p.889.

Tan, H., Wang, N. and Feng, Y. (2016). Autophagy mediated activation of RelB/p52 responsible for the reprogramming of tumour associated macrophages. European Journal of Cancer.

Tanaka, Y., Kamohara, H., Kinoshita, K., Kurashige, J., Ishimoto, T., Iwatsuki, M., Watanabe, M. and Baba, H. (2013). Clinical impact of serum exosomal microRNA-21 as a clinical biomarker in human esophageal squamous cell carcinoma. Cancer, 119(6), pp.1159-1167.

Tang, C., Chuang, J., Fong, Y., Maa, M., Way, T. and Hung, C. (2008). Bone-derived SDF-1 stimulates IL-6 release via CXCR4, ERK and NF-kappaB pathways and promotes osteoclastogenesis in human oral cancer cells. Carcinogenesis, 29 (8), pp.1483–1492.

Tao, S. and Guo, S. (2019). Extracellular vesicles in bone:“dogrobbers” in the “eternal battle field”. Cell Communication and Signaling, 17(1), p.6.

Teitelbaum, S. (2000). Bone resorption by osteoclasts. Science, 289(5484), pp.1504-1508.

Tejada, M., Yu, L., Dong, J., Jung, K., Meng, G., Peale, F., Frantz, G., Hall, L., Liang, X., Gerber, H. and Ferrara, N. (2006). Tumor-driven paracrine platelet-derived growth factor receptor α signaling is a key determinant of stromal cell recruitment in a model of human lung carcinoma. Clinical Cancer Research, 12(9), pp.2676-2688.

te Poele, R.H., Okorokov, A.L., Jardine, L., Cummings, J. and Joel, S.P. (2002). DNA damage is able to induce senescence in tumor cells in vitro and in vivo. *Cancer*

research, *62*(6), pp.1876-1883.

Theill, L., Boyle, W. and Penninger, J. (2002). RANK-L and RANK: T cells, bone loss, and mammalian evolution. Annual Review of Immunology, 20(1), pp.795-823.

Théry, C., Witwer, K., Aikawa, E., Alcaraz, M., Anderson, J., Andriantsitohaina, R., Antoniou, A., Arab, T., Archer, F., Atkin-Smith, G., Ayre, D. *et al.* (2018). Minimal information for studies of extracellular vesicles 2018 (MISEV2018): a position statement of the International Society for Extracellular Vesicles and update of the MISEV2014 guidelines. Journal of Extracellular Vesicles, 7(1), p.1535750.

Théry, C., Zitvogel, L. and Amigorena, S. (2002). Exosomes: composition, biogenesis and function. Nature Reviews Immunology, 2(8), p.569.

Thode, C., Jørgensen, T.G., Dabelsteen, E., Mackenzie, I. and Dabelsteen, S., (2011). Significance of myofibroblasts in oral squamous cell carcinoma. Journal of Oral Pathology & Medicine, 40(3), pp.201-207.

Totsuka, Y., Usui, Y., Tei, K., Fukuda, H., Shindo, M., Iizuka, T., and Amemiya, A. (1991). Mandibular involvement by squamous cell carcinoma of the lower alveolus: analysis and comparative study of histologic and radiologic features. Head Neck. 13, pp.40-50.

Trajkovic, K., Hsu, C., Chiantia, S., Rajendran, L., Wenzel, D., Wieland, F., Schwille, P., Brügger, B. and Simons, M. (2008). Ceramide triggers budding of exosome vesicles into multivesicular endosomes. Science, 319(5867), pp.1244-1247.

Trepel, J., Mollapour, M., Giaccone, G. and Neckers, L. (2010). Targeting the dynamic HSP90 complex in cancer. Nature reviews cancer, 10(8), p.537.

Turley, E., Veiseh, M., Radisky, D. and Bissell, M. (2008). Mechanisms of Disease: epithelial–mesenchymal transition—does cellular plasticity fuel neoplastic progression? Nature Clinical Practice Oncology, 5(5), pp.280-290.

Vader, P., Breakefield, X. and Wood, M. (2014). Extracellular vesicles: emerging targets for cancer therapy. Trends in Molecular Medicine, 20(7), pp.385-393.

Van den Boorn, J., Daßler, J., Coch, C., Schlee, M. and Hartmann, G. (2013). Exosomes as nucleic acid nanocarriers. Advanced Drug Delivery Reviews, 65(3), pp.331-335.

Vered, M., Allon, I., Buchner, A. and Dayan, D. (2009). Stromal myofibroblasts accompany modifications in the epithelial phenotype of tongue dysplastic and malignant lesions. Cancer Microenvironment, 2(1), pp.49-57.

Vered, M., Dayan, D., Yahalom, R., Dobriyan, A., Barshack, I., Bello, I., Kantola, S. and Salo, T. (2010). Cancer-associated fibroblasts and epithelial-mesenchymal transition in metastatic oral tongue squamous cell carcinoma. International Journal of Cancer, 127(6), pp.1356-1362.

Vered, M., Dobriyan, A., Dayan, D., Yahalom, R., Talmi, Y., Bedrin, L., Barshack, I. and Taicher, S. (2010). Tumor-host histopathologic variables, stromal myofibroblasts and risk score, are significantly associated with recurrent disease in tongue cancer. Cancer Science, 101(1), pp.274-280.

Vincent, C., Kogawa, M., Findlay, D. and Atkins, G. (2009). The generation of osteoclasts from RAW 264.7 precursors in defined, serum-free conditions. Journal of Bone and Mineral Metabolism, 27(1), pp.114-119.

Wada, T., Nakashima, T., Hiroshi, N. and Penninger, J. (2006). RANKL–RANK signaling in osteoclastogenesis and bone disease. Trends in Molecular Medicine, 12(1), pp.17-25.

Wagner, W., Horn, P., Castoldi, M., Diehlmann, A., Bork, S., Saffrich, R., Benes, V., Blake, J., Pfister, S., Eckstein, V. and Ho, A. (2008). Replicative senescence of mesenchymal stem cells: a continuous and organized process. PLOS One, 3(5), p.e2213.

Waldenström, A., Gennebäck, N., Hellman, U. and Ronquist, G. (2012). Cardiomyocyte microvesicles contain DNA/RNA and convey biological messages to target cells. PLOS One, 7(4), p.e34653.

Walsh, M., Kim, N., Kadono, Y., Rho, J., Lee, S. and Lorenzo, J. (2006). Osteoimmunology: interplay between the immune system and bone metabolism. Annual Review of Immunology. 24, pp.33–63.

Wan, L., Pantel, K. and Kang, Y. (2013). Tumor metastasis: moving new biological insights into the clinic. Nature medicine, 19(11), p.1450.

Wang, E. (1995). Senescent human fibroblasts resist programmed cell death, and failure to suppress bcl2 is involved. Cancer Research, 55(11), pp.2284-2292.

Wang, W., Li, Q., Yamada, T., Matsumoto, K., Matsumoto, I., Oda, M., Watanabe, G., Kayano, Y., Nishioka, Y., Sone, S. and Yano, S. (2009). Crosstalk to stromal fibroblasts induces resistance of lung cancer to epidermal growth factor receptor tyrosine kinase inhibitors. Clinical Cancer Research, 15(21), pp.6630-6638.

Warnakulasuriya, S. (2009). Global epidemiology of oral and oropharyngeal cancer. Oral Oncology. 45(4–5), pp.309–316.

Warnakulasuriya, S. (2010). Living with oral cancer: epidemiology with particular reference to prevalence and life-style changes that influence survival. Oral Oncology, 46(6), pp.407-410.

Webber, J., Steadman, R., Mason, M., Tabi, Z. and Clayton, A. (2010). Cancer exosomes trigger fibroblast to myofibroblast differentiation. Cancer Research, 70(23), pp.9621-9630.

Weiss, A. and Attisano, L. (2013). The TGFbeta superfamily signaling pathway. Wiley Interdisciplinary Reviews: Developmental Biology, 2(1), pp.47-63.

Werner, S. and Grose, R. (2003). Regulation of wound healing by growth factors and cytokines. Physiological Reviews, 83(3), pp.835-870.

Winck, F., Ribeiro, A., Domingues, R., Ling, L., Riaño-Pachón, D., Rivera, C., Brandão, T., Gouvea, A., Santos-Silva, A., Coletta, R. and Leme, A. (2015). Insights into immune responses in oral cancer through proteomic analysis of saliva and salivary extracellular vesicles. Scientific Reports, 5, p.16305.

Wipff, P., Rifkin, D., Meister, J. and Hinz, B. (2007). Myofibroblast contraction activates latent TGF-β1 from the extracellular matrix. The Journal of Cell Biology, 179(6), pp.1311-1323.

Xing, F., Saidou, J. and Watabe, K. (2010). Cancer associated fibroblasts (CAFs) in tumor microenvironment. Frontiers in Bioscience: A Journal and Virtual Library, 15, p.166.

Xouri, G. and Christian, S. (2010). Origin and function of tumor stroma fibroblasts. In Seminars in Cell & Developmental Biology, (21) pp.40-46. Academic Press.

Xu, J., Lamouille, S. and Derynck, R. (2009). TGF-beta-induced epithelial to mesenchymal transition. Cell Research. 19, pp.156–172.

Xu, R., Rai, A., Chen, M., Suwakulsiri, W., Greening, D. and Simpson, R. (2018). Extracellular vesicles in cancer—implications for future improvements in cancer care. *Nature reviews Clinical oncology*, *15*(10), p.617.

Yamada, T., Matsumoto, K., Wang, W., Li, Q., Nishioka, Y., Sekido, Y., Sone, S. and Yano, S. (2010). Hepatocyte growth factor reduces susceptibility to an irreversible epidermal growth factor receptor inhibitor in EGFR-T790M mutant lung cancer. Clinical Cancer Research, 16(1), pp.174-183.

Yao, K., Wu, X., Thompson, J.E. and Carlson, J.C. (1993). Isolation and characterization of deteriosomes from rat liver. Journal of Cellular Biochemistry, 51(4), pp.488-494.

Yin, P., Lv, H., Li, Y., Deng, Y., Zhang, L. and Tang, P. (2017). exosome-Mediated Genetic information transfer, a Missing piece of osteoblast–osteoclast Communication puzzle. Frontiers in endocrinology, *8*, p.336.

Yu, Q. and Stamenkovic, I. (2000). Cell surface-localized matrix metalloproteinase-9 proteolytically activates TGF-β and promotes tumor invasion and angiogenesis. Genes & Development, 14(2), pp.163-176.

Zhao, C., Irie, N., Takada, Y., Shimoda, K., Miyamoto, T. and Nishiwaki, T. (2006). Bidirectional ephrinB2–EphB4 signaling controls bone homeostasis. Cell Metabolism. 4, pp.111–21.

Zhou, H., Kartsogiannis, V., Hu, Y., Elliott, J., Quinn, J. and McKinstry, W. (2001). A novel osteoblast-derived C-type lectin that inhibits osteoclast formation. Journal of Biological Chemistry. 276, pp.14916–23.

Zhu, G., Wang, S., Chen, J., Wang, Z., Liang, X., Wang, X., Jiang, J., Lang, J. and Li, L. (2017). Long noncoding RNA HAS2-AS1 mediates hypoxia-induced invasiveness of oral squamous cell carcinoma. Molecular carcinogenesis, 56(10), pp.2210-2222.

Zhu, Y., Armstrong, J., Tchkonia, T. and Kirkland, J. (2014). Cellular senescence and the senescent secretory phenotype in age-related chronic diseases. Current Opinion in Clinical Nutrition & Metabolic Care, 17(4), pp.324-328.

Zhu, Y., Doornebal, E., Pirtskhalava, T., Giorgadze, N., Wentworth, M., Fuhrmann-Stroissnigg, H., Niedernhofer, L., Robbins, P., Tchkonia, T. and Kirkland, J. (2017). New

agents that target senescent cells: the flavone, fisetin, and the BCL-XL inhibitors, A1331852 and A1155463. Aging (Albany NY), 9(3), p.955.

Zhu, Y., Tchkonia, T., Fuhrmann-Stroissnigg, H., Dai, H.M., Ling, Y., Stout, M., Pirtskhalava, T., Giorgadze, N., Johnson, K., Giles, C., Wren, J., Niedernhofer, L., Robbins, P. and Kirkland, J. (2016). Identification of a novel senolytic agent, navitoclax, targeting the Bcl-2 family of anti-apoptotic factors. Aging cell, 15(3), pp.428-435.

Zhu, Y., Tchkonia, T., Pirtskhalava, T., Gower, A., Ding, H., Giorgadze, N., Palmer, A., Ikeno, Y., Hubbard, G., Lenburg, M., O'Hara, S., LaRusso, N., Miller, J., Roos, C., Verzosa, G., LeBrasseur, N., Wren, J., Farr, J., Khosla, S., Stout, M., McGowan, S., Fuhrmann-Stroissnigg, H., Gurkar, A., Zhao, J., Colangelo, D., Dorronsoro, A., Ling, Y., Barghouthy, A., Navarro, D., Sana, T., Robbins, P., Niedernhofer, L. and Kirkland, J. (2015). The Achilles' heel of senescent cells: from transcriptome to senolytic drugs. Aging cell, 14(4), pp.644-658.